PETROGRAPHIC CHARACTERISATION AND ZIRCON GEOCHRONOLOGY OF THE COBUNGRA GRANITE AND LOW–P HIGH–T OMEO METAMORPHIC COMPLEX, LACHLAN FOLD BELT

NICHOLAS TEFAY

Morning snow in Omeo, Snowy Mountains, Victoria. Photo by N. Daczko

PRESENTED TO THE DEPARTMENT OF EARTH AND PLANETARY SCIENCES,
FACULTY OF SCIENCE
IN PARTIAL FULFILMENT OF THE REQUIREMENTS OF THE DEGREE OF

HONOURS, BSC

MACQUARIE UNIVERSITY, SYDNEY

JUNE 2011

MACQUARIE UNIVERSITY

GEMOC

STATEMENT OF ORIGINALITY

All the work submitted in this thesis is the original work of the author except where otherwise acknowledged. No part of this thesis has been previously submitted to any university or institution.

_____ _____

Signed *– Nicholas Tefay* ***Dated***

ACKNOWLEDGEMENTS

I would like to thank the following people for their help and support during my Honours year.

- My supervisor Nathan Daczko, for being so generous with his time and for his willingness and patience to help me with all aspects of the project. He planned fieldwork and lab work, reviewed my writing and was a constant source of knowledge and motivation.
- My co-supervisor Norm Pearson, for sharing his wealth of knowledge and experience, and especially for his help in reviewing geochemical data.
- Cameron Quinn of the Geological Survey of New South Wales, for his help in choosing a study location and for his guidance during fieldwork.
- Steve Craven, for help in the initial processing the rock samples, for help using the SelFrag© and for making the zircon mount.
- Manal Bebbington, for making thin sections.
- Kevin Grant, for his instruction on the EMP and SEM and setting up the sessions; and for his understanding when I turned up the air-conditioning and shutdown the EMP.
- Will Powell, for assistance with LA-ICP-MS. He was always keen to help me out and answer my questions.
- Peter Wieland, for preparing the whole-rock samples for analysis by XRF and ICP-MS, and for carrying out the analyses.
- Rosanna Murphy, for help in processing geochronological data.
- Dick Flood, for his good cheer and contagious enthusiasm for geology.
- And finally to my family, for their ongoing support and encouragement in the past year and for providing a productive environment to work in.

ABSTRACT

The low-P high-T Omeo Metamorphic Complex, located in the Lachlan Fold Belt, formed in the Silurian by amphibolite-grade metamorphism of quartz-rich Ordovician turbidites. I-type and S-type granites intruded the complex in the Silurian and Devonian. The study area is a 15 km by 15 km area of this terrane located near the town of Omeo in the Snowy Mountains of Victoria. I-type and S-type granites (predominantly the S-type Cobungra Granite) make up the western part of the study area with the metasedimentary rocks of the Omeo Metamorphic Complex decreasing in grade toward the east away from the Cobungra Granite, forming a regional aureole. This study involved the sampling and characterisation of rocks in the study area, focusing on petrography, mineral chemistry and whole-rock chemistry. Zircon morphology, U/Pb geochronology and major and trace element chemistry was characterised for four samples to determine whether the high-T metasedimentary rocks of the Omeo Metamorphic Complex are the source for the adjacent S-type Cobungra Granite. A crystallisation age of 423.6 ± 4.8 Ma was resolved for one Cobungra Granite sample which marks the first time this granite has been dated using U/Pb in zircon. Unfortunately, the U/Pb zircon data from the other samples was too disturbed to be useful. However, zircon trace element data showed that the metasedimentary sample was distinct from the granite samples suggesting the source of the S-type magmatism is different to the exposed high-T metasedimentary rocks. Zircon trace element data was also useful in making links between geochronological and morphological data.

TABLE OF CONTENTS

LIST OF FIGURES

LIST OF TABLES

CHAPTER 1

INTRODUCTION

1.1 STUDY AREA

The low-P high-T Omeo Metamorphic Complex (OMC) is located at the southern end of the Wagga-Omeo Metamorphic Belt in the Lachlan Fold Belt (Figure 1.1). The quartz-rich Ordovician turbidites of the Pinnak Sandstone were metamorphosed in the Silurian to amphibolite-grade to form the OMC with peak P/T conditions of ≈3.5 kbar and ≈700°C (Morand 1990). I-type and S-type granites were also intruded at this time. The study area is approximately 15 km by 15 km and is located in the south of the OMC near the town of Omeo in the Victorian Snowy Mountains (Figures 1.1 & 1.2). I-type and S-type granites (predominantly the S-type Cobungra Granite) make up the western part of the study area. The metasedimentary rocks of the OMC decrease in grade toward the east away from the Cobungra Granite, forming a regional aureole similar to those described by White et al. (1974). The lower grade metasedimentary rocks are biotite–muscovite–cordierite schists and the higher grade rocks are K-feldspar–cordierite–sillimanite gneisses. At the higher grade end, the metasedimentary rocks grade into nebulitic migmatites and a very heterogeneous S-type granite (Cobungra) with up to metre-scale gneissic xenoliths (Willman et al. 1999). The rocks have also undergone widespread retrogression to lower greenschist facies.

1.2 GEOCHRONOLOGY OF THE SE LACHLAN FOLD BELT

The first geochronological studies of the south-eastern Lachlan Fold Belt, apart from those using stratigraphic relationships, were the reconnaissance K/Ar age measurements on igneous rocks in south-eastern New South Wales by Evernden and Richards (1962) and

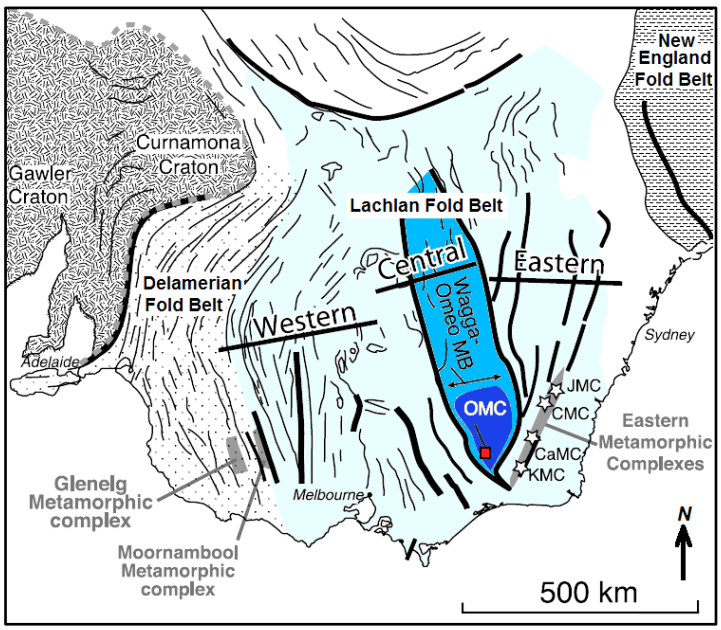

Figure 1.1. Metamorphic complexes and fold belts of south-eastern Australia. OMC=Omeo Metamorphic Complex. MB=Metamorphic Belt. Location of study area indicated in red (see Figure 1.2). From Gray and Foster (2004).

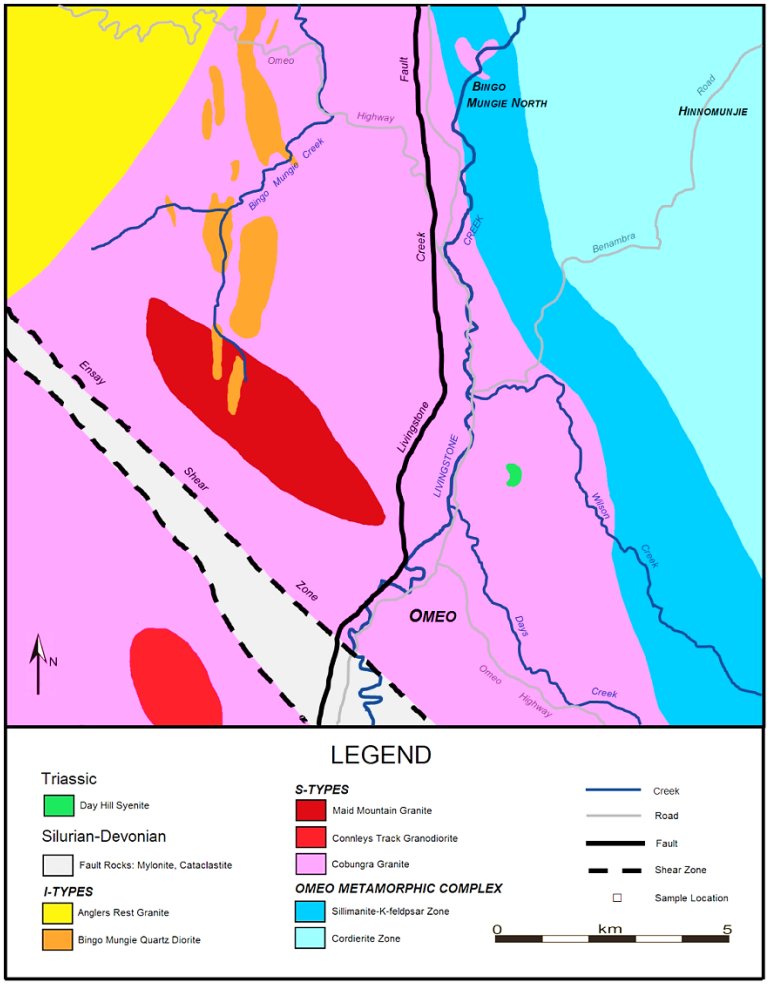

Figure 1.2. Simplified geological map of the study area. Map modified from Morand et al. 1999.

the reconnaissance traverse of K/Ar and Rb/Sr ages of igneous rocks across Victoria (Richard and Singleton 1981). The researchers emphasised that the ages are not necessarily the intrusion ages, particularly in regions subject to slow cooling or protracted magmatism. The researchers also pointed out the susceptibility of the K/Ar biotite system to thermal overprinting. Sensitive high resolution ion microprobe (SHRIMP) dating using U/Pb in zircon from I-type and S-type granites in the Lachlan Fold Belt showed an age pattern of inherited grains (Williams 1992). The difference between the two granite types was that inherited zircon was rare in I-types, but most zircon grains in the S-types contained an inherited core. Backscatter electron imaging showed most cores to be rounded fragments of formerly larger grains, consistent with the cores originally having been detrital grains (Paterson et al. 1992). The ages and relative abundances of detrital zircon in the sediments match those of the inherited zircon in the granites (Williams 1995). Detrital zircon age groupings of 450-600 Ma, 750-1200 Ma and >1200 Ma occur in the Ordovician turbidites of the Lachlan Fold Belt (Williams et al. 1994). Studies of Victorian granites have compared inherited and detrital zircon ages in S-type granites, their deep-sourced enclaves and their host sediments and found a similar age pattern in all three (Anderson et al. 1996; Keay et al. 1999). Crystallisation ages of granites from the south-eastern Lachlan Fold Belt have also been estimated using U/Pb zircon dating (Keay et al. 1999; Kemp et al. 2005; Belousova et al. 2006) which generally reported ages slightly older than the K/Ar biotite age.

1.3 AIMS OF THE STUDY

The specific aims of the study are as follows:

- Collect approximately 30 representative rock samples from the study area and characterise their petrography from thin sections including mineral modes and grain sizes, textures and any interpretations.

- Characterise the mineral chemistry of the samples by EMP analysis of eight thin sections for minerals including biotite, muscovite and feldspars. Check for the presence of fresh cordierite in any of the metasedimentary samples.
- For the granites and high-grade metasedimentary rocks, characterise whole-rock major element chemistry by XRF and whole-rock trace element chemistry by both XRF and ICPMS.
- Separate zircon grains from the I-type and S-type granite samples and a high-grade metasedimentary sample. Characterise and compare the zircon morphology (SEM), U/Pb age of magmatic, inherited and detrital grains (LA-ICP-MS), major elements (EMP) and trace elements (LA-ICP-MS).
- Investigate the nature of the interaction between the high-T metasedimentary rocks and the adjacent S-type granites by analysis of zircon from various samples and determine whether the high-T metasedimentary rocks are the source for the S-type granites.

CHAPTER 2

REGIONAL GEOLOGY

2.1 REGIONAL SETTING

The eastern third of Australia is mostly composed of the Palaeozoic Tasman Orogenic System. In the southern part of this system, there are three major belts of deformed rocks. These are the Delamerian Fold Belt to the west, the New England Fold Belt to the east and the Lachlan Fold Belt (LFB) to the south (Figure 2.1). The LFB represents a prolonged period during which mainly Cambrian to Devonian marine sedimentary wedges accreted westward onto the Australian craton. Structural divisions of the LFB include the Omeo Zone in which the present study area is located (Figure 2.1). The multiple orogenic events experienced by the LFB are summarised in Table 2.1 along with the local effects of these events in the Omeo Zone.

Table 2.1. Effects of orogenic events in the Lachlan Fold Belt in Victoria and local effects in the Omeo Zone. (VandenBerg et al. 1998; Willman et al. 1999; VandenBerg et al. 2000)

Orogenic Event	Geological Period	Overall effects on Lachlan Fold Belt	Local effects in Omeo Zone
Benambran	Early – Middle Silurian *(440-430 Ma)*	• Widespread uplift throughout Victoria • Deformation and metamorphism of quartz-rich Ordovician turbidites	• Formation of the Omeo Metamorphic Complex through regional metamorphism of Pinnak Sandstone • Tight folding
Bindian	Early Devonian *(418-410 Ma)*	• Uplift and deformation in central and eastern Victoria	• Widespread retrogression of the Omeo Metamorphic Complex to lower greenschist facies assemblages • Intrusion of granites near end of event • Shearing and faulting near edges of Omeo Zone
Tabbera-bberan	Middle Devonian *(385-380 Ma)*	• Uplift forming the Tabberabberan Highlands resulting in major changes in patterns of sedimentation • Deformation of Cambrian to Early Devonian sedimentary rocks throughout Victoria • Extensive granitic intrusive activity throughout Victoria	• Further deformation: formation of open folds, crenulation cleavages, kink folds and reactivation of pre-existing faults
Kanimblan	Carboniferous *(≈340 Ma)*	• Widespread, low-intensity uplifting of central and eastern Victoria • Folding of Upper Devonian rocks across Victoria	• No obvious effects

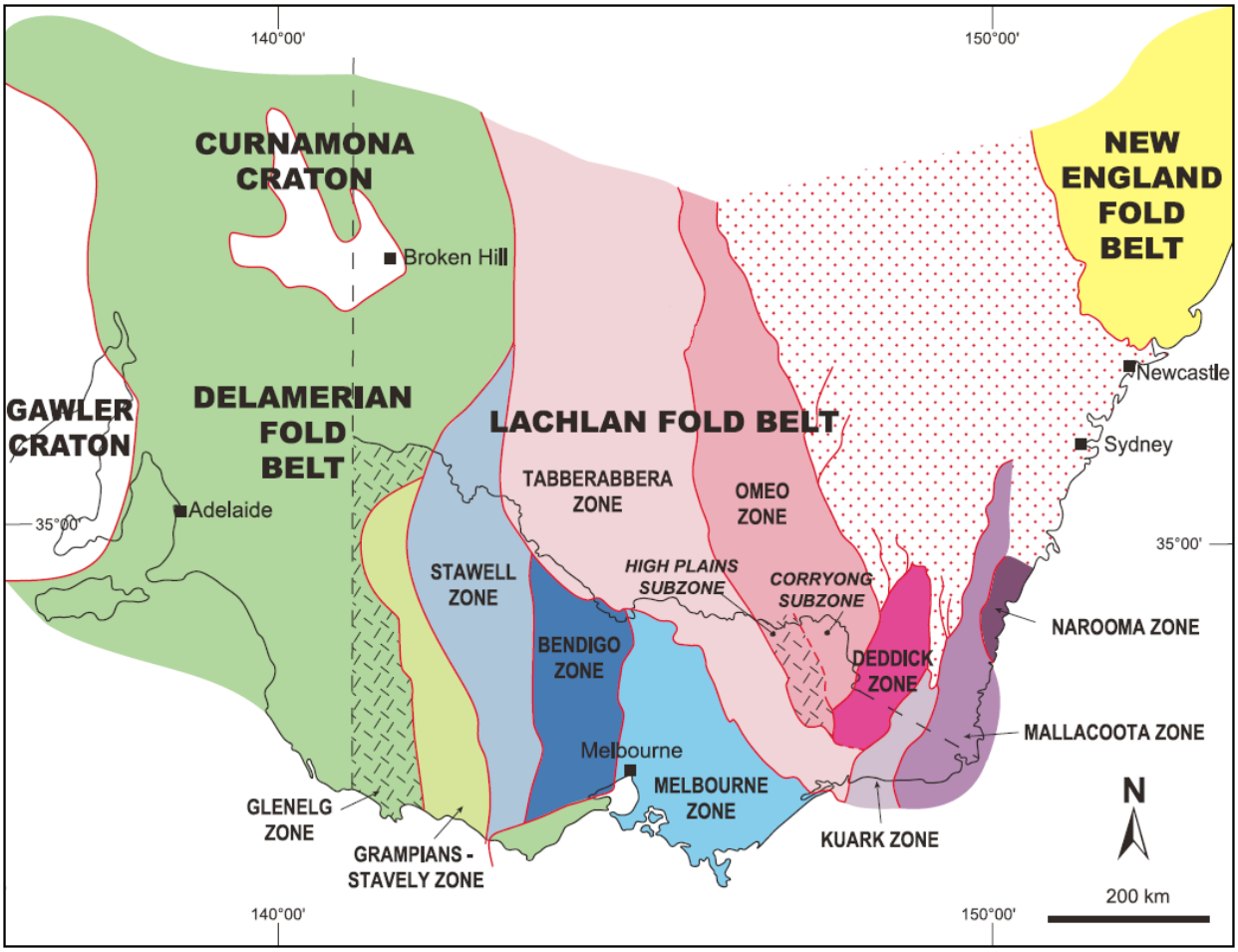

Figure 2.1. Map of the South-eastern Australian fold belts and Victorian structural zones. From VandenBerg et al. (2000).

2.2 GEOLOGY

2.2.1 PINNAK SANDSTONE

The Pinnak Sandstone, a formation of the Adaminaby Group, was deposited in the Ordovician and subsequently metamorphosed during the Silurian Benambran Orogeny to form the Omeo Metamorphic Complex in the Omeo Zone. These quartz-rich sediments were derived from the erosion of Proterozoic and Cambrian granites and metamorphic rocks of the Delamerian Fold Belt and equivalent Ross Orogen in Antarctica (Fergusson &

Tye 1999). The Pinnak Sandstone is dominated by turbidites and has lithofacies associations that include thick-bedded sandstone, thin-bedded sandstone, generally thin-bedded mudstone and thin-bedded chert (Figure 2.2) (VandenBerg et al. 1991, 1998; Hendrickx et al. 1996; Simpson et al. 1997). The rocks occur in poorly defined, laterally and vertically discontinuous packages up to 100 m thick that are either dominated by sandstone or mudstone or occur in approximately equal proportions (Cas & VandenBerg 1988).

Thick-bedded sandstone (>50 cm) is massive to graded, poorly-sorted, medium to coarse, with some layers having scattered granule-sized particles at the base (Simpson et al. 1996). Thin-bedded sandstone is finer, normally graded, planar and cross-laminated. Quartz grains are angular to subrounded, and feldspar (dominantly plagioclase) and muscovite are common accessory minerals. Mudstone is yellow, grey and rarely black, and generally consists of alternating quartz-rich and clay-rich beds 0.2-5 cm thick in packages up to 5 m thick. Sporadic thin bands of chert (<1 m) are composed of thin 5-20 cm beds of pale to very dark grey chert and cherty siltstone, which are internally massive or have fine parallel laminations (VandenBerg et al. 1991, 1998; Hendrickx et al. 1996; Simpson et al. 1997).

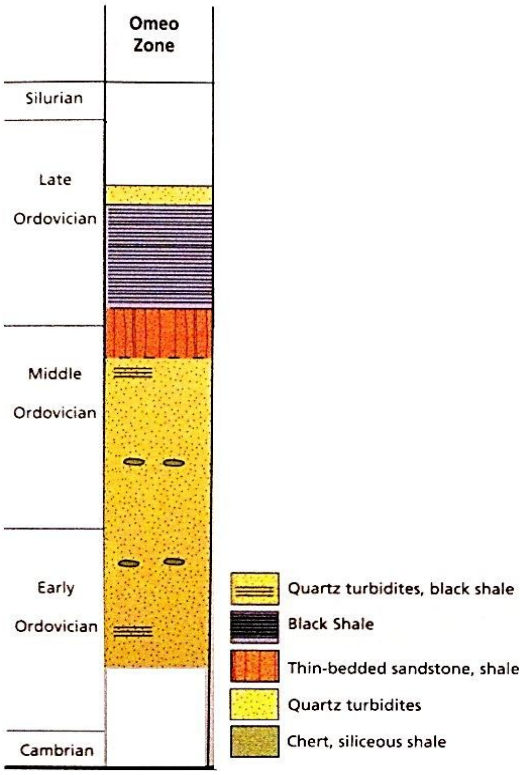

Figure 2.2. Stratigraphic column of Ordovician units in the Omeo zone. From Fergusson & VandenBerg (2003).

2.2.2 GRANITES

The Omeo Province is dominated by S-type granites with subordinate I-types (Figure 2.3). Available radiometric ages for Omeo Province granites (VandenBerg et al. 2000) cluster around 420 Ma and 400 Ma with a few in between and both age groups containing S- and I-type varieties.

Several granites in the Omeo Province belong to the Cooma Supersuite. These include Yabba, Bethanga, House Creek and Cobungra (William et al. 1999). Like the well-studied Cooma pluton in NSW, these are foliated, often heterogenous S-type granodiorites and monzogranites emplaced into migmatitic hosts. They contain abundant quartz, red-brown biotite, primary muscovite, cordierite, sillimanite and in places, a little garnet, but lack calcic plagioclase cores. These granites are characterised by an abundance of metasedimentary enclaves indicating that they have not moved far from their sources. The apparent concentration of Cooma Supersuite granites in the Omeo Province may be due to deeper crustal levels being exposed here as suggested by the high metamorphic grade (Rossiter 2003).

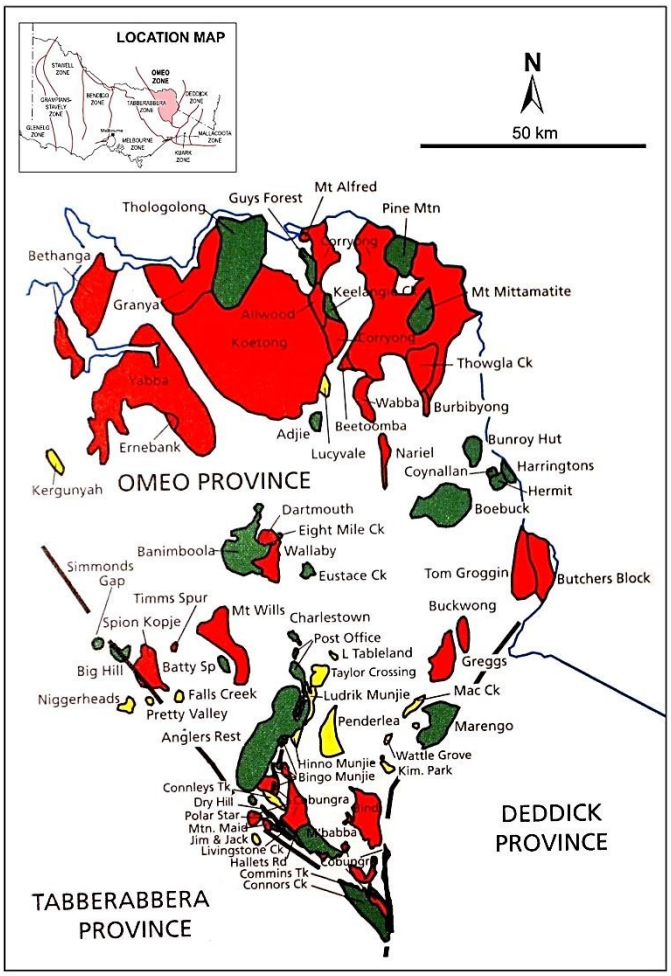

Figure 2.3. Distribution of Siluro-Devonian granite plutons of the Omeo Province, Victoria. S-types are in red; I-types in green; those difficult to classify in yellow. From Rossiter (2003).

Many of the I-type granites in the Omeo Province belong to the Boggy Plains Supersuite (Wyborn et al. 1987). This supersuite is a group of plutons and associated volcanics occupying an elongate belt over 500 km long. The composition of the rocks varies greatly from pyroxenites and gabbros to syenogranites. Wyborn et al. (1987) proposed that this chemical variation is the result of high-temperature fractional crystallisation and that most mafic rocks are cumulates. I-type plutons of the Boggy Plains Supersuite that occur in the Omeo Province include Mount Mittamatite, Pine Mountain, Thologolong, Banimboola, Boebuck and Anglers Rest. Willman et al. (1999) consider the Bingo Munjie Suite bodies (Bingo Munjie, Charlestown, Post Office) to belong to the Boggy Plains Supersuite.

2.2.2.1 COBUNGRA GRANITE

The S-type Cobungra Granite (Figure 2.3) of the Cooma Supersuite in the Omeo Metamorphic Complex has been subdivided into the main Cobungra Granite and the subtype of Biotite Granodiorite (Willman et al. 1999). The main Cobungra Granite is a very heterogenous rock, but is typically a medium-grained, grey biotite-muscovite granite containing scattered anhedral phenocrysts of perthitic K-feldspar or xenoliths of intergrown K-feldspar and quartz up to 7 cm across. It typically has small 10 mm ovoid, fine-grained, biotite-rich xenoliths, as well as numerous xenoliths of gneiss up to two metres long (Willman et al. 1999). Gneissic xenoliths include quartz-rich, biotite-rich, cordierite-rich and calc-silicate types. There are also small grains of altered cordierite scattered throughout the rock, and rare garnet. The rock may be massive or foliated, grading locally into mylonite, may be intruded by pegmatites, and may display a weak, streaky layering (Willman et al. 1999).

Biotite Granodiorite generally forms smaller bodies than the main Cobungra Granite and they are typically interlayered. Biotite Granodiorite is better separated from its source rocks and is clean with few xenoliths (Willman et al. 1999). The two granites are considered to be the same age due to the gradational contacts between them. A K/Ar determination on biotite from the Biotite Granodiorite has given an age of 411±6 Ma (Willman et al. 1999), placing it near the Siluro-Devonian boundary. This is not the emplacement age but is considered to be the age of an Early Devonian regional thermal event that resulted in I-type granite intrusion (Willman et al. 1999).

2.2.2.2 ANGLERS REST GRANITE

The Anglers Rest Granite (Figure 2.3), also known as the Knocker Granite, is very homogenous, being a medium-grained, massive, equigranular monzogranite with very few xenoliths – only one small xenolith (1 x 2 cm) was found during the course of mapping by VandenBerg et al. (1998). It is leucocratic, with a small amount of green-brown biotite, and is pink due to abundant K-feldspar. However, weathered outcrops are white (VandenBerg et al. 1998). Two K/Ar biotite determinations on the Anglers Rest Granite have given ages of 390±16 Ma and 400±16 Ma (Richards & Singleton 1981) placing it in the Early Devonian.

2.3 STRUCTURAL HISTORY

The Omeo Zone is a NNW-trending belt of complexly deformed metamorphic rocks bounded by the Kiewa-Kancoona, Indi-Long Plains and Gilmore fault zones (Figure 2.4). Structures within the Omeo Zone show a trend of increased complexity with increasing metamorphic grade (Willman et al. 1999, 2002). Regional structural trends are mostly defined by Benambran S_2 schistosity and gneissosity. These fabrics show a dominant

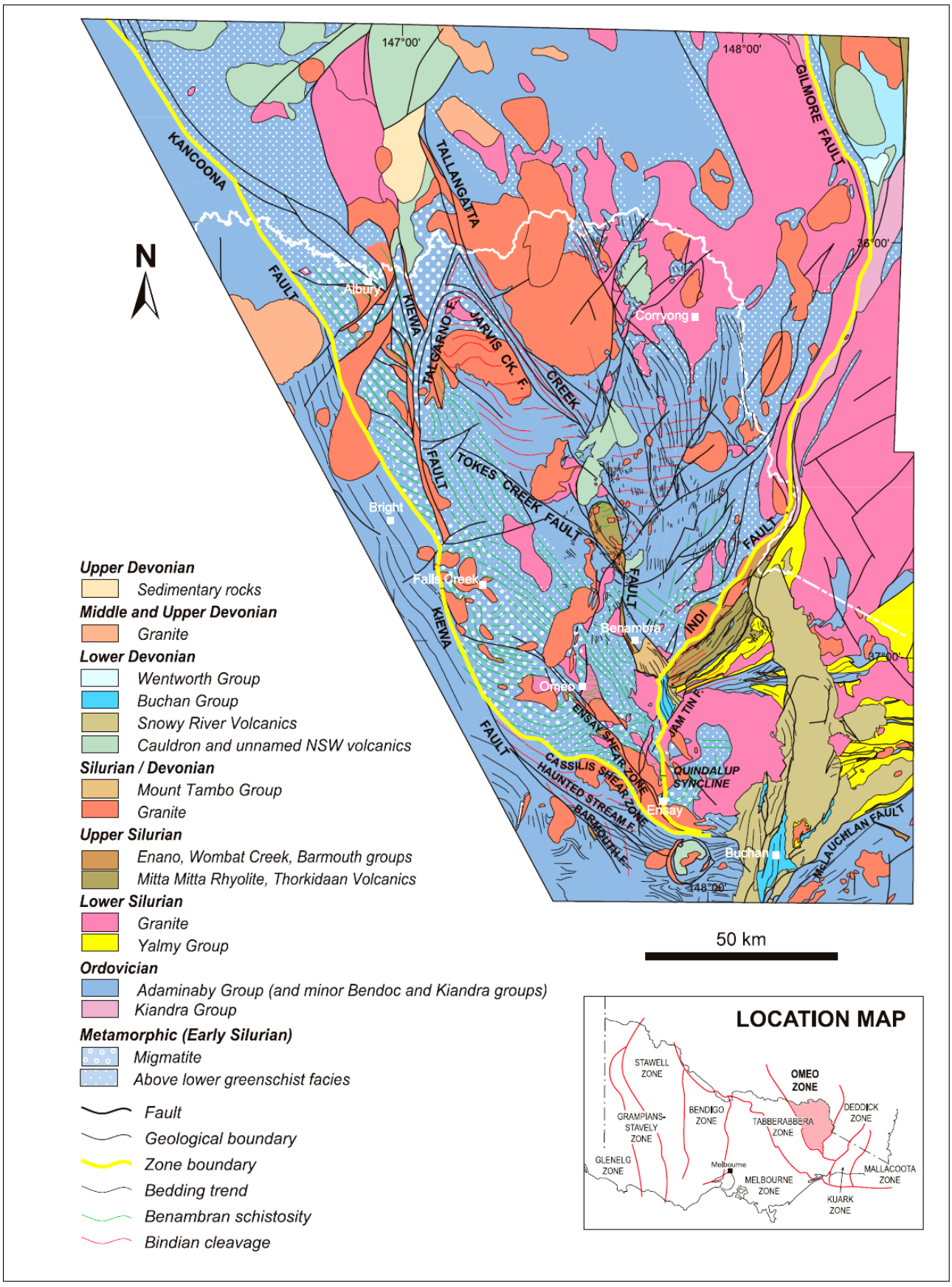

Figure 2.4. Solid geological map of the Omeo Zone showing main rock units and structural information. From VandenBerg et al. (2000).

WNW strike which in places swings to the NW near the western boundary faults (Figure 2.4). S_2 in the Cordierite Zone is defined by well-aligned muscovite and biotite, while an internal fabric in cordierite porphyroblasts records an earlier S_1 foliation (Morand 1990). Retrogression of these cordierite porphyroblasts occurred after the S_2 cleavage developed. F_2 folds are usually upward facing, close to tight and have fold half-wavelengths of up to hundreds of metres (Willman et al. 1999).

The present structural framework of the Omeo Zone is shaped by a number of major, NW- and NE-trending, mostly dextral, strike-slip faults which record a significant period of southeast tectonic transport during the Bindian Orogeny (VandenBerg et al. 2000). Thrusting occurred at this time along the Indi Fault, Old Tallangatta Shear Zone and parts of the Ensay Shear Zone (Morand & Gray, 1991; Willman et al. 1999). These shear zones are 1-2 km wide and contain S-C fabrics within mylonitised schist, gneiss and granite (Morand & Gray 1991).

2.4 METAMORPHIC HISTORY

During the Benambran Orogeny, much of the Pinnak Sandstone in the Omeo Zone was metamorphosed to upper amphibolite facies with maximum P/T conditions estimated at 3.5 kbar and 650-700°C, forming the Omeo Metamorphic Complex (Figure 2.5) (Crohn 1950; Beavis 1962; Fagan 1979; Morand 1990). Morand (1990) described a low-pressure series of metamorphic zones including chlorite, biotite, cordierite, andalusite-K-feldspar, sillimanite-K-feldspar and migmatite zones, and a slightly higher-pressure series with sillimanite-muscovite instead of andalusite-K-feldspar.

Chlorite and biotite zone rocks appear identical to Pinnak Sandstone throughout eastern Victoria, with original sedimentary features preserved (Morand 1990). For this reason, the cordierite isograd can be taken as the boundary of the metamorphic complex. Minerals in metamorphic zones are shown in Table 2.2 and the distribution of zones in Figure 2.5.

Table 2.2. Prograde minerals in metamorphic zones of the Omeo Metamorphic Complex formed from mudstone and sandstone protoliths. Modified from VandenBerg et al. (2000).

Protolith	Cordierite zone	Sillimanite-muscovite zone	Andalusite-K-feldspar zone	Sillimanite-K-feldspar zone	Migmatite zone
Mudstone	biotite, muscovite, cordierite, albite, andalusite, staurolite, quartz	biotite, muscovite, cordierite, sillimanite, quartz, albite	biotite, cordierite, andalusite, K-feldspar, quartz, plagioclase	biotite, cordierite, sillimanite, K-feldspar, quartz, garnet, plagioclase	biotite, cordierite, sillimanite, K-feldspar, titanite, garnet, plagioclase
Sandstone	quartz, muscovite, biotite	quartz, muscovite, biotite	quartz, biotite, K-feldspar, plagioclase	quartz, biotite, K-feldspar, plagioclase	quartz, biotite, K-feldspar, plagioclase

The cordierite zone is characterised by ‘knotted schists’ in which porphyroblasts of cordierite are wrapped by a schistose matrix of biotite and muscovite (Morand 1990). An early foliation, defined by fine inclusions of muscovite, opaques and quartz is commonly preserved in cordierite grains. In the north of the zone, andalusite and cordierite commonly occur together, although throughout the complex both are commonly retrogressed to muscovite, biotite and chlorite. Grain size increases in the andalusite-K-feldspar zone and the schistose character is lost as the amount of muscovite decreases with increasing grade (Morand 1990). These rocks become gneissic and exhibit only a poorly developed foliation, although biotite-rich layers still appear schistose. The sillimanite-K-feldspar zone has the same assemblage as the andalusite-K-feldspar zone except that andalusite is replaced by sillimanite (Morand 1990). Bedding can still be recognised at this grade.

Migmatites and S-type granites formed by partial melting of gneiss are common up-grade of the Sillimanite-K-feldspar Zone, where bedding is destroyed by the partial melting (Fagan 1979; Morand 1990). The migmatite zone is identified by significant amounts

(>20%) of granitic segregation within the gneiss (Willman et al. 1999). The leucosomes consist of quartz, plagioclase, orthoclase or microcline and myrmekite. The melanosomes consist of red-brown biotite, sillimanite, cordierite, and some with andalusite and/or muscovite. There is gradation in places into S-type granite with increase in granitic component, and some migmatites are nebulitic without clear separation of granitic and metasedimentary components (Willman et al. 1999).

Morand (1990) and Willman et al. (1999) have made P/T estimates of the prograde mineral isograds based on studies by Fagan (1979) and Xu et al. (1994). These are summarised in Table 2.3 along with the reactions that produced the minerals.

Table 2.3. P/T estimates of prograde mineral isograds in the Omeo Metamorphic Complex and the reactions that produced the minerals.

Mineral / Isograd	Pressure (kbar)	Temp. (°C)	Reaction(s)
Biotite	Difficult to estimate	400	–
Cordierite	2.5	530	chlorite + muscovite + quartz = cordierite + biotite + water
Andalusite	2-3	550	chlorite + muscovite = biotite + cordierite + andalusite + water
K-feldspar	2.8	630	1. biotite + muscovite + quartz = K-feldspar + cordierite + water 2. muscovite + quartz = K-feldspar + andalusite + water
Sillimanite	2.8	630	–
Migmatite	3.25	660	–

A lower greenschist facies retrogressive event occurred during Bindian Orogeny (Morand 1990; William et al. 1999). The most common retrograde mineral is muscovite which can be very abundant in high grade rocks replacing sillimanite, andalusite, feldspar and cordierite. Biotite and chlorite are also common minerals replacing cordierite and andalusite.

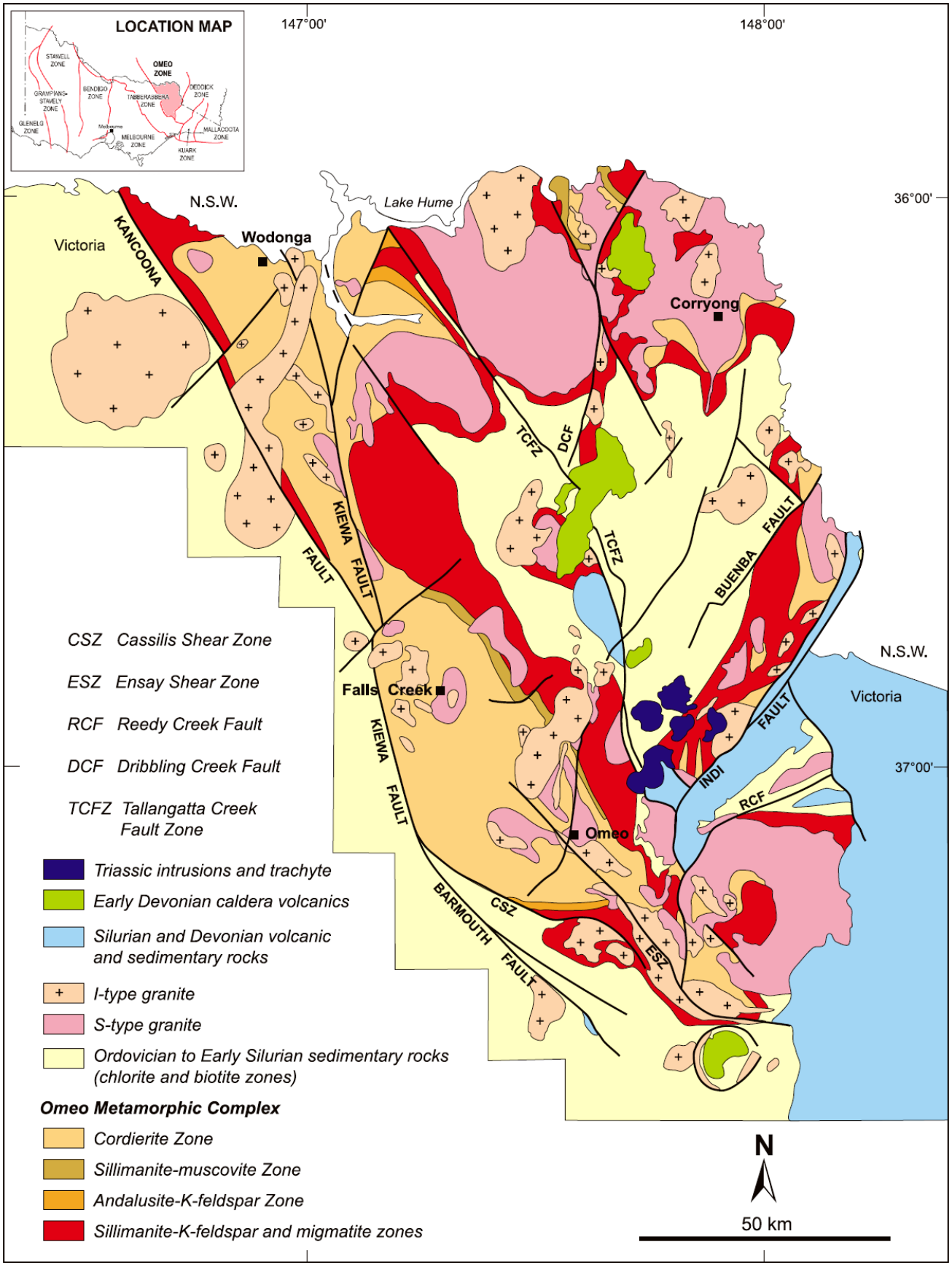

Figure 2.5. Geological map of the Omeo Zone showing distribution of metamorphic zones and major faults. From VandenBerg et al. (2000).

CHAPTER 3

FIELDWORK

Fieldwork was carried out in the Omeo Metamorphic Complex to the north and east of the town of Omeo, Victoria over five days (23-27 August 2010). The aim was to become familiar with the geology of the area and to collect representative samples of the main lithologies for petrographic characterisation, geochemistry and zircon geochronology. The land around Omeo is mainly used for livestock and permission was acquired from owners before entering private property. Cameron Quinn of the Geological Survey of NSW, who has had previous experience in the area, accompanied Nathan Daczko and myself for two days. We used a map published by the Geological Survey of Victoria (Morand et al. 1999) to decide on several locations to visit and potentially sample. These locations were mainly restricted to road cuttings and creeks as there is limited exposure elsewhere.

The Biotite and Chlorite Zones of the complex could not be sampled as there were no exposures in the study area. Rocks sampled include Cordierite and Sillimanite–K-feldspar Zone meta-sedimentary rocks, three lithologies of S-type Cobungra Granite (main granite, biotite granodiorite and garnet-bearing leucogranite) (Willman et al. 1999) and I-type Anglers Rest Granite. The Anglers Rest Granite was sampled to provide an example of an I-type in the study area. Metamorphic grade decreases to the east, away from the Cobungra Granite (Figure 3.2), forming a regional aureole like those described by White et al. (1974). Sample numbers associated with the lithologies and field descriptions are given in Table 3.1 with field photographs in Figure 3.1. Four samples were selected especially for characterisation of whole-rock chemistry and zircon analysis, in addition to general petrographic characterisation and mineral chemistry analysis. These are 1019C, 1010B, 1012A and 1015A and were chosen because they represent the granites and metamorphic rocks in the area. Sample locations are shown in Figure 3.2.

Table 3.1. Sample numbers and field descriptions of main lithologies in study area. Samples used for whole-rock chemical analysis and zircon analysis are in red.

Lithology	Field Description	Sample number
Cordierite Zone	• Bedding preserved. Psammitic, porphyroblastic and pelitic varieties present. • Good exposures in road cuttings along Benambra Road.	1001A, 1001B, 1001C, 1001D, 1002A, 1002B, 1003A, 1004A, 1004B, 1024A, 1025A, 1025B
Sillimanite-K-feldspar Zone	• No decent exposures in road cuttings but some sporadic outcrops were found along Wilson Creek. • Genuine leucosome development is not as common as the map (Morand et al. 1999) indicated. Most of what is mapped as migmatite is xenolith-rich Cobungra Granite.	1017A, 1017B, 1018A, 1019A, 1019B, 1019C, 1023A
S-type Cobungra Granite	• Very heterogeneous with up to 50% incorporated country rock. Large centimetre- to metre-scale gneissic xenoliths. Up to 7 cm K-feldspar megacrysts • Good exposures in creeks but weathered in road cuttings and elsewhere.	1007A, 1008A, 1009A, 1010A, 1010B, 1011A, 1013A, 1013B, 1013C, 1013D, 1014A
S-type Biotite Granodiorite *(subtype of Cobungra Granite)*	• Homogenous. No country rock xenoliths. Interlayered with the main Cobungra Granite and pegmatite. • Well exposed along Days Creek.	1012A
S-type Garnet-bearing Leucogranite *(subtype of Cobungra Granite)*	• Very weathered sample from bank of Livingstone Creek.	1016A
I-type Anglers Rest Granite	• Very homogenous. Only weathered and hydrothermally altered outcrops were found. • Sampled in a creek near the Omeo Highway.	1015A

Universal Transverse Mercator (AGD66 datum) grid references of sample sites were recorded using a Garmin 12L GPS with an accuracy of ± 5-10 m. A list of the grid references of sample sites is given in Appendix A. In-situ samples were removed from outcrops using a geological hammer and chisel, labelled and bagged to avoid contamination. In total, 33 samples were collected from the field area.

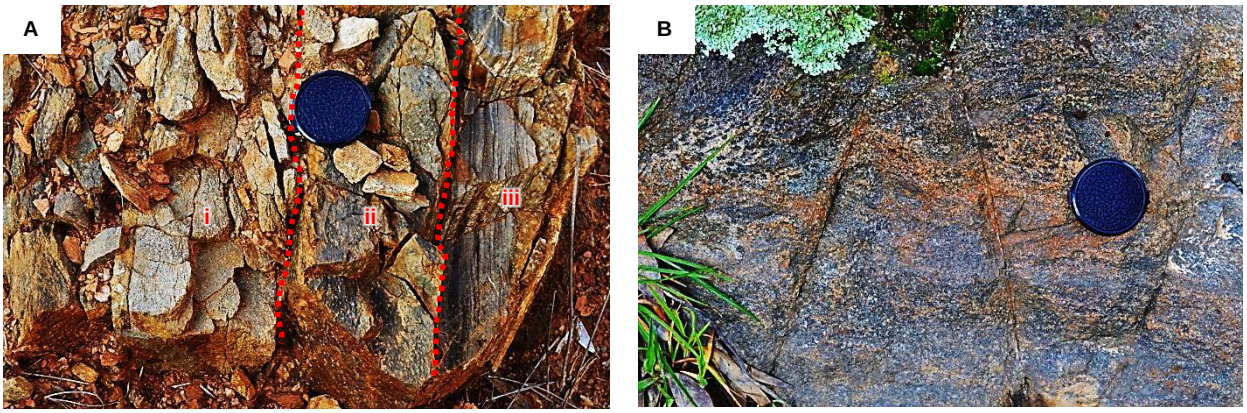

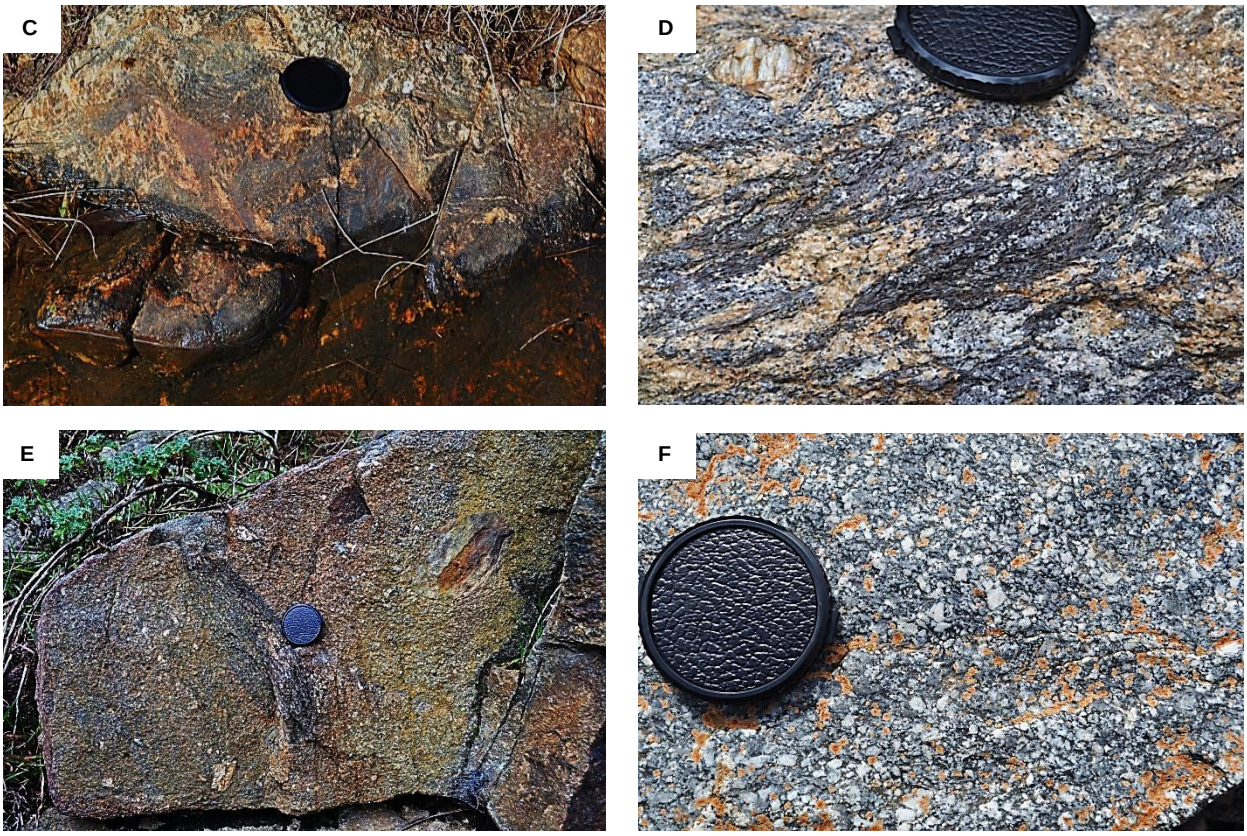

Figure 3.1. Field photographs of lithologies in field area. See Figure 3.2 for photo locations. (Locations noted here in brackets). **A.** *(1001)* **(i)** Psammitic, **(ii)** porphyroblastic and **(iii)** pelitic varieties of Cordierite Zone meta-sediments. **B.** *(1019)* Sillimanite–K-feldspar Zone meta-sediments. **C.** *(1023)* Sillimanite–K-feldspar Zone migmatite. **D.** *(1009)* Cobungra Granite. **E.** *(1010)* Biotite-rich xenoliths and K-feldspar megacrysts of Cobungra Granite. **F.** *(1012)* Clean-looking S-type Biotite Granodiorite. Orange material is lichen. **G.** *(1015)* Hand specimen of Anglers Rest Granite. Width of view is 75 mm. (Lens cap is 60 mm across. Photographs by Nathan Daczko.)

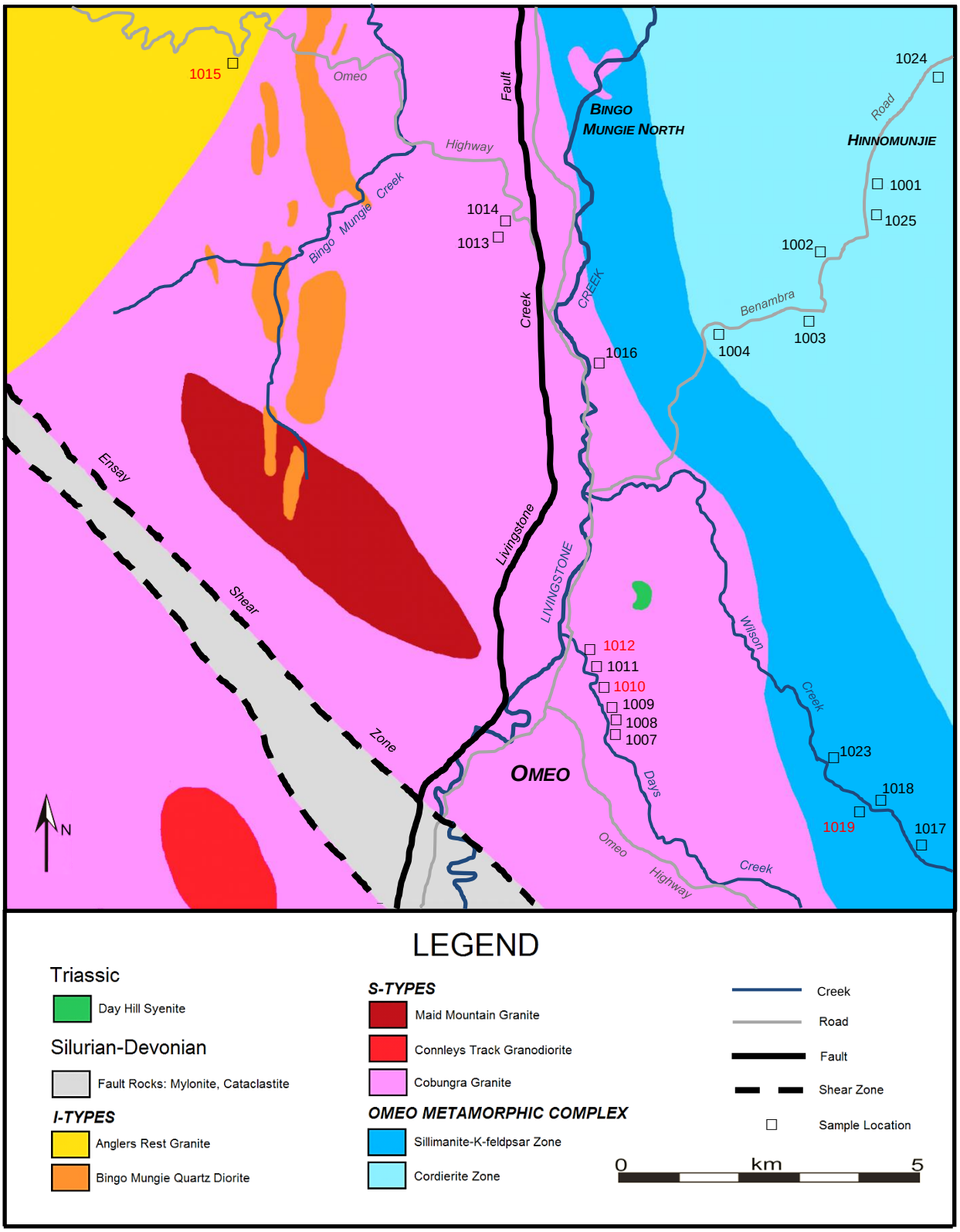

Figure 3.2. Geological map of the field area north of Omeo showing the location of sample sites. Locations of samples used for whole-rock chemistry and zircon analysis are shown in red. Map modified from Morand et al. 1999.

CHAPTER 4

PETROGRAPHY

4.1 INTRODUCTION

This section details the key petrographic features of the rocks examined from the Omeo study area to characterise the samples and to give context to the geochemical and zircon analyses that follow. The samples examined include Cordierite and Sillimanite-K-feldspar Zone rocks of the Omeo Metamorphic Complex and granites of the Cobungra and Anglers Rest plutons. Thin sections of 32 samples were visually inspected under a petrographic microscope.

4.2 METHODOLOGY

Samples collected from fieldwork (see Chapter 3) were cut using a circular saw to obtain fresh samples minimally affected by weathering. Samples were then cut to expose a cross-section of significant features such as foliation, before being thin sectioned for petrographic analysis. Polished thin sections (30 μm thick) were examined specifically to characterise mineral assemblages, mode, grain size, and metamorphic and igneous textures. Thin sections were analysed using a Nikon Eclipse E400 POL binocular petrographic microscope, and mineral modes were estimated visually. Photomicrographs of representative or unusual samples were taken using a Canon EOS 300 digital SLR camera. Mineral abbreviations used in this chapter are those used by Winter (2010).

4.3 RESULTS AND DISCUSSION

4.3.1 CORDIERITE ZONE

Samples 1001A, 1001B, 1001C, 1001D, 1002A, 1002B, 1003A, 1004A, 1004B, 1024A, 1025A, 1025B

The psammites of the Cordierite Zone have the mineral assemblage quartz–biotite–K-feldspar–muscovite, with accessory plagioclase. A schistosity is defined by alignment of biotite (15-25 vol.%; 0.05-0.25 mm) and muscovite (5-10 vol.%; 0.05-0.3 mm) and the elongation of some coarser quartz grains (40-60 vol.%; 0.05-1.1 mm) and K-feldspar grains (10-15 vol.%; 0.03-0.8 mm) (Figure 4.1A-D). Some K-feldspar grains are coarse and some are fine with irregular grain boundaries (Figure 4.1C-E). A particularly conspicuous mass of aligned micas can be seen running lower-left to upper-right in the middle of Figure 4.1C-D. Most of the quartz grains have migrated grain boundaries and have a reduced grain size resulting from dynamic recrystallization. Undulose extinction and subgrain formation is also evident in the quartz grains of the Cordierite Zone psammites (Figure 4.1E).

Most of the relict porphyroblasts in the pelitic layers have been completely pseudomorphed by muscovite, biotite, chlorite and/or clay minerals, and the porphyroblasts have a large range of shapes and sizes (0.3-5 mm). Some porphyroblasts are circular to hexagonal, suggesting they were originally cordierite, and other porphyroblasts are rhomboidal, suggesting they were originally andalusite. These shapes can be seen in Figure 4.1F. The pseudomorphing minerals were analysed with an electron microprobe in an attempt to determine precursor minerals (see Section 5.3.4). The matrix contains a schistosity defined by well-aligned biotite (20-35 vol.%; 0.05-0.3 mm) and muscovite (15-30 vol.%; 0.04-0.6 mm), with some fine-grained quartz (10-20 vol.%; 0.05-0.1 mm) and accessory K-

feldspar. The muscovite of the matrix is concentrated around and is commonly deflected around the porphyroblasts (Figure 4.1G). Matrix deflection is consistent with pre-tectonic porphyroblast growth. The matrix is also slightly crenulated adjacent to some porphyroblasts (Figure 4.1G). At the lower-grade end of the Cordierite Zone, only relict cordierite porphyroblasts are present and they preserve an earlier foliation than the matrix foliation (Figure 4.1H).

In the higher-grade end of the Cordierite Zone, fresh andalusite is preserved. It has a skeletal texture and contains inclusions of biotite, K-feldspar and quartz (Figure 4.1I-J). Cordierite porphyroblasts pseudomorphed by sericite and biotite are very abundant in these samples (Figure 4.1K). Quartz grains have been dynamically recrystallised and biotite is concentrated between porphyroblasts (Figure 4.1K).

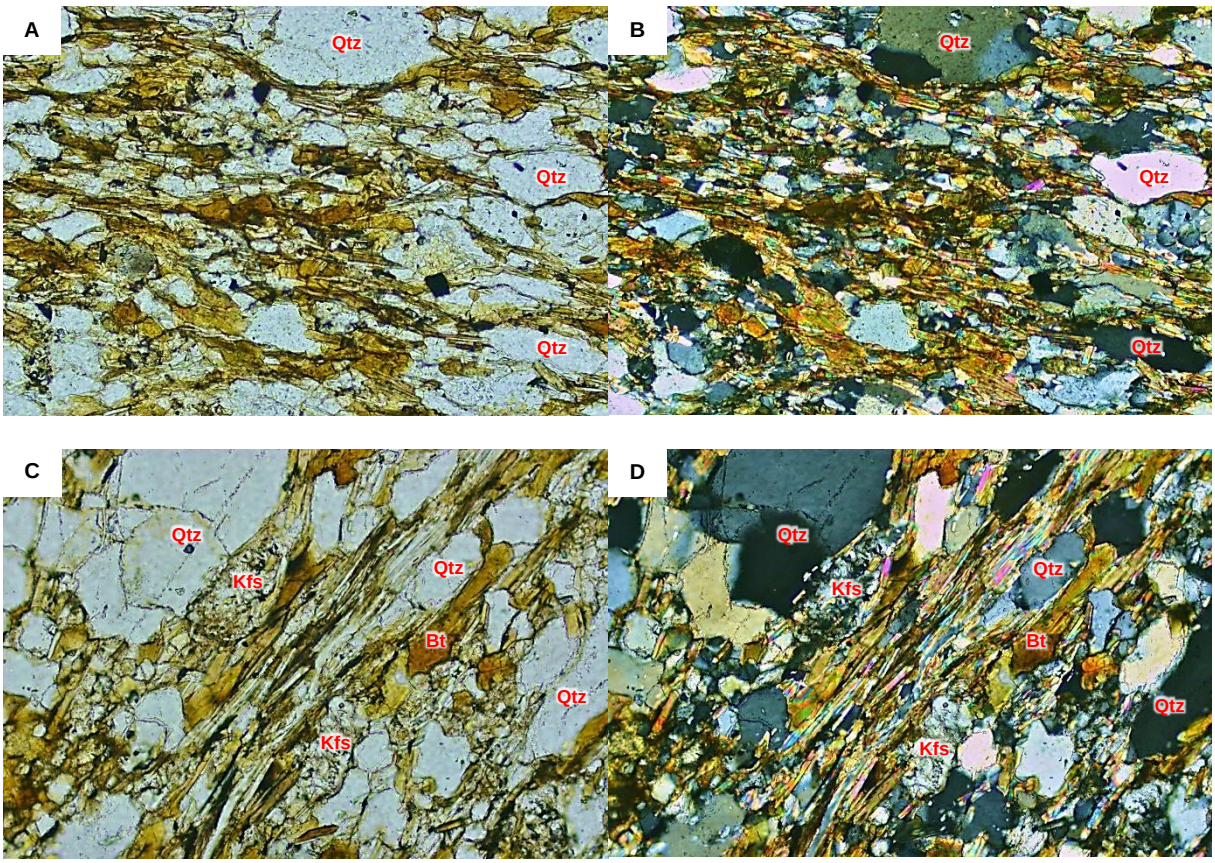

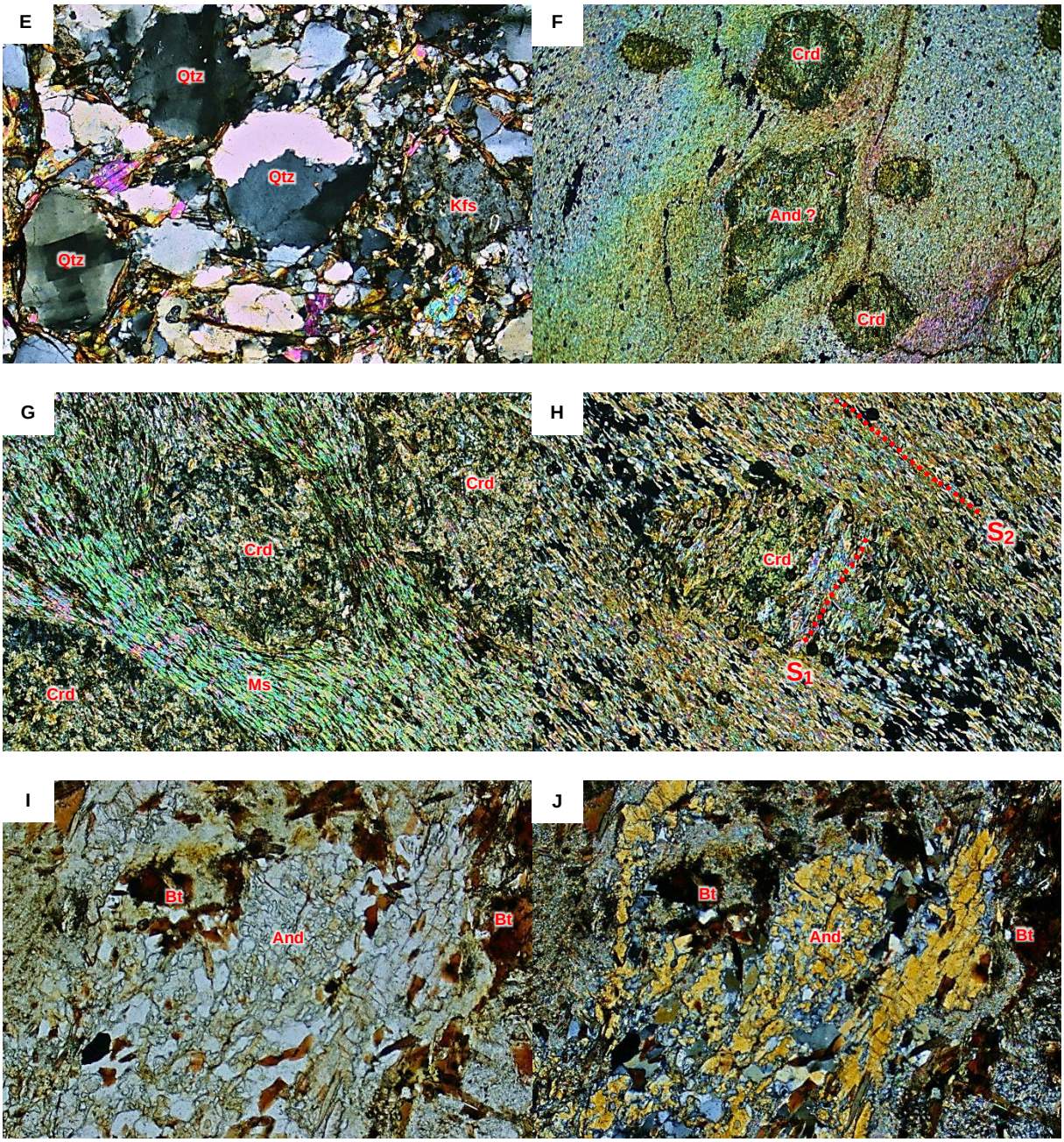

Figure 4.1. Photomicrographs of Cordierite Zone meta-sedimentary rocks, Omeo Metamorphic Complex. **A-E.** Psammite displaying schistosity and quartz microstructure. **F.** Relict porphyroblast shapes. **G.** Matrix deflection around porphyroblast and crenulation. **H.** Earlier foliation preserved in porphyroblast than matrix foliation. **I-J.** Skeletal andalusite **K.** Fresh andalusite porphyroblasts, cordierite porphyroblasts and recrystallised quartz. (Width of view: A-E,G-J=2.5 mm; F,K=10.5 mm. A-D=1001A; E=1004B; F=1001D; G=1002A; H=1025A; I-K=1004A. A,C,I,=PPL; B,D-H,J,K=XPL)

4.3.2 SILLIMANITE-K-FELDSPAR ZONE

Samples 1017A, 1017B, 1018A, 1019A, 1019B, 1019C, 1023A

Sillimanite-K-feldspar Zone meta-sedimentary rocks have the mineral assemblage K-feldspar (10-30 vol.%) – biotite (15-25 vol.%) – cordierite (5-25 vol.%) – muscovite (10-20 vol.% including sericite) – quartz (10-15 vol.%) – sillimanite (accessory-15 vol.%), with accessory tourmaline and zircon. Cordierite porphyroblasts (0.5-4 mm) are commonly retrogressed and partially to completely pseudomorphed by muscovite, biotite and chlorite, with or without clay minerals (Figure 4.2A-G). Pseudomorphous muscovite after cordierite is much larger than the surrounding matrix retrogressive product. Where the porphyroblasts are adjacent to quartz or K-feldspar, straight to curviplanar grain boundaries are well-preserved. The middle-left of Figure 4.2A shows part of a hexagonal grain of retrogressed cordierite with well-preserved grain boundaries. Figure 4.2G shows a retrogressed cordierite grain with a moat of sericite.

Sillimanite commonly occurs in this zone as fibrolite, nucleating near or on biotite (Figure 4.2G-J). Preserved biotite enclosed by sillimanite is shown in Figure 4.2H. To the middle-left of this figure, sillimanite fibres have developed into adjacent K-feldspar. Quartz (0.05-1.8 mm) at the high-grade end of the Sillimanite-K-feldspar Zone has irregular grain boundaries and is commonly interstitial (Figure 4.2F). Muscovite poikiloblasts (up to 5 mm) have inclusions of K-feldspar, quartz and biotite (Figure 4.2G,I,J). K-feldspar is present in this zone as ordinary crystals, inclusions in cordierite porphyroblasts (Figure 4.2E) and as poikiloblasts up to 3.5 mm in length (Figure 4.2I-K). The main inclusion mineral in the K-feldspar poikiloblasts is biotite, with quartz inclusions being less prevalent (Figure 4.2I-K). Inclusions in K-feldspar poikiloblasts are concentrated in cores and are sub-rounded. The rims commonly exhibit flame perthite (Figure 4.2K). Brown tourmaline is also evident in this zone (lower-right of Figure 4.2F).

Migmatites have formed at the higher-grade end of the Sillimanite-K-feldspar Zone from partial melting of and/or melt injection into the highest grade metamorphic rocks in the area. The andalusite poikiloblasts at this location commonly have a moat of sericite and contain elongate biotite inclusions that are aligned with the external biotite foliation (Figure 4.2L-N). These poikiloblasts were distinguished from K-feldspar by their higher relief and from sillimanite by being length-fast. In Figure 4.2N, a 1-3.5 mm biotite-rich selvedge seperates neosome on the left from paleosome on the right. The neosome is dominated by light-coloured minerals of quartz (35-55 vol.%) and K-feldspar (25-40 vol.%), with accessory plagioclase and biotite, making it a leucosome. In the leucosome, originally coarse quartz grains (up to 7 mm) and coarse K-feldspar grains (up to 8 mm), some with straight boundaries, have been recrystallised into smaller grains (Figure 4.2O-P). Biotite has melted and filled cracks in the quartz and K-feldspar (Figure 4.2O-P). Muscovite (5-15 vol.%; 0.2-2 mm) has pseudomorphed K-feldspar during retrogression of the leucosome (Figure 4.2N-P).

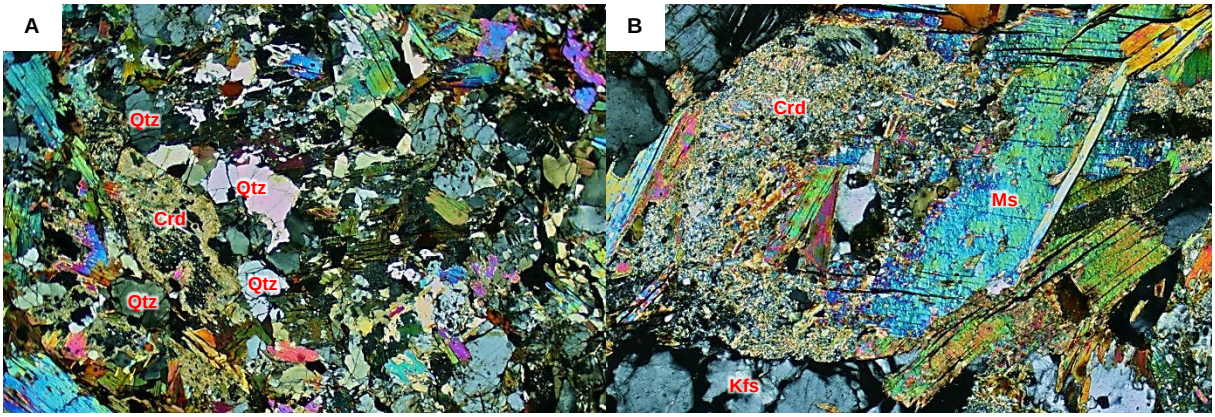

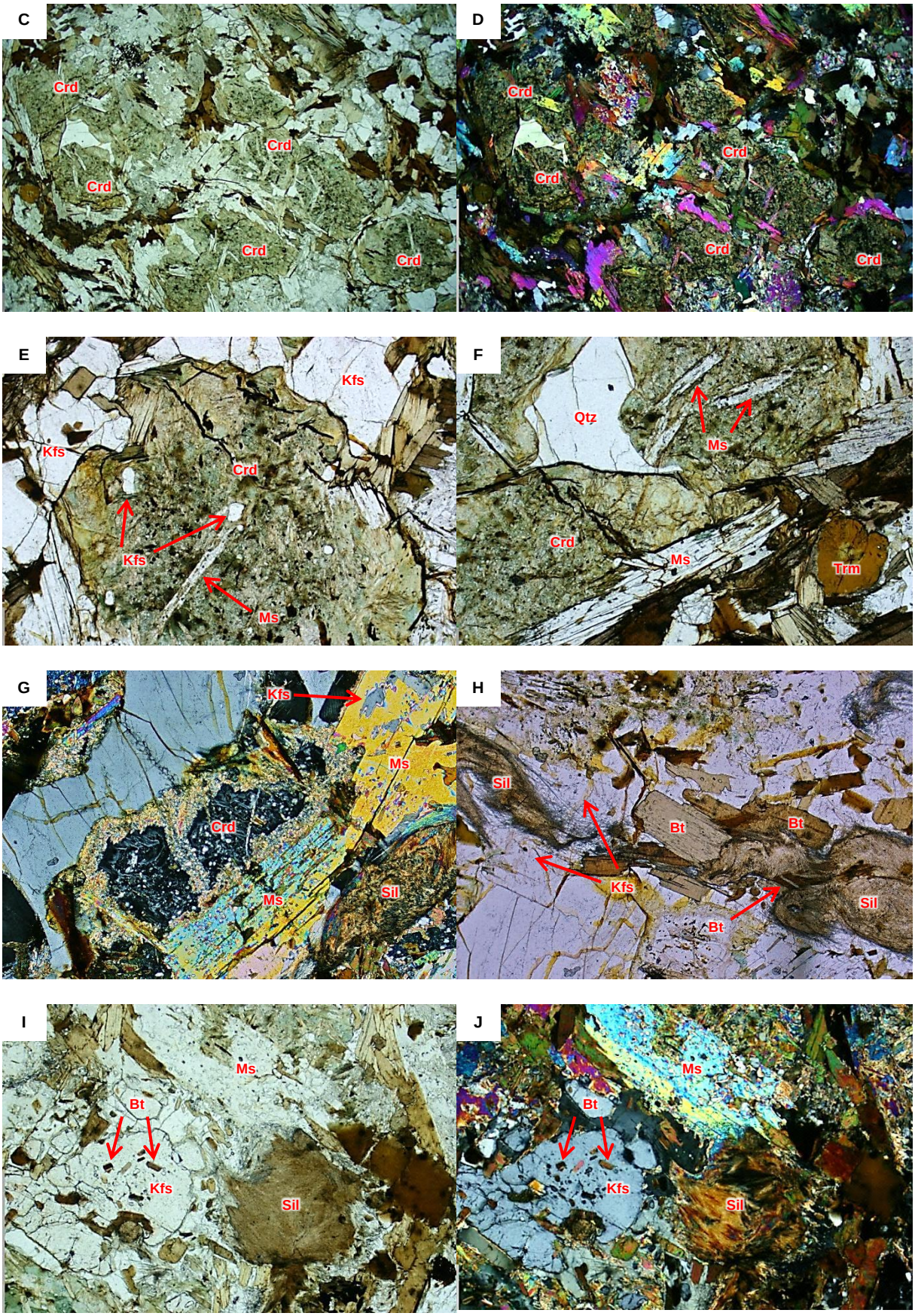
C
Crd
Crd
Crd
Crd
Crd
D
Crd
Crd
Crd
Crd
Crd
E
Kfs
Kfs
Crd
Kfs
Ms
F
Qtz
Ms
Crd
Ms
Trm
G
Kfs
Ms
Crd
Ms
Sil
H
Sil
Bt
Bt
Kfs
Bt
Sil
I
Ms
Bt
Kfs
Sil
J
Ms
Bt
Kfs
Sil

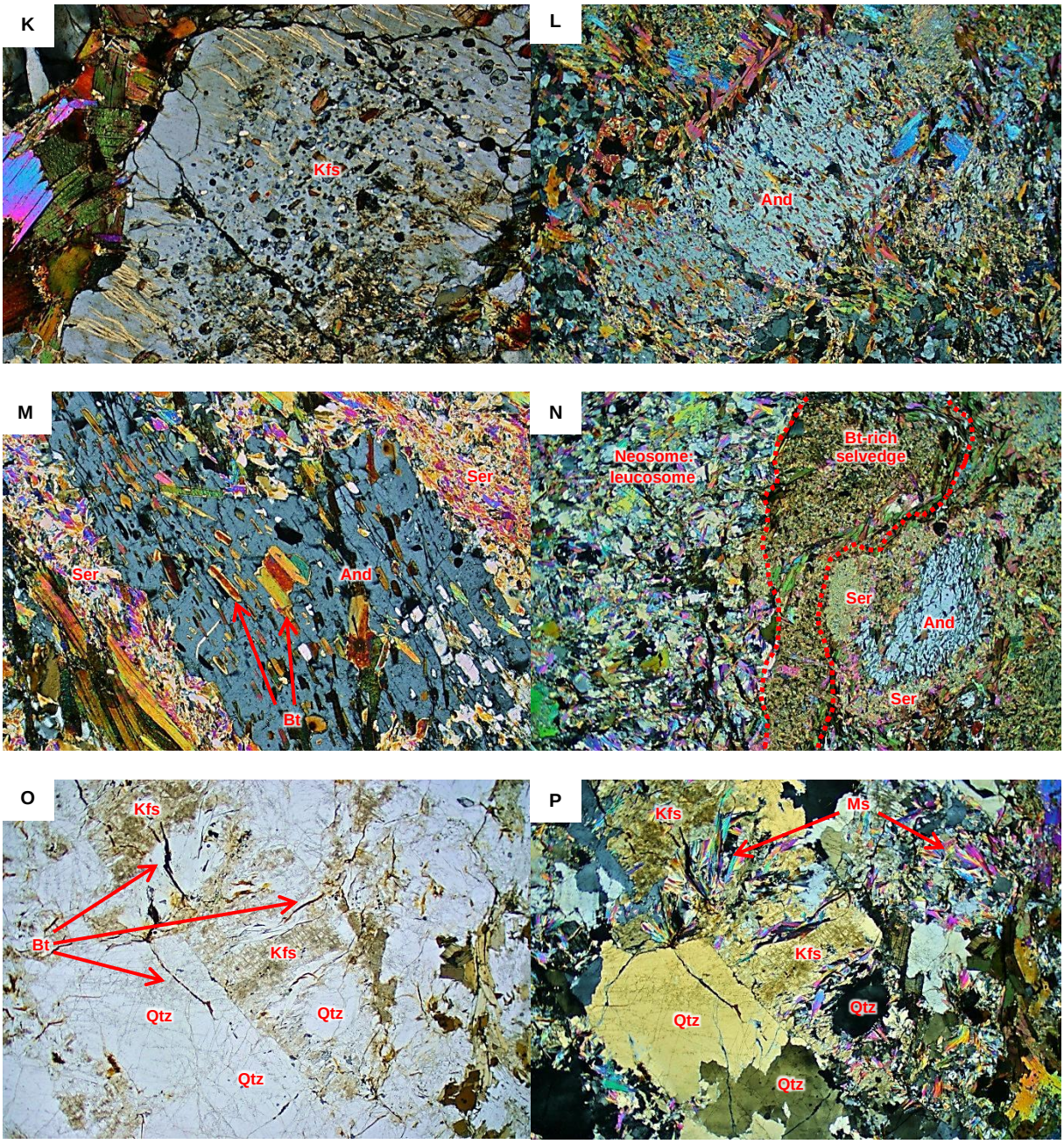

Figure 4.2. Photomicrographs of Sillimanite-K-feldspar Zone meta-sedimentary rocks and migmatites, Omeo Metamorphic Complex. **A-G.** Retrogressed cordierite porphyroblasts. Brown tourmaline and interstitial quartz in F. Muscovite poikiloblasts in G. **H.** Sillimanite as fibrolite. **I-K.** K-feldspar poikiloblasts. Muscovite poikiloblasts in I & J. **L-N.** Andalusite poikiloblasts. Biotite-rich selvedge and leucosome in N. **O-P.** Leucosome. (Width of view: B,E-K,M=2.5 mm; A,C,D,L,N-P=10.5 mm. A,B,K=1017A; C-F,I,J=1019C; G,H=1019A; L-N=1023A; O,P=1019B. C,E,F,H,I,O=PPL; A,B,D,G,J,K-N,P=XPL)

4.3.3 COBUNGRA GRANITE

Samples 1007A, 1008A, 1009A, 1010A, 1010B, 1011A, 1013A, 1013B, 1013C, 1013D 1014A

S-type Cobungra Granite has the mineral assemblage quartz (30-45 vol.%) – K-feldspar (15-25 vol.%) – plagioclase (5-15 vol.%) – biotite (5-15 vol.%) – cordierite (5-15 vol.%) – muscovite (5-10 vol.%) – sillimanite (0-40 vol.%, commonly ≈10 vol.%), with accessory tourmaline and zircon. As mentioned in the fieldwork chapter (Chapter 3), the Cobungra Granite is an extremely variable rock. Some samples display a typical igneous microstructure (Figure 4.3A) while other samples have incorporated varied amounts of country rock. In samples where igneous microstructure is preserved, euhedral plagioclase (0.2-4 mm) has maintained its original elongate shape (Figure 4.3A,B). The plagioclase has been partially altered to sericite though multiple twinning remains visible (Figure 4.3B). Deformation twinning is evident in the plagioclase of a sample with large amounts of country rock (Figure 4.3F). Coarse-grained K-feldspar (0.5-7 mm) has also been partially altered to sericite but to a lesser extent compared to the plagioclase (Figure 4.3A). In all varieties of the Cobungra Granite sampled, the quartz has recrystallised from coarse grains (0.4-3.5 mm) to fine grains, forming sutured to granoblastic polygonal aggregates with triple junctions of approximately 120° (Figure 4.3A-C,E-H). In some quartz domains, there has been subgrain formation and undulose extinction. Much of the primary biotite (0.2-1.8 mm) of this granite has been partially altered to chlorite and opaque minerals, exhibiting either a green (Figure 4.3A) or a light brown (Figure 4.3E-J) colour. Some biotite grains have developed sericite rims (Figure 4.3E-F).

The entrainment of country rock into the Cobungra Granite has formed 1-10 mm layers of biotite, sillimanite and muscovite (Figure 4.3D). Similar to the adjacent high-grade metamorphic rocks, fibrous sillimanite has nucleated near or on biotite, though some fine

prismatic grains have been preserved (Figure 4.3D). Cordierite (0.5-4 mm) has mostly been pseudomorphed by pinite, muscovite and biotite (Figure 4.3I-J) however some fresh cordierite (Figure 4.3G-H) appears to have been preserved. Electron microprobe analysis was undertaken to determine whether the cordierite is fresh or pseudomorphed (see Section 5.3.2). Pinite and coarser muscovite are the main pseudomorphic minerals, with biotite being more minor. Many of the original grain boundaries of the cordierite grains are preserved. The alteration textures of the two feldspars and biotite, along with the pinitised cordierite, is consistent with retrograde metamorphism and hydration of granite mineralogy. It is difficult to determine what proportion of the muscovite is primary. However, most of the muscovite is likely to be secondary because of the widespread retrogression.

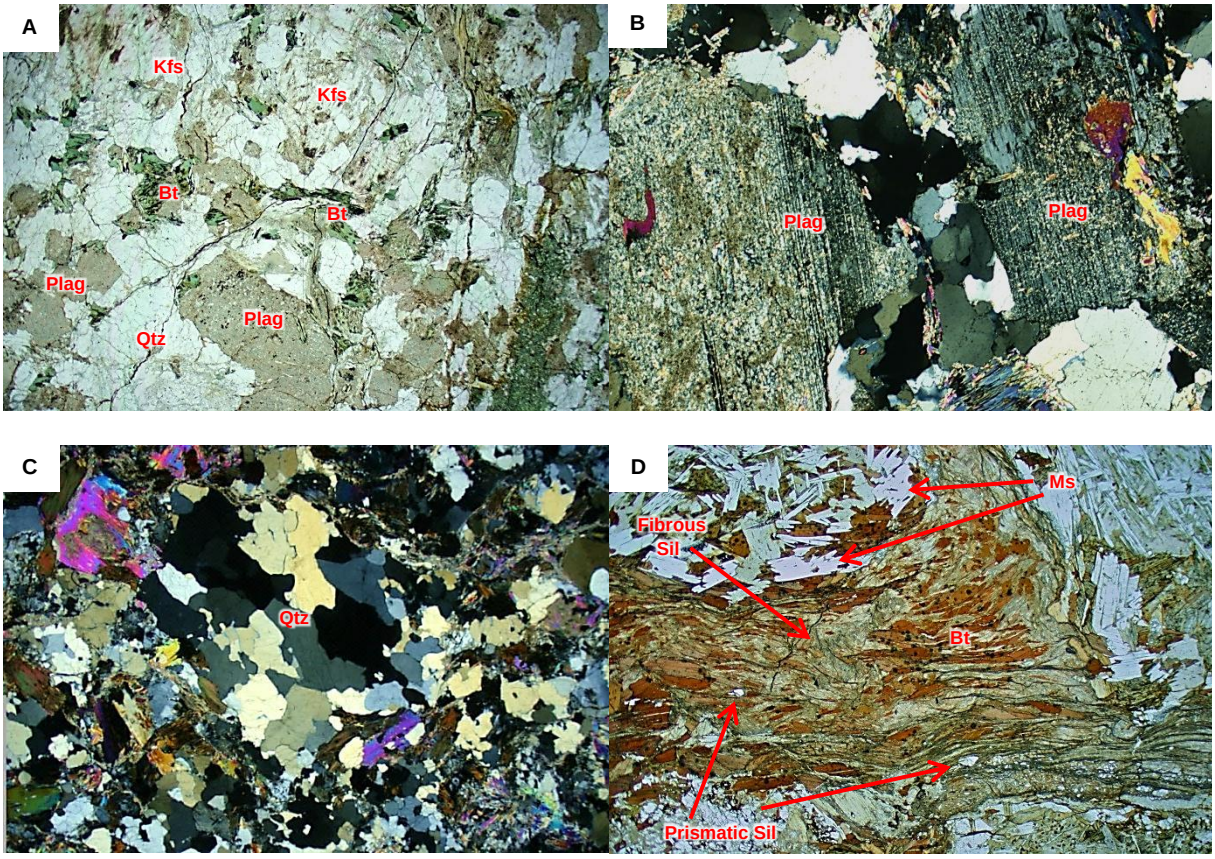

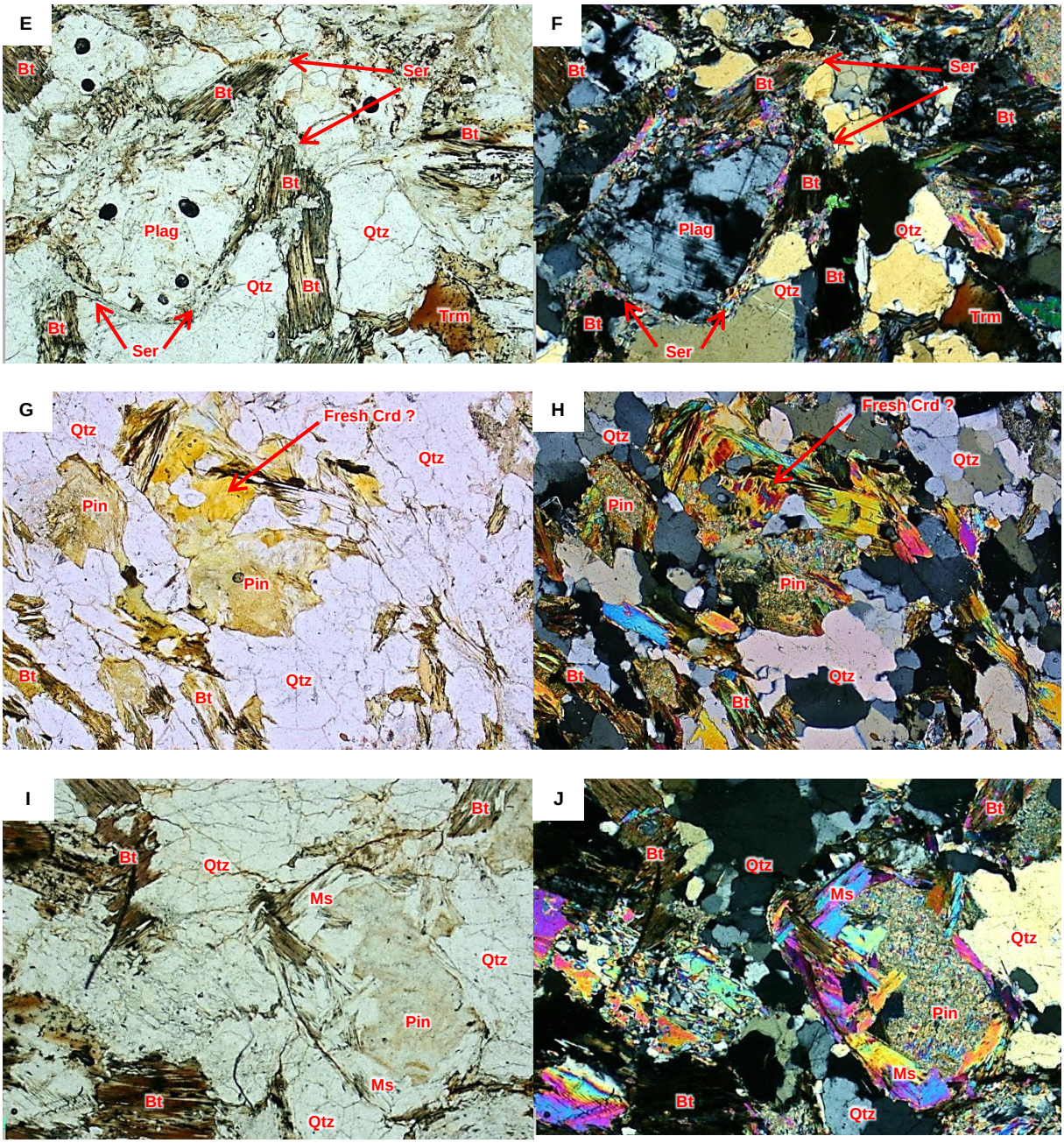

Figure 4.3 Photomicrographs of the Cobungra Granite, Lachlan Fold Belt. **A.** Preservation of igneous microstructure with elongate grains of euhedral plagioclase. Feldspars with sericitic alteration. Biotite altered to chlorite and opaques. **B.** Plagioclase with sericitic alteration and multiple twinning. **C.** Recrystallised quartz domain. **D.** Country rock entrained into granite. **E-F.** Partially altered biotite with sericite rims. Plagioclase with deformation twinning. Recrystallised quartz. **G-H.** Potentially fresh cordierite and pinitised cordierite. Recrystallised quartz domains. Partially altered biotite. **I-J.** Pinitised cordierite with some coarse muscovite. Partially altered biotite. (Width of view: A,C,D=10.5 mm; B,E-J=2.5 mm. A,B=1007A; C,E,F,I,J=1010B; D=1013B; G,H=1010A. A,D,E,G,I=PPL; B,C,F,H,J=XPL)

4.3.4 BIOTITE GRANODIORITE

Sample 1012A

S-type Biotite Granodiorite has the mineral assemblage plagioclase (40-65 vol.%) – K-feldspar (15-25 vol.%) – quartz (15-25 vol.%) – biotite (12-20 vol.%), with accessory tourmaline and muscovite. Similar to some samples of the Cobungra Granite, the Biotite Granodiorite has preserved igneous microstructure (Figure 4.4A). The K-feldspar (0.5-3 mm) displays simple twinning (Figure 4.4A) and the plagioclase (0.5-5.5 mm) displays a range of interesting textures as follows. Some plagioclase grains have altered cores containing sericite and biotite (Figure 4.4B-D). Deformation and growth twinning are also evident in the plagioclase (Figure 4.4C,E,H). Oscillatory zoning is preserved in the plagioclase (Figure 4.4D) indicating that the rock was under igneous conditions for part of its history. Some plagioclase grains have been boudinaged (Figure 4.4E) which is consistent with the rock undergoing some deformation. Most of the biotite (0.3-2 mm) in the sample is primary and is fresher than that of the Cobungra Granite (Figure 4.4A-F,I). When fresh, the biotite is dark brown to tan, but when the biotite has been replaced by chlorite and opaque minerals, it displays a pale green colouration (Figure 4.4G-H). An example of kinked biotite cleavage is shown in Figure 4.4F. There is a great deal of suturing in the quartz (original grain size: 0.4-4 mm) and can be described as smoky quartz (Figure 4.4A,B,D,H). Blue tourmaline is also preserved (Figure 4.4I).

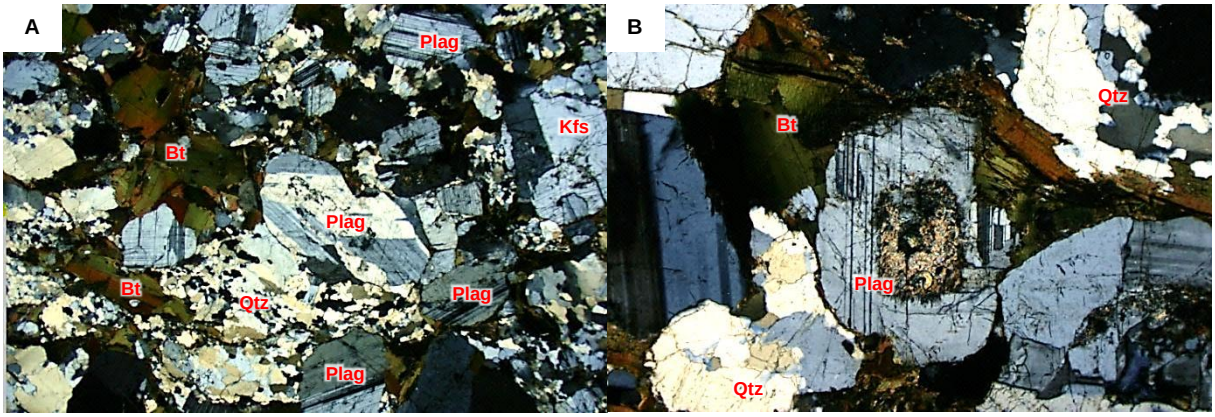

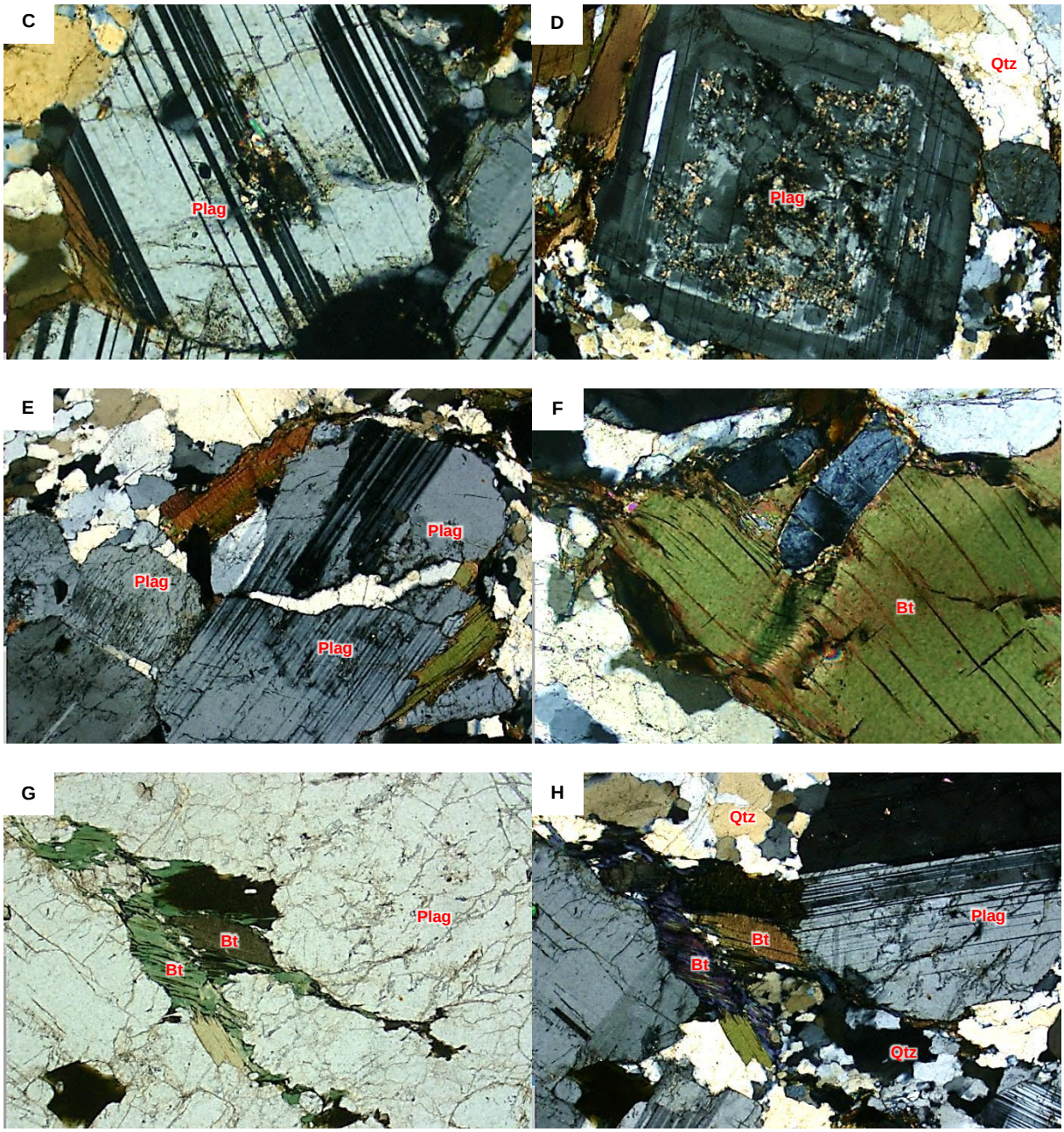

Figure 4.4. Photomicrographs of Biotite Granodiorite (Cobungra Granite), Lachlan Fold Belt. **A.** Preservation of igneous microstructure. Simple twinning is K-feldspar. Smoky quartz. **B-D.** Plagioclase with altered core. Smoky quartz in B. Growth and deformation twinning in C. Oscillatory zoned plagioclase in D. **E.** Boudinaged plagioclase with deformation twinning. **F.** Kinked biotite cleavage. **G-H.** Replacement of biotite with chlorite and opaques. Growth and deformation twinning in plagioclase. Smoky quartz. **I.** Blue tourmaline. (Width of view: A=10.5 mm; B-I=2.5 mm. A-I=1012A. G,I=PPL; A-F,H=XPL)

4.3.5 ANGLERS REST GRANITE

Sample 1015A

The Anglers Rest Granite is a leucocratic I-type granite containing the minerals quartz (30-45 vol.%) – K-feldspar (30-40 vol.%) – plagioclase (15-25 vol.%), with accessory pseudomorphed biotite and retrogressive sericite. This rock has the largest grain-size of all rocks sampled with coarse K-feldspar (1-6 mm) and quartz (0.7-5 mm) composing most of the rock. Both K-feldspar and plagioclase (0.7-2.5 mm) have been partially altered to sericite whereas the quartz has remained relatively unaltered (Figure 4.5A-C). Deformation twinning is widespread in the plagioclase (Figure 4.5C,D) along with the bending of a plagioclase grain shown in Figure 4.5D indicating that some deformation has occurred. The quartz is coarser and tends to be more euhedral compared to that of other rock types, but shows some similar suturing of grain boundaries (Figure 4.5A,B,F). Figure 4.5E shows deformation lamellae in quartz running upper-left to lower-right with the bulging of a plagioclase grain into the quartz. Perthitic exsolution of some K-feldspar grains is preserved in the rock (Figure 4.5G). All of the biotite in this sample (0.3-0.8 mm) has been pseudomorphed by opaque minerals (Figure 4.5F) suggesting this rock has been significantly altered and is likely to have been metasomatised.

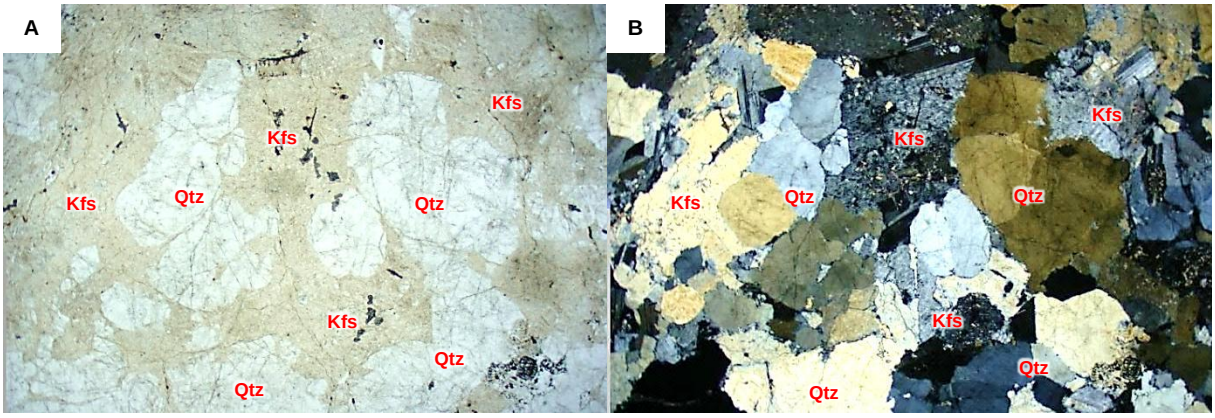

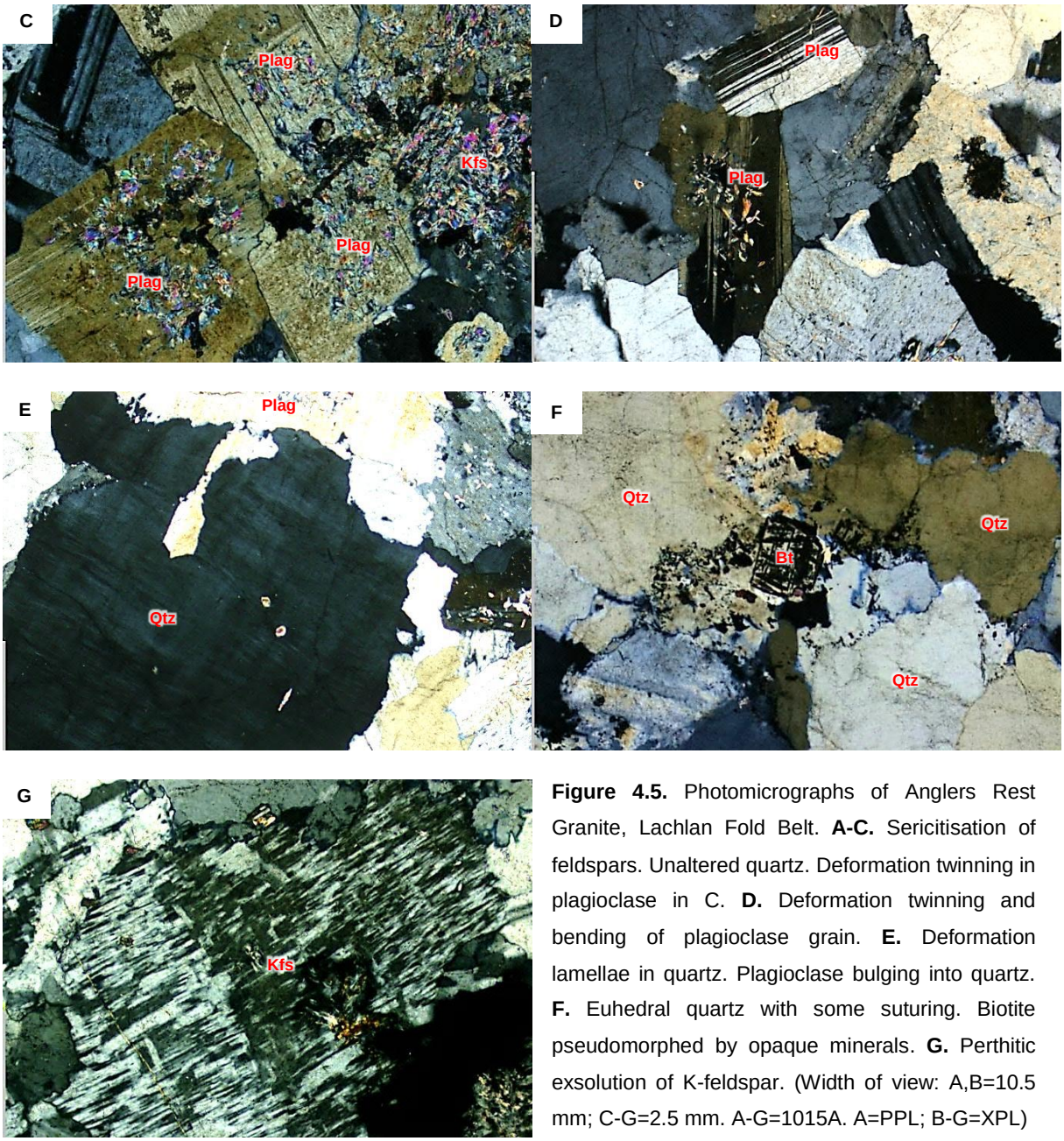

Figure 4.5. Photomicrographs of Anglers Rest Granite, Lachlan Fold Belt. **A-C.** Sericitisation of feldspars. Unaltered quartz. Deformation twinning in plagioclase in C. **D.** Deformation twinning and bending of plagioclase grain. **E.** Deformation lamellae in quartz. Plagioclase bulging into quartz. **F.** Euhedral quartz with some suturing. Biotite pseudomorphed by opaque minerals. **G.** Perthitic exsolution of K-feldspar. (Width of view: A,B=10.5 mm; C-G=2.5 mm. A-G=1015A. A=PPL; B-G=XPL)

CHAPTER 5

MINERAL CHEMISTRY

5.1 INTRODUCTION

Mineral chemistry analysis of the metamorphic rocks and granites in the study area was carried out using an electron microprobe (EMP). Determinations of the chemistry of individual minerals were made in order to make comparisons between the different lithologies. Differences in mineral chemistry across lithologies provide information about the history of the rocks.

5.2 METHODOLOGY

Eight samples were chosen to undergo EMP analysis to obtain information on mineral chemistry in the Omeo Metamorphic Complex. Polished thin sections of approximately 30 μm in thickness previously prepared for examination with a petrographic microscope were selected for EMP analysis. Thin section preparation included cleaning the section using ethanol solution and lint-free wipes before the desired areas of each slide were circled and photographed to enable ease of locating grains when using the EMP. A carbon coat of ≈20 nm was also applied to the thin sections to increase the conductivity of the sample.

These analyses were carried out using a CAMECA SX100 Electron Probe Microanalyser in the Geochemical Analysis Unit, GEMOC, Macquarie University. Operating conditions were 15 kV accelerating voltage and 20 nA beam current. Standards used for EMP

calibration were: orthoclase for K, wollastonite for Ca, albite for Na, hematite for Fe, kyanite for Al and Si, chromite for Cr, olivine for Mg, rutile for Ti and spessartine garnet for Mn. Lower limits of detection and relative standard deviation for all elements are listed in Table 5.1. PAP matrix corrections were automatically applied by CAMECA software. Major element oxides assessed include SiO_2, TiO_2, Al_2O_3, Cr_2O_3, FeO, MnO, MgO, CaO, Na_2O and K_2O.

Table 5.1. Lower limits of detection (LLD) and relative standard deviation (%rsd) of elements analysed by the CAMECA SX100 Electron Probe Microanalyser.

CAMECA SX100 ELECTRON MICROPROBE Large area LIF, PET and TAP Lower limits of detection for 15 kV		
Element	**LLD (wt%)**	**% rsd**
SiO_2	0.03	0.27
TiO_2	0.02	0.19
Al_2O_3	0.01	0.18
Cr_2O_3	0.04	0.56
FeO	0.03	0.34
MnO	0.03	0.55
MgO	0.03	0.22
CaO	0.02	0.27
Na_2O	0.02	0.56
K_2O	0.01	0.49

5.3 RESULTS AND DISCUSSIONS

5.3.1 BIOTITE

Biotite follows the formula:

$$K_2(Mg,Fe^{2+})_{6-4}(Fe^{3+},Al,Ti)_{0-2}[Si_{6-5}Al_{2-3}O_{20}](OH,F)_4$$

METHODOLOGY

Biotite was analysed in seven out of the eight thin sections chosen for EMP work. The biotite of the Angler Rest Granite sample (1015A) has been pseudomorphed by opaque minerals and hence was not analysed.

The biotite Fe:Mg ratio was calculated as follows:

$$X_{Fe} = Fe^{2+}/(Mg+Fe^{2+})$$

where Fe and Mg values are the number of cations per formula unit. The number of Ti cations was calculated to 22 oxygen anions per formula unit.

RESULTS AND DISCUSSION

Considering all samples except the Lower Cordierite Zone (addressed in the next paragraph), X_{Fe} values for biotite across all lithologies range between 0.54 and 0.61, and are therefore typically iron-rich (X_{Fe}>0.50) (Table 5.2). Fe^{2+} and Mg commonly substitute for each other in biotite so the Fe:Mg ratio can vary as a result of differing metamorphic grades – the higher temperature biotite being more Mg-rich (Deer et al. 1992). However, the X_{Fe} values of biotite in this study do not vary greatly across the metamorphic grades and granites (Table 5.2). One characteristic of note concerning X_{Fe} values is that the range of values for the Lower and Upper Sillimanite-K-feldspar Zone is larger than that of the Upper Cordierite Zone, Cobungra Granite and Biotite Granodiorite. A similar lack of variation is apparent in the Ti cations of the biotite across lithologies in this study (excluding the Lower Cordierite Zone) (Table 5.2). The similarity of biotite composition across lithologies possibly reflects re-equilibration upon cooling.

The X_{Fe} values and Ti cation of biotite in the Lower Cordierite Zone have a discrepancy with the other samples in this study. The X_{Fe} values have a larger range and the Ti cations are significantly lower than the other samples (Table 5.2). This discrepancy is possibly due to the electron beam of the EMP being unable to pinpoint the fine-grained biotite in the matrix. Alternatively, perhaps the biotite has partially altered to chlorite and/or opaque minerals, therefore giving a wide range of compositions. This alteration hypothesis is consistent with many of the other rocks sampled (see Chapter 4: Petrography).

Table 5.2. Characteristics of biotite chemistry in the Omeo Metamorphic Complex and nearby granite plutons. Sample numbers are in brackets.

Lithology	X_{Fe}	Ti cations
Lower Cordierite Zone *(1001D)*	0.45 – 0.81	0.03 – 0.12
Upper Cordierite Zone *(1001A)*	0.54 – 0.56	0.29 – 0.37
Lower Sillimanite-K-feldspar Zone *(1019A, 1019C)*	0.56 – 0.61	0.22 – 0.37
Upper Sillimanite-K-feldspar Zone *(1023A)*	0.56 – 0.59	0.18 – 0.39
Cobungra Granite *(1010B)*	0.54 – 0.56	0.27 – 0.36
Biotite Granodiorite *(1012A)*	0.57 – 0.59	0.19 – 0.33
Anglers Rest Granite *(1015A)*	–	–

5.3.2 MUSCOVITE

Muscovite is common in pelites of a range of metamorphic grades. Because of the scarcity of muscovite in sedimentary rocks, muscovite in the Omeo Metamorphic Complex is therefore related to metamorphic and intrusive events. Although there is muscovite in the Cordierite Zone that formed from the recrystallization of clay minerals during amphibolite-

grade metamorphism, a great deal of the muscovite in the Sillimanite-K-feldspar Zone and Cobungra Granite texturally appears to be secondary, arising from the later greenschist facies retrogressive event (see Chapter 4: Petrography).

The formula for muscovite is:

$$K_2Al_4[Si_6Al_2O_{20}](OH,F)_4$$

METHODOLOGY

The chemical composition of paragonite differs from muscovite in that Na replaces K. Muscovite may contain up to 20% paragonite in solid solution and is calculated as follows:

$$\text{Paragonite component} = Na/(Na+K)$$

The name phengite is used to describe muscovites in which the Si:Al ratio is greater than 3:1, and in which increase of Si is accompanied by substitution of Mg and Fe^{2+} for Al in octahedral sites. The "4" in the phengite component calculation below comes from the four octahedral Al atoms in the standard muscovite formula.

$$\text{Phengite component} = (Fe^{2+}+Mg)/4$$

X_{Fe} was also calculated as was done for biotite (see above).

RESULTS AND DISCUSSION

Muscovite was analysed in both metamorphic zones and in the Cobungra Granite. For all of these samples, excluding muscovite after cordierite in the Cobungra Granite, the end-member ranges are paragonite$_{9\text{-}18}$ and phengite$_{5\text{-}10}$ (Table 5.3). The Lower Cordierite Zone and Upper Sillimanite-K-feldspar Zone have larger paragonite components than the other lithologies. Phengite components and X_{Fe} values are similar across all lithologies with some exceptions. The large range of X_{Fe} values for the Lower Cordierite Zone may be due to alteration of the fine-grained matrix minerals, as explained in the biotite section above (Section 5.3.1).

Section 4.3.3 outlined the petrographic characteristics of the Cobungra Granite which included potentially fresh cordierite. The results of EMP analysis show that the chemistry of these porphyroblasts is closer to muscovite, and hence no fresh cordierite has been preserved. The low paragonite$_{2}$ and high phengite$_{24\text{-}31}$ of the muscovite after cordierite in Cobungra Granite (Table 5.3) is probably due to the influence of cordierite chemistry on the pseudomorphous muscovite. This muscovite is pale yellow under plane polarised light (Figure 4.3G) instead of the normal colourless appearance, which further lends support to the muscovite being influenced by cordierite chemistry.

Table 5.3. Characteristics of muscovite chemistry in the Omeo Metamorphic Complex. Sample numbers in brackets.

Lithology	Paragonite component	Phengite component	X_{Fe}
Lower Cordierite Zone *(1001D)*	0.16 – 0.18	0.06 – 0.10	0.49 – 0.72
Upper Cordierite Zone *(1001A)*	0.09 – 0.10	0.06	0.48
Lower Sillimanite-K-feldspar Zone *(1019A, 1019C)*	0.09 – 0.12	0.05 – 0.06	0.43 – 0.52
Upper Sillimanite-K-feldspar Zone *(1023A)*	0.12 – 0.17	0.05 – 0.06	0.42 – 0.48
Cobungra Granite *(1010B)*	0.10 – 0.11	0.05 – 0.08	0.47 – 0.55
Cobungra Granite: Muscovite after Cordierite	0.02	0.24 – 0.31	0.47 – 0.50
Biotite Granodiorite *(1012A)*	–	–	–
Anglers Rest Granite *(1015A)*	–	–	–

5.3.3 FELDSPAR

Feldspars are commonly classified in terms of chemistry using a ternary system. The three end-members of this system are as follows:

Anorthite (*X*An) = $CaAl_2Si_2O_8$

Albite (*X*Ab) = $NaAlSi_3O_8$

Orthoclase (*X*Or) = $KAlSi_3O_8$

Plagioclase refers to feldspar compositions with complete solid solutions between the end-members of anorthite and albite. Within metamorphic systems, plagioclase composition is determined by metamorphic grade and composition of the host rock (Deer et al. 1992). Plagioclase in low temperature systems is commonly stable as albite. In higher temperature systems, including igneous systems, anorthite increases in plagioclase.

METHODOLOGY

Feldspars were analysed from the Sillimanite-K-feldspar Zone, Cobungra Granite, Biotite Granodiorite and Anglers Rest Granite. K-feldspar from Cordierite Zone psammites was unable to be analysed because of constraints on the number of thin sections able to be analysed with the EMP for this project. Feldspar end-members were calculated using the following formulas before being classified using a ternary plot.

$$\boldsymbol{X}\mathbf{An} = Ca/(Na+Ca+K)$$

$$\boldsymbol{X}\mathbf{Ab} = Na/(Na+Ca+K)$$

$$\boldsymbol{X}\mathbf{Or} = K/(Na+Ca+K)$$

RESULTS AND DISCUSSION

The composition of plagioclase grains across all lithologies analysed has the range $X\text{An}_{0\text{-}59}$. The plagioclase of the Biotite Granodiorite is the most calcic. One group of the Biotite Granodiorite plagioclase analyses range in composition $X\text{An}_{40\text{-}47}$ and plot as andesine, and two other analyses of composition $X\text{An}_{59}$ plot as labradorite (Figure 5.1). Calcic plagioclase is consistent with the typical igneous microstructure of this rock type, described in Section 4.3.4. The plagioclase of the Sillimanite K-feldspar Zone and Cobungra Granite has similar composition to each other. Both sets of analyses plot as oligoclase (Figure 5.1) but the Cobungra Granite oligoclase has a slightly higher calcium content ($X\text{An}_{21\text{-}23}$) than that of the Sillimanite K-feldspar Zone ($X\text{An}_{14\text{-}19}$). This higher calcium content possibly reflects a higher temperature of crystallisation or may be a bulk rock composition effect. Petrographic analysis of the Anglers Rest Granite (Section 4.3.5) identified both plagioclase and K-feldspar, and sericitisation of those feldspars. However, analysis of feldspar chemistry has revealed that all feldspars have been recrystallised to nearly pure

albite (XAb$_{97-99}$) (Figure 5.1). Therefore, significant sodium metasomatism has occurred. This hydrothermal alteration is likely to have had a significant effect on the whole-rock chemistry and zircon characteristics of this rock (Chapters 6 and 7).

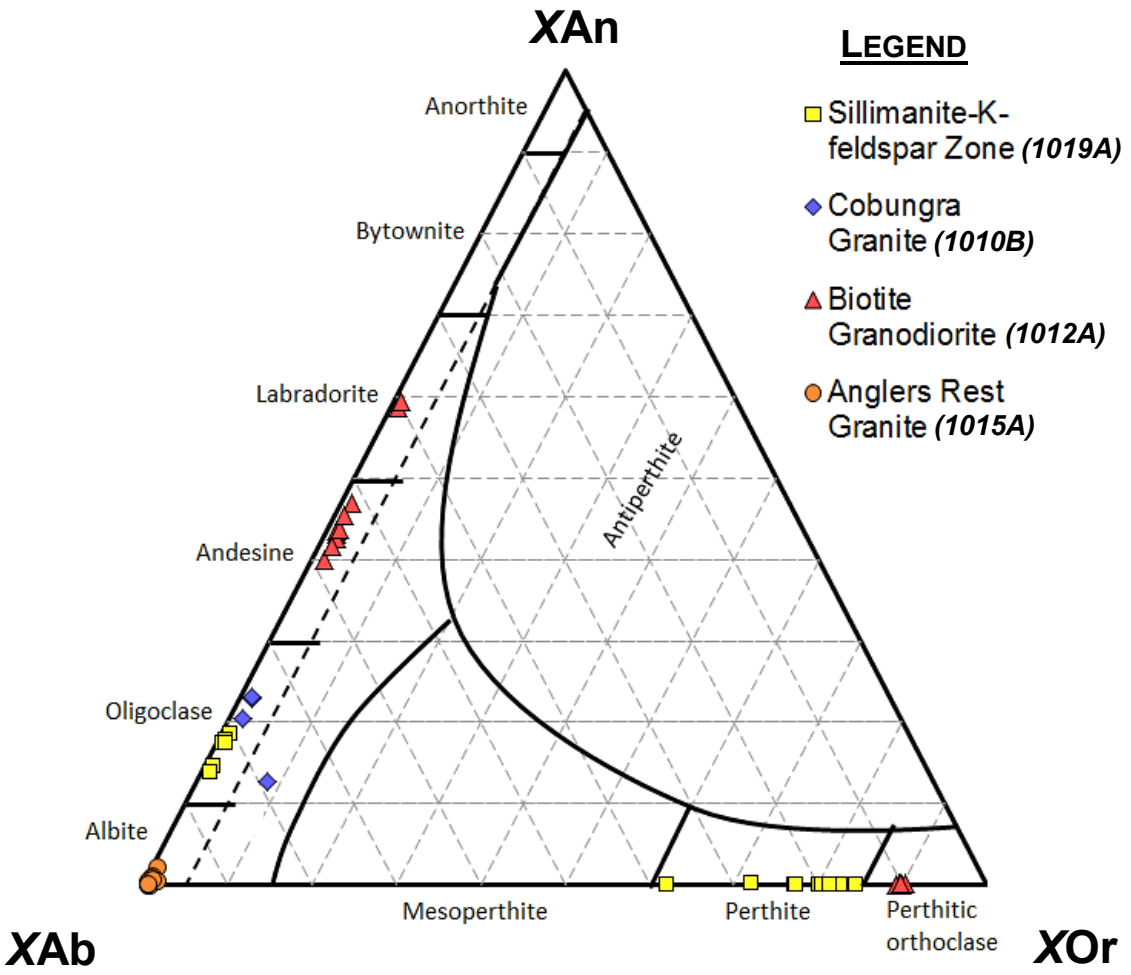

Figure 5.1. Feldspar ternary plot of EMP analyses, Omeo Metamorphic Complex. Feldspar ternary boundaries from Deer et al. (1992). Sample numbers in brackets.

Electron microprobe analyses of K-feldspar in the Sillimanite K-feldspar Zone gave a compositional range of XOr$_{62-84}$. This range, with all analyses plotting in the perthite field on Figure 5.1, is due to the variable incorporation in the analysis of flames of albite, which are observed as exsolution lamellae in thin section (Figure 4.2K). The K-feldspar of the Biotite Granodiorite is more potassium-rich (XOr$_{89-90}$) and is characterised as perthitic orthoclase (Figure 5.1).

5.3.4 PORPHYROBLAST CHEMISTRY

The pseudomorphed porphyroblasts (0.3-5 mm) in the Cordierite Zone have a variety of shapes (see Section 4.3.1) including rhomboidal, hexagonal and circular (Figure 5.2). The variety of shapes means that andalusite and cordierite are both potential precursor minerals as andalusite porphyroblasts are commonly rhomboidal (E.g. Figure 5.3A) and cordierite porphyroblasts are commonly circular (E.g. Figure 5.3B), but can also be hexagonal (Deer et al. 1992). The aim was to use the EMP to determine whether pseudomorphed andalusite porphyroblasts (as well as pseudomorphed cordierite porphyroblasts) are present in the Cordierite Zone by comparing the chemistry of the pseudomorphing minerals to published data on the chemistry of the potential precursor minerals.

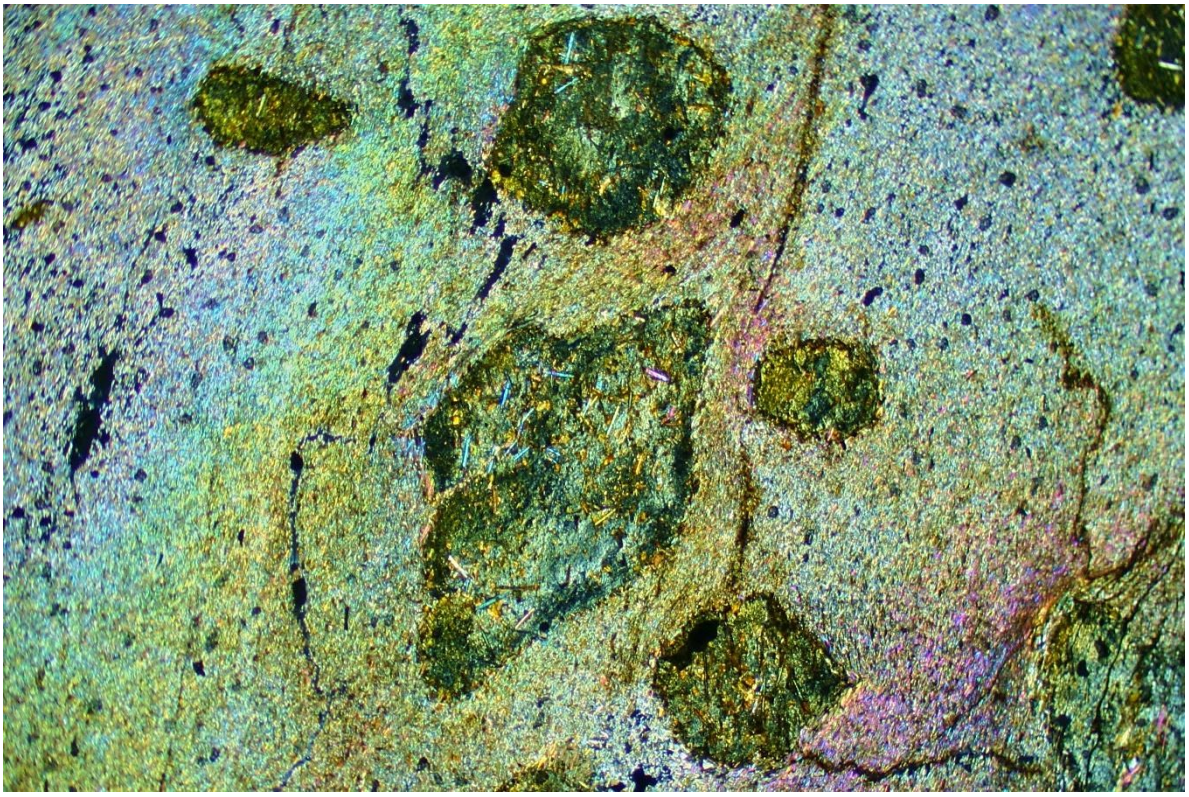

Figure 5.2. Photomicrograph showing the shapes of pseudomorphed porphyroblasts from the Cordierite Zone, Omeo Metamorphic Complex (Sample 1001D). Width of view = 10.5 mm. Cross-polarised light.

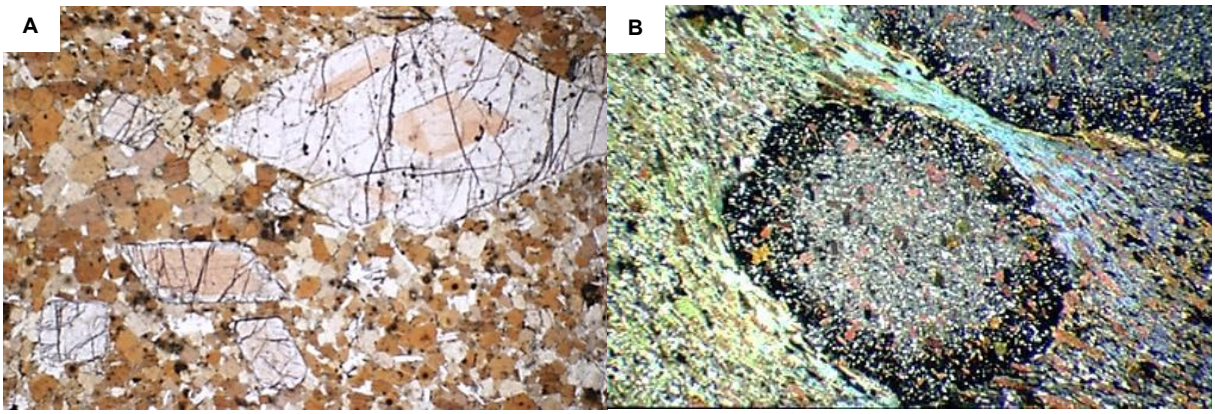

Figure 5.3. A. Rhomboidal shape of a typical andalusite porphyroblast. Width of view = 10.5 mm. (From Jerangle, NSW). **B.** Circular shape of a typical cordierite porphyroblast. Width of view = 9 mm. (From Slave Province, Canada).

METHODOLOGY

The pseudomorphing minerals of eight porphyroblasts from the Cordierite Zone (Sample 1001D) were analysed with a defocused beam on the EMP. Based on shape, porphyroblast numbers 1 and 6 are possibly relict andalusite, whereas the remaining six porphyroblasts are thought to be relict cordierite (Figure 5.4). The operating conditions and the oxides chosen to be measured were the same as those mentioned in the methodology section at the beginning of this chapter. Five analyses were made on each of the eight porphyroblasts (a total of 40 analyses) and SiO_2, Al_2O_3, FeO and MgO were averaged for each porphyroblast. These porphyroblast averages were compared to published major element oxide concentrations for andalusite and cordierite from Deer et al. (1992).

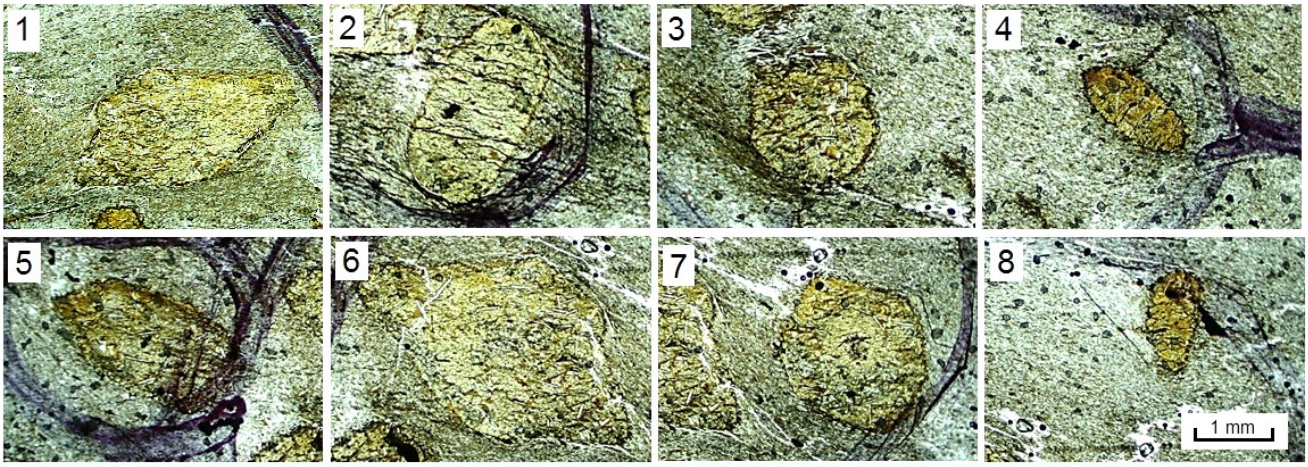

Figure 5.4. Photomicrographs of eight porphyroblasts from the Cordierite Zone (Sample 1001D) analysed for pseudomorphing mineral chemistry. Five EMP analyses were made per porphyroblast.

RESULTS AND DISCUSSION

The major element chemistry of pseudomorphing minerals of porphyroblasts from the Cordierite Zone was successfully obtained by performing 40 EMP analyses of eight porphyroblasts. Two analyses were rejected because of low totals. Figure 5.5 shows average SiO_2, Al_2O_3, FeO and MgO concentrations for each of the eight porphyroblasts. Results for porphyroblasts numbers 1 and 6 (those that are possibly relict andalusite) show no significant difference in chemistry to the other porphyroblasts. Because of the lack of variation in chemistry, weighted averages of SiO_2, Al_2O_3, FeO and MgO across all porphyroblasts were calculated using Isoplot v3.6 (Ludwig 2009) to give an indication of overall porphyroblast chemistry. Table 5.4 shows the weighted averages along with published element oxide concentrations for andalusite and cordierite from Deer et al. (1992) for comparison.

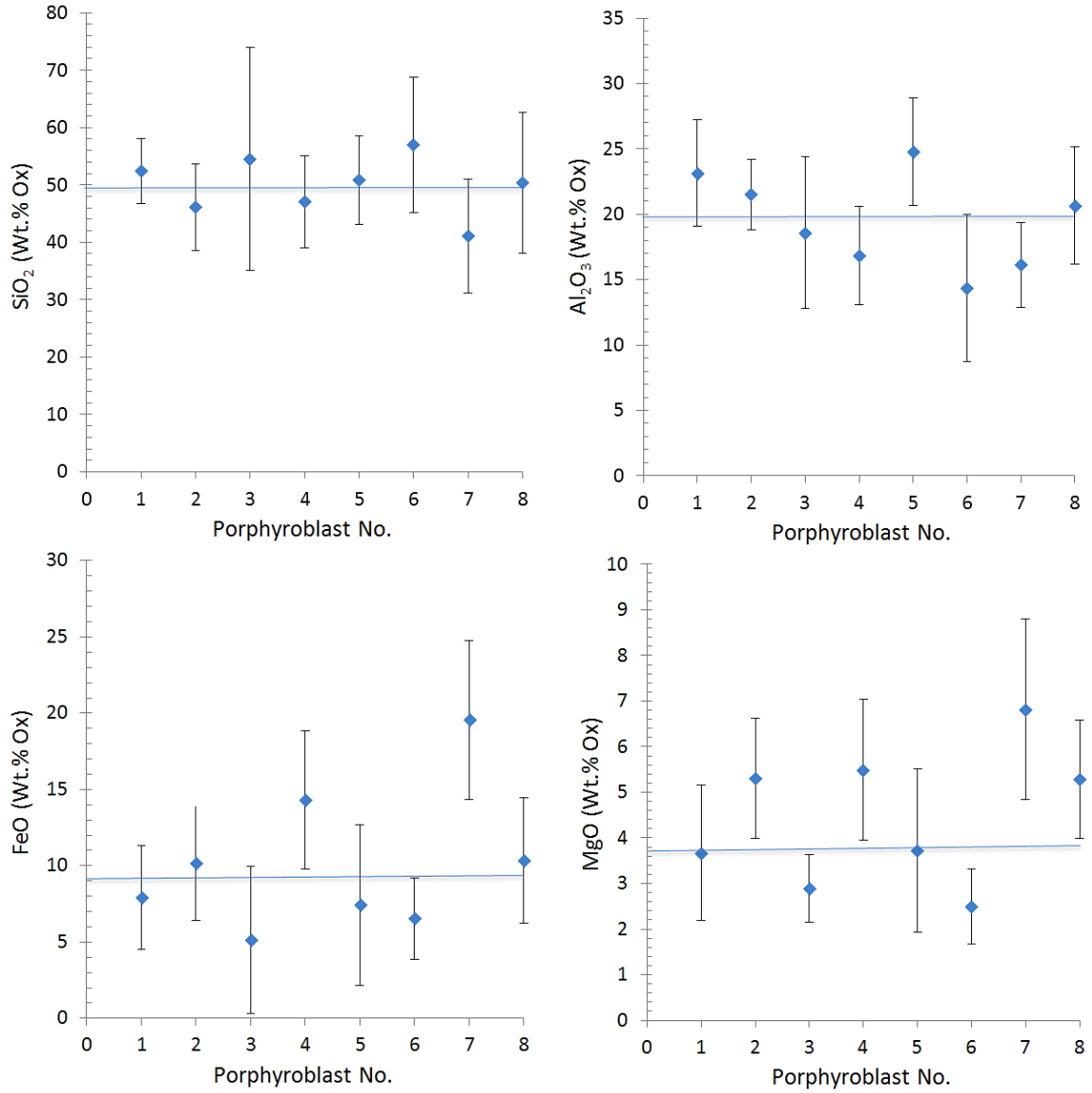

Figure 5.5. Average SiO_2, Al_2O_3, FeO and MgO concentrations for pseudomorphing minerals of eight porphyroblasts from the Cordierite Zone. Five analyses were made per porphyroblast. Error bars are 1 standard deviation. Blue lines are weighted averages.

The concentrations of SiO_2, FeO and MgO for the sampled porphyroblasts are within the ranges given for cordierite and are considerably higher than those given for andalusite (see Table 5.4). Al_2O_3 concentration for the sampled porphyroblasts (19.80 wt.%) is closer to that of cordierite (29.96-33.50 wt.%.) than andalusite (61.70 wt.%). These results are consistent with cordierite being the precursor mineral of the sampled porphyroblasts. The rhomboidal shaped porphyroblasts are probably just hexagonal shaped relict cordierite

porphyroblasts with two sides of the hexagon being very short. The aluminium discrepancy between the sampled porphyroblasts and published data on cordierite means that some aluminium has been lost from the porphyroblasts during pseudomorphism.

Table 5.4. Element oxide concentrations for pseudomorphing minerals of porphyroblasts from the Cordierite Zone, Omeo Metamorphic Complex. Values for cordierite and andalusite are from Deer et al. (1992).

Element Oxide (wt.%)	Weighted Average of Sampled Porphyroblasts (Errors = 2σ)	Cordierite	Andalusite
SiO_2	49.50 ± 6.10	44.64 – 50.20	36.65
Al_2O_3	19.80 ± 2.70	29.96 – 33.50	61.70
FeO	9.30 ± 2.70	0.84 – 11.02	1.75
MgO	3.73 ± 0.83	3.08 – 12.80	0.03

CHAPTER 6

WHOLE-ROCK CHEMISTRY

6.1 INTRODUCTION

Whole-rock chemistry, traditionally assessed by x-ray fluorescence (XRF), is used to define the bulk chemical composition of a rock sample. In this study, the granite plutons and the highest grade metamorphic rocks in the field area were analysed by XRF using pressed pellets and by dissolving powdered sample in solution with inductively coupled plasma mass spectrometry (ICP-MS). Glass disks were prepared for a more accurate measure of major elements by XRF however equipment problems at a university lab outside Macquarie University meant that data was not sent in time for inclusion in this thesis. Whole-rock chemistry used to characterise and compared the samples will also be considered in the interpretation of zircon chemistry (Chapter 7).

6.2 METHODOLOGY

Four rock samples (1010B, 1012A, 1015A and 1019C) were cut with a circular saw to remove any weathered outer surfaces, ensuring representative sampling for whole-rock analysis. The samples were then crushed using a hydraulic press and powdered using a tungsten carbide ring mill. The press and mill were cleaned thoroughly with MQ water and ethanol between samples to avoid contamination. Quartz sand was run through the mill between samples to further ensure contamination did not occur. The powders were used for analysis by XRF and solution ICP-MS.

6.2.1 XRF

Pressed pellets were prepared from the powder samples for XRF analysis using 5.5 – 6 g of powder and 15 drops of polyvinyl acetate dissolved in ethanol. These components were mixed well before being pressed to 80 kN. The ethanol was subsequently dried off in an oven. A Spectro XLAB2000 energy dispersive spectrometer, housed in the Geochemical Analysis Unit, GEMOC, Macquarie University was used for analysis. Table 6.1 presents the lower limits of detection (LLD) of elements that were assessed. Table 6.2 shows the standards that are used by the lab to determine accuracy and instrument drift.

Table 6.1. Major and trace element lower limits of detection analysed by XRF.

Element	wt.%	Element	ppm	Element	ppm
SiO_2	0.01	V	1	Cd	0.2
TiO_2	0.01	Cr	0.3	In	0.3
Al_2O_3	0.03	Co	0.4	Sn	0.4
Fe_2O_3	0.01	Ni	0.3	Sb	0.5
MnO	0.01	Cu	0.3	Te	1.0
MgO	0.02	Zn	0.3	I	1.0
CaO	0.01	Ga	0.3	Cs	1.5
Na_2O	0.04	Ge	0.2	Ba	1.5
K_2O	0.01	As	0.3	La	2.0
P_2O_5	0.01	Se	0.2	Ce	3.0
		Br	0.3	Hf	2.0
		Rb	0.3	Tl	0.7
		Sr	0.2	Pb	0.2
		Y	0.2	Bi	0.5
		Zr	0.2	Th	0.5
		Nb	0.2	U	0.5
		Mo	0.2		

Table 6.2. Published and measured concentrations of major and trace elements for reference samples used for XRF analysis. Published values are from GeoReM.

	BHVO-1				BIR-1			
Element	Published concentration		Measured concentration (*n*=8)		Published concentration		Measured concentration (*n*=6)	
		1sd		*1sd*		*1sd*		*1sd*
wt.%								
SiO_2	49.94		49.80	0.11	47.77		47.53	0.07
TiO_2	2.71		2.78	0.02	0.96		0.97	0.01
Al_2O_3	13.80		13.46	0.12	15.35		15.43	0.10
Fe_2O_3	12.23		12.46	0.06	11.26		11.55	0.05
MnO	0.17		0.17	0.00	0.17		0.17	0.00
MgO	7.23		7.27	0.06	9.68		9.73	0.08
CaO	11.40		11.57	0.04	13.24		13.47	0.06
Na_2O	2.26		2.34	0.12	1.75		1.79	0.07
K_2O	0.52		0.51	0.01	0.03			
P_2O_5	0.273		0.271	0.01	0.046		0.02	0.00

	BHVO-2				BIR-1			
Element	Published concentration		Measured concentration (*n*=10)		Published concentration		Measured concentration (*n*=8)	
		1sd		*1sd*		*1sd*		*1sd*
ppm								
V	317	11	330.0	13.1	319	18	324.3	17.6
Cr	280	19	325.2	7.0	391	15	445.9	14.2
Ni	119	7	115.5	3.7	166	7	158.1	4.3
Cu	127	7	126.8	4.4	119	8	127.9	3.7
Zn	103	6	100.0	2.0	72	18	66.1	2.9
Ga	22	2	20.9	1.7	15.3	0.8	14.6	2.3
Ge	1.6	0.1	2.0	0.8	1.4	0.2	1.5	0.3
As			0.7	0.3	0.44		0.8	
Se			0.3	0.1	0.024	0.002	0.2	0.0
Rb	9.11	0.04	9.0	0.3	0.2	0.01	0.5	0.2
Sr	396	1	391.9	2.4	109	2	109.9	0.7
Y	26	2	27.9	0.8	15.6	0.9	17.9	0.8
Zr	172	11	168.3	1.5	14	0.1	15.8	0.7
Nb	18.1	1	17.1	0.8	0.55	0.05	1.0	0.2
Mo	4	0.2	3.8	0.5	0.07		0.4	0.1
Cd	0.06	0.006	1.3	0.9	0.097		0.8	0.5
Sn	1.7	0.2	2.8	1.4	0.6		1.2	0.6
Sb	0.13	0.04	1.9	1.0	0.46	0.07	1.6	0.6
Te			0.9	0.4	0.0057	0.0002	1.3	0.6
Cs	0.1	0.01	4.1		0.007	0.003	1.4	0.2
Ba	131	1	129.5	3.0	7.14		7.0	1.0
La	15.2	0.1	11.8	1.8	0.615	0.021	3.0	0.6
Ce	37.5	0.2	36.7	2.0	1.92	0.08	4.8	1.7
Hf	4.36	0.14	2.4	1.0	0.582	0.004		
Tl			1.5	1.0			1.7	0.1
Pb	1.6	0.3	1.2	0.4	3.1	0.3	2.7	1.0
Bi			1.0	0.5			1.4	0.1
Th	1.22	0.06	2.5	0.8	0.032	0.004	1.4	0.6
U	0.403	0.001	1.4	0.8	0.01	0.001	2.1	0.9

6.2.2 ICP-MS

Trace element analysis by ICP-MS was conducted at the Geochemical Analysis Unit, GEMOC, Macquarie University. Digestion of ≈0.1 g of powdered sample in Teflon beakers using 2% HNO_3 and HF was done by Peter Wieland. Precisely measured spikes of an internal standard (containing ^{6}Li, ^{75}As, ^{103}Rh, ^{115}In, ^{169}Tm and ^{209}Bi) were added to the sample. The dilution factors used for HNO_3 were 1/1000, 1/2000 and 1/5000. The samples were analysed on an Agilent 7500cs ICP-MS Octopole reaction system with the operating conditions shown in Table 6.3. One run was performed with the four unknown samples being analysed in the middle of the run. HNO_3 was used as a rinse and to measure background counts. A series of external calibration standards (BCR-2) and reference samples (BIR-1 and BHVO-2) were analysed at the start and end of the run and concentrations were compared to USGS preferred values (Table 6.4).

Table 6.3. Agilent 7500s ICP-MS Operating Conditions

Condition	Property
ICP-MS type	Octopole Reaction System
Make and Model	Agilent 7500s
Nebulizer type and model	Self-aspiring concentric
Nebulizer gas and rate flow	Ar 100mL/min
Nebulizer pump	0.1 rps
RF Power	1550 W
RF Matching	1.66v
Sample depth	5.5 - 7mm
Torch H	-0.2 mm
Torch V	0.5 mm
Dwell time (individual)	100ms
Number of replicates	3
Total dwell time	300ms
Acquisition time	187 s
Carrier (plasma) Gas	Ar
Carrier gas flow rate	0.83 L/min (Ar)
Collision Cell Gas	He
Make-up gas flow rate	0.47 L/min (Ar)
External Calibration standard	BCR-2 (USGS)
Individual sample digestion checks	BHVO-2 (USGS) BIR-1 (USGS)

Table 6.4. Published and measured concentrations (ppm) of trace elements for reference samples BHVO-2 and BIR-1 used during ICP-MS analysis. Published values are from GeoReM.

	BHVO-2				BIR-1			
Element	Published concentration		Measured concentration (*n*=2)		Published concentration		Measured concentration (*n*=2)	
		2se		*2se*		*2se*		*2se*
Li	4.8	0.4	4.23	0.06	3.2	0.4	3.19	0.03
Be	1	0.2	1.3	0.02	0.12	0.02	0.120	0.002
Sc	32	2	34.0	0.8	43	4	45.7	1.9
Ti	16300	4000	17153.0	348.6	5600	1000	5856.2	189.5
V	317	22	316.2	3.4	319	36	316.3	7.8
Cr	280	38	257.2	3.0	391	30	296.4	5.8
Mn	1317	77	1365.6	19.3	1394	124	1359.0	26.8
Co	45	6	45.2	0.1	52	6	51.7	0.9
Ni	119	14	130.9	1.9	166	14	182.1	4.9
Cu	127	14	136.2	0.8	119	16	120.7	1.1
Zn	103	12	106.7	0.05	72	36	66.9	1.5
Ga	22	4	20.8	0.02	15.3	1.6	15.10	0.30
Rb	9.11	0.08	9.360	0.159	0.2	0.2	0.19	0.002
Sr	389	46	383.2	1.3	109	4	104.2	0.2
Y	26	4	27.7	0.04	15.6	1.8	16.82	0.12
Zr	172	22	175.2	1.5	14	0.2	15.0	0.19
Nb	18.1	2	18.43	0.1	0.55	0.1	0.528	0.01
Mo	4	0.4	3.3	0.01	0.07		0.126	0.002
Cs	0.1	0.02	0.10	0.00003	0.01	0.006	0.005	0.0003
Ba	130	26	127.8	0.99	7.14		6.808	0.138
La	15	2	14.95	0.12	0.62	0.042	0.671	0.0881
Ce	38	4	36.0	0.3	1.92	0.16	1.981	0.186
Pr	5.35	0.34	5.205	0.011	0.37	0.04	0.387	0.023
Nd	25	3.6	23.5	0.03	2.38	0.02	2.310	0.089
Sm	6.2	0.8	6.01	0.05	1.12	0.04	1.114	0.007
Eu	2.07	0.4	1.942	0.03	0.53		0.490	0.004
Tb	0.9	0.06	0.93	0.009	0.36	0.06	0.353	0.002
Gd	6.3	0.4	6.15	0.07	1.87	0.08	1.900	0.030
Dy	5.31	0.04	5.145	0.084	2.51		2.519	0.032
Ho	0.98	0.08	0.983	0.018	0.56	0.1	0.581	0.007
Er	2.54	0.02	2.495	0.023	1.66		1.706	0.013
Yb	2	0.04	1.9	0.047	1.65		1.613	0.019
Lu	0.28	0.02	0.268	0.003	0.25	0.06	0.240	0.005
Hf	4.1	0.6	4.21	0.07	0.582	0.008	0.5642	0.0148
Ta	1.14	0.06	1.101	0.025	0.04	0.0008	0.036	0.0009
Pb	1.6	0.3	1.37	0.06	3.1	0.6	2.78	0.13
Th	1.2	0.6	1.27	0.09	0.032	0.08	0.0351	0.002
U	0.403	0.001	0.4208	0.0288	0.01	0.002	0.010	0.0008

6.3 RESULTS AND DISCUSSION

6.3.1 MAJOR ELEMENTS

Major elements of four samples were analysed by XRF using pressed pellets of powdered rock samples. These measurements are rough estimates and do not provide the accuracy of XRF analysis with glass disks. However, they still give some indication of major element concentration. The results are given in Table 6.5. The Anglers Rest Granite is about 80% SiO_2 and has high Na_2O content (9.27 wt.%). The high Na_2O content is on account of the pervasive albitisation of the feldspars (Section 5.3.3). Concentrations of all other major elements in this sample are very low, except for 13.5 wt.% Al_2O_3 found in the feldspars. The high Al_2O_3 of the Sillimanite-K-feldspar Zone sample is expected because these rocks were derived from sedimentary rocks, which are known to have high Al content. The Biotite Granodiorite has the highest CaO (3.97 wt.%), which is consistent with the calcium-rich plagioclase of this sample (Section 5.3.3). Na_2O is below LLD for the Cobungra Granite and Sillimanite-K-feldspar Zone samples.

Table 6.5. Major element concentrations (wt.%) of four whole-rock samples from the study area. Analyses were made by XRF using pressed pellets. No totals were provided.

Element	Cobungra Granite *(1010B)*	Biotite Granodiorite *(1012A)*	Anglers Rest Granite *(1015A)*	Sillimanite-K-feldspar Zone *(1019C)*
SiO_2	58.18	63.28	81.19	57.37
TiO_2	0.82	0.61	0.07	0.76
Al_2O_3	18.43	15.26	13.48	23.10
FeO	4.24	3.70	0.01	4.79
MnO	0.07	0.06	0.001	0.05
MgO	3.14	2.56	0.41	2.78
CaO	0.46	3.97	0.07	0.29
Na_2O	< 0.08	0.46	9.27	< 0.11
K_2O	4.17	3.17	0.45	6.19
P_2O_5	0.13	0.21	0.02	0.14

6.3.2 TRACE ELEMENTS

6.3.2.1 COMPARISON OF XRF AND ICP-MS

Table 6.6 reports the trace element concentrations measured by the two techniques for the four unknown samples. Twenty-nine elements were measured by XRF and 38 elements were measured by ICP-MS. For XRF, all samples have a number of elements below LLD. Sample 1015A has the most with nine elements below LLD and sample 1010B has the least with five elements below LLD. Due to the incomplete dissolution of zircon during preparation of the samples for ICP-MS, one of the advantages of XRF is a more accurate measurement of Zr. Hafnium and Y are also present in the zircon crystal lattice so XRF is generally better at measuring these elements as well. As seen in Table 6.6, the Zr and Y concentrations are higher when measured by XRF so these were used for further data interpretation. However, Hf by XRF for two samples was below LLD so ICP-MS values were used. The two samples with Hf above LLD for XRF are similar to the ICP-MS values. ICP-MS values were chosen for all other elements because of better LLD, except for those only analysed by XRF. Another advantage of ICP-MS is its ability to measure the concentrations of 13 rare earth elements, as these are useful petrogenetic tracers.

Figures 6.1 and 6.2 identify the ICP-MS zircon dissolution problem outlined above by having Zr plot below and away from the 1:1 line for samples 1010B, 1012A and 1019C and having Y plot below and away from the 1:1 line for samples 1010B, 1015A and 1019C. Interestingly, Zr of sample 1015A has been measured in similar concentrations by both techniques (XRF=93.3 ppm, ICP-MS=87 ppm) suggesting zircon dissolution was better in this sample (Table 6.6 & Figure 6.2). A reason for this better zircon dissolution is given in Section 7.3.3. Fewer elements are plotted for sample 1015A because of the large number

of elements below LLD for XRF. Most of the elements that were plotted for sample 1015A had ICP-MS values less than the corresponding XRF values (plotted below 1:1 line) (Table 6.6 & Figure 6.1). Since poor zircon dissolution for this sample cannot explain this discrepancy, perhaps the reason for this discrepancy is the poor dissolution of the oxides that pseudomorphed the biotite of the sample (Section 4.3.5). Uranium and Mo plotting above and below the 1:1 line (respectively) for samples 1010B, 1012A and 1019C (Figure 6.1) is likely to be because U and Mo are near the LLD. Similarly, Cu and Cs of sample 1015A are probably near the LLD.

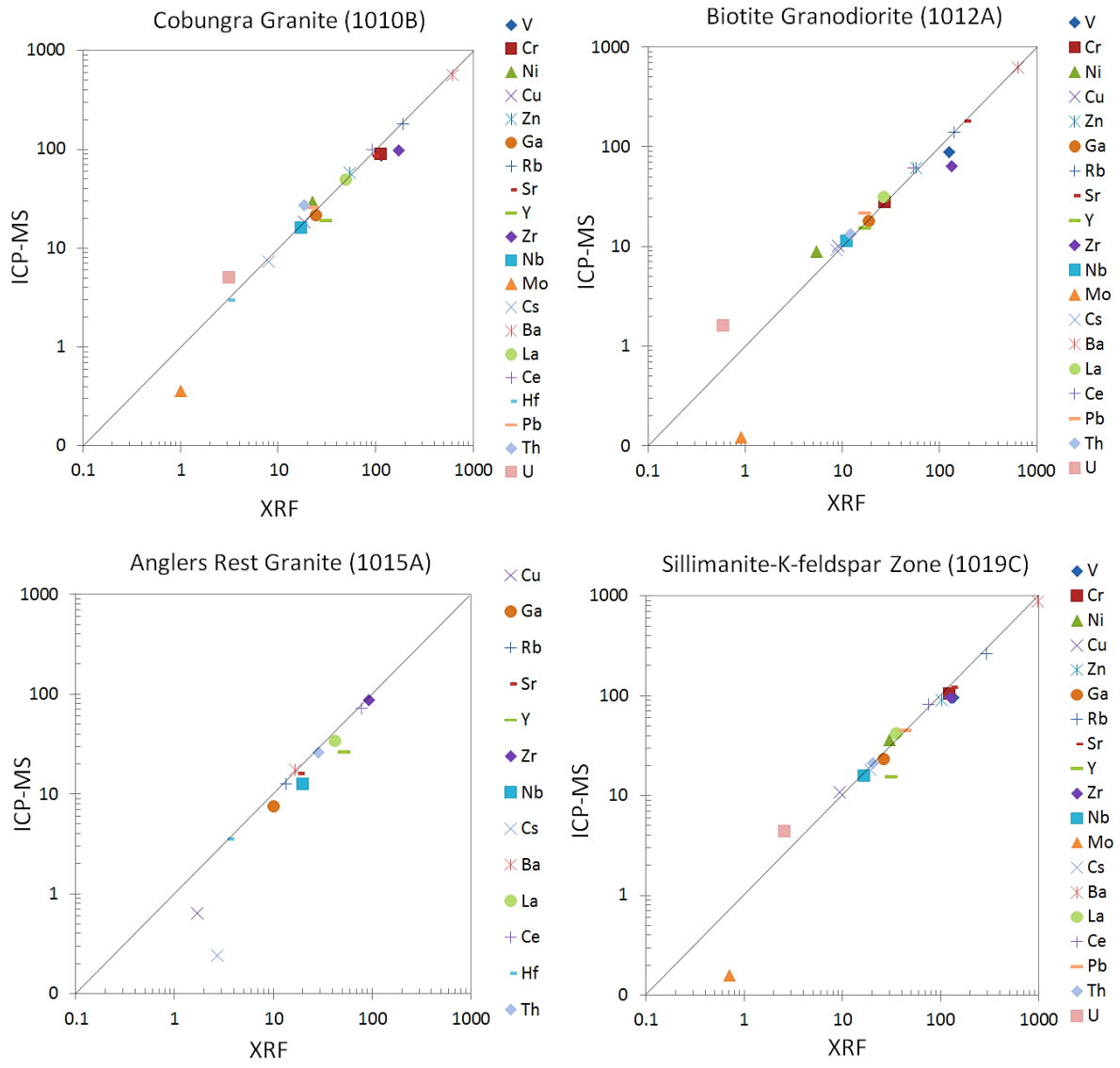

Figure 6.1. Comparison of whole-rock trace element concentrations (ppm) by XRF and ICP-MS of four samples from the study area.

Table 6.6. Trace element concentrations (ppm) measured by XRF and ICP-MS of four whole-rock samples from the study area.

	XRF				ICP-MS			
Element	*1010B*	*1012A*	*1015A*	*1019C*	*1010B*	*1012A*	*1015A*	*1019C*
Li	–	–	–	–	31.3	29.5	1.4	17.8
Be	–	–	–	–	4.3	1.8	1.2	4.4
Sc	–	–	–	–	13.6	17.0	3.7	15.1
Ti	–	–	–	–	4061	3296	378	3928
V	114.2	125.8	< 1.9	134.2	86	90	2.2	97
Cr	110.7	27.7	< 0.7	124.5	90.8	28.2	2.8	106.0
Mn	–	–	–	–	457	456	5.3	371
Co	–	–	–	–	30.3	38.2	71.3	24.1
Ni	22.4	5.4	< 0.8	29.8	29	9	0.55	36
Cu	18.5	8.9	1.7	9.3	19	10	0.65	11
Zn	54	56.6	< 0.4	102.3	57	63	2.4	90
Ga	24.3	18.9	10.1	26.8	21.4	18	7.6	23
Ge	1.9	0.3	5	< 0.3	–	–	–	–
As	< 0.3	0.4	0.7	18.3	–	–	–	–
Se	< 0.2	< 0.2	0.9	< 0.2	–	–	–	–
Rb	188.1	140.2	13.4	288.2	180	142	12.6	264
Sr	92.7	184.8	17.9	131.1	86	182	16.2	122
Y	30.7	17	51.8	31.5	19	16	26.8	16
Zr	172.6	132.5	93.3	125	98	65	87	96
Nb	17.1	11.2	19.8	16.6	16.2	11.4	12.6	15.8
Mo	1	0.9	< 0.2	0.7	0.36	0.13	0.21	0.16
Cd	< 0.2	< 0.2	< 0.2	0.3	–	–	–	–
Sn	2.8	6	1.9	9.6	–	–	–	–
Sb	< 0.5	< 0.5	< 0.5	< 0.5	–	–	–	–
Te	< 0.2	< 0.2	0.3	< 0.2	–	–	–	–
Cs	8	8.7	2.7	19.3	7.32	9.39	0.24	18.07
Ba	610.4	643.2	16.5	962.5	562	635	17.5	887
La	48.7	27.2	42.2	35.7	49.9	31.5	34.2	42.0
Ce	92.6	53.9	78.5	73.8	98.7	62.3	72.3	81.6
Pr	–	–	–	–	11.5	7.3	8.5	9.6
Nd	–	–	–	–	42.6	26.7	31.0	35.3
Sm	–	–	–	–	8.22	5.30	6.28	6.91
Eu	–	–	–	–	1.39	1.40	0.26	1.87
Gd	–	–	–	–	6.55	4.69	4.97	5.48
Tb	–	–	–	–	0.93	0.68	0.75	0.75
Dy	–	–	–	–	4.37	3.46	4.19	3.41
Ho	–	–	–	–	0.75	0.64	0.89	0.58
Er	–	–	–	–	1.87	1.48	2.67	1.42
Yb	–	–	–	–	1.58	0.93	2.73	1.26
Lu	–	–	–	–	0.23	0.13	0.42	0.19
Hf	3.1	< 2.0	3.5	< 2.0	3.02	1.95	3.55	2.82
Ta	–	–	–	–	1.76	1.70	1.93	1.69
Tl	0.6	< 0.7	3.2	< 0.7	–	–	–	–
Pb	22.6	17	< 0.5	44.4	26.16	21.83	1.81	45.49
Bi	0.8	< 0.5	1.1	< 0.5	–	–	–	–
Th	18.3	12.1	28.7	20.1	27.13	13.42	25.97	21.00
U	3.1	0.6	< 0.5	2.6	5.10	1.60	2.03	4.42

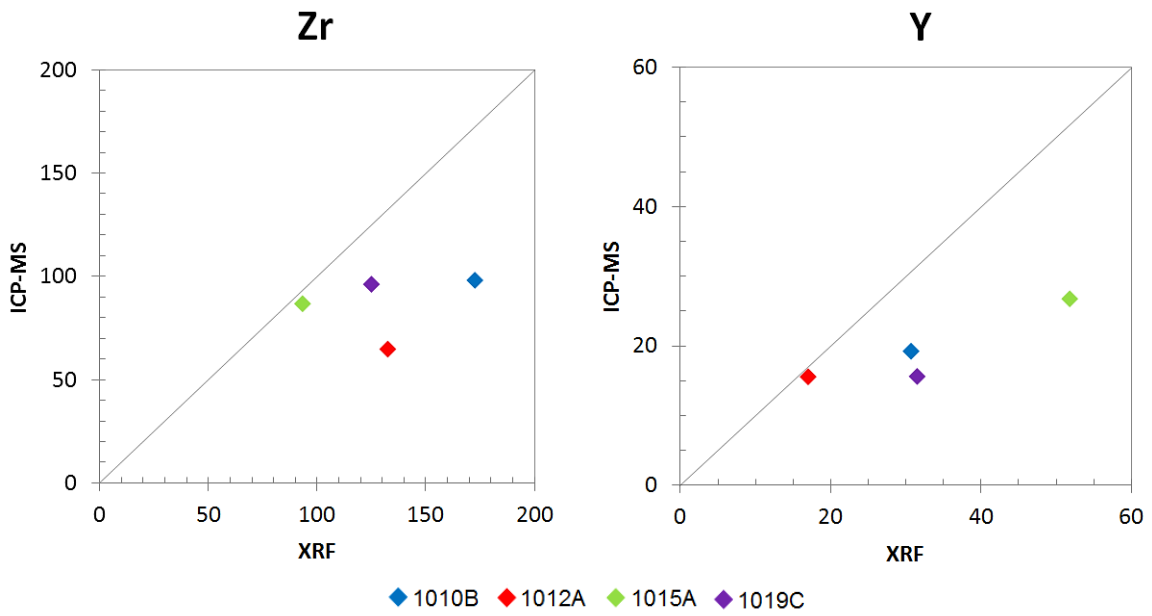

Figure 6.2. Comparison of whole-rock zirconium and yttrium concentrations (ppm) by XRF and ICP-MS for four samples from the study area.

6.3.2.2 RARE EARTH ELEMENTS

Rare earth elements (REE) are regarded as amongst the least soluble trace elements and are relatively immobile (Rollinson 1993). This property means REE are generally retained in rocks and can therefore provide information about their histories. However, REE patterns can be affected in heavily hydrothermally altered rocks or highly metamorphosed rocks (Humphries 1984). All whole-rock samples in this study are enriched in light REE (100 times chondrite), which is typical of crustal rocks (Figure 6.3). There is approximately one order of magnitude difference between the light REE and the heavy REE. The Anglers Rest Granite is more enriched in heavy REE compared to the other samples. This heavy REE discrepancy with the other samples may be associated with the hydrothermal alteration this rock has experienced as evidenced from feldspar chemistry (Section 5.3.3), where nearly pure albite has replaced K-feldspar and plagioclase seen in thin section.

The samples all show a negative Eu anomaly that varies in magnitude from sample to sample (Figure 6.3). A Eu anomoly is primarily controlled by feldspars because Eu (present in the divalent state) is compatible in plagioclase and K-feldspar, in contrast to the trivalent REE which are incompatible. Therefore, the removal of feldspar from a felsic melt by fractional crystallisation will cause a negative Eu anomaly in the melt. Eu anomalies were calculated using the formula: Eu_N / √(Sm_N x Gd_N). The Anglers Rest Granite has a very large negative Eu anomoly (0.14) whereas the Sillimanite-K-feldspar Zone sample has the smallest negative Eu anomaly (0.93) of the samples (Figure 6.3). The apparent negative Yb anomaly of the Biotite Granodiorite is an artificial one as Tm has been omitted from the ICP-MS analyses. If Tm was included between Er and Yb on the plot, then the gentle slope would continue through these elements.

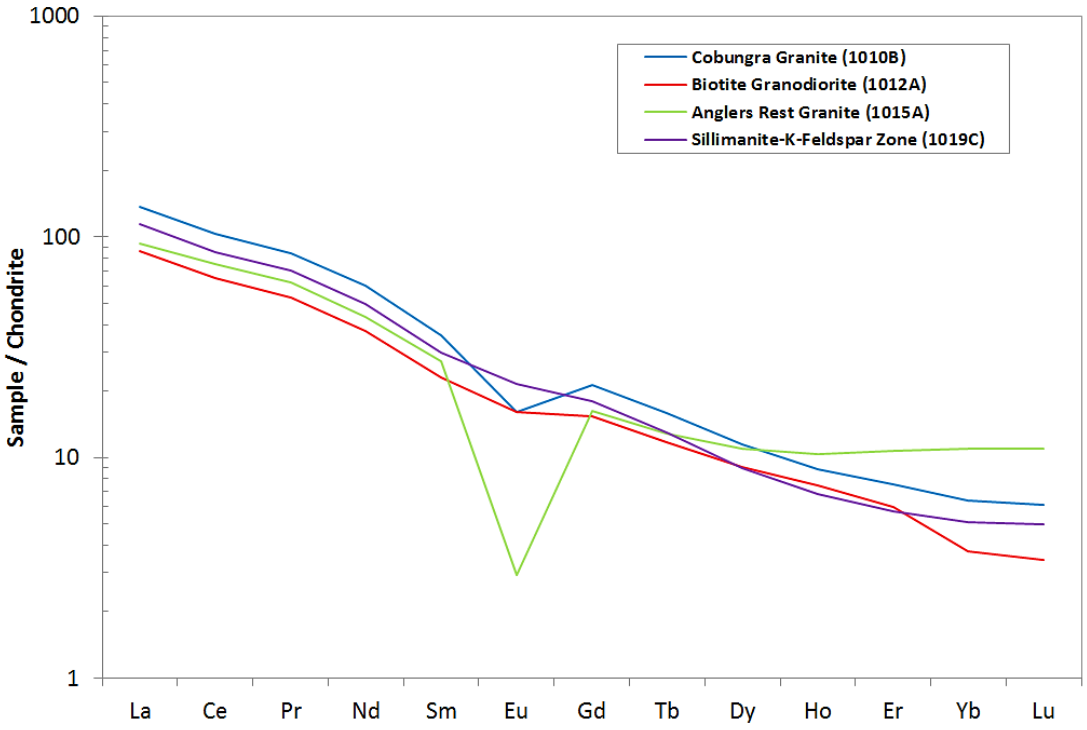

Figure. 6.3. Rare earth element plot of four whole-rock samples from the study area. Chondrite values from Taylor and McLennon (1985).

6.3.2.3 OTHER TRACE ELEMENTS

The multi-element diagram presented here has samples normalised to the composition of typical mid-ocean ridge basalt (MORB) (Figure 6.4). MORB was used for normalisation rather than estimates of primitive mantle or chondrite used for other diagrams, because it is closer to the parental composition of the crustal rocks in this study. The more mobile elements are on the left of the diagram, listed left-to-right in increasing incompatibility, and the less mobile elements are listed in increasing incompatibility from right-to-left. The four samples generally follow the trend of upper continental crust (Figure 6.4). There are slight deviations from upper continental crust for the elements Ta, Zr and Hf. The Anglers Rest Granite is different from the other samples in that it is depleted in the mobile elements of Sr, Rb and Ba. The hydrothermal alteration this rock has undergone (Section 5.3.3) is probably linked to the low concentration of mobile elements. Furthermore, of all samples, this sample had the most elements below LLD for XRF. The Anglers Rest Granite is also depleted in the transition metals Ti and Cr, however relatively enriched in Y and Yb. The Biotite Granodiorite is depleted in most elements compared to the Cobungra Granite and Sillimanite-K-Feldspar Zone samples and the two latter samples show the most similar pattern on the plot (Figure 6.4). These whole-rock analyses were carried out with one sample per lithology. The results might be more illuminating if several samples were analysed for each lithology.

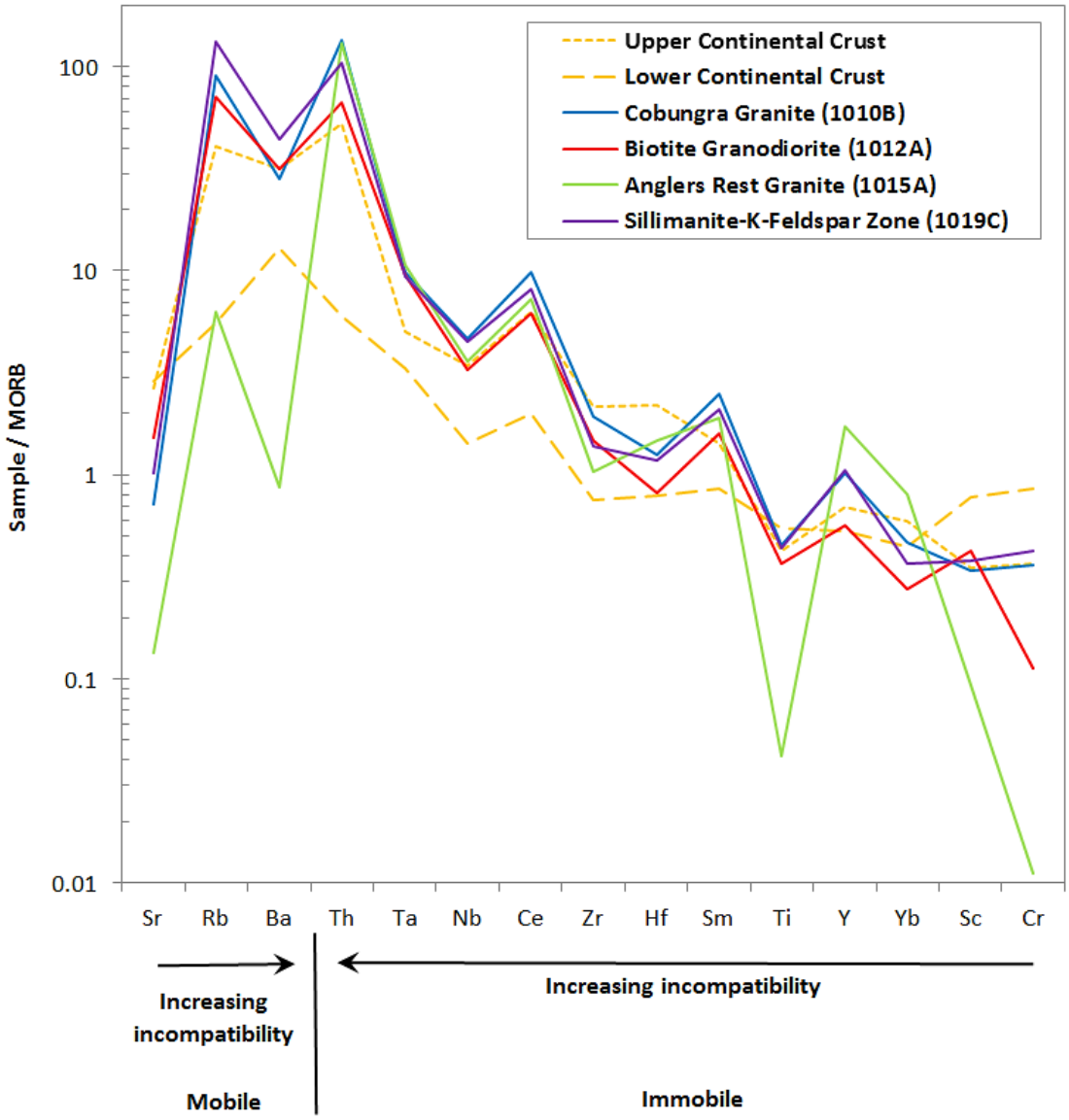

Figure 6.4. Incompatible element diagram of four whole-rock samples from the study area. MORB values from Pearce (1983). Values for upper and lower continental crust from Rudnick and Gao (2004).

CHAPTER 7

ZIRCON MORPHOLOGY, GEOCHRONOLOGY AND CHEMISTRY

7.1 INTRODUCTION

Zircon is a common accessory mineral found in many different rocks types and has become one of the most widely used minerals for the extraction of information on the history and genesis of magmatic, metamorphic and sedimentary rocks. One of the major advantages of zircon is its physical and chemical durability, allowing it to survive processes that destroy most other common minerals (Finch & Hanchar 2003). The usefulness of zircon comes from its suitability as a geochronometer based on the decay of U and Th to Pb (Kosler & Sylvester 2003), and its rare earth element (REE) and other trace element contents (Hoskin & Schaltegger 2003). Zircon-forming events also tend to preserve distinct morphological segments on pre-existing zircon grains, each preserving a particular period of zircon-formation or consumption (Corfu et al. 2003). All these characteristics provide useful clues concerning the history of the host rock, and in some cases, the parent rock in which the precursor zircon crystallised.

In this study, an inquiry into the morphological, geochronological and chemical features of zircon from four lithologies in the field area was undertaken in order to characterise and compare the samples and to determine whether the high-T metasedimentary rocks of the Omeo Metamorphic Complex are the source for the adjacent S-type granites of the Cobungra pluton. This involved attempting to determine crystallisation ages for the S-type granitoids (Cobungra Granite and Biotite Granodiorite) and comparing the ages of any

inherited grains of these granites to the detrital pattern of the Sillimanite-K-feldspar Zone sample. An age estimate was also attempted for the Anglers Rest Granite which may have implications for the other granitoids. Morphological characteristics and major and trace elements patterns (particularly REE) will be compared to further investigate the interaction between the rocks.

7.2 METHODOLOGY

The four samples used for zircon analysis were also used for whole-rock chemistry analysis. These included a sample from each of the following: Cobungra Granite (1010B), Biotite Granodiorite (1012A), Anglers Rest Granite (1015A) and the Sillimanite-K-feldspar Zone (1019C). The samples were firstly cut into small pieces up to 3 cm long and then processed with a SelFrag©. This instrument uses high-powered electrical pulses to disaggregate rocks along the grain boundaries. Because zircon grains are generally small (up to 500 µm), a series of sieves were used to separate the zircon grains from the larger grains in each sample. The samples were panned with an 80 cm two-directional fibreglass pan and finally with a watchglass, exploiting zircon's relatively high specific gravity. Approximately 150 zircon grains were selected from each sample using an optical microscope and these were mounted in epoxy. All shapes and sizes of grains were chosen to ensure representative sampling. The mount was ground down to reveal the cores of the zircons. Cathodoluminescence (CL) images showing the internal structure of the grains were produced using a ZEISS EVO MA15 Scanning Electron Microscope (SEM), and each grain was numbered and had its dimensions measured and morphology described. From these descriptions, about 40 to 65 representative grains were selected from each sample to undergo major element, trace element and U-Th-Pb isotopic analysis in the Geochemical Analysis Unit, GEMOC, Macquarie University.

Major element concentrations were determined using a CAMECA SX100 Electron Probe Microanalyser with operating conditions of 15 kV accelerating voltage and 20 nA beam current. SiO_2, ZrO_2, HfO_2 and Y_2O_3 were analysed to confirm zircon composition and to use the Hf concentration as an internal standard for trace element analysis by laser ablation inductively coupled plasma mass spectrometry (LA-ICP-MS). Standards used for EMP calibration were: zircon for Si and Zr, Hf wire for Hf, and yttrium aluminium garnet for Y. The lower limits of detection and relative standard deviation for these elements are shown in Table 7.1.

Table 7.1. Lower limits of detection (LLD) and relative standard deviation (%rsd) of elements analysed by the CAMECA SX100 Electron Probe Microanalyser.

CAMECA SX100 ELECTRON MICROPROBE Large area LIF, PET and TAP Lower limits of detection for 15 kV		
Element	**LLD (wt%)**	**% rsd**
SiO_2	0.03	0.19
ZrO_2	0.09	0.19
HfO_2	0.03	0.30
Y_2O_3	0.03	0.34

Concentrations of 22 trace elements (including all 14 naturally occurring REE) and U-Th-Pb isotopes (^{206}Pb, ^{207}Pb, ^{208}Pb, ^{232}Th, ^{238}U and ^{235}U) were measured using an Agilent 7700 series LA-ICP-MS attached to a New Wave UP-213 nm Nd:YAG laser. A pulse rate of 5 Hz was used with a spot size of 40 µm. Other operating conditions are listed in Table 7.2. Hafnium was used as an internal standard to calculate the concentrations of other trace elements. The calibration standards GJ (Jackson et al. 2004) and NIST 610 (Norman et al. 1996) were used for U-Th-Pb dating and trace elements (respectively). Each of a total of 17 runs consisted of: two analyses of each calibration standard at the beginning of each run and two at the end; one analysis of the standard reference material 91500 to

monitor accuracy; and 10–14 unknown samples in the middle of each run. Published and measured values for the standards are shown in Table 7.3. When lasering the unknown samples, any inclusions in the zircon grains were avoided and grains were sampled to one side of obvious boundaries in internal structure. For some grains, both the core and rim were analysed and analyses were made at the location of the EMP analysis for that grain. The data were processed with GLITTER software v4.4 (Griffin et al. 2008). A common Pb correction was applied to all U-Th-Pb analyses using the program ComPbCorr (Anderson 2002) due to the low ^{204}Pb count rates and the isobaric interference from Hg (a contaminant from the Ar gas supply of the LA-ICP-MS). Trace elements were normalised to chondrite using values from Taylor and McLennon (1985). Isoplot v3.6 (Ludwig 2009) was used to produce concordia plots, cumulative probability plots and weighted averages of ages of individual grains.

Table 7.2. Agilent 7700s LA-ICP-MS operating conditions.

Condition	Property
ICP-MS type	Quadrupole
Make and Model	Agilent 7700 series
Type of laser	Nd:YAG
Make and model	New Wave UP-213 nm
Laser Wavelength	213 nm
Beam diameter used	40 µm
Carrier Gas	He (0.8 L/min)
Make Up Gas	Ar (0.7 L/min)
Laser Power	8 J/cm^2
Laser Pulse Rate	5 Hz
Calibration standards used	GJ, NIST 610
Standard reference material used	91500
Data reduction software used	GLITTER software v4.4
Typical signal length for background counts	60 seconds
Typical signal length for age/ trace elements	100-120 seconds
Isotope dwell times	All 10 ms except: 15 ms for ^{206}Pb, 30 ms for ^{207}Pb & 15 ms for ^{238}U

Table 7.3. Published and measured values of standards used during LA-ICP-MS analysis of U-Th-Pb isotopes and trace elements in zircon.

Standard	Published value	*1sd*	Measured value	*1sd*
GJ (Jackson et al. 2004)				
$^{206}Pb/^{238}U$ age (Ma)	600.39	0.65	600.74 (*n*=68)	4.12
91500 (Weidenbeck et al. 1995)				
$^{207}Pb/^{206}Pb$ age (Ma)	1065.00	1.01	1058 (*n*=19)	12
91500 (Belousova et al. 2002)				
ppm			(*n*=19)	
Y	147	22	134	11
Ce	2.5	0.5	2.42	0.41
Sm	0.41	0.2	0.43	0.09
Eu	0.37	0.17	0.22	0.04
Dy	12	2.1	9.83	1.34
Yb	66	7.3	64.3	4.26
Th	31	4.9	28.4	3.60
U	88	15	72.9	12.5

7.3 RESULTS AND DISCUSSION

7.3.1 ZIRCON MORPHOLOGY

Morphological variety in zircon arises from the range of settings in which zircon can form. The major controlling factor of length-to-width ratio (L/W) of zircon is the velocity of crystallisation (Corfu et al. 2003). Needle-shaped acicular zircon crystals with large L/W are common in rapidly crystallised intrusions whereas stubby and equant crystals are more common in slowly cooled environments. Oscillatory zoning in zircon reflects variation in trace element concentration (especially Hf, P, Y, the REE, U and Th) and is associated with a magmatic environment. Metamorphically grown or metamorphically modified zircon crystals can show oscillatory zoning but they are generally characterised by subrounded or

highly resorbed shapes. Cathodoluminescence response is closely related to the structural perfection in the zircon crystal lattice (Nasdala et al. 2003). A low CL response (i.e. dark) often coincides with high concentrations of Fe, Y, P, Ca and U (Kempe et al. 2000). Uranium plays a particularly important role in reducing CL response because of its radiation effects in causing damage to the zircon crystal lattice (Poller et al. 2001).

After inspection of the CL images, it was noted that some of the 150 or so grains of each sample were not zircon. These grains were ignored and the zircon grains were described in terms of size, shape and internal structure. The length and width of the zircon grains from each sample were measured and a L/W was calculated (see Table 7.4 and Figure 7.1). The dimensions of incomplete grains were estimated by assuming the grains were complete and using the appearance of other grains in a sample as a guide. Several types of grains within each sample were recognised and described based on morphology and representative examples of these types are shown in Figures 7.2 – 7.5.

The zircon grains across all samples have a range in length of 70-470 µm but are commonly 100-250 µm (Figure 7.1). Both elongate and stubby grains are present, as well as rounded grains, rectangular grains and grains with pointed tips. The grains exhibit a variety of textures including oscillatory zoning, sector zoning, evidence of multiple phases of growth and grains with new zircon mantles.

Table 7.4. Size distribution of zircon grains from four samples in the study area. L/W = Length-to-width ratio.

	Cobungra Granite			**Biotite Granodiorite**			**Anglers Rest Granite**			**Sillimanite-K-feldspar Zone**		
	(1010B)		*(n*=133)	*(1012A)*		*(n*=145)	*(1015A)*		*(n*=134)	*(1019C)*		*(n*=128)
	Length	Width	L/W	Length	Width	L/W	Length	Width	L/W	Length	Width	L/W
Minimum	80	25	1.14	75	25	1.55	80	40	1.18	70	30	1.14
1st Quart.	125	50	2.06	160	45	3.17	125	60	1.78	125	50	2.20
Median	150	60	2.50	190	50	3.67	140	70	2.00	145	55	2.58
3rd Quart.	175	70	3.00	235	65	4.30	165	80	2.36	170	70	3.09
Maximum	435	150	7.80	470	125	7.83	320	125	4.57	340	125	5.50

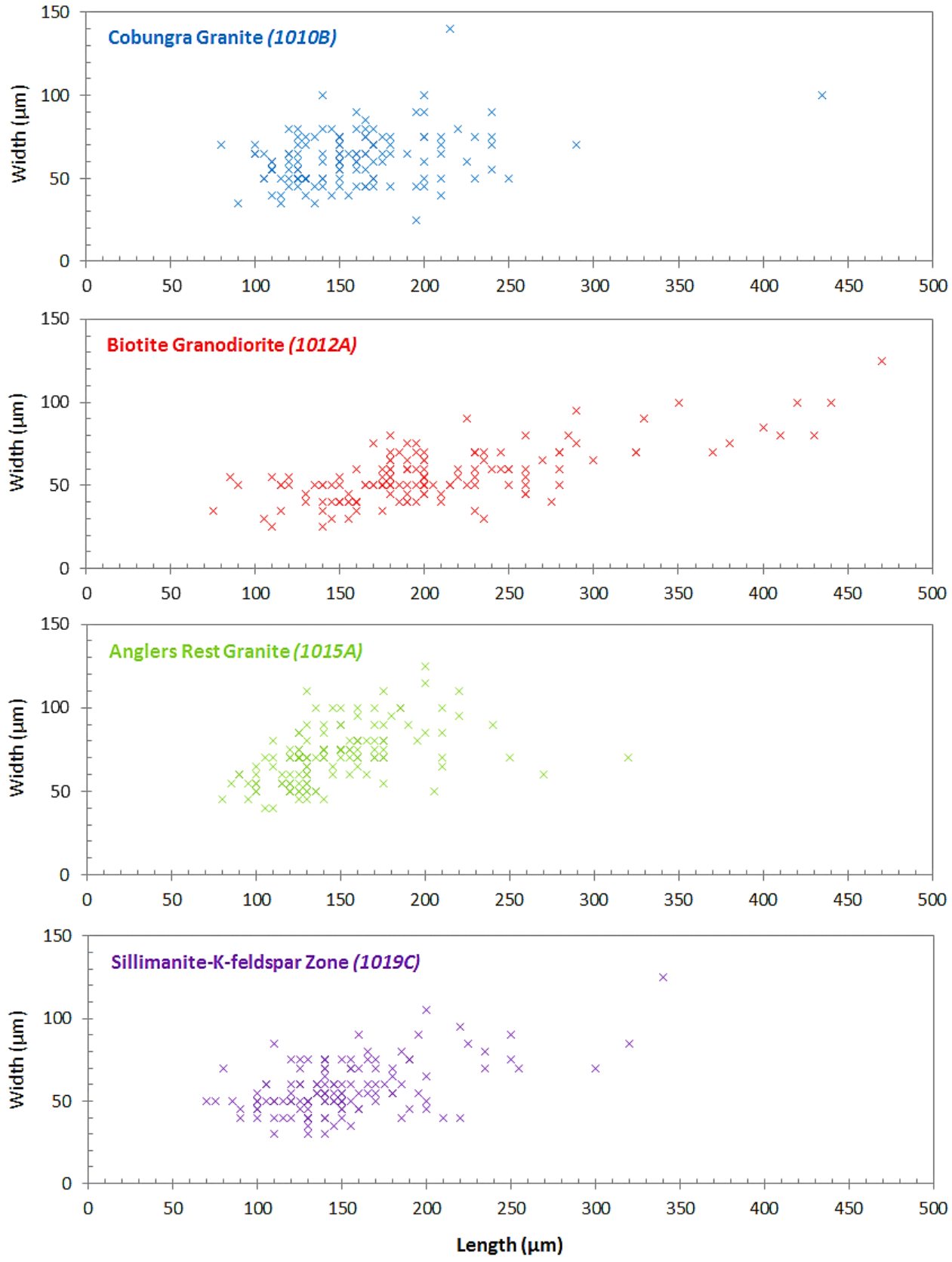

Figure 7.1. Size distribution of zircon grains of four samples in the study area. All axes have equal scales. Bold markers indicate two or more analyses.

BIOTITE GRANODIORITE

The Biotite Granodiorite has the largest proportion of oscillatory zoned elongate grains out of all the samples. This sample has the largest median L/W (3.67) of the four samples which reflects rapid crystallisation. The longest zircon grains across all lithologies belong to this sample with 12 grains ≥300 µm and no more than three grains above this length for the other samples. Some grains of the Biotite Granodiorite have a thin acicular shape like those of Figure 7.2A-B and some grains are slightly more rounded with a round zoning pattern (Figure 7.2C-E). There are some grains with pointed tips that generally have a structureless interior (Figure 7.2H-I) and some with complex zoning patterns, different to regular oscillatory zoning (Figure 7.2G). A small number of grains have an obvious core/rim texture with the cores commonly having a higher CL response than the oscillatory zoned rims (Figure 7.2J-K). A few grains also show evidence of a slight ghosting of oscillatory zoning (Figure 7.2F).

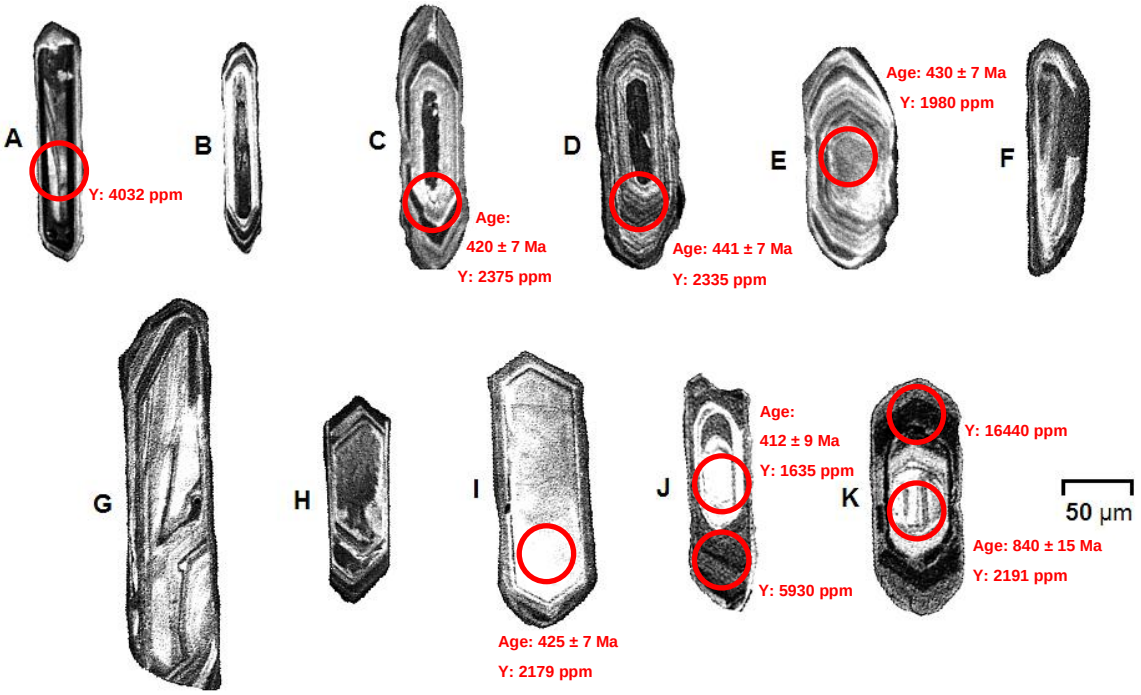

Figure 7.2. Cathodoluminescence images of representative zircon grains from the Biotite Granodiorite. Circles indicate location of analysis by LA-ICP-MS (spot size=40 µm). The ages are the $^{206}Pb/^{238}U$ age and were not included if the analysis had >2% common Pb and/or >30-33% central discordance. Y=Yttrium concentration. See Sections 7.3.2–7.3.5 for an explanation of results.

COBUNGRA GRANITE

The Cobungra Granite has the largest variation in grain type of all samples. Ovoid grains are common, many with truncated zoning patterns and evidence of multiple phases of growth (Figure 7.3A-F). These grains are thought to be inherited from a sedimentary source as they are rounded due to sedimentary processes. New zircon mantles are observed on many grains, with the mantles having a darker CL response to the central domains (Figure 7.3D-H). These mantles range in thickness from 5-30 µm and were too thin to analyse by LA-ICP-MS as the spot size used by the laser was 40 µm. The Cobungra Granite zircon has a smaller median L/W (2.50) than the Biotite Granodiorite (see Table 7.4) due to the high number of subrounded grains. The Cobungra Granite does however have many grains that appear to be of igneous origin (Figure 7.3I-P). Textures include rectangular oscillatory zoning, ovoid to hexagonal oscillatory zoning, banding and grains with pointed tips. Some grains exhibit ghosting of their oscillatory zoning which commonly causes a dark CL response (Figure 7.3I-K,P).

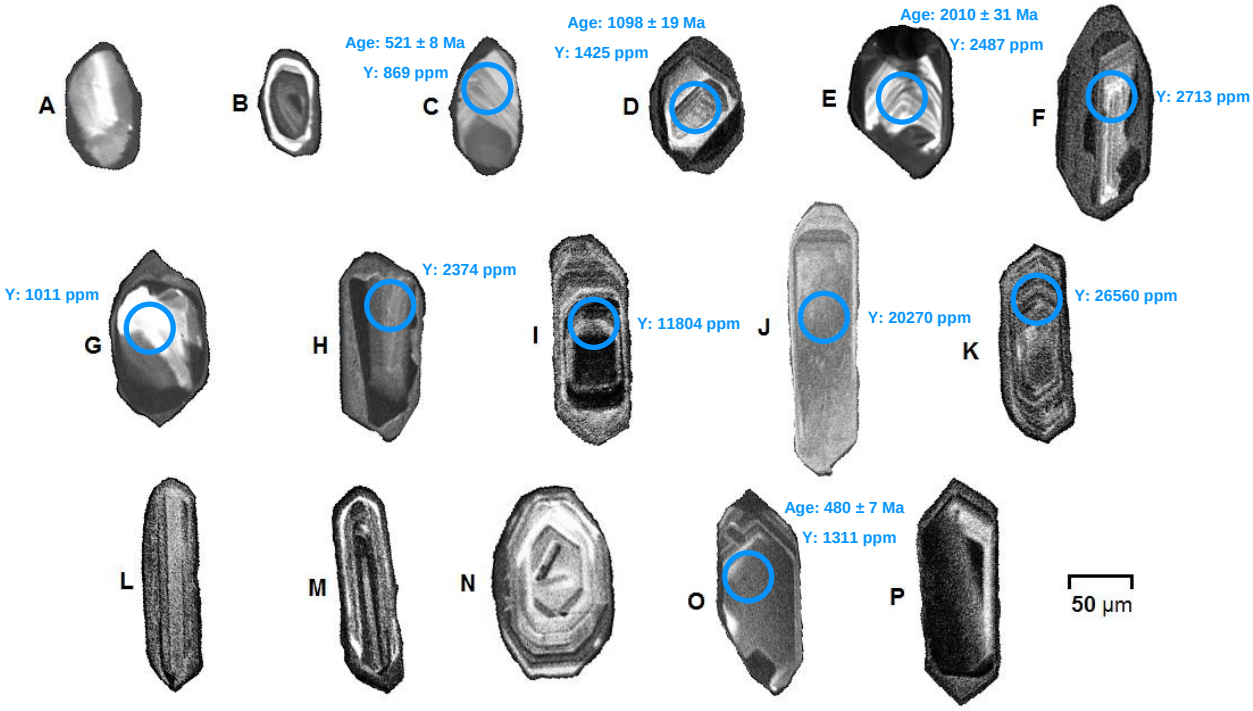

Figure 7.3. Cathodoluminescence images of representative zircon grains from the Cobungra Granite. See Figure 7.2 caption.

SILLIMANITE-K-FELDSPAR ZONE

Zircon grains from the Sillimanite-K-feldspar Zone sample are most similar to those of the Cobungra Granite. They have a similar size distribution (Figure 7.1), median L/W (Table 7.4) and are mostly ovoid or rectangular in shape (Figure 7.4). The ovoid grains are commonly composed of cores with unusual shapes (Figure 7.4D,G,H) or truncated zoning patterns (Figure 7.4A-C) and are surrounded by either rings of new zircon growth (Figure 7.4B-D), new zircon mantles (Figure 7.4A,E) or more conventional oscillatory zoning (Figure 7.4F-H). The new zircon generally has a darker CL response to the cores. However, some lighter rings are present. Rounding of these grains is a consequence of having a sedimentary protolith. The rectangular grains (Figure 7.4L-P) commonly have a structureless central domain surrounded by coarse oscillatory zoning. Some of these grains are particularly stubby (Figure 7.4L-M) which is consistent with a slow velocity of crystallisation. The Sillimanite-K-feldspar Zone sample also contains some grains with odd structural patterns (Figure 7.4I-J) and grains with obvious oscillatory zoning (Figure 7.4Q).

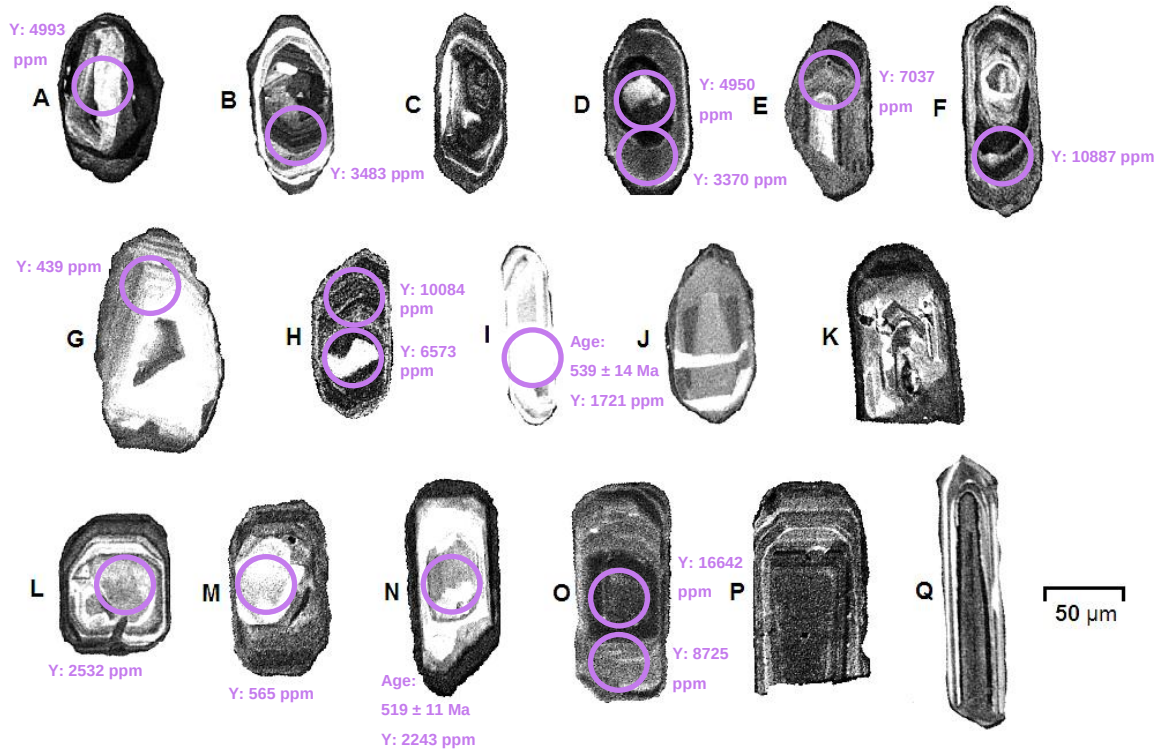

Figure 7.4. Cathodoluminescence images of representative zircon grains from the Sillimanite-K-feldspar Zone, Omeo Metamorphic Complex. See Figure 7.2 caption.

ANGLERS REST GRANITE

Approximately 90% of the zircon grains of the Angler Rest Granite sample have the appearance of those in Figure 7.5A-E. The basic shape of these grains is hexagonal but many are broken into fragments and have unusual shapes. These grains appear to be nearly structureless and exhibit ghosting of their oscillatory zoning and a dark CL response. Many of these grains have inclusions (Figure 7.5D-E). The Angler Rest Granite sample has the lowest median L/W of all samples (2.00) and highest median width (70 µm). In approximately ten grains, oscillatory zoning is more visible and these grains tend to have a lighter CL response (Figure 7.5G-K). Five grains exhibit sector zoning (e.g. Figure 7.5F).

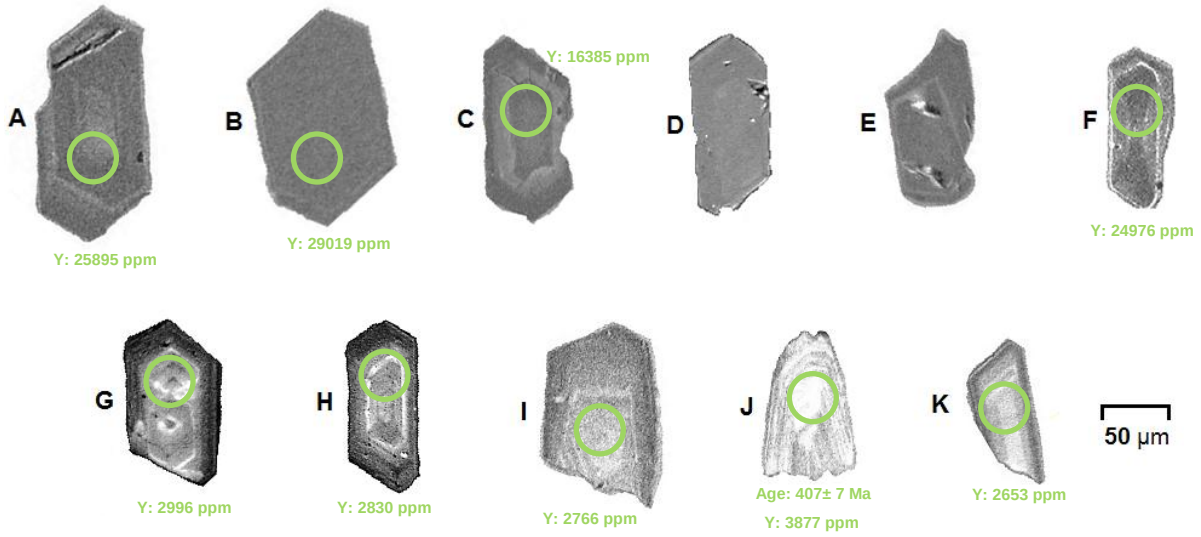

Figure 7.5. Cathodoluminescence images of representative zircon grains from the Anglers Rest Granite. See Figure 7.2 caption.

7.3.2 ZIRCON GEOCHRONOLOGY

After applying a common Pb correction (Anderson 2002) to all analyses, particularly high common Pb contents and high central discordances were observed for many analyses across all four samples. Plots were produced using Isoplot v3.6 (Ludwig 2009), with some plots including all analyses of a sample and some including analyses with <2% common Pb and <30-33 % central discordance (depending on sample). These conditions are noted with each plot below. A common Pb concentration of >2% was considered too inaccurate to provide reliable age information. For U/Pb concordia plots, analyses coloured green and blue both indicate <2% common Pb but differing amounts of central discordance (green: <20 % central discordance; blue: 20 to 30-33% central discordance). Thirty-three percent was considered the absolute maximum value of central discordance to provide reliable age information. Cumulative probability plots were produced using $^{206}Pb/^{238}U$ age data, except for grains of ages >1000 Ma for which $^{207}Pb/^{206}Pb$ age data was used as it is considered to be more accurate. A crystallisation age was calculated for the Biotite Granodiorite by taking a weighted average of ages of individual grains but no age estimates could be made for the other two granitoids because of the lack of reliable data. Analyses for these two granitoids had either high common Pb content or gave inherited grain ages. The Sillimanite-K-feldspar Zone data provided a detrital age pattern but many analyses also had high common Pb content.

The Biotite Granodiorite had the most concordant data and the least number of samples with >2% common Pb. A U/Pb concordia plot of all analyses shows the less discordant analyses clustering around 400-420 Ma (Figure 7.6). The analysis at approximately 850 Ma (on the inset plot) is most likely to be from an inherited grain. Figure 7.7A shows the same information on a cumulative probability plot with a spike between 400-450 Ma and a younger shoulder on the data pattern. Figure 7.7B shows the data filtered for analyses with

<2% common Pb and <30% central discordance and it shows the same younger shoulder. Accurate ages cannot be attained for zircon grains that have undergone excessive Pb loss. These grains commonly give ages younger than the correct age, hence the younger shoulders. The analyses with <30% central discordance and <2% common Pb were then used to calculate an age for the granite by taking a weighted average. The statistics were improved by rejecting analyses one by one until the probability was >0.05 (Figure 7.7C). Four older and five younger grains of the population were rejected, giving an age of 423.6 ± 4.8 Ma. This study marks the first time the Biotite Granodiorite has been dated using U/Pb in zircon. A previous age estimate was made using K/Ar in biotite (Willman et al. 1999) which gave an age of 411 ± 6 Ma (2σ). These ages are very similar but were just outside the uncertainty of each other.

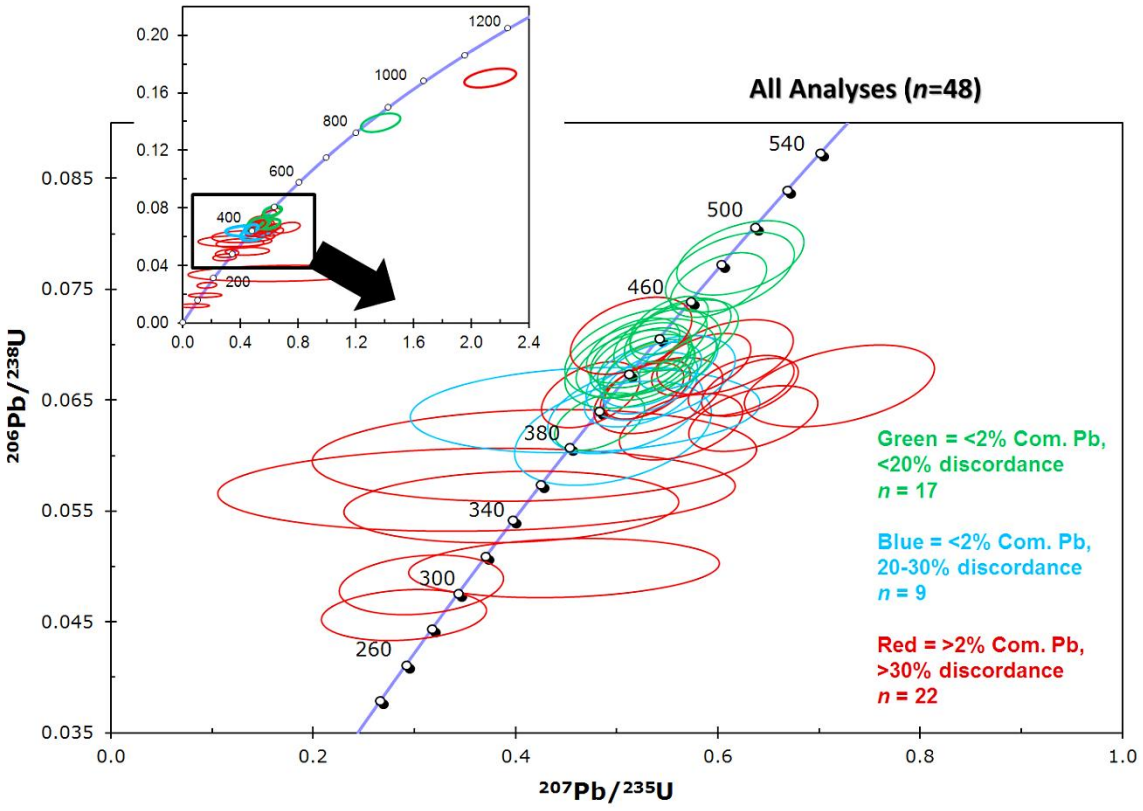

Figure 7.6. U/Pb Concordia plot for zircon analyses of the Biotite Granodiorite.

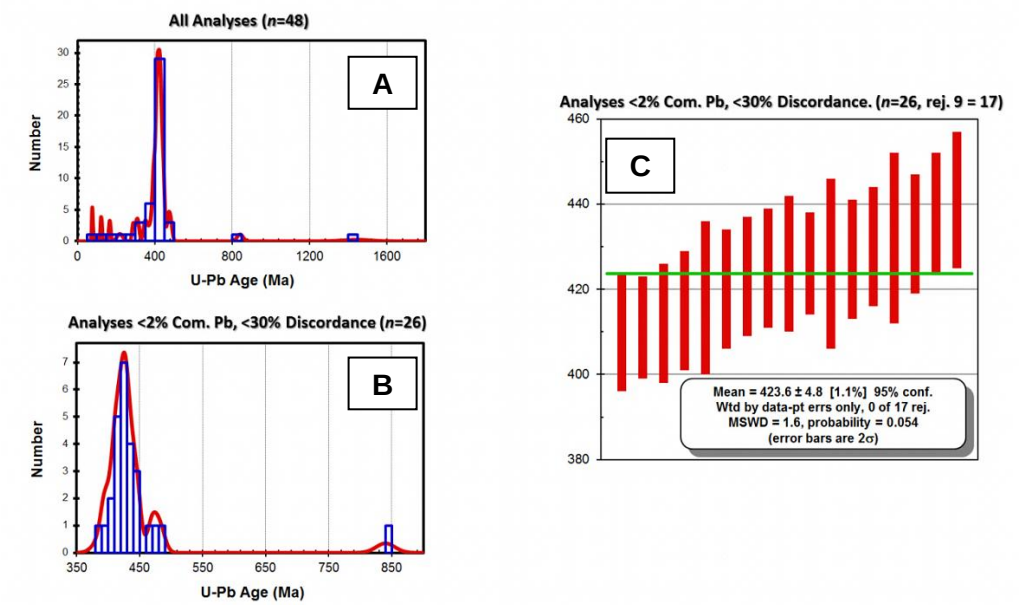

Figure 7.7. Cumulative probability plots (**A,B**) and a weighted average plot (**C**) for zircon analyses of the Biotite Granodiorite.

Many zircon grains from the Cobungra Granite have ages of ≈500 Ma (Figure 7.8A,C), but the central discordance and common Pb content of most grains is too high to provide accurate ages. Figure 7.8B shows the age pattern of the most reliable analyses which gave ages of inherited grains of 500 Ma, 1100 Ma, 2000 Ma and 3100 Ma. Many grains in this sample have suffered extensive Pb loss as shown by the spread of ages from 0-600 Ma. A similar result occurred for grains from the Sillimanite-K-feldspar Zone (Figure 7.9A,C) and the Angler Rest Granite (Figure 7.10A,B). The Sillimanite-K-feldspar Zone had seven analyses with acceptable common Pb content and central discordance giving a detrital age pattern with ages of 500-550 Ma, 850-950 Ma and 2200 Ma (Figure 7.9B). Data for the Anglers Rest Granite show many analyses with $^{206}Pb/^{238}U$ ages at ≈400 Ma but vastly different $^{207}Pb/^{235}U$ ages (Figure 7.10A). This spread of ages may however be some indication of an age for the granite which would be similar to two previous K/Ar biotite ages of 400 ± 16 Ma and 390 ± 16 Ma (Richards & Singleton 1981). However, only one grain had <2% common Pb and <31% discordance which provided an extremely poor precision concordia age of 408 ± 190 Ma (Figure 7.10C). Therefore, no crystallisation ages could be established for the Anglers Rest Granite or the Cobungra Granite due to extensive Pb loss.

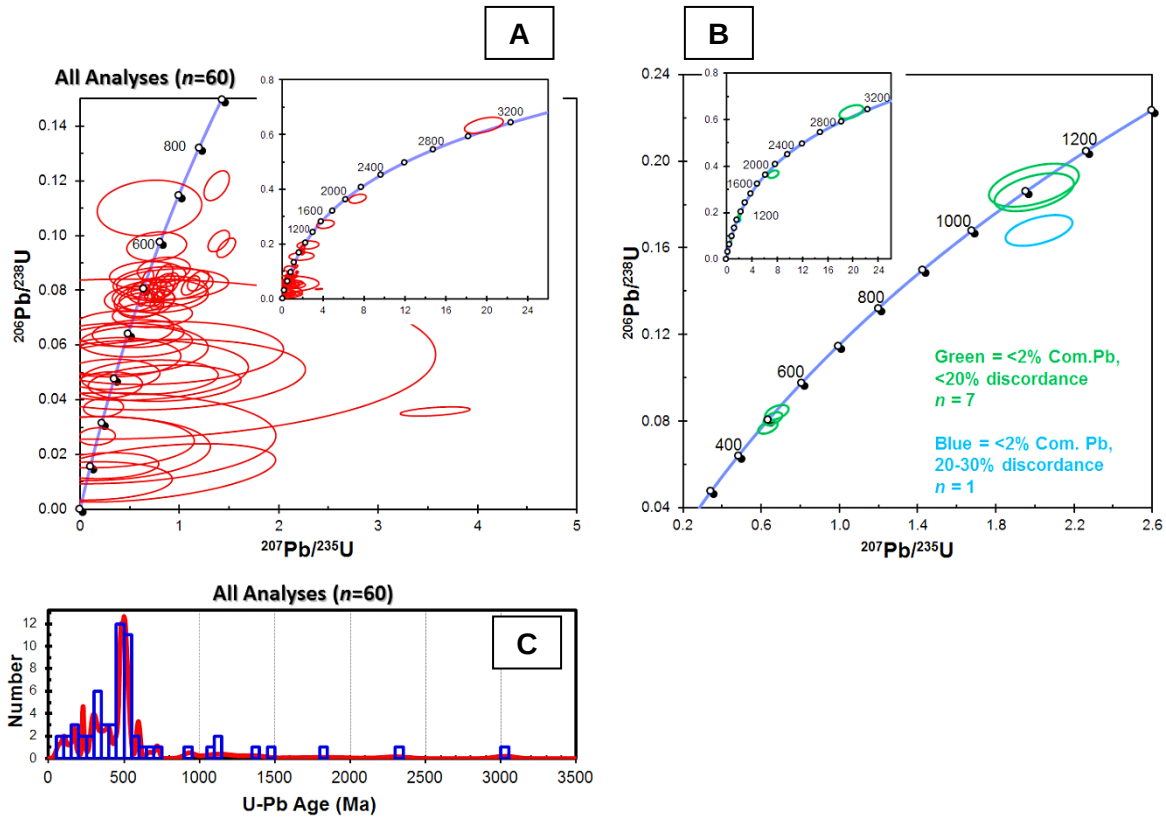

Figure 7.8. U/Pb Concordia plots (**A,B**) and a cumulative probability plot (**C**) for zircon analyses of the Cobungra Granite.

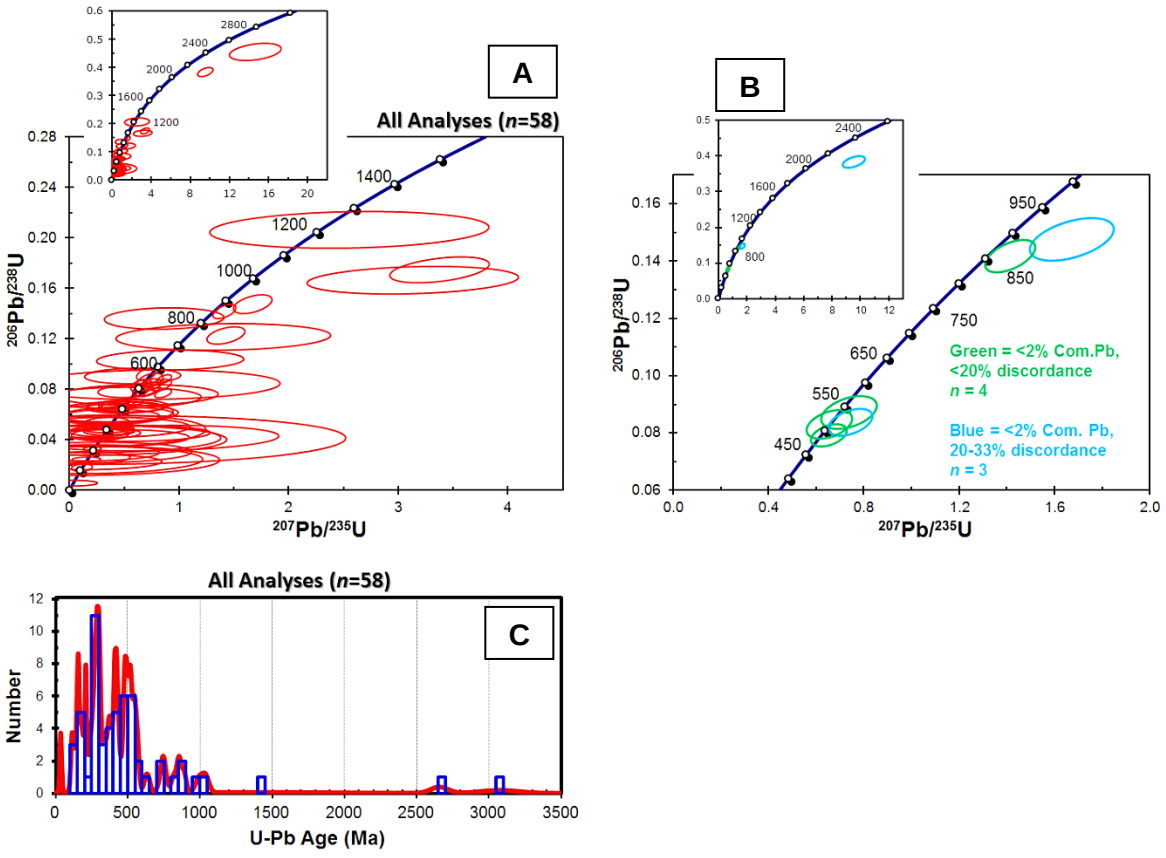

Figure 7.9. U/Pb Concordia plots (**A,B**) and a cumulative probability plot (**C**) for zircon analyses of the Sillimanite-K-feldspar Zone.

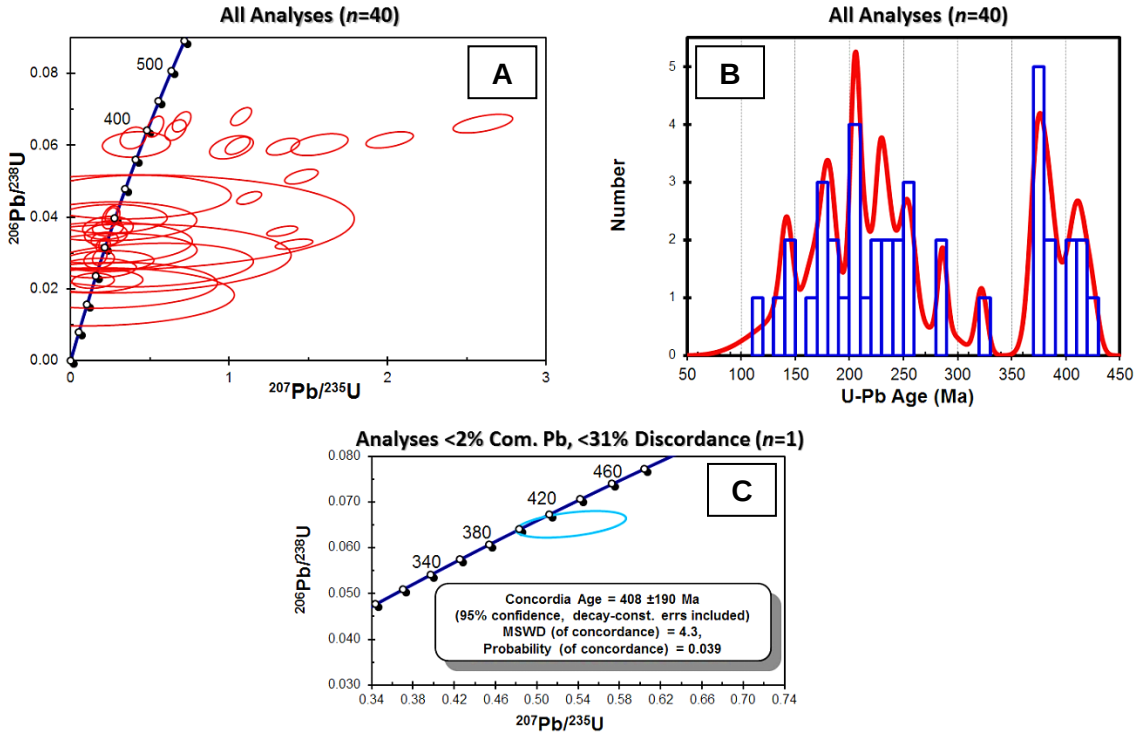

Figure 7.10. U/Pb Concordia plots (**A,C**) and cumulative probability plot (**B**) for zircon analyses of the Anglers Rest Granite.

7.3.3 ZIRCON MAJOR ELEMENTS

For all zircon samples, ZrO_2 and SiO_2 have a positive correlation, and ZrO_2 and Y_2O_3 have a negative correlation (Figure 7.11). Hafnium oxide is unaffected by ZrO_2 (Figure 7.11). Major element concentrations are fairly similar for the Cobungra Granite, Biotite Granodiorite and Sillimanite-K-feldspar Zone samples (Table 7.5). First to third quartile ranges for the three abovementioned samples are: 31.1–32.8 wt.% for SiO_2, 65.4–66.7 wt.% for ZrO_2, 1.47–1.55 wt.% for HfO_2 and 0.27–0.32 wt.% for Y_2O_3. For these three samples, HfO_2 has an even spread of concentrations between 1-2 wt.%, whereas the other elements are focused towards the upper end of their ranges (Figure 7.11).

Major element content of zircon from the Anglers Rest Granite is significantly different to the other samples. Values for SiO_2, ZrO_2, and Y_2O_3 are spread evenly within their ranges (Figure 7.11). The Anglers Rest Granite sample had low SiO_2, ZrO_2, HfO_2 and totals, and high Y_2O_3 (median=2.67 wt.%). Yttrium content is generally indicative of the concentration of other trace elements (Hoskin & Schaltegger 2003). The low totals (median=84.73 wt.%) means that zircon of the Anglers Rest Granite commonly contains up to 20 wt.% trace elements (including Y and Hf). The high trace element content of this zircon may explain the near-complete dissolution of the zircon during ICP-MS analysis of whole-rock chemistry (Section 6.3.2.1). Hydrothermal alteration of this rock (Section 5.3.3) and the accumulation of trace elements in the zircon, means that the zircon crystal lattice is likely to have been damaged and distorted. The zircon would consequently be easier to dissolve during sample preparation for whole-rock analysis.

Table 7.5. Major element oxide data (wt.%) of zircon from four samples in the study area.

Element	Minimum	1st Quart.	Median	3rd Quart.	Maximum
	Cobungra Granite (*n*=71)				
SiO_2	18.99	31.73	32.56	32.79	33.42
ZrO_2	46.99	64.58	65.95	66.37	67.04
HfO_2	1.05	1.42	1.55	1.64	2.00
Y_2O_3	0.05	0.19	0.30	0.51	6.35
Total	72.60	97.96	100.36	100.78	101.98
	Biotite Granodiorite (*n*=49)				
SiO_2	25.05	32.06	32.46	32.68	33.21
ZrO_2	52.26	66.08	66.71	67.07	69.39
HfO_2	1.07	1.41	1.47	1.58	2.03
Y_2O_3	0.05	0.17	0.27	0.47	3.30
Total	81.85	100.29	101.06	101.50	102.75
	Anglers Rest Granite (*n*=43)				
SiO_2	16.99	20.44	23.43	27.07	32.94
ZrO_2	44.50	53.41	57.25	60.93	67.53
HfO_2	1.16	1.25	1.29	1.38	1.80
Y_2O_3	0.18	1.52	2.67	3.67	4.94
Total	70.46	78.46	84.73	90.72	101.66
	Sillimanite-K-feldspar Zone (*n*=74)				
SiO_2	21.30	31.10	32.45	32.80	33.11
ZrO_2	53.42	63.71	65.35	65.84	66.41
HfO_2	1.06	1.34	1.53	1.67	1.97
Y_2O_3	0.05	0.18	0.32	0.62	3.54
Total	80.21	96.76	99.72	100.30	101.18

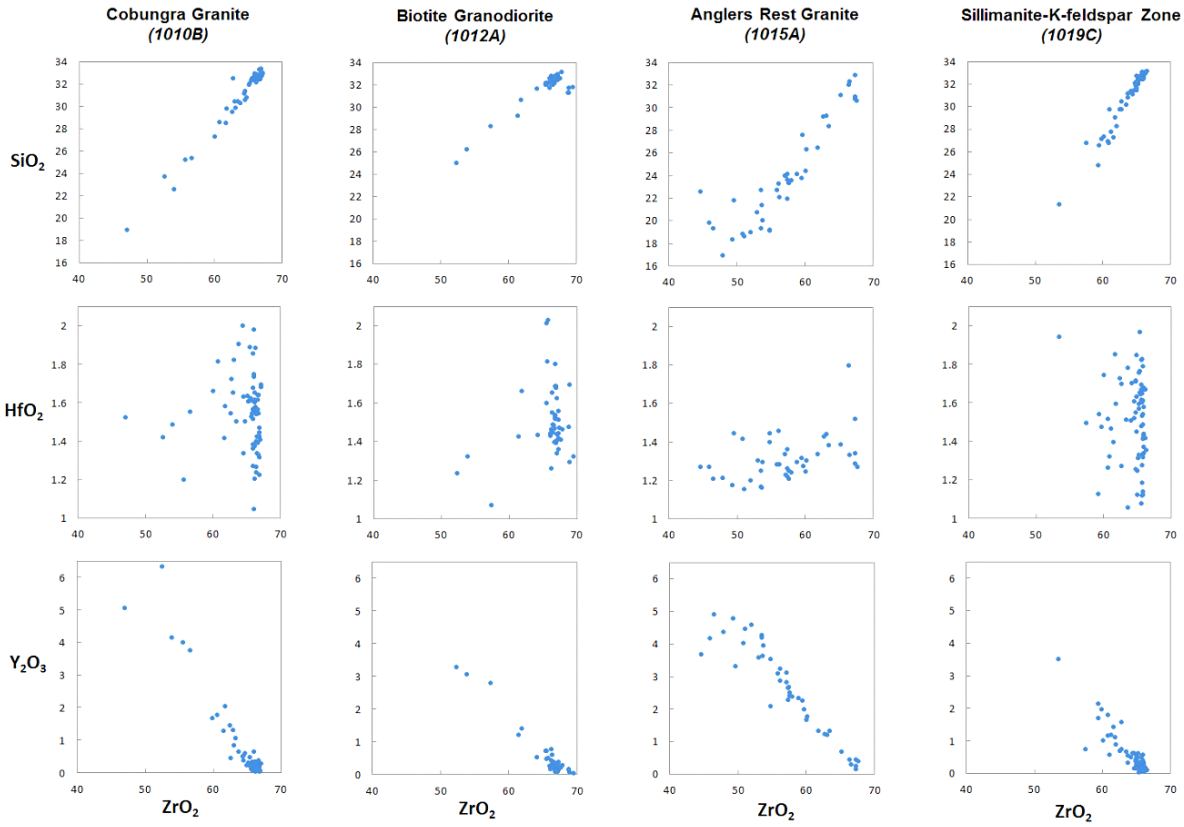

Figure 7.11. Major element oxide (wt.%) plots of zircon grains of four samples from the study area.

7.3.4 ZIRCON TRACE ELEMENTS

Zircon trace element data was attained for all 14 naturally occurring REE as well as P, Ti, Y, Nb, Hf, Ta, Th and U. Since Hf was used as an internal standard to calculate the concentrations of other trace elements from raw counts, the Hf values are actually from the EMP. Nevertheless, these Hf values have been reproduced in the data tables below in ppm for comparison with other trace elements. The REE data were processed in several ways. The ratios of $(Lu/La)_N$, $(Sm/La)_N$ and $(Lu/Gd)_N$ were calculated to determine the degree of fractionation of all REE, LREE and HREE respectively. The 'N' subscript denotes chondrite normalised values. Europium and Ce anomalies were calculated in the manner: $Ce_N / \sqrt{(La_N \times Pr_N)}$, where positive anomalies are >1 and negative anomalies are <1. Total REE content was also calculated. These REE characteristics are presented in the tables below along with individual element concentrations (Tables 7.6-7.9).

Percentiles (10^{th}, 30^{th}, 50^{th}, 70^{th} and 90^{th}) were used to produce chondrite normalised REE plots for all analyses of each sample (Figures 7.12 & 7.13). Minimum, maximum, median and quartile values were not used to construct these plots because the percentiles were thought to better represent the samples due to outliers at low and high concentrations. No chondrite normalised REE plots showing individual analyses were included in the thesis as they did not convey any more information than the abovementioned percentile REE plots or the bivariate plots of REE characteristics included below (Figure 7.14). On the bivariate plots, Y has frequently been plotted on horizontal axes to allow ease of comparison of different trace elements and ratios. There are three reasons for this repetitive plotting of Y on horizontal axes. (1) Yttrium is the most abundant trace element being plotted and therefore it varies the most in concentration. (2) Yttrium concentration is considered to be indicative of the concentration of other trace elements (including REE), i.e. the concentration of different trace elements increases with increasing Y. (3) It was found that when Y is plotted against other trace elements and ratios, the four samples are distinguishable from each other for analyses with greater than ≈4000 ppm Y. An orange line has been used to indicate 4000 ppm Y on the plots. Bivariate plots of non-REE (P, Ti, Nb, Ta & U) were included to distinguish the four samples and interpret their petrogenetic histories (Figure 7.15).

Yttrium content of crustal zircon generally ranges from tens-of-ppm up to ≈5000 ppm (Hoskin & Schaltegger 2003). Some zircon in this study has high Y content (Tables 7.6-7.9). Third quartile values of Y for the four samples are 7102, 4105, 25725 and 6499 ppm. The Anglers Rest Granite consistently has zircon with high Y content (first quartile=16014 ppm) which is probably associated with the hydrothermal alteration this rock has experienced.

Table 7.6. Trace element data of zircon from the Cobungra Granite. Values are in ppm or are ratios. 'N' subscript denotes chondrite normalised values using chondrite values from Taylor and McLennon (1985). Eu and Ce anomalies were calculated in the manner: $Ce_N / \sqrt{(La_N \times Pr_N)}$.

	Cobungra Granite (*n*=58)				
Element	**Minimum**	**1st Quart.**	**Median**	**3rd Quart.**	**Maximum**
P	183	462	902	2492	7412
Ti	3.3	11	20	32	228
Y	651	1617	2616	7102	30934
Nb	1.0	2.5	4.0	7.2	28
La	0.38	3.2	10	67	453
Ce	3.3	25	52	220	1596
Pr	0.42	2.2	7.0	41	278
Nd	3.9	16	47	261	1649
Sm	5.2	15	31	139	973
Eu	0.85	3.5	9.9	47	536
Gd	20	46	75	275	1716
Tb	6.5	14	25	81	427
Dy	68	158	273	722	3223
Ho	23	52	90	199	768
Er	90	223	364	712	2567
Tm	18	47	75	140	481
Yb	161	447	695	1314	4102
Lu	27	79	117	215	548
Hf	8896	12120	13207	13888	16990
Ta	0.43	1.10	1.8	3.7	106
Th	26	213	336	778	4126
U	70	381	674	1477	6503
$(Lu/La)_N$	9.3	28	79	230	2973
$(Sm/La)_N$	1.96	3.4	4.2	5.7	114
$(Lu/Gd)_N$	2.0	5.9	10.9	14	22
Ce/Ce*	0.64	1.08	1.3	1.9	23
Eu/Eu*	0.16	0.38	0.56	0.77	1.4
ΣREE	427	1191	1886	4396	17513

Table 7.7. Trace element data of zircon from the Biotite Granodiorite. See Table 7.6 caption.

	Biotite Granodiorite (*n*=48)				
Element	**Minimum**	**1st Quart.**	**Median**	**3rd Quart.**	**Maximum**
P	216	495	637	817	1468
Ti	4.2	8.2	16	45	638
Y	1047	2024	2488	4105	16440
Nb	1.7	3.8	4.8	8.7	30
La	0.02	1.5	8.2	94	1038
Ce	8.6	22	52	334	5975
Pr	0.07	1.5	6.1	51	750
Nd	1.5	10	37	311	4259
Sm	4.0	11	26	145	2319
Eu	0.89	2.9	5.9	52	510
Gd	26	46	76	261	3011
Tb	7.8	16	22	61	528
Dy	93	187	242	495	2996
Ho	35	70	87	145	572
Er	159	314	382	619	1416
Tm	31	67	82	133	223
Yb	285	647	791	1254	2023
Lu	57	124	146	223	322
Hf	9084	11997	12467	13319	17217
Ta	0.74	1.4	1.8	3.0	13
Th	102	198	279	484	1480
U	169	407	648	1221	3096
$(Lu/La)_N$	2.8	15	141	994	86957
$(Sm/La)_N$	2.1	3.8	5.4	10.5	583
$(Lu/Gd)_N$	0.79	4.2	16	25	40
Ce/Ce*	0.82	1.3	1.6	3.5	66
Eu/Eu*	0.25	0.35	0.52	0.65	1.09
ΣREE	877	1561	2050	4203	25721

Table 7.8. Trace element data of zircon from the Anglers Rest Granite. See Table 7.6 caption.

	Angler Rest Granite (*n*=41)				
Element	**Minimum**	**1st Quart.**	**Median**	**3rd Quart.**	**Maximum**
P	564	6019	8664	10931	17284
Ti	9.1	292	395	454	589
Y	2653	16014	24079	25725	40633
Nb	27	1742	2855	3397	4444
La	4.5	79	133	211	347
Ce	54	1163	2083	2744	5963
Pr	3.6	172	290	366	497
Nd	24	1254	2149	2601	3922
Sm	29	972	1646	1911	2630
Eu	2.7	49	83	96	135
Gd	92	1667	2515	2840	4178
Tb	27	383	546	637	1151
Dy	281	2760	3841	4549	8507
Ho	96	648	893	1030	1777
Er	408	2119	2874	3211	5496
Tm	88	394	545	585	1009
Yb	861	3535	4579	4931	8177
Lu	146	513	656	679	1044
Hf	9817	10592	10942	11661	15273
Ta	2.6	42	51	76	216
Th	691	6380	11904	17937	40676
U	764	2632	3558	4046	6101
$(Lu/La)_N$	14.63	31	46	64	419
$(Sm/La)_N$	6.39	11.4	16	20	76
$(Lu/Gd)_N$	1.6	1.9	2.1	2.4	15
Ce/Ce*	1.86	2.1	2.4	2.6	4.0
Eu/Eu*	0.10	0.12	0.12	0.13	0.21
ΣREE	2227	16746	23607	26029	37847

Table 7.9. Trace element data of zircon from the Sillimanite-K-feldspar Zone. See Table 7.6 caption.

	Sillimanite-K-feldspar Zone (*n*=56)				
Element	**Minimum**	**1st Quart.**	**Median**	**3rd Quart.**	**Maximum**
P	154	732	1829	3963	15843
Ti	7.8	17	43	85	267
Y	439	1717	3146	6499	16642
Nb	0.85	2.7	4.2	6.2	19
La	0.11	4.3	17	60	558
Ce	5.2	40	97	275	2022
Pr	0.13	5.3	17	58	419
Nd	1.8	42	110	423	2893
Sm	2.0	24	72	214	1218
Eu	0.61	12	49	192	599
Gd	8.5	60	129	396	1630
Tb	3.0	17	36	87	281
Dy	33	183	331	707	1972
Ho	14	59	104	201	511
Er	65	246	391	739	1784
Tm	17	52	81	153	370
Yb	154	503	796	1394	3385
Lu	28	85	125	211	536
Hf	9165	11476	12867	14204	16708
Ta	0.51	1.4	2.2	4.2	21.1
Th	68	223	466	855	4208
U	89	542	1104	1817	10653
$(Lu/La)_N$	8.4	36	64	210	7794
$(Sm/La)_N$	2.2	5.2	8.4	13	137
$(Lu/Gd)_N$	2.3	4.7	6.8	13	36
Ce/Ce*	0.94	1.08	1.3	1.7	37
Eu/Eu*	0.19	0.94	1.4	2.1	3.1
ΣREE	374	1324	2581	5568	17625

7.3.4.1 ZIRCON RARE EARTH ELEMENTS

All samples are LREE-depleted and HREE-enriched which is typical for crustal zircon (Hoskin & Schaltegger 2003) (Figures 7.12 & 7.13). Most analyses of each sample have a positive Ce anomaly and a negative Eu anomaly except for the Sillimanite-K-feldspar Zone sample which has many analyses with positive Eu anomalies (addressed below). Negative Eu anomalies commonly arise from divalent Eu being compatible in plagioclase and being removed from a melt in contrast to the other trivalent REE which are incompatible. Thus when plagioclase is retained in the source region of a magma, a negative Eu anomaly will be present in the melt.

The median ΣREE concentration of zircon from Anglers Rest Granite is more than an order of magnitude larger than those of the other three samples (Tables 7.6-7.9). Furthermore, the 90th percentile REE concentrations of the other three samples are less than the median concentrations of the Anglers Rest Granite (Figure 7.13). The Anglers Rest Granite has a large negative Eu anomaly which is fairly consistent in magnitude across the analyses with a first to third quartile range of 0.12-0.13. The Eu anomaly in the zircon of this sample is a similar size to the Eu anomaly of the whole-rock which is 0.14 (Section 6.3.2.2). There are a small number of analyses of this sample that have significantly less REE concentration (and other trace elements) than the rest. This is shown by the 10th percentile line in Figure 7.12C plotting away from the other percentile lines and the lower Y concentration of some of the analyses in Figure 7.14A-F.

Excluding the Anglers Rest Granite, the Biotite Granodiorite has the largest range of values for LREE, but the smallest range of values for HREE (Figure 7.13). This sample also has the largest range of $(Lu/Gd)_N$ values (HREE fractionation) (Figure 7.14C) which is reflected in Figure 7.13 by the steep 10th percentile line and the flat 90th percentile line for

the sample. The Sillimanite-K-feldspar Zone sample has the second largest median REE concentrations except for the heavier HREE (Figure 7.13). This sample is unique in that 73% of its analyses have a positive Eu anomaly (>1) (Figures 7.12D & 7.14E), whereas the Biotite Granodiorite and Cobungra Granite only have two and three analyses respectively with a positive Eu anomaly. Large positive Eu anomalies in zircon are very uncommon. Europium values were checked to see whether they were in fact within 2σ of being a negative Eu anomaly. For most analyses, the anomalies were simply too large for analytical uncertainty to explain the positive anomalies. This will be discussed further when comparing Eu anomalies to geochronological data (Section 7.3.5).

Yttrium and ΣREE content have a strong positive linear correlation (Figure 7.14A) which is expected as Y concentration is generally indicative of the concentration of other trace elements. Figure 7.14A has analyses from each sample that have >4000 ppm Y grouped together which is a feature mirrored in many other bivariate plots of REE characteristics (Figure 7.14). Values of $(Sm/La)_N$ (LREE fractionation) for analyses with <4000 ppm Y have a large range (2.0-583) and do not distinguish the samples, whereas analyses with >4000 ppm Y have a small range (mostly 2.0-31.4) and do distinguish the samples (Figure 7.14B). Values of $(Lu/Gd)_N$ (HREE fractionation) having a negative linear correlation with Y (Figure 7.14C), is a trend that is also seen in Figure 7.13 by the HREE pattern becoming more flat with increasing REE content. The Biotite Granodiorite has the largest range of $(Lu/Gd)_N$ values (0.79-40) and has analyses grouped at both ends of the range (Figure 7.14C).

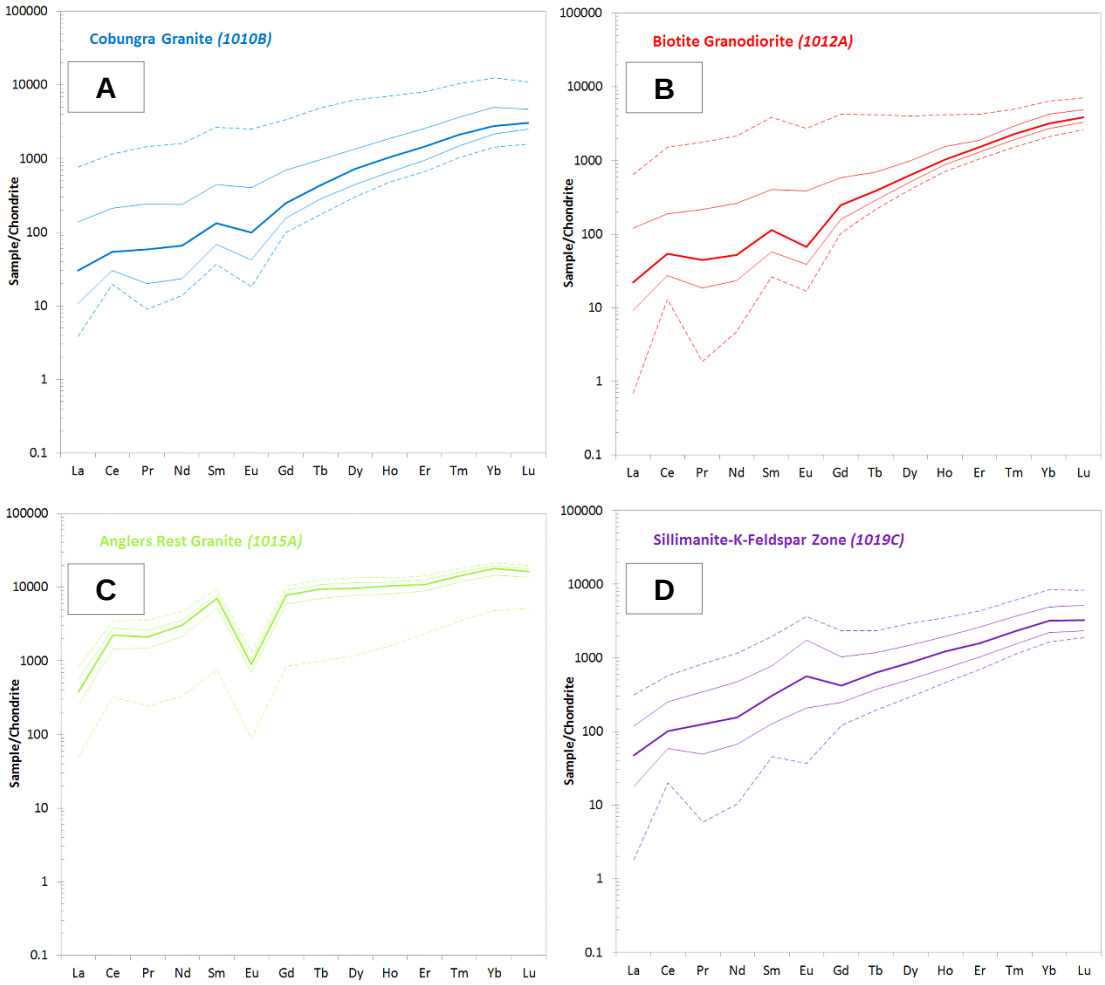

Figure 7.12. Distribution of rare earth element concentrations from zircon of four samples. See Figure 7.13 for key.

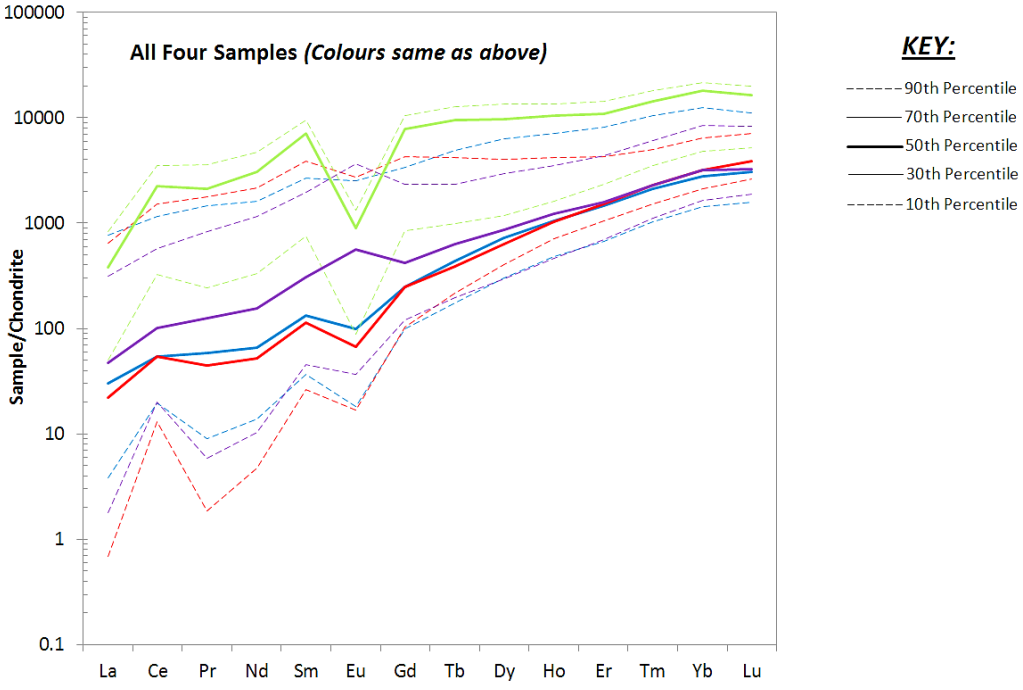

Figure 7.13. Distribution of rare earth element concentrations from zircon of four samples.

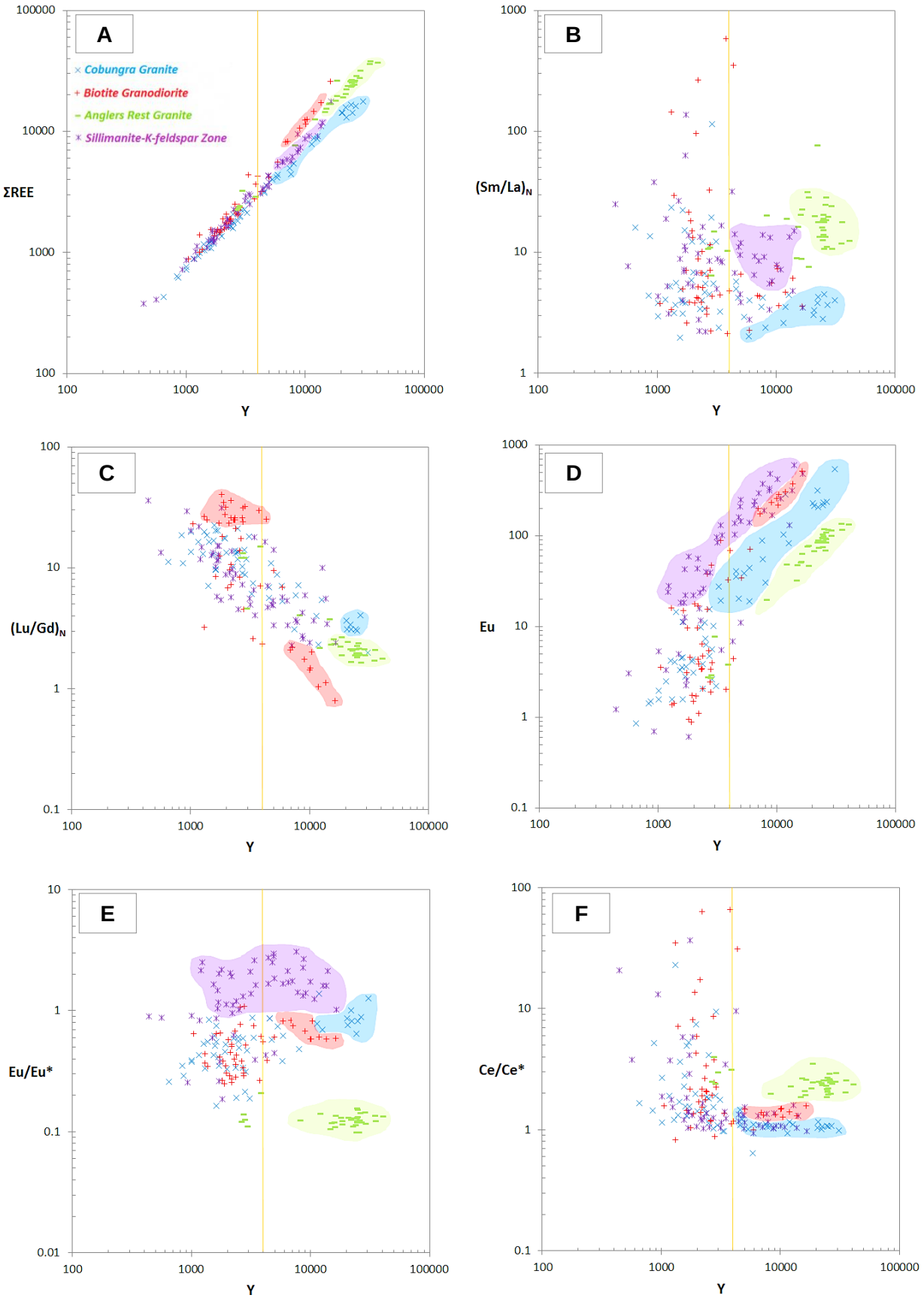
A
Cobungra Granite
Biotite Granodiorite
Anglers Rest Granite
Sillimanite-K-feldspar Zone
ΣREE
Y
B
(Sm/La)N
Y
C
(Lu/Gd)N
Y
D
Eu
Y
E
Eu/Eu*
Y
F
Ce/Ce*
Y

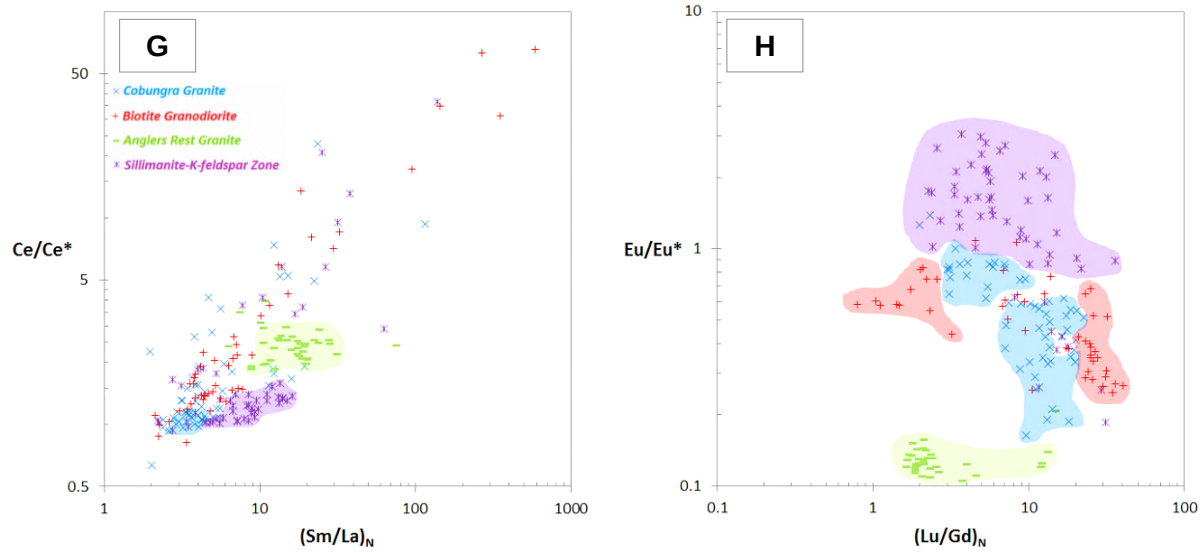

Figure 7.14. Bivariate plots of yttrium and rare earth element characteristics of zircon (in ppm or ratios) from four samples. Trace element patterns of analyses with >4000 ppm yttrium are different in comparison to analyses with <4000 ppm yttrium (orange line). 'N' subscript denotes chondrite normalised values.

Europium and Y have a positive correlation and Eu concentration is a good distinguisher of all four samples for analyses with >4000 ppm Y (Figure 7.14D). Europium anomalies are a good distinguisher of the Sillimanite-K-feldspar Zone sample in particular (Figure 7.14E) because of the high number of analyses with large positive Eu anomalies (median=1.4; maximum=3.1). Also of note from Figure 7.14E is the broad range of Eu/Eu* values for each sample for analyses with <4000 ppm Y and the narrow range for analyses >4000 ppm Y. There is also a weak positive correlation between Eu/Eu* and Y for all samples except the Anglers Rest Granite. For analyses >4000 ppm Y, Ce anomalies distinguish the Biotite Granodiorite and Cobungra Granite from each other but not the Sillimanite-K-feldspar Zone sample from the former two (Figure 7.14F). The Ce/Ce* and $(Sm/La)_N$ patterns are very similar when plotted against Y (Figure 7.14B,F). These two characteristics do in fact have a weak positive correlation (Figure 7.14G). The analyses in Figure 7.14G grouped in different samples are mostly those with >4000 ppm Y. Figure 7.14H shows that the degree of HREE fractionation and Eu anomalies are good ways of differentiating the samples.

7.3.4.2 ZIRCON NON-RARE EARTH ELEMENTS

All non-REE analysed have a positive correlation with Y and each other (Figure 7.15). Similar to REE, the patterns of non-REE (P, Ti, Nb, Ta & U) can distinguish the samples for analyses >4000 ppm Y (Figure 7.15A-D). These elements are generally better than the REE at distinguishing the Biotite Granodiorite from the other samples. The differing concentrations of P and Ti in each of the samples for analyses >4000 ppm Y (Figure 7.15A,B) is possibly associated with accessory minerals. Phosphorus and Ti are major components of the common crustal accessory minerals apatite and rutile, respectively. These minerals may have been present in some of the zircon grains as inclusions and consequently processed by the laser during analysis, or the minerals may have been crystallising in the magma at the same time as the zircon, thus influencing the composition of the zircon. Another explanation is that the zircon crystal lattices have been damaged and fluids have brought in ions that have been accommodated into the zircon. This hypothesis is supported by the geochronological data which shows all samples with disturbed U/Pb systems. Different fluids may contain differing concentrations of Ti and P ions (and other trace element ions), therefore producing the various trace element patterns of the samples, particularly for zircon with high trace element content (>4000 ppm Y).

Niobium plotted against Y distinguishes three of the samples well (Figure 7.15C), but not the Cobungra Granite (not included). Uranium content distinguishes the Cobungra Granite and Sillimanite-K-feldspar Zone samples from each other but not from either of the other two samples (Figure 7.15D). Thorium content and Th/U were not good distinguishers of the samples and hence were not included. Plots of P versus Ti and Nb versus Ta distinguish the samples well at high concentrations (Figure 7.15E,F). Niobium and Ta substitute at the same site in the zircon crystal lattice, and thus reflect the condition of the melt during crystallisation of zircon.

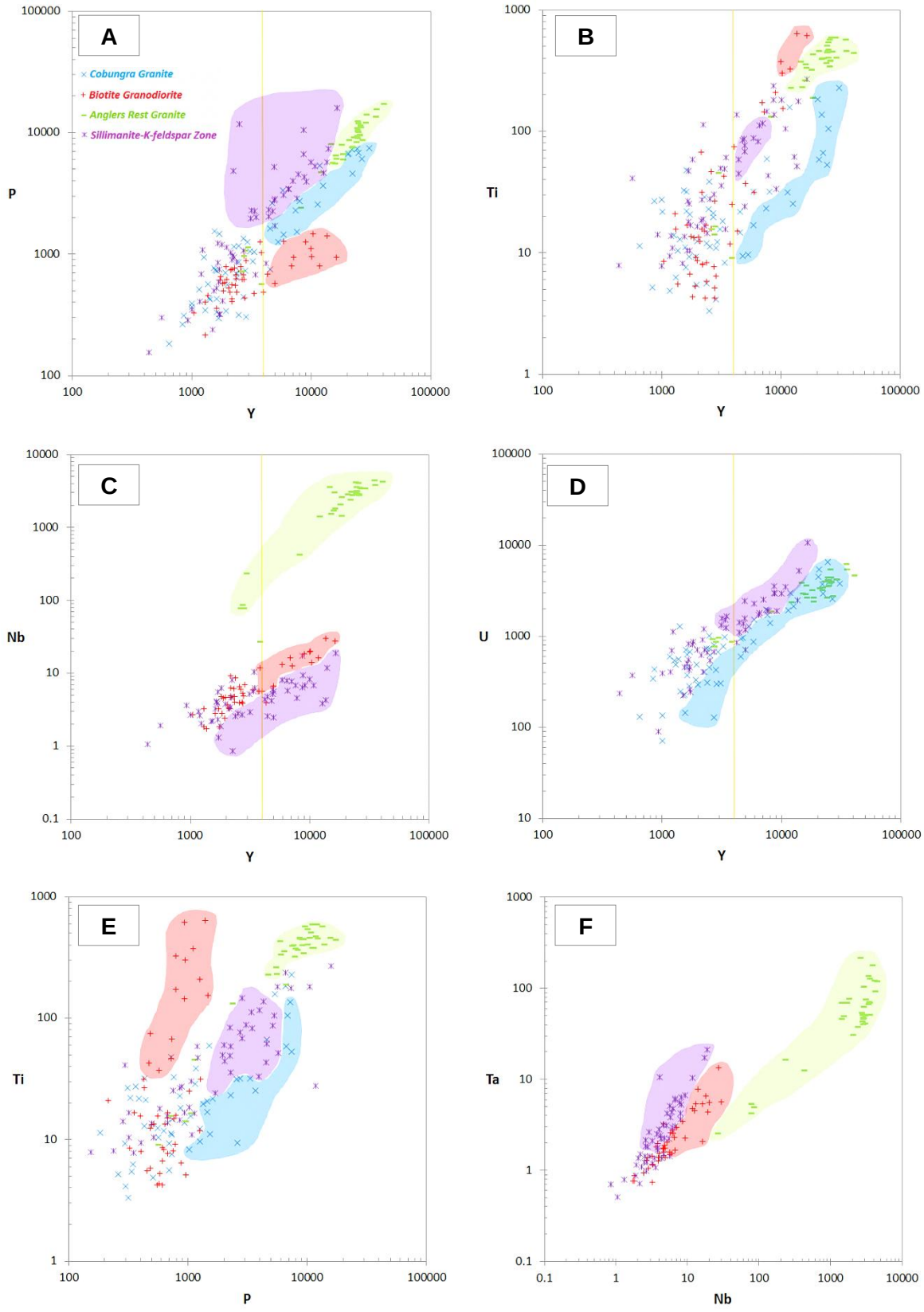

Figure 7.15. Bivariate plots of non-rare earth elements (ppm) in zircon of four samples. Patterns of analyses with >4000 ppm yttrium are different in comparison to analyses with <4000 ppm yttrium (orange line).

7.3.5 COMPARISON OF ZIRCON MORPHOLOGY, GEOCHRONOLOGY AND TRACE ELEMENTS

Zircon trace element data were compared to morphological and U/Pb data to investigate any relationships between the three. Yttrium was used to represent all trace elements in comparisons of zircon characteristics because of its positive correlation with other trace elements (Section 7.3.4). The $^{206}Pb/^{238}U$ ages were used to represent geochronological data. The concentration of ≈4000 ppm Y is an important value for distinguishing trace element patterns in different samples (Section 7.3.4). This value is also important for geochronological data, since only 8% of analyses yielding reliable ages (<30-33% central discordance and <2% common Pb) had >4000 ppm Y. This finding is shown on Figure 7.16A in the way that the analyses of the Biotite Granodiorite used for an age estimate of the rock (423.6 Ma) commonly have <4000 ppm Y. There is also a clustering of the Sillimanite-K-feldspar Zone and Cobungra Granite analyses at around ≈500 Ma (Figure 7.16A). These are the analyses that produced reliable detrital and inherited grain ages for those samples, and most of these analyses have <4000 ppm Y. Five analyses of the Anglers Rest Granite with <4000 ppm Y cluster at ≈400 Ma and these are thought to give some indication of an age for the rock (see Section 7.3.2). There is a negative correlation between Y and $^{206}Pb/^{238}U$ age, for analyses less than ≈600 Ma. The high-Y analyses have the greatest degree of Pb loss and hence the youngest ages. Central discordance and common Pb content both increase with increasing Y (Figure 7.16B,C). Analyses that produced reliable age data commonly have low Eu/Eu* values (Figure 7.16D). The samples show similar clustering patterns for low Eu/Eu* and $^{206}Pb/^{238}U$ age (Figure 7.16D) as they do for low-Y and $^{206}Pb/^{238}U$ age (Figure 7.16A). The range of ages of the Sillimanite-K-feldspar Zone analyses potentially provides an explanation for the large positive Eu anomalies of this sample. Evidently, the U/Pb system of these zircon grains has been open to the external environment and the crystal lattice is damaged. If a fluid

with anomalously high Eu content made contact with this zircon, then the ions could be accommodated into the zircon crystal lattice and produce zircon with large positive Eu anomalies. This sample also has the highest Eu anomaly value for whole-rock chemical analysis (0.93) (Section 6.3.2.2). Table 7.10 summarises the comparison of geochronological data and trace element data along with other comparisons addressed below.

There is also a link between trace element concentration and morphology of zircon. Analyses with low trace element concentrations had a high CL response and the analyses were commonly of clear oscillatory zoning, cores or towards the centre of grains. Conversely, analyses with high trace element concentrations had a low CL response and the analyses were commonly of ghosted oscillatory zoning or new zircon mantles. Figures 7.2-7.5 show examples of these textures along with $^{206}Pb/^{238}U$ ages and Y concentrations. The relationship between trace elements and CL response of the zircon in this study is in agreement that of other studies (Kempe et al. 2000; Poller et al. 2001) which reported a low CL response coinciding with high trace element concentrations. The findings are summarised in Table 7.10 using 4000 ppm Y to discriminate low and high trace element content. Ranges of Eu and Ce anomalies are also included in Table 7.10 with analyses >4000 ppm Y having higher Eu/Eu* values and a narrower range of Ce/Ce* values (except the Anglers Rest Granite). The samples in Table 7.10 are also ranked by percentage of sample with >4000 ppm Y. The five grains of the Anglers Rest Granite with <4000 ppm Y are shown in Figure 7.5G-K.

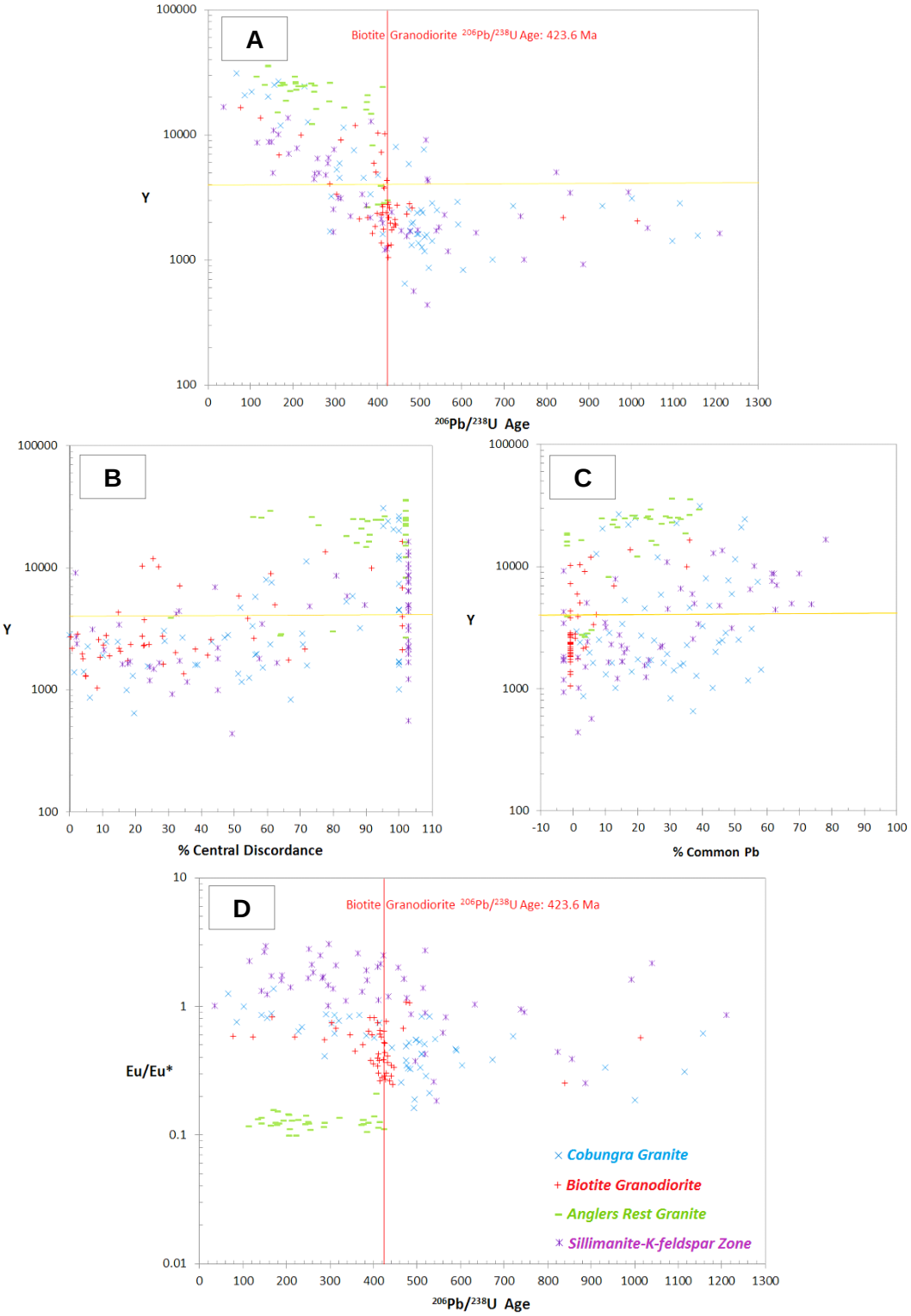

Figure 7.16. Comparison of yttrium, europium anomalies and U/Pb data of zircon including $^{206}Pb/^{238}U$ age (Ma), % central discordance and % common Pb. Common Pb percentages were estimated using the program ComPbCorr (Anderson 2002). Very few grains with >4000 ppm yttrium (orange line) yielded reliable age estimates (<30-33% central discordance and <2% common Pb). Plot A is truncated at 1300 Ma because of the few analyses above that age. Analyses of ≥100% central discordance may have values far greater than 100%. Anaylses with ≤0% common Pb have 0% common Pb – analyses were seperated from each other for ease of viewing.

Table 7.10. Comparison of morphological, geochronological and trace element characteristics of zircon from four samples for analyses with <4000 ppm and >4000 ppm yttrium. Outliers were ignored.

	<4000 ppm Y					>4000 ppm Y				
	% of Sample	CL & Morphology	$^{206}Pb/^{238}U$ age	Eu/Eu*	Ce/Ce*	% of Sample	CL & Morphology	$^{206}Pb/^{238}U$ age	Eu/Eu*	Ce/Ce*
Biotite Granodiorite	73%		357 – 483 Ma Age: 423.6 Ma	0.25 – 0.68	0.82 – 66	27%		77 – 423 Ma	0.39 – 0.84	1.00 – 1.6
Cobungra Granite	65%	High-CL / Light – Clear oscillatory zoning	Inherited grain ages	0.16 – 0.88	0.97 – 23	35%	Low-CL / Dark – Ghosting of oscillatory zoning	67 – 510 Ma	0.39 – 1.39	0.94 – 1.5
Sillimanite-K-feldspar Zone	57%	– Cores – Towards the centre of grains	Detrital ages	0.19 – 2.6	1.03 – 37	43%	– New zircon mantles	36 – 519 Ma	1.03 – 3.1	0.94 – 1.6
Anglers Rest Granite	13% (5 grains)		377 – 424 Ma	0.11 – 0.21	2.4 – 4.0	87%		114 – 412 Ma	0.10 – 0.16	1.9 – 3.5

CHAPTER 8

DISCUSSION

This chapter will summarise the main findings from the characterisation of petrography, mineral chemistry, whole-rock chemistry and zircon characteristics, as well as address the aim of determining whether the high-T metasedimentary rocks are the source of the S-type granites. Any unexpected results will be attempted to be explained and interpreted.

8.1 Metamorphic Rocks

Petrography and mineral chemistry was successfully documented for the Cordierite Zone and Sillimanite-K-feldspar Zone and whole-rock chemistry and zircon characteristics were analysed for one of the samples from the latter metamorphic zone. No fresh cordierite was found in any of these samples. The variety in shape of relict porphyroblasts in the Lower Cordierite Zone meant that both andalusite and cordierite were potential precursor minerals. However, analysis of the chemistry of pseudomorphing minerals indicated that cordierite is likely to be the only precursor mineral (Section 5.3.4).

Zircon in the Sillimanite-K-feldspar Zone, though heavily affected by Pb loss, had seven reliable analyses (from 58 analyses) providing the detrital age groupings of 500-550 Ma, 850-950 Ma and 2200 Ma (Section 7.3.2). This age pattern is consistent with published data from the widespread Ordovician turbidites of the Adaminaby Group from which the Omeo Metamorphic Complex rocks are derived (Fergusson & Fanning 2002). The data from Fergusson and Fanning (2002) show large peaks at approximately 500 Ma and 1000 Ma, and other groups of ages at 1700 Ma, 2200 Ma and 2700 Ma (Figure 8.1). These results are similar to the abovementioned values from the present study.

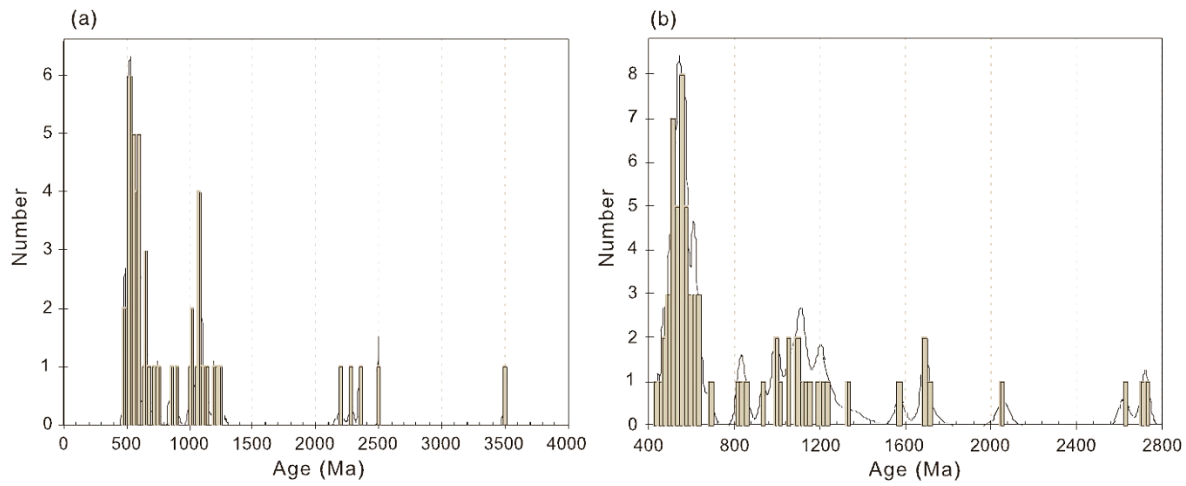

Figure 8.1. Combined histogram and relative probability distribution of detrital-zircon age spectra for the quartz sandstone samples of the Adaminaby Group from the (a) Genoa River and (b) Shoalhaven River.

The Sillimanite-K-feldspar Zone zircon exhibited relatively large positive Eu anomalies with median and maximum values of 1.4 and 3.1 respectively (Section 7.3.4.1). This is a very uncommon result as Eu anomalies in zircon are commonly <1 or sightly >1 (Hoskin & Schaltegger 2003). Analyses with Eu anomalies >1 did not provide reliable age data which means that the U/Pb system of these grains is open and their crystal lattices are damage. These grains are therefore able to accommodate trace elements into their crystal lattices from the outside the grains and potentially develop large positive Eu anomalies. Diagenesis can provide the environment for fluids to have a positive Eu anomaly (MacRae et al. 1992; Martinez-Ruiz et al. 1999). These studies found that positive Eu anomalies can be produced during deposition and early diagenesis of sediment under strong reducing conditions. The process is rare but it is possible that the zircon in Sillimanite-K-feldspar Zone metasedimentary rocks have undergone this process at some point. A future study could examine trace elements in zircon from the Cordierite Zone to investigate whether large Eu anomalies are present in zircon from that location and for a comparison of other trace element characteristics.

8.2 Granites

Two varieties of the S-type Cobungra Granite were sampled in this study including eleven samples of the xenolithic main variety of Cobungra Granite (referred to in this study simply as Cobungra Granite) and one sample of a subtype that is free of any country rock, known as the Biotite Granodiorite. The Biotite Granodiorite had a typical igneous microstructure in thin section and had the most calcic plagioclase of all samples. The Cobungra Granite had abundant country rock material visible in thin section although one particularly igneous sample was described (Section 4.3.3). There were differences in the zircon characteristics of these two contrasting varieties of Cobungra Granite. The Biotite Granodiorite zircon grains were commonly oscillatory zoned, generally had lower trace element content and provided a crystallisation age of 423.6 ± 4.8 Ma. This age is ≈10 Ma older than the K/Ar biotite age of 411 ± 6 Ma given by Willman et al. (1999). The discrepancy is probably due to the slow cooling of the pluton and the K/Ar system being set at a later stage. The crystallisation age attained in this study is similar to other U/Pb zircon ages of S-type granites in the south-eastern Lachlan Fold Belt: 416.1 ± 4 Ma for the Round Flat Tonalite of the Jindabyne Suite (Kemp et al. 2005); 422.0 ± 1.5 Ma for the Hawksview Adamellite (Keay et al. 1999); 419.9 ±1.7 Ma for the Bethanga Granite (Keay et al. 1999); and 418 ± 4 Ma for the Kosciusko Tonalite (Belousova et al. 2006).

Only one analysis of the Biotite Granodiorite had an inherited grain age. This analysis was of the core of a grain (see Figure 7.2K) and gave an age of 840 ± 15 Ma. This age is similar to some analyses of the detrital age pattern from the Sillimanite-K-feldspar Zone. If more of these core/rim grains were present in the Biotite Granodiorite sample and more analyses of the cores yielded reliable age information, then an argument could be made for the high-T metasedimentary rocks being the source for the adjacent S-type granites. To make this connection, a single sample must have both a crystallisation age and have an

age pattern of inherited grains similar to the detrital pattern. The eight reliable age analyses of the Cobungra Granite gave an age pattern of inherited grains similar to the detrital age pattern but no crystallisation age so this sample could not be used to support the abovementioned hypothesis. Therefore, the U/Pb data was too disturbed to be useful. However, the trace element data from zircon analyses showed that the metasedimentary sample was distinct from the granite samples suggesting that the source of the S-type magmatism is different to the exposed high-T metasedimentary rocks. Detailed mapping of Cobungra Granite exposures in creeks and the contact with the metasedimentary rocks would be beneficial in investigating the nature of the interaction between these rocks as the outcrops show a complex relationship.

High trace element content is a feature of all zircon samples in this study and this is typical for granites (Belousova et al. 2002). A significant finding of this study is that zircon trace element patterns are able to distinguish all four samples for analyses with >4000 ppm Y. A link between trace element content and geochronological data was found in that analyses with high trace element content did not yield reliable age measurements. This connection is complimented by morphological data since analyses with high trace element content were commonly of ghosted oscillatory zoning or new zircon mantles, and analyses with high trace element content were commonly of clear oscillatory zoning, of cores or towards the centre of grains. The fact that trace elements are concentrated towards the exterior of grains means that the event that formed these high trace element domains was relatively recent. A possible event is the greenschist facies retrogressive event that formed much of the secondary muscovite seen in thin sections of Cordierite Zone, Sillimanite-K-feldspar Zone and Cobungra Granite samples. This interpretation only applies to the three zircon samples other than the Anglers Rest Granite as 90% of the zircon grains from this sample are structureless.

Zircon from the Anglers Rest Granite has exceptionally high trace element content (median Y=24079 ppm; median ΣREE=33607 ppm; median P=8664 ppm). There is evidence that this rock has been hydrothermally altered as plagioclase and K-feldspar identified in thin section have been recrystallised to nearly pure albite (Section 5.3.3). The combination of hydrothermal alteration and high trace element content in the zircon points to a damaged crystal lattice. The near-complete dissolution of zircon during ICP-MS analysis (Section 6.3.2.1) gives support to a damaged crystal lattice which would readily accept trace elements from hydrothermal fluids. REE characteristics of hydrothermally altered zircon from the Boggy Plain Zoned Pluton (south-eastern Lachlan Fold Belt) (Hoskin 2005) are similar to those of zircon from the Anglers Rest Granite. Both are enriched in REE relative to igneous zircon and both have reduced Ce anomalies (Anglers Rest Granite <4.0; Boggy Plain Zoned Pluton <4.2). An unaltered sample of the Anglers Rest Granite would be useful in investigating the effects of hydrothermal alteration on zircon but no such sample was found.

REFERENCES

ANDERSON J. A. C., WILLIAMS I. S., PRICE R. C. & FLEMING P. D. 1996. U-Pb zircon ages from the Koetong Adamellite: Implication for granite genesis and the local basement in NE Victoria. *Geological Society of Australia Abstracts 42,* 1-2.

ANDERSON T. 2002. Correction of common lead in U-Pb analyses that do not report ^{204}Pb. *Chemical Geology 192*, 59-79.

BEAVIS F. C. 1962. The geology of the Kiewa area. *Proceedings of the Royal Society of Victoria 75*, 349-410.

BELOUSOVA E. A., GRIFFIN W. L., O'REILLY S. Y. & FISHER N. I. 2002. Igneous zircon: Trace element composition as an indicator of source rock type. *Contributions to Mineralogy and Petrology 143*, 602-622.

BELOUSOVA E. A., GRIFFIN W. L. & O'REILLY S. Y. 2006. Zircon crystal morphology, trace element signatures and Hf isotope composition as a tool for petrogenetic modelling: examples from eastern Australian granitoids. *Journal of Petrology 47,* 329-353.

CAS R. A. F. & VANDENBERG A. H. M. 1988. Ordovician. *In:* Douglas J.G. & Ferguson J.A. eds. *Geology of Victoria,* pp. 63-102. Geological Society of Australia, Victorian Division, Melbourne.

CAS R. A. F., O'HALLORAN G. J., LONG J. A. & VANDENBERG A. H. M. 2003. Middle Devonian to Carboniferous: Late to post-tectonic sedimentation and magmatism in an arid continental setting. *In:* Birch W. D. ed. *Geology of Victoria*, pp. 157-193. Geological Society of Australia Special Publication 23. Geological Society of Australia (Victoria Division).

CORFU F., HANCHAR J. M., HOSKIN P. W. O. & KINNY P. 2003. Atlas of Zircon Textures. *Reviews in Mineralogy and Geochemistry 53*, 469-500.

CROHN P. W. 1950. The geology, petrology and physiography of the Omeo district, North-Eastern Victoria. *Proceedings of the Royal Society of Victoria 62*, 1-70.

DEER W. A., HOWIE R. A. & ZUSSMAN J. 1992. *An Introduction to the Rock-Forming Minerals: 2nd Ed.* Pearson Education Limited, England.

EVERNDEN J. F. & RICHARDS J. R. 1962. Potassium-argon ages in eastern Australia. *Journal of the Geological Society of Australia 9,* 1-49.

FAGAN R. K. 1979. Deformation, metamorphism and anatexis of an Early Palaeozoic flysch sequence in northeastern Victoria. PhD thesis. University of New England, Armidale (unpubl.).

FERGUSSON C. L. & TYE S. C. 1999. Provenance of Early Palaeozoic sandstones, southeastern Australia, Part 1: vertical changes through the Bengal fan-type deposit. *Sedimentary Geology 125*, 135-151.

FERGUSSON C. L. & FANNING C. M. 2002. Late Ordovician stratigraphy, zircon provenance and tectonics, Lachlan Fold Belt, south-eastern Australia. *Australian Journal of Earth Sciences 52,* 423-436.

FERGUSSON C. L. & VANDENBERG A. H. M. 2003. Ordovician: The development of craton-derived deep-sea turbidite successions. *In:* Birch W. D. ed. *Geology of Victoria*, pp. 95-115. Geological Society of Australia Special Publication 23. Geological Society of Australia (Victoria Division).

FINCH R. J. & HANCHAR J. M. 2003. Structure and Chemistry of Zircon and Zircon Group Minerals. *Reviews in Mineralogy and Geochemistry 53*, 1-25.

GRAY D. R. & FOSTER D. A. 2004. Tectonic evolution of the Lachlan Orogen, southeast Australia: historical review, data synthesis and modern perspectives. *Australian Journal of Earth Sciences 51*, 773-817.

GRIFFIN W. L., POWELL W. J., PEARSON N. J., & O'REILLY S. Y. 2008. Glitter: Data reduction software for Laser Ablation ICP-MS. *Mineralogical Association of Canada Short Course 40, Vancouver, B.C, Appendix A2,* 204-207.

HENDRICKX M. A., WILLMAN C. E., MAGART A. P. M., ROONEY S., VANDENBERG A.H.M., ORANSKAIA A. & WHITE A. J. R. 1996. The geology and prospectivity of the Murrungowar 1:100 000 map geological report. *Victorian Initiative for Minerals and Petroleum Report 26*. Geological Survey of Victoria, Department of Natural Resources & Environment.

HOSKIN P. W. O. & SCHALTEGGER U. 2003. The Composition of Zircon and Igneous and Metamorphic Petrogenesis. *Reviews in Mineralogy and Geochemistry 53*, 27-62.

HOSKIN P. W. O. 2005. Trace-element composition of hydrothermal zircon and the alteration of Hadean zircon from the Jack Hills, Australia. *Geochimica et Cosmochimica Acta 69,* 637-648.

HUMPHRIES S. E. 1984. The mobility of the rare earth elements in the crust. *In:* Henderson P. ed. *Rare earth element chemistry*. pp. 315-341. Elsevier, Amsterdam.

JACKSON S. E., PEARSON N. J., GRIFFIN W. L. & BELOUSOVA E. A. 2004. The application of laser ablation-inductively coupled plasma-mass spectrometry to in situ U-Pb zircon geochronology. *Chemical Geology 211*, 47-69.

KEAY S., STEELE D. & COMPSTON W. 1999. Identifying granite sources by SHRIMP U-Pb zircon geochronology: An application to the Lachlan Fold Belt. *Contributions to Mineralogy and Petrology 137,* 323-341.

KEMP A. I. S., WHITEHOUSE M. J., HAWKESWORTH C. J., ALARCON M. K. 2005. A zircon U-Pb study of metaluminous (I-type) granites of the Lachlan Fold Belt, southeastern Australia: Implication for the high/low temperature classification and magma differentiation processes. *Contributions to Mineralogy and Petrology 150,* 230-249.

KEMPE U., GRUNER T., NASDALA L. & WOLF D. 2000. Relevance of cathodoluminescence for the interpretation of U-Pb zircon ages, with an example of an application to a study of zircons from the Saxonian Granulite Complex, Germany. *In:* Pagel M., Barbin V., Blanc P. & Ohnenstetter D. eds. *Cathodoluminescence in Geosciences.* pp. 415-455. Springer-Verlag, Berlin–Heidelberg.

KOSLER J. & SYLVESTER P. J. 2003. Present trends and the future of zircon in geochronology: Laser Ablation ICPMS. *Reviews in Mineralogy and Geochemistry 53*, 243-275.

LUDWIG K. R. 2009. *Isoplot v3.6. A Geochronological Toolkit for Microsoft Excel.* Berkeley Geochronology Center. Berkeley, CA.

MACRAE N. D., NESBITT H. W. & KRONBERG B. I. 1992. Development of a positive Eu anomaly during diagenesis. *Earth and Planetary Science Letters 109,* 585-591.

MARTINEZ-RUIZ F., ORTEGA-HUERTAS M. & PALOMO I. 1999. Positive Eu anomaly development during diagenesis of the K/T boundary ejecta layer in the Agost section (SE Spain): Implications for trace element remobilization. *Terra Nova 11,* 290-296.

MORAND V. J. 1990. Low-pressure regional metamorphism in the Omeo Metamorphic Complex, Victoria, *Australia. Journal of Metamorphic Geology 8*, 1-12.

MORAND V. J. & GRAY D. R. 1991. Major fault zones related to the Omeo Metamorphic Complex, northeastern Victoria. *Australian Journal of Earth Sciences 38*, 203-221.

MORAND V. J., VANDENBERG A. H. M., HAYDON S. J & HENDRICKX M. A. 1999. *Omeo 1:50 000 geological map.* Geological Survey of Victoria.

NASDALA L., ZHANG M., KEMPE U., PANCZER G., GAFT M., ANDRUT M. & PLOTZE M. 2003. Spectroscopic methods applied to zircon. *Reviews in Mineralogy and Geochemistry 53*, 427-467.

NORMAN M. D., PEARSON N. J., SHARMA A. & GRIFFIN W. L. 1996. Quantitative analysis of trace elements in geological materials by laser ablation ICPMS: Instrumental operating conditions and calibration values of NIST glasses. *Geostandards Newsletter 20*, 247-261.

PATERSON B. A., STEPHENS W. E., ROGERS G., WILLIAMS I. S., HINTON R. W. & HERD D. A. 1992. The nature of zircon inheritance in two granite plutons. *Transactions of the Royal Society of Edinburgh: Earth Sciences 83,* 459-471.

PEARCE J. A. 1983. Role of the sub-coninental lithosphere in magma genesis at active continental margins. *In:* Hawkesworth C. J. & Norry M. J. eds. *Continental basalts and mantle xenoliths.* pp. 230-249. Shiva, Nantwich.

POLLER U., HUTH J., HOPPE P., WILLIAMS I. S. 2001. REE, U, Th, and Hf distribution in zircon from Western Carpathian Variscan granitoids: A combined cathodoluminescence and ion microprobe study. *American Journal of Science 301*, 858-876.

RAMSAY W. R. H. & VANDENBERG A. H. M. 1986. Metallogeny and tectonic development of the Tasman Fold Belt System in Victoria. *Ore Geology Reviews 1*, 213-257.

RICHARDS J. R. & SINGLETON O. P. 1981. Palaeozoic Victoria, Australia: Igneous rocks ages and their interpretation. *Journal of the Geological Society of Australia 28*, 395-421.

ROSSITER A. G. 2003. Granitic Rocks of the Lachlan Fold Belt in Victoria: Potential keys to the composition of the lower-middle crust. *In:* Birch W. D. ed. *Geology of Victoria*, pp. 217-237. Geological Society of Australia Special Publication 23. Geological Society of Australia (Victoria Division).

ROLLINSON H. 1993. *Using geochemical data: Evaluation, presentation, evaluation.* Longman House, Harlow.

RUDNICK R. L. & GAO S. 2004. Composition of the continental crust. *In:* Holland H. D. & Turekian. K. K. (eds.) *Treatise on Geochemistry.* Amsterdam, Elsevier, 3: 1-64.

SIMPSON C. J., SIMS, J. P. & ORANSKAIA A. 1996. The geology and prospectivity of the Mt Elizabeth area, Eastern Highlands VIMP area. *Victorian Initiative for Minerals and Petroleum Report 19*. Department of Agriculture, Energy & Minerals, Victoria.

SIMPSON C. J., FERGUSSON, C. L. & ORANSKAIA A. 1997. Craigie 1:100 000 map area geological report. *Geological Survey of Victoria Report 111*.

SIMPSON C. J., HENDRICKS M. A., BIBBY L. M., ALLEN R., PAGE D., WOODFULL C. J., FERGUSSON C. L. & CARNEY C. 2001. Corryong 1:100 000 map area geological report. *Geological Survey of Victoria Report 120*.

SUN S. S. & MCDONOUGH W. F. 1989. Chemical and isotopic systematics of oceanic basalts: implications for mantle composition and processes. *In:* Saunders A. D. & Norry H. J. eds. *Magmatism in ocean basins.* pp. 313-345. Geological Society of London Special Publication No. 42.

TAYLOR S. R. & MCLENNON S. M. 1985. *The continental crust: Its composition and evolution.* Blackwell Scientific Publications, Oxford.

VANDENBERG A. H. M. 2003. Silurian to Early Devonian: The Lachlan Fold Belt at its most diverse. *In:* Birch W. D. ed. *Geology of Victoria*, pp. 117-155. Geological Society of Australia Special Publication *23*. Geological Society of Australia (Victoria Division).

VANDENBERG A. H. M., NOTT R. J. & GLEN R. A. 1991. Bendoc 1:100 000 Map Geological Report. *Geological Survey Report 90*.

VANDENBERG A. H. M., HENDRICKX M. A., WILLMAN C. E., MAGART A. P. M., SIMONS B. A. & RYAN S. M. 1998. Benambra 1:100 000 map area geological report. *Geological Survey Report 114*.

VANDENBERG A. H. M., WILLMAN C. E., MAHER S., SIMONS B. A., CAYLEY R. A., TAYLOR D. H., MORAND V. J., MOORE D. H. & RADOJKOVIC A. 2000. The Tasman Fold Belt System in Victoria. *Geological Survey of Victoria Special Publication.*

WEIDENBECK M., ALLE P., CORFU F., GRIFFIN W. L., MEIER M., OBERLI F., VON QUADT A., RODDICK J. C. & SPIEGEL W. 1995. Three natural zircon standards for U-Th-Pb, Lu-Hf, trace element and REE analyses. *Geostandards Newsletter 19*: 1-24.

WHITE A. J. R., CHAPPELL B. W. & CLEARY J. R. 1974. Geologic setting and emplacement of some Australian Palaeozoic batholiths and implications for intrusive mechanisms. *Pacific Geology 8,* 159-171.

WILLIAMS I. S. 1992. Some observations on the use of zircon U-Pb geochronology in the study of granitic rocks. *Transactions of the Royal Society of Edinburgh: Earth Sciences 83,* 447-458.

WILLIAMS I. S. 1995. Zircon analysis by ion microprobe: The case of the eastern Australian granites. *In: Leon T. Silver 70th Birthday Symposium and Celebration,* pp. 27-31. California Institute of Technology, Pasadena.

WILLIAMS I. S., CHAPPELL B. W., CROOK K. A. W. & NICOLL R. S. 1994. In search of the provenance of the ealy Palaeozoic flysch in the Lachlan Fold Belt, southeastern Australia. *Geological Society of Australia Abstracts 37,* 464.

WILLMAN C. E., MORAND V. J., HENDRICKX M. A., VANDENBERG A. H. M., HAYDON S. J. & CARNEY C. 1999. Omeo 1:100 000 map geological report. *Geological Survey of Victoria Report 118*.

WILLMAN C. E., VANDENBERG A. H. M. & MORAND V. J. 2002. Evolution of the southeastern Lachlan Fold Belt in Victoria. *Austalian Journal of Earth Sciences 49*, 271-289.

WINTER J. D. 2010. *An Introduction to Igneous and Metamorphic Petrology. (2nd Ed.)* Pearson Education, New Jersey.

WYBORN D., TURNER B. S. & CHAPPELL B. W. 1987. The Boggy Plain Supersuite: a distinctive belt of I-type igneous rocks of potential economic significance in the Lachlan Fold Belt. J*ournal of the Geological Society of Australia 34*, 21-43.

XU G., POWELL R., WILSON C. J. L. & WILL T. M. 1994. Contact metamorphism around the Stawell granite, Victoria, Australia. *Journal of Metamorphic Geology 12*, 609-624.

APPENDICES

Appendix A: GPS Coordinates of Sample Locations

GPS points – AGD66 Datum

Lithology	Sample Number	Northing	Easting
Cordierite Zone	1001 A, B, C & D	0557742	5902331
	1002 A & B	0557214	5901123
	1003 A	0556932	5900274
	1004 A & B	0555322	5900077
Cobungra Granite	1007 A	0553725	5893778
	1008 A	0553688	5893868
	1009 A	0553633	5894045
	1010 A & B	0553486	5894410
	1011 A	0553365	5894710
Biotite Granodiorite	1012 A	0553314	5894932
Cobungra Granite	1013 A, B, C & D	0552160	5901804
	1014 A	0552171	5901736
Anglers Rest Granite	1015 A	0547918	5904381
Garnet-bearing leucogranite	1016 A	0553350	5899510
Sillimanite-K-feldspar Zone	1017 A & B	0558467	5891849
	1018 A	0558009	5892477
	1019 A, B & C	0557911	5892420
	1023 A	0557079	5893200
Cordierite Zone	1024 A	0558772	5904098
	1025 A & B	0557723	5901894

Appendix B: Mineral Chemistry Data

Sample No.	1012A	1012A	1012A	1012A	1012A	1012A	1010B	1010B	1010B	1010B	1010B	1010B	1010B	1010B	1010B	1010B	1010B
Analysis No.	2.1	2.8	1.4	1.5	1.6	2.2	1.8	2.10	2.2	2.3	2.4	2.5	3.4	3.6	2.15	2.16	2.17
Mineral	Biotite	Biotite	Biotite	Biotite	Biotite	Biotite	Biotite	Biotite	Biotite	Biotite	Biotite	Biotite	Biotite	Biotite	Biotite	Biotite	Biotite
SiO_2	35.21	34.88	35.08	35.42	34.86	35.68	35.35	35.28	34.68	34.96	35.03	34.86	35.09	34.90	35.11	33.23	34.72
TiO_2	2.83	1.63	2.45	2.51	2.75	2.67	2.54	2.66	2.79	2.76	2.63	2.53	2.44	2.31	3.13	2.28	3.09
Al_2O_3	17.49	17.03	16.78	17.64	17.18	17.51	18.70	20.13	19.58	19.29	19.92	19.02	19.09	19.38	19.73	19.48	19.42
Cr_2O_3	0.01	0.02	0.01	0.03	0.07	0.04	0.01	0.02	0.06	0.04	0.03	0.05	0.03	0.07	0.10	0.06	0.05
Fe_2O_3	0.00	0.00	0.00	0.00	0.00	0.00	0.00	0.00	0.00	0.00	0.00	0.00	0.00	0.00	0.00	0.00	0.00
FeO	20.83	21.54	21.21	20.48	20.90	20.96	19.26	19.14	19.22	19.21	18.73	19.67	19.08	19.62	19.41	21.38	19.32
MnO	0.27	0.29	0.31	0.24	0.27	0.25	0.16	0.20	0.24	0.21	0.21	0.21	0.21	0.22	0.20	0.22	0.17
MgO	8.77	8.82	8.42	8.02	8.61	8.35	8.40	8.68	8.60	8.79	8.46	9.07	8.97	8.90	8.42	9.37	8.47
CaO	0.00	0.05	0.03	0.02	0.06	0.01	0.06	0.00	0.02	0.00	0.01	0.00	0.05	0.00	0.02	0.04	0.03
Na_2O	0.28	0.25	0.31	0.27	0.28	0.26	0.46	0.31	0.39	0.34	0.37	0.31	0.37	0.34	0.28	0.32	0.31
K_2O	9.76	9.53	9.65	9.57	9.70	9.73	9.12	9.47	9.17	9.25	9.10	9.23	9.04	8.49	9.17	7.22	9.18
Total	95.45	94.03	94.26	94.21	94.69	95.45	94.06	95.89	94.75	94.85	94.49	94.95	94.36	94.24	95.58	93.59	94.76
Cations	Numbers of cations on the basis of 22O																
Si	5.423	5.476	5.491	5.505	5.424	5.489	5.450	5.330	5.313	5.349	5.355	5.342	5.387	5.360	5.326	5.170	5.319
Ti	0.328	0.192	0.288	0.293	0.321	0.309	0.295	0.303	0.322	0.318	0.303	0.291	0.282	0.267	0.357	0.266	0.356
Al	3.176	3.152	3.096	3.234	3.152	3.174	3.400	3.584	3.536	3.479	3.591	3.437	3.454	3.509	3.528	3.574	3.508
Cr	0.001	0.002	0.002	0.004	0.009	0.004	0.001	0.003	0.007	0.005	0.004	0.006	0.004	0.009	0.013	0.007	0.006
Fe^{3+}	0.000	0.000	0.000	0.000	0.000	0.000	0.000	0.000	0.000	0.000	0.000	0.000	0.000	0.000	0.000	0.000	0.000
Fe^{2+}	2.683	2.829	2.776	2.663	2.719	2.696	2.484	2.418	2.463	2.457	2.395	2.522	2.449	2.520	2.463	2.783	2.475
Mn	0.035	0.038	0.041	0.031	0.036	0.032	0.021	0.025	0.031	0.027	0.027	0.027	0.027	0.029	0.026	0.030	0.023
Mg	2.014	2.064	1.963	1.858	1.997	1.913	1.930	1.954	1.964	2.003	1.927	2.072	2.052	2.036	1.904	2.173	1.934
Ca	0.001	0.008	0.005	0.004	0.010	0.002	0.010	0.000	0.003	0.000	0.002	0.000	0.008	0.000	0.003	0.006	0.005
Na	0.083	0.077	0.094	0.083	0.085	0.078	0.137	0.091	0.115	0.101	0.109	0.092	0.110	0.102	0.081	0.095	0.091
K	1.918	1.910	1.927	1.898	1.926	1.909	1.794	1.824	1.792	1.806	1.775	1.804	1.770	1.663	1.774	1.432	1.794
Total	15.662	15.748	15.683	15.573	15.679	15.606	15.521	15.532	15.546	15.545	15.487	15.593	15.543	15.496	15.475	15.537	15.511
K-site	2.002	1.995	2.026	1.985	2.021	1.989	1.941	1.915	1.910	1.907	1.886	1.896	1.888	1.766	1.858	1.534	1.890
Ti cations	0.328	0.192	0.288	0.293	0.321	0.309	0.295	0.303	0.322	0.318	0.303	0.291	0.282	0.267	0.357	0.266	0.356
X_{Fe}	0.571	0.578	0.586	0.589	0.577	0.585	0.563	0.553	0.556	0.551	0.554	0.549	0.544	0.553	0.564	0.561	0.561

Sample No.	1019C	1019C	1019C	1019C	1019C	1019C	1019C	1001D	1001D	1001D	1001D	1001D	1001D	1004A	1004A	1004A	1004A
Analysis No.	1.3	1.4	2.2	3.1	3.2	4.6	4.7	1.15	2.12	2.14	3.8	4.18	4.19	1.6	1.7	2.8	2.9
Mineral	Biotite	Biotite	Biotite	Biotite	Biotite	Biotite	Biotite	Biotite	Biotite	Biotite	Biotite	Biotite	Biotite	Biotite	Biotite	Biotite	Biotite
SiO_2	34.88	34.63	35.65	35.04	34.59	34.30	34.13	46.70	49.64	50.31	46.67	42.52	47.17	35.65	35.12	35.97	35.76
TiO_2	3.24	3.02	2.90	2.23	1.93	2.56	2.68	0.73	0.33	0.57	0.54	1.07	0.54	2.53	3.04	2.96	2.97
Al_2O_3	19.81	19.25	19.96	19.53	19.56	19.56	19.49	35.32	33.36	27.63	32.03	23.19	31.39	18.86	19.49	19.54	19.52
Cr_2O_3	0.10	0.10	0.08	0.07	0.03	0.06	0.06	0.01	0.02	0.02	0.00	0.00	0.04	0.09	0.12	0.08	0.08
Fe_2O_3	0.00	0.00	0.00	0.00	0.00	0.00	0.00	0.00	0.00	0.00	0.00	0.00	0.00	0.00	0.00	0.00	0.00
FeO	20.31	20.49	20.43	20.18	20.11	20.24	20.24	1.01	1.56	4.99	2.85	11.73	3.90	19.34	18.88	18.15	18.77
MnO	0.12	0.16	0.17	0.16	0.22	0.17	0.17	0.00	0.00	0.02	0.01	0.08	0.03	0.12	0.10	0.14	0.14
MgO	7.70	7.49	7.32	8.00	8.74	8.42	8.04	0.69	0.54	0.68	1.83	5.85	1.36	9.31	8.47	8.59	8.39
CaO	0.05	0.06	0.00	0.04	0.04	0.05	0.02	0.06	0.03	0.07	0.01	0.11	0.04	0.01	0.05	0.07	0.06
Na_2O	0.31	0.38	0.31	0.29	0.32	0.35	0.28	1.19	1.12	1.00	0.88	0.17	0.65	0.20	0.26	0.19	0.30
K_2O	9.02	9.01	9.25	9.00	8.92	9.14	9.16	8.51	8.60	7.37	8.67	7.16	7.74	8.60	8.74	8.82	8.83
Total	95.52	94.60	96.07	94.54	94.45	94.84	94.27	94.27	95.25	92.71	93.59	92.14	92.98	95.05	94.50	94.80	95.08
Cations	Numbers of cations on the basis of 22O																
Si	5.313	5.343	5.394	5.390	5.330	5.279	5.287	6.209	6.520	6.862	6.326	6.190	6.421	5.430	5.373	5.456	5.429
Ti	0.371	0.351	0.330	0.258	0.224	0.296	0.313	0.073	0.032	0.058	0.055	0.117	0.055	0.290	0.349	0.338	0.339
Al	3.557	3.502	3.561	3.540	3.554	3.549	3.559	5.536	5.166	4.443	5.118	3.981	5.038	3.388	3.516	3.494	3.493
Cr	0.012	0.013	0.009	0.008	0.003	0.007	0.007	0.001	0.002	0.002	0.000	0.000	0.004	0.011	0.014	0.010	0.009
Fe^{3+}	0.000	0.000	0.000	0.000	0.000	0.000	0.000	0.000	0.000	0.000	0.000	0.000	0.000	0.000	0.000	0.000	0.000
Fe^{2+}	2.588	2.644	2.586	2.596	2.591	2.605	2.623	0.112	0.171	0.569	0.323	1.428	0.444	2.464	2.416	2.302	2.383
Mn	0.015	0.021	0.022	0.021	0.029	0.022	0.022	0.000	0.000	0.002	0.001	0.010	0.003	0.015	0.012	0.018	0.018
Mg	1.747	1.721	1.650	1.833	2.007	1.932	1.856	0.137	0.105	0.138	0.370	1.270	0.276	2.115	1.932	1.943	1.898
Ca	0.008	0.009	0.000	0.006	0.007	0.008	0.003	0.008	0.004	0.010	0.002	0.017	0.005	0.002	0.008	0.011	0.010
Na	0.091	0.114	0.090	0.087	0.096	0.104	0.084	0.305	0.285	0.266	0.232	0.048	0.171	0.059	0.076	0.057	0.088
K	1.752	1.774	1.786	1.767	1.753	1.794	1.811	1.443	1.441	1.283	1.499	1.329	1.343	1.672	1.706	1.707	1.710
Total	15.454	15.493	15.429	15.505	15.593	15.596	15.565	13.824	13.727	13.632	13.926	14.391	13.760	15.446	15.403	15.336	15.380
K-site	1.851	1.897	1.876	1.860	1.856	1.906	1.898	1.757	1.730	1.559	1.733	1.395	1.519	1.733	1.790	1.775	1.809
Ti cations	0.371	0.351	0.330	0.258	0.224	0.296	0.313	0.073	0.032	0.058	0.055	0.117	0.055	0.290	0.349	0.338	0.339
X_{Fe}	0.597	0.606	0.610	0.586	0.563	0.574	0.586	0.450	0.619	0.805	0.466	0.529	0.617	0.538	0.556	0.542	0.557

Sample No.	1004A	1004A	1019A	1019A	1019A	1019A	1019A	1019A	1019A	1019A	1019A	1019A	1019A	1019A	1023A	1023A	1023A	1023A
Analysis No.	2.10	2.12	1.2	1.5	1.1	2.10	2.2	2.3	2.6	2.24	2.26	3.6	3.9	3.11	1.9	2.5	2.8	2.2
Mineral	Biotite	Biotite	Biotite	Biotite	Biotite	Biotite	Biotite	Biotite	Biotite	Biotite	Biotite	Biotite	Biotite	Biotite	Biotite	Biotite	Biotite	Biotite
SiO_2	34.69	35.16	36.14	34.75	34.25	34.25	33.36	33.57	34.70	34.68	34.40	34.33	34.53	34.85	35.13	35.06	35.02	35.18
TiO_2	2.91	3.22	2.28	2.41	2.86	2.50	2.72	2.83	2.46	1.92	2.32	2.61	2.69	2.66	2.45	2.00	2.94	1.53
Al_2O_3	19.28	19.10	19.90	19.60	18.97	19.09	18.18	18.59	19.47	19.04	19.34	19.12	19.03	19.12	18.87	19.27	18.83	19.48
Cr_2O_3	0.02	0.07	0.01	0.07	0.10	0.07	0.04	0.08	0.06	0.02	0.01	0.07	0.05	0.06	0.09	0.06	0.07	0.00
Fe_2O_3	0.00	0.00	0.00	0.00	0.00	0.00	0.00	0.00	0.00	0.00	0.00	0.00	0.00	0.00	0.00	0.00	0.00	0.00
FeO	18.11	18.88	18.55	19.98	20.09	19.54	19.49	19.74	20.31	19.91	19.55	19.62	19.69	19.86	20.35	19.67	20.08	20.37
MnO	0.10	0.14	0.14	0.14	0.12	0.11	0.15	0.17	0.15	0.12	0.14	0.09	0.09	0.14	0.16	0.21	0.20	0.17
MgO	8.19	8.58	7.83	7.93	7.79	7.64	7.37	7.40	7.75	7.99	7.75	7.70	7.66	7.78	8.68	8.84	8.57	8.81
CaO	0.11	0.02	0.04	0.02	0.01	0.03	0.12	0.05	0.04	0.01	0.04	0.06	0.06	0.03	0.03	0.02	0.01	0.02
Na_2O	0.32	0.25	0.35	0.31	0.28	0.26	0.27	0.27	0.21	0.20	0.24	0.37	0.34	0.27	0.36	0.41	0.36	0.41
K_2O	8.71	8.92	8.45	8.64	8.74	8.76	7.98	8.57	8.70	8.54	8.62	8.72	8.72	8.76	8.43	8.36	8.40	8.43
Total	92.74	94.66	93.98	94.08	93.50	92.43	89.84	91.58	94.08	92.80	92.67	92.94	93.11	93.89	94.78	94.16	94.77	94.60
Cations	Numbers of cations on the basis of 22O																	
Si	5.402	5.384	5.522	5.371	5.351	5.391	5.400	5.359	5.374	5.439	5.394	5.379	5.398	5.407	5.395	5.400	5.377	5.404
Ti	0.340	0.371	0.262	0.280	0.336	0.296	0.332	0.340	0.286	0.226	0.274	0.308	0.316	0.310	0.283	0.231	0.339	0.177
Al	3.539	3.448	3.584	3.571	3.493	3.542	3.469	3.498	3.555	3.521	3.576	3.531	3.507	3.498	3.415	3.499	3.408	3.528
Cr	0.003	0.008	0.001	0.009	0.012	0.008	0.005	0.010	0.008	0.002	0.001	0.009	0.006	0.007	0.011	0.007	0.009	0.000
Fe^{3+}	0.000	0.000	0.000	0.000	0.000	0.000	0.000	0.000	0.000	0.000	0.000	0.000	0.000	0.000	0.000	0.000	0.000	0.000
Fe^{2+}	2.358	2.418	2.371	2.582	2.624	2.572	2.638	2.635	2.630	2.613	2.564	2.570	2.574	2.578	2.614	2.534	2.579	2.617
Mn	0.013	0.018	0.018	0.018	0.016	0.015	0.021	0.023	0.020	0.015	0.018	0.012	0.012	0.019	0.020	0.027	0.026	0.022
Mg	1.901	1.958	1.783	1.827	1.813	1.792	1.779	1.760	1.788	1.868	1.812	1.797	1.785	1.799	1.986	2.030	1.960	2.017
Ca	0.019	0.003	0.007	0.004	0.001	0.005	0.020	0.009	0.007	0.002	0.007	0.009	0.009	0.005	0.004	0.003	0.002	0.004
Na	0.097	0.074	0.103	0.093	0.084	0.078	0.086	0.084	0.064	0.061	0.072	0.111	0.104	0.080	0.106	0.124	0.107	0.123
K	1.730	1.742	1.647	1.703	1.742	1.759	1.648	1.746	1.719	1.709	1.724	1.742	1.739	1.733	1.652	1.643	1.645	1.652
Total	15.401	15.424	15.298	15.457	15.473	15.457	15.399	15.463	15.450	15.457	15.442	15.469	15.451	15.437	15.487	15.499	15.452	15.543
K-site	1.846	1.818	1.757	1.800	1.827	1.841	1.755	1.839	1.789	1.772	1.803	1.862	1.852	1.819	1.762	1.770	1.754	1.778
Ti cations	0.340	0.371	0.262	0.280	0.336	0.296	0.332	0.340	0.286	0.226	0.274	0.308	0.316	0.310	0.283	0.231	0.339	0.177
X_{Fe}	0.554	0.552	0.571	0.586	0.591	0.589	0.597	0.599	0.595	0.583	0.586	0.588	0.590	0.589	0.568	0.555	0.568	0.565

Sample No.	1023A	1023A	1023A
Analysis No.	1.12	1.13	2.11
Mineral	Biotite	Biotite	Biotite
SiO_2	35.11	35.35	35.31
TiO_2	3.41	3.22	2.37
Al_2O_3	18.96	19.21	19.01
Cr_2O_3	0.08	0.07	0.07
Fe_2O_3	0.00	0.00	0.00
FeO	20.53	20.29	20.04
MnO	0.20	0.19	0.19
MgO	8.11	8.26	8.75
CaO	0.00	0.03	0.02
Na_2O	0.40	0.38	0.40
K_2O	8.49	8.39	8.42
Total	95.45	95.53	94.81
Cations	Numbers of ions on the basis of 22O		
Si	5.357	5.371	5.409
Ti	0.391	0.368	0.273
Al	3.410	3.441	3.433
Cr	0.010	0.009	0.008
Fe^{3+}	0.000	0.000	0.000
Fe^{2+}	2.620	2.578	2.567
Mn	0.026	0.024	0.025
Mg	1.845	1.871	1.997
Ca	0.001	0.006	0.003
Na	0.117	0.113	0.118
K	1.651	1.625	1.646
Total	15.427	15.406	15.479
K-site	1.769	1.744	1.767
Ti cations	0.391	0.368	0.273
X_{Fe}	0.587	0.580	0.562

Sample No.	1010B	1010B	1010B	1010B	1010B	1010B	1010B	1010B	1010B	1010B	1010B	1010B	1010B	1010B
Analysis No.	1.4	1.5	1.6	2.11	2.12	2.13	2.14	3.1	3.5	1.1	1.2	2.6	3.2	3.3
Mineral	Muscovite	Muscovite	Muscovite	Muscovite	Muscovite	Muscovite	Muscovite	Muscovite	Muscovite	Muscovite	Muscovite	Muscovite	Muscovite	Muscovite
SiO_2	45.16	44.48	45.01	45.17	45.49	45.76	44.94	45.70	45.72	47.43	48.84	49.57	47.51	48.01
TiO_2	0.34	1.10	0.08	0.57	0.39	0.60	1.16	0.03	0.58	0.08	0.08	0.05	0.06	0.06
Al_2O_3	35.65	35.24	35.74	35.66	35.98	35.28	34.90	35.67	36.06	29.06	29.83	28.92	29.05	28.94
Cr_2O_3	0.00	0.04	0.03	0.00	0.00	0.00	0.06	0.00	0.04	0.05	0.00	0.00	0.00	0.01
Fe_2O_3	0.00	0.00	0.00	0.00	0.00	0.00	0.00	0.00	0.00	0.00	0.00	0.00	0.00	0.00
FeO	1.08	0.93	1.30	0.99	0.89	1.03	0.94	1.42	0.94	4.85	4.03	5.21	5.49	5.09
MnO	0.01	0.03	0.04	0.01	0.01	0.02	0.00	0.00	0.00	0.04	0.04	0.04	0.06	0.06
MgO	0.59	0.58	0.69	0.59	0.52	0.65	0.43	0.74	0.54	2.77	2.44	3.26	3.08	2.82
CaO	0.00	0.03	0.00	0.00	0.00	0.00	0.02	0.00	0.00	0.25	0.20	0.26	0.19	0.16
Na_2O	0.75	0.85	0.80	0.78	0.77	0.80	0.83	0.80	0.86	0.12	0.13	0.11	0.11	0.10
K_2O	10.59	10.37	10.49	10.54	10.54	10.57	10.46	10.60	10.57	8.99	9.58	8.50	9.21	9.24
Total	94.16	93.66	94.19	94.31	94.60	94.71	93.72	94.96	95.31	93.64	95.18	95.92	94.76	94.50
Cations	Numbers of cations on the basis of 22O													
Si	6.090	6.036	6.075	6.079	6.095	6.132	6.091	6.117	6.085	6.491	6.550	6.593	6.457	6.521
Ti	0.034	0.112	0.008	0.058	0.039	0.060	0.118	0.003	0.058	0.008	0.008	0.005	0.006	0.006
Al	5.668	5.637	5.687	5.659	5.684	5.574	5.577	5.630	5.658	4.688	4.716	4.534	4.654	4.634
Cr	0.000	0.004	0.004	0.000	0.000	0.000	0.006	0.000	0.004	0.005	0.000	0.000	0.000	0.001
Fe^{3+}	0.000	0.000	0.000	0.000	0.000	0.000	0.000	0.000	0.000	0.000	0.000	0.000	0.000	0.000
Fe^{2+}	0.121	0.106	0.147	0.112	0.100	0.116	0.106	0.159	0.105	0.555	0.452	0.579	0.624	0.579
Mn	0.001	0.003	0.004	0.002	0.001	0.002	0.000	0.000	0.000	0.005	0.005	0.004	0.007	0.007
Mg	0.118	0.117	0.139	0.118	0.105	0.130	0.087	0.148	0.107	0.565	0.489	0.647	0.623	0.571
Ca	0.000	0.005	0.000	0.000	0.000	0.000	0.003	0.000	0.000	0.036	0.029	0.037	0.028	0.023
Na	0.197	0.225	0.210	0.203	0.200	0.207	0.219	0.207	0.223	0.031	0.033	0.029	0.028	0.028
K	1.822	1.796	1.807	1.809	1.801	1.807	1.808	1.810	1.795	1.569	1.639	1.443	1.597	1.602
Total	14.051	14.041	14.080	14.040	14.025	14.028	14.013	14.074	14.035	13.954	13.920	13.871	14.023	13.971
K-site	2.019	2.025	2.017	2.012	2.002	2.014	2.029	2.017	2.018	1.636	1.701	1.508	1.654	1.653
Para comp.	0.098	0.111	0.104	0.101	0.100	0.103	0.108	0.102	0.111	0.019	0.020	0.020	0.017	0.017
Phen comp.	0.060	0.056	0.072	0.057	0.051	0.061	0.048	0.077	0.053	0.280	0.235	0.307	0.312	0.287
X_{Fe}	0.508	0.474	0.514	0.487	0.489	0.471	0.551	0.517	0.494	0.495	0.481	0.472	0.500	0.503

Sample No.	1019C	1019C	1019C	1019C	1019C	1019C	1019C	1019C	1019C	1001D	1001D	1001D	1004A	1004A
Analysis No.	1.5	1.7	1.9	2.3	2.7	3.3	3.4	4.2	4.3	2.13	3.6	3.7	1.13	2.13
Mineral	Muscovite	Muscovite	Muscovite	Muscovite	Muscovite	Muscovite	Muscovite	Muscovite	Muscovite	Muscovite	Muscovite	Muscovite	Muscovite	Muscovite
SiO_2	45.61	45.08	43.55	46.49	45.24	45.61	45.47	47.01	44.37	46.77	48.77	45.15	47.00	47.05
TiO_2	0.43	0.44	0.46	0.26	0.22	0.25	0.32	0.37	0.25	0.35	0.61	0.66	0.53	1.24
Al_2O_3	36.63	35.72	36.87	36.73	36.38	36.31	35.81	35.46	36.15	35.62	36.15	34.66	35.46	35.87
Cr_2O_3	0.00	0.00	0.00	0.00	0.03	0.04	0.00	0.02	0.00	0.03	0.02	0.03	0.07	0.08
Fe_2O_3	0.00	0.00	0.00	0.00	0.00	0.00	0.00	0.00	0.00	0.00	0.00	0.00	0.00	0.00
FeO	0.91	0.83	0.83	0.80	0.98	0.86	0.93	0.96	0.91	1.08	1.11	2.53	0.98	0.96
MnO	0.01	0.00	0.00	0.02	0.00	0.02	0.00	0.01	0.02	0.00	0.00	0.00	0.00	0.00
MgO	0.55	0.51	0.54	0.48	0.57	0.57	0.57	0.56	0.64	0.62	0.53	0.55	0.59	0.60
CaO	0.01	0.06	0.00	0.00	0.02	0.00	0.04	0.02	0.01	0.02	0.05	0.01	0.03	0.05
Na_2O	0.80	0.77	0.86	0.82	0.91	0.66	0.79	0.80	0.84	1.19	1.27	1.13	0.67	0.69
K_2O	10.59	10.48	10.33	10.35	10.42	10.03	10.29	10.59	10.35	9.14	8.79	8.54	9.69	9.93
Total	95.53	93.90	93.43	95.95	94.76	94.35	94.23	95.79	93.54	94.95	97.37	93.29	95.04	96.54
Cations	Numbers of cations on the basis of 22O													
Si	6.053	6.087	5.918	6.120	6.054	6.101	6.108	6.211	6.018	6.201	6.274	6.127	6.223	6.153
Ti	0.043	0.045	0.047	0.026	0.022	0.025	0.033	0.037	0.025	0.035	0.059	0.068	0.052	0.122
Al	5.732	5.685	5.906	5.700	5.740	5.726	5.672	5.524	5.781	5.567	5.482	5.545	5.536	5.530
Cr	0.001	0.000	0.000	0.000	0.003	0.004	0.000	0.002	0.000	0.004	0.002	0.004	0.007	0.008
Fe^{3+}	0.000	0.000	0.000	0.000	0.000	0.000	0.000	0.000	0.000	0.000	0.000	0.000	0.000	0.000
Fe^{2+}	0.101	0.094	0.094	0.088	0.110	0.096	0.104	0.106	0.103	0.120	0.119	0.287	0.109	0.105
Mn	0.001	0.000	0.000	0.002	0.000	0.002	0.000	0.001	0.002	0.000	0.000	0.000	0.000	0.000
Mg	0.108	0.104	0.110	0.093	0.113	0.114	0.114	0.110	0.128	0.123	0.102	0.111	0.116	0.116
Ca	0.001	0.009	0.000	0.000	0.003	0.000	0.006	0.002	0.002	0.003	0.007	0.002	0.004	0.007
Na	0.205	0.200	0.226	0.210	0.235	0.170	0.206	0.204	0.221	0.305	0.317	0.298	0.172	0.175
K	1.792	1.804	1.790	1.739	1.778	1.711	1.764	1.785	1.792	1.545	1.442	1.479	1.638	1.657
Total	14.037	14.028	14.091	13.978	14.059	13.949	14.008	13.983	14.072	13.904	13.805	13.920	13.857	13.872
K-site	1.999	2.014	2.017	1.949	2.016	1.881	1.976	1.991	2.015	1.853	1.766	1.780	1.813	1.839
Para comp.	0.103	0.100	0.112	0.108	0.117	0.090	0.105	0.103	0.110	0.165	0.180	0.168	0.095	0.096
Phen comp.	0.052	0.049	0.051	0.045	0.056	0.053	0.055	0.054	0.058	0.061	0.055	0.099	0.056	0.055
X_{Fe}	0.483	0.476	0.461	0.485	0.493	0.456	0.479	0.491	0.444	0.494	0.538	0.722	0.482	0.476

Sample No.	1019A	1019A	1019A	1019A	1019A	1019A	1019A	1023A	1023A	1023A	1023A	1023A
Analysis No.	1.3	1.4	1.6	1.9	2.5	3.10	3.12	1.4	1.6	1.7	2.6	2.7
Mineral	Muscovite	Muscovite	Muscovite	Muscovite	Muscovite	Muscovite	Muscovite	Muscovite	Muscovite	Muscovite	Muscovite	Muscovite
SiO_2	47.03	46.92	45.97	46.20	46.63	46.81	46.51	46.66	46.80	46.82	46.91	46.76
TiO_2	0.27	0.42	0.64	0.59	0.43	0.84	0.82	0.24	0.21	0.92	0.15	0.24
Al_2O_3	36.02	35.20	34.96	35.96	35.64	35.69	35.13	35.75	35.96	35.07	35.76	36.13
Cr_2O_3	0.00	0.00	0.00	0.03	0.00	0.06	0.03	0.03	0.00	0.01	0.00	0.03
Fe_2O_3	0.00	0.00	0.00	0.00	0.00	0.00	0.00	0.00	0.00	0.00	0.00	0.00
FeO	0.77	0.90	0.84	0.88	0.91	0.96	0.94	1.04	0.96	0.79	0.72	0.88
MnO	0.02	0.01	0.00	0.00	0.01	0.04	0.02	0.02	0.00	0.03	0.00	0.01
MgO	0.57	0.63	0.64	0.52	0.56	0.55	0.48	0.68	0.62	0.54	0.55	0.52
CaO	0.00	0.01	0.03	0.01	0.01	0.01	0.00	0.00	0.00	0.03	0.00	0.00
Na_2O	0.79	0.83	0.70	0.74	0.68	0.73	0.74	0.95	1.17	0.89	1.20	1.16
K_2O	9.98	9.97	9.96	9.87	10.04	10.04	10.05	9.65	9.23	9.80	9.17	9.61
Total	95.54	94.93	93.82	94.88	94.95	95.84	94.75	95.05	94.95	94.98	94.55	95.36
Cations	Numbers of cations on the basis of 22O											
Si	6.202	6.234	6.187	6.143	6.194	6.173	6.199	6.187	6.193	6.217	6.228	6.175
Ti	0.027	0.042	0.064	0.059	0.043	0.083	0.082	0.024	0.021	0.092	0.015	0.024
Al	5.601	5.514	5.548	5.637	5.582	5.548	5.520	5.589	5.610	5.490	5.597	5.625
Cr	0.001	0.000	0.000	0.003	0.000	0.006	0.004	0.003	0.000	0.001	0.000	0.003
Fe^{3+}	0.000	0.000	0.000	0.000	0.000	0.000	0.000	0.000	0.000	0.000	0.000	0.000
Fe^{2+}	0.085	0.100	0.095	0.097	0.101	0.105	0.105	0.115	0.107	0.088	0.080	0.097
Mn	0.002	0.001	0.000	0.000	0.001	0.005	0.002	0.002	0.000	0.003	0.000	0.001
Mg	0.113	0.124	0.128	0.103	0.111	0.109	0.096	0.134	0.122	0.107	0.109	0.103
Ca	0.000	0.002	0.004	0.002	0.001	0.001	0.000	0.000	0.000	0.004	0.000	0.001
Na	0.203	0.214	0.184	0.192	0.176	0.185	0.190	0.243	0.299	0.230	0.310	0.296
K	1.679	1.690	1.710	1.674	1.701	1.689	1.708	1.632	1.557	1.660	1.553	1.618
Total	13.912	13.920	13.921	13.910	13.911	13.904	13.906	13.930	13.909	13.891	13.891	13.944
K-site	1.882	1.906	1.897	1.867	1.878	1.875	1.899	1.876	1.857	1.894	1.863	1.916
Para comp.	0.108	0.112	0.097	0.103	0.094	0.099	0.100	0.130	0.161	0.121	0.166	0.155
Phen comp.	0.050	0.056	0.056	0.050	0.053	0.054	0.050	0.062	0.057	0.049	0.047	0.050
X_{Fe}	0.430	0.446	0.426	0.485	0.476	0.492	0.523	0.462	0.465	0.452	0.424	0.485

Sample No.	1012A	1012A	1012A	1012A	1012A	1012A	1012A	1012A	1012A	1012A	1010B	1010B
Analysis No.	2.3	1.7	1.8	1.10	1.11	2.9	1.2	1.3	4.5	4.6	1.12	2.7
Mineral	Plagioclase	Plagioclase	Plagioclase	Plagioclase	Plagioclase	Plagioclase	Plagioclase	Plagioclase	Plagioclase	Plagioclase	Plagioclase	Plagioclase
SiO_2	52.57	55.29	56.37	52.02	56.99	56.11	56.31	56.96	55.62	55.85	61.35	60.99
TiO_2	0.02	0.00	0.02	0.00	0.00	0.00	0.00	0.01	0.02	0.00	0.00	0.00
Al_2O_3	30.39	28.19	27.53	30.18	27.13	27.72	27.66	27.06	27.63	28.02	24.33	24.25
Cr_2O_3	0.02	0.00	0.00	0.00	0.00	0.03	0.01	0.00	0.00	0.00	0.00	0.01
Fe_2O_3	0.00	0.00	0.00	0.00	0.00	0.00	0.00	0.00	0.00	0.00	0.00	0.00
FeO	0.06	0.03	0.02	0.07	0.03	0.03	0.09	0.06	0.10	0.08	0.04	0.05
MnO	0.01	0.00	0.00	0.00	0.01	0.02	0.01	0.00	0.02	0.00	0.01	0.01
MgO	0.00	0.00	0.00	0.00	0.00	0.00	0.00	0.00	0.00	0.00	0.00	0.00
CaO	12.03	9.92	9.11	12.15	8.51	9.18	9.06	8.73	9.33	9.49	4.96	5.04
Na_2O	4.59	6.03	6.48	4.47	6.91	6.44	6.53	6.56	6.45	6.18	9.07	9.12
K_2O	0.15	0.23	0.25	0.16	0.29	0.22	0.29	0.28	0.27	0.20	0.26	0.26
Total	99.83	99.69	99.78	99.05	99.87	99.74	99.96	99.66	99.44	99.81	100.02	99.73
Cations	Numbers of cations on the basis of 8O											
Si	2.384	2.498	2.538	2.379	2.561	2.528	2.533	2.564	2.519	2.516	2.726	2.721
Ti	0.001	0.000	0.001	0.000	0.000	0.000	0.000	0.000	0.001	0.000	0.000	0.000
Al	1.625	1.502	1.461	1.627	1.438	1.473	1.467	1.436	1.475	1.488	1.275	1.276
Cr	0.001	0.000	0.000	0.000	0.000	0.001	0.000	0.000	0.000	0.000	0.000	0.000
Fe^{3+}	0.000	0.000	0.000	0.000	0.000	0.000	0.000	0.000	0.000	0.000	0.000	0.000
Fe^{2+}	0.002	0.001	0.001	0.003	0.001	0.001	0.003	0.002	0.004	0.003	0.002	0.002
Mn	0.000	0.000	0.000	0.000	0.000	0.001	0.000	0.000	0.001	0.000	0.000	0.000
Mg	0.000	0.000	0.000	0.000	0.000	0.000	0.000	0.000	0.000	0.000	0.000	0.000
Ca	0.584	0.480	0.439	0.595	0.410	0.443	0.436	0.421	0.453	0.458	0.236	0.241
Na	0.403	0.528	0.566	0.397	0.602	0.563	0.570	0.573	0.566	0.540	0.781	0.789
K	0.009	0.013	0.014	0.009	0.016	0.013	0.016	0.016	0.015	0.011	0.015	0.015
Total	5.009	5.022	5.021	5.010	5.029	5.023	5.027	5.012	5.034	5.016	5.034	5.043
Si+Al (=4?)	4.009	3.999	4.000	4.006	3.999	4.001	4.000	4.000	3.994	4.004	4.001	3.996
Na+Ca (=1?)	0.987	1.008	1.006	0.992	1.012	1.006	1.006	0.994	1.019	0.998	1.017	1.030
***X*An**	0.587	0.470	0.431	0.595	0.399	0.435	0.427	0.417	0.438	0.454	0.229	0.230
***X*Ab**	0.405	0.517	0.555	0.396	0.585	0.552	0.557	0.567	0.547	0.535	0.757	0.756
***X*Or**	0.009	0.013	0.014	0.009	0.016	0.013	0.016	0.016	0.015	0.011	0.014	0.014

Sample No.	1015A	1015A	1015A	1015A	1015A	1015A	1015A	1015A	1015A	1015A	1015A	1015A
Analysis No.	1.2	1.3	1.4	1.1	1.2	1.3	1.4	1.5	1.6	2.9	2.10	2.11
Mineral	Plagioclase	Plagioclase	Plagioclase	Plagioclase	Plagioclase	Plagioclase	Plagioclase	Plagioclase	Plagioclase	Plagioclase	Plagioclase	Plagioclase
SiO_2	68.16	67.00	68.85	68.38	67.13	67.46	69.03	68.78	68.51	68.48	68.64	67.96
TiO_2	0.01	0.00	0.00	0.01	0.01	0.00	0.00	0.00	0.01	0.00	0.00	0.00
Al_2O_3	19.35	19.58	19.38	19.62	19.47	19.87	19.63	19.64	19.97	19.78	19.69	19.27
Cr_2O_3	0.00	0.00	0.01	0.00	0.00	0.00	0.02	0.02	0.00	0.03	0.02	0.00
Fe_2O_3	0.00	0.00	0.00	0.00	0.00	0.00	0.00	0.00	0.00	0.00	0.00	0.00
FeO	0.02	0.04	0.01	0.00	0.00	0.05	0.00	0.02	0.02	0.00	0.00	0.01
MnO	0.01	0.02	0.00	0.00	0.01	0.01	0.00	0.00	0.00	0.00	0.00	0.00
MgO	0.03	0.02	0.01	0.00	0.01	0.03	0.03	0.02	0.00	0.01	0.01	0.00
CaO	0.10	0.09	0.07	0.13	0.14	0.53	0.11	0.03	0.29	0.09	0.05	0.10
Na_2O	12.22	12.57	12.20	12.30	12.32	11.97	12.24	12.45	12.25	12.44	12.51	12.14
K_2O	0.14	0.11	0.11	0.09	0.14	0.09	0.15	0.08	0.09	0.09	0.08	0.10
Total	100.05	99.43	100.65	100.53	99.24	100.01	101.22	101.05	101.16	100.92	101.00	99.59
Cations	Numbers of cations on the basis of 8O											
Si	2.985	2.960	2.993	2.980	2.969	2.959	2.986	2.982	2.969	2.974	2.978	2.988
Ti	0.000	0.000	0.000	0.000	0.000	0.000	0.000	0.000	0.000	0.000	0.000	0.000
Al	0.999	1.020	0.994	1.008	1.015	1.028	1.001	1.004	1.020	1.013	1.007	0.999
Cr	0.000	0.000	0.000	0.000	0.000	0.000	0.001	0.001	0.000	0.001	0.001	0.000
Fe^{3+}	0.000	0.000	0.000	0.000	0.000	0.000	0.000	0.000	0.000	0.000	0.000	0.000
Fe^{2+}	0.001	0.001	0.000	0.000	0.000	0.002	0.000	0.001	0.001	0.000	0.000	0.000
Mn	0.000	0.001	0.000	0.000	0.000	0.000	0.000	0.000	0.000	0.000	0.000	0.000
Mg	0.002	0.002	0.001	0.000	0.001	0.002	0.002	0.001	0.000	0.001	0.001	0.000
Ca	0.005	0.004	0.003	0.006	0.007	0.025	0.005	0.001	0.014	0.004	0.003	0.005
Na	1.038	1.077	1.029	1.040	1.056	1.018	1.026	1.047	1.029	1.048	1.052	1.035
K	0.008	0.006	0.006	0.005	0.008	0.005	0.009	0.004	0.005	0.005	0.004	0.006
Total	5.038	5.071	5.027	5.038	5.056	5.039	5.030	5.041	5.038	5.045	5.046	5.033
Si+Al (=4?)	3.984	3.980	3.987	3.988	3.984	3.987	3.987	3.986	3.989	3.987	3.985	3.987
Na+Ca (=1?)	1.043	1.081	1.032	1.045	1.063	1.043	1.032	1.048	1.043	1.052	1.055	1.040
***X*An**	0.005	0.004	0.003	0.006	0.006	0.024	0.005	0.001	0.013	0.004	0.002	0.004
***X*Ab**	0.988	0.991	0.991	0.990	0.986	0.971	0.987	0.995	0.982	0.991	0.994	0.990
***X*Or**	0.008	0.006	0.006	0.005	0.007	0.005	0.008	0.004	0.005	0.004	0.004	0.006

Sample No.	1015A	1015A	1015A	1015A	1015A	1015A	1015A	1015A	1015A	1015A	1015A	1019A
Analysis No.	2.12	2.13	2.2	2.3	2.4	2.5	2.7	1.6	1.7	1.8	1.9	2.8
Mineral	Plagioclase	Plagioclase	Plagioclase	Plagioclase	Plagioclase	Plagioclase	Plagioclase	Plagioclase	Plagioclase	Plagioclase	Plagioclase	Plagioclase
SiO_2	68.01	68.29	67.35	66.91	68.69	68.28	68.33	68.01	68.23	68.28	67.21	64.91
TiO_2	0.00	0.01	0.00	0.00	0.01	0.00	0.00	0.02	0.00	0.00	0.00	0.00
Al_2O_3	19.31	19.67	19.46	19.81	19.43	19.38	19.82	19.37	19.74	19.65	19.67	22.22
Cr_2O_3	0.00	0.02	0.01	0.01	0.00	0.00	0.00	0.00	0.00	0.00	0.00	0.00
Fe_2O_3	0.00	0.00	0.00	0.00	0.00	0.00	0.00	0.00	0.00	0.00	0.00	0.00
FeO	0.00	0.00	0.02	0.02	0.00	0.03	0.04	0.00	0.02	0.01	0.03	0.04
MnO	0.04	0.00	0.01	0.00	0.00	0.00	0.01	0.00	0.00	0.00	0.00	0.01
MgO	0.01	0.00	0.01	0.01	0.01	0.02	0.00	0.01	0.05	0.01	0.01	0.00
CaO	0.13	0.15	0.23	0.07	0.07	0.08	0.15	0.04	0.13	0.06	0.10	3.27
Na_2O	12.17	12.39	12.52	12.64	12.44	12.21	12.65	12.06	12.10	12.49	12.55	10.48
K_2O	0.12	0.08	0.06	0.10	0.07	0.14	0.05	0.13	0.26	0.09	0.10	0.20
Total	99.79	100.62	99.67	99.58	100.72	100.14	101.04	99.64	100.53	100.59	99.67	101.15
Cations	Numbers of cations on the basis of 8O											
Si	2.986	2.975	2.967	2.953	2.987	2.986	2.968	2.987	2.975	2.976	2.961	2.839
Ti	0.000	0.000	0.000	0.000	0.000	0.000	0.000	0.001	0.000	0.000	0.000	0.000
Al	1.000	1.010	1.011	1.031	0.996	0.999	1.015	1.003	1.015	1.010	1.022	1.145
Cr	0.000	0.001	0.000	0.001	0.000	0.000	0.000	0.000	0.000	0.000	0.000	0.000
Fe^{3+}	0.000	0.000	0.000	0.000	0.000	0.000	0.000	0.000	0.000	0.000	0.000	0.000
Fe^{2+}	0.000	0.000	0.001	0.001	0.000	0.001	0.001	0.000	0.001	0.001	0.001	0.001
Mn	0.002	0.000	0.000	0.000	0.000	0.000	0.000	0.000	0.000	0.000	0.000	0.000
Mg	0.001	0.000	0.001	0.000	0.001	0.001	0.000	0.001	0.003	0.001	0.001	0.000
Ca	0.006	0.007	0.011	0.003	0.003	0.004	0.007	0.002	0.006	0.003	0.005	0.153
Na	1.036	1.047	1.069	1.082	1.049	1.036	1.065	1.027	1.023	1.055	1.073	0.889
K	0.007	0.005	0.003	0.006	0.004	0.008	0.003	0.007	0.014	0.005	0.006	0.011
Total	5.036	5.045	5.064	5.076	5.041	5.036	5.059	5.028	5.037	5.050	5.067	5.039
Si+Al (=4?)	3.985	3.985	3.978	3.983	3.984	3.986	3.982	3.990	3.989	3.985	3.983	3.984
Na+Ca (=1?)	1.042	1.054	1.080	1.085	1.052	1.040	1.072	1.028	1.029	1.058	1.077	1.042
***X*An**	0.006	0.007	0.010	0.003	0.003	0.004	0.006	0.002	0.006	0.003	0.004	0.145
***X*Ab**	0.988	0.989	0.987	0.992	0.993	0.989	0.991	0.991	0.980	0.993	0.991	0.844
***X*Or**	0.007	0.004	0.003	0.005	0.004	0.007	0.003	0.007	0.014	0.005	0.005	0.011

Sample No.	1019A	1019A	1019A	1019A	1019A
Analysis No.	2.11	2.12	2.13	2.14	2.15
Mineral	Plagioclase	Plagioclase	Plagioclase	Plagioclase	Plagioclase
SiO_2	63.79	64.02	63.51	63.77	64.97
TiO_2	0.00	0.00	0.00	0.03	0.00
Al_2O_3	22.72	22.27	22.58	22.51	22.07
Cr_2O_3	0.00	0.00	0.00	0.01	0.00
Fe_2O_3	0.00	0.00	0.00	0.00	0.00
FeO	0.03	0.03	0.01	0.01	0.00
MnO	0.00	0.00	0.00	0.00	0.01
MgO	0.01	0.00	0.00	0.00	0.00
CaO	3.89	4.02	4.04	3.88	3.12
Na_2O	10.10	9.59	10.19	9.97	10.55
K_2O	0.16	0.21	0.19	0.20	0.19
Total	100.71	100.15	100.56	100.38	100.94
Cations	Numbers of cations on the basis of 8O				
Si	2.806	2.827	2.802	2.813	2.845
Ti	0.000	0.000	0.000	0.001	0.000
Al	1.178	1.159	1.175	1.170	1.139
Cr	0.000	0.000	0.000	0.000	0.000
Fe^{3+}	0.000	0.000	0.000	0.000	0.000
Fe^{2+}	0.001	0.001	0.001	0.001	0.000
Mn	0.000	0.000	0.000	0.000	0.000
Mg	0.001	0.000	0.000	0.000	0.000
Ca	0.183	0.190	0.191	0.183	0.146
Na	0.861	0.821	0.872	0.853	0.896
K	0.009	0.012	0.011	0.011	0.011
Total	5.040	5.010	5.052	5.032	5.038
Si+Al (=4?)	3.984	3.986	3.977	3.984	3.985
Na+Ca (=1?)	1.045	1.011	1.063	1.036	1.042
***X*An**	0.174	0.186	0.178	0.175	0.139
***X*Ab**	0.818	0.803	0.812	0.814	0.851
***X*Or**	0.008	0.012	0.010	0.011	0.010

Sample No.	1012A	1012A	1012A	1012A	1019A	1019A	1019A	1019A	1019A	1019A	1019A	1019A	1019A
Analysis No.	2.4	3.1	3.2	4.1	2.9	2.10	3.13	3.14	3.15	3.16	3.17	3.18	3.19
Mineral	K-feldspar	K-feldspar	K-feldspar	K-feldspar	K-feldspar	K-feldspar	K-feldspar	K-feldspar	K-feldspar	K-feldspar	K-feldspar	K-feldspar	K-feldspar
SiO_2	63.60	64.21	63.57	63.11	64.84	64.97	65.94	64.78	65.62	64.16	65.76	64.80	66.09
TiO_2	0.00	0.00	0.01	0.00	0.00	0.01	0.01	0.00	0.00	0.00	0.00	0.00	0.01
Al_2O_3	18.84	18.69	18.54	18.24	18.52	18.11	18.68	18.38	19.07	18.00	18.62	18.35	18.73
Cr_2O_3	0.00	0.01	0.00	0.00	0.00	0.05	0.00	0.00	0.00	0.00	0.00	0.00	0.01
Fe_2O_3	0.00	0.00	0.00	0.00	0.00	0.00	0.00	0.00	0.00	0.00	0.00	0.00	0.00
FeO	0.01	0.02	0.01	0.05	0.07	0.04	0.02	0.00	0.01	0.01	0.01	0.03	0.01
MnO	0.00	0.00	0.00	0.01	0.00	0.01	0.00	0.00	0.03	0.00	0.02	0.00	0.00
MgO	0.01	0.00	0.00	0.01	0.00	0.00	0.00	0.01	0.01	0.00	0.00	0.01	0.00
CaO	0.03	0.03	0.05	0.04	0.00	0.00	0.03	0.01	0.02	0.03	0.02	0.03	0.05
Na_2O	1.12	1.21	1.07	1.12	2.20	1.67	2.51	2.49	4.25	1.87	2.15	2.03	3.13
K_2O	15.35	15.26	15.44	15.00	13.49	13.77	12.88	13.00	10.57	13.60	13.54	13.50	12.27
Total	98.95	99.44	98.67	97.58	99.13	98.63	100.08	98.69	99.59	97.69	100.13	98.74	100.30
Cations	Numbers of cations on the basis of 8O												
Si	2.968	2.979	2.976	2.983	2.994	3.013	3.004	2.999	2.985	3.007	3.002	3.002	3.000
Ti	0.000	0.000	0.000	0.000	0.000	0.000	0.000	0.000	0.000	0.000	0.000	0.000	0.000
Al	1.036	1.022	1.023	1.017	1.009	0.990	1.003	1.003	1.023	0.995	1.002	1.002	1.002
Cr	0.000	0.000	0.000	0.000	0.000	0.002	0.000	0.000	0.000	0.000	0.000	0.000	0.000
Fe^{3+}	0.000	0.000	0.000	0.000	0.000	0.000	0.000	0.000	0.000	0.000	0.000	0.000	0.000
Fe^{2+}	0.000	0.001	0.000	0.002	0.003	0.001	0.001	0.000	0.000	0.000	0.000	0.001	0.000
Mn	0.000	0.000	0.000	0.000	0.000	0.001	0.000	0.000	0.001	0.000	0.001	0.000	0.000
Mg	0.001	0.000	0.000	0.001	0.000	0.000	0.000	0.001	0.000	0.000	0.000	0.000	0.000
Ca	0.001	0.001	0.002	0.002	0.000	0.000	0.001	0.001	0.001	0.001	0.001	0.001	0.002
Na	0.101	0.109	0.097	0.103	0.197	0.150	0.222	0.224	0.375	0.170	0.191	0.183	0.275
K	0.914	0.903	0.922	0.905	0.795	0.815	0.748	0.768	0.614	0.814	0.789	0.798	0.711
Total	5.022	5.016	5.022	5.012	4.997	4.973	4.979	4.995	4.998	4.987	4.986	4.987	4.991
Si+Al (=4?)	4.004	4.001	3.999	4.000	4.003	4.004	4.007	4.002	4.007	4.002	4.004	4.004	4.002
*X*An	0.001	0.001	0.002	0.002	0.000	0.000	0.001	0.001	0.001	0.001	0.001	0.001	0.002
*X*Ab	0.100	0.107	0.095	0.102	0.199	0.155	0.228	0.226	0.379	0.172	0.194	0.186	0.279
*X*Or	0.899	0.892	0.902	0.896	0.801	0.845	0.770	0.774	0.620	0.826	0.805	0.812	0.719

Sample No.	1004A	1004A	1004A	1004A	1004A	1004A	1004A	1004A	1023A	1023A	1023A	1023A	1023A	1023A
Analysis No.	1.1	1.2	2.1	2.2	2.3	2.4	2.5	2.7	1.10	1.11	2.1	2.3	2.9	2.10
Mineral	Andalusite	Andalusite	Andalusite	Andalusite	Andalusite	Andalusite	Andalusite	Andalusite	Andalusite	Andalusite	Andalusite	Andalusite	Andalusite	Andalusite
SiO_2	36.63	36.73	36.84	36.85	36.95	37.02	36.87	36.59	36.72	36.64	36.98	36.66	37.06	36.97
TiO_2	0.03	0.04	0.00	0.03	0.02	0.00	0.02	0.02	0.02	0.03	0.09	0.01	0.02	0.03
Al_2O_3	61.36	61.33	61.68	61.60	61.50	61.52	61.59	61.53	61.60	61.26	61.53	61.03	61.77	61.55
Cr_2O_3	0.10	0.09	0.03	0.00	0.01	0.08	0.02	0.03	0.02	0.06	0.00	0.02	0.00	0.01
Fe_2O_3	0.00	0.00	0.00	0.00	0.00	0.00	0.00	0.00	0.00	0.00	0.00	0.00	0.00	0.00
FeO	0.16	0.22	0.22	0.20	0.19	0.16	0.20	0.31	0.17	0.21	0.27	0.25	0.22	0.20
MnO	0.01	0.00	0.01	0.00	0.00	0.00	0.01	0.00	0.00	0.00	0.00	0.01	0.00	0.03
MgO	0.03	0.04	0.03	0.02	0.03	0.03	0.03	0.06	0.02	0.03	0.06	0.03	0.04	0.04
CaO	0.04	0.01	0.00	0.02	0.02	0.00	0.00	0.01	0.00	0.00	0.00	0.00	0.00	0.01
Na_2O	0.03	0.02	0.02	0.01	0.00	0.01	0.01	0.01	0.01	0.01	0.02	0.03	0.00	0.01
K_2O	0.01	0.02	0.01	0.00	0.00	0.01	0.00	0.01	0.00	0.00	0.01	0.02	0.00	0.00
Total	98.40	98.50	98.86	98.76	98.75	98.87	98.77	98.58	98.56	98.24	98.96	98.07	99.12	98.85
Cations	Numbers of cations on the basis of 5O													
Si	1.005	1.007	1.006	1.007	1.010	1.011	1.008	1.003	1.006	1.007	1.009	1.009	1.009	1.010
Ti	0.001	0.001	0.000	0.001	0.000	0.000	0.000	0.000	0.000	0.001	0.002	0.000	0.000	0.001
Al	1.985	1.982	1.986	1.985	1.982	1.980	1.984	1.988	1.988	1.984	1.979	1.981	1.983	1.981
Cr	0.002	0.002	0.001	0.000	0.000	0.002	0.000	0.001	0.001	0.001	0.000	0.000	0.000	0.000
Fe^{3+}	0.000	0.000	0.000	0.000	0.000	0.000	0.000	0.000	0.000	0.000	0.000	0.000	0.000	0.000
Fe^{2+}	0.004	0.005	0.005	0.005	0.004	0.004	0.005	0.007	0.004	0.005	0.006	0.006	0.005	0.004
Mn	0.000	0.000	0.000	0.000	0.000	0.000	0.000	0.000	0.000	0.000	0.000	0.000	0.000	0.001
Mg	0.001	0.002	0.001	0.001	0.001	0.001	0.001	0.003	0.001	0.001	0.002	0.001	0.002	0.001
Ca	0.001	0.000	0.000	0.001	0.001	0.000	0.000	0.000	0.000	0.000	0.000	0.000	0.000	0.000
Na	0.002	0.001	0.001	0.001	0.000	0.000	0.000	0.001	0.001	0.001	0.001	0.001	0.000	0.000
K	0.000	0.001	0.000	0.000	0.000	0.000	0.000	0.000	0.000	0.000	0.000	0.001	0.000	0.000
Total	3.001	3.001	3.001	3.000	2.999	2.998	3.000	3.003	3.000	3.000	3.000	3.001	2.999	2.999

Sample No.	1012A	1019C	1019C	1019A	1019A	1023A	1023A
Analysis No.	4.2	1.6	2.9	3.7	3.8	1.8	2.4
Mineral	Tourmaline	Tourmaline	Tourmaline	Tourmaline	Tourmaline	Tourmaline	Tourmaline
SiO_2	39.04	35.39	35.39	36.73	36.40	36.12	35.76
TiO_2	0.60	1.16	1.20	0.48	0.50	0.69	1.07
Al_2O_3	28.52	34.89	34.84	35.04	34.73	34.60	33.53
Cr_2O_3	0.00	0.08	0.11	0.06	0.06	0.10	0.14
Fe_2O_3	0.00	0.00	0.00	0.00	0.00	0.00	0.00
FeO	8.56	7.41	7.37	7.28	7.13	7.63	7.56
MnO	0.05	0.03	0.01	0.01	0.00	0.02	0.02
MgO	5.43	5.23	5.11	4.63	4.77	4.86	5.33
CaO	1.22	0.72	0.74	0.36	0.42	0.56	0.85
Na_2O	1.68	1.82	1.86	1.67	1.75	1.77	1.88
K_2O	2.27	0.06	0.05	0.05	0.04	0.04	0.06
Total	87.37	86.79	86.69	86.44	85.95	86.60	86.53
Cation	Numbers of cations on the basis of 31O						
Si	8.116	7.270	7.277	7.528	7.509	7.438	7.408
Ti	0.093	0.180	0.186	0.074	0.077	0.107	0.166
Al	6.992	8.450	8.447	8.466	8.445	8.399	8.188
Cr	0.000	0.013	0.018	0.011	0.009	0.016	0.024
Fe^{3+}	0.000	0.000	0.000	0.000	0.000	0.000	0.000
Fe^{2+}	1.489	1.273	1.268	1.248	1.231	1.313	1.310
Mn	0.009	0.005	0.001	0.002	0.001	0.003	0.004
Mg	1.683	1.600	1.566	1.414	1.465	1.491	1.646
Ca	0.273	0.158	0.163	0.079	0.094	0.123	0.188
Na	0.676	0.726	0.740	0.666	0.702	0.708	0.756
K	0.603	0.016	0.013	0.012	0.010	0.011	0.017
Total	19.933	19.690	19.680	19.499	19.543	19.608	19.706

Sample No.	1001D	1001D	1001D	1001D	1001D	1001D	1001D	1001D	1001D	1001D	1001D	1001D	1001D	1001D	1001D	1001D	1001D	1001D
Porph. No.	1	1	1	1	1	2	2	2	2	2	3	3	3	3	4	4	4	4	4
Analysis No.	1.1	1.2	1.3	1.4	1.5	2.1	2.2	2.3	2.4	2.5	3.1	3.2	3.4	3.5	4.1	4.2	4.3	4.4	4.5
SiO_2	46.21	53.90	46.94	59.07	56.17	48.95	47.87	36.67	40.72	56.20	31.16	49.46	59.71	77.67	54.25	33.98	48.08	52.61	46.44
TiO_2	0.55	0.10	0.10	0.12	0.09	0.10	0.09	2.24	0.76	0.06	0.42	0.11	0.07	0.04	0.09	0.57	0.17	0.12	0.10
Al_2O_3	24.74	28.78	20.11	18.36	23.75	23.81	24.14	19.56	17.95	22.17	19.22	24.71	19.66	10.73	13.47	15.47	13.56	21.60	20.13
Cr_2O_3	0.03	0.00	0.01	0.02	0.00	0.00	0.00	0.10	0.03	0.02	0.02	0.00	0.00	0.00	0.00	0.03	0.01	0.02	0.02
Fe_2O_3	0.00	0.00	0.00	0.00	0.00	0.00	0.00	0.00	0.00	0.00	0.00	0.00	0.00	0.00	0.00	0.00	0.00	0.00	0.00
FeO	10.72	3.54	11.88	7.21	6.17	9.78	8.08	16.72	8.52	7.76	12.13	0.00	6.15	2.25	14.78	20.74	14.29	8.01	13.83
MnO	0.10	0.00	0.04	0.03	0.05	0.04	0.08	0.09	0.05	0.04	0.03	0.00	0.00	0.02	0.02	0.06	0.08	0.02	0.06
MgO	6.10	3.12	3.44	2.08	3.60	5.58	4.40	7.49	4.55	4.52	2.54	3.59	3.43	2.00	4.68	6.40	6.44	3.15	6.79
CaO	0.41	0.28	0.64	0.49	0.48	1.02	0.73	0.05	0.31	0.66	0.16	0.57	0.51	0.38	0.84	0.89	0.94	0.40	0.96
Na_2O	0.20	0.08	0.10	0.13	0.09	0.11	0.09	0.25	0.11	0.06	0.22	0.10	0.09	0.07	0.10	0.18	0.08	0.07	0.14
K_2O	6.47	8.08	5.44	3.93	6.33	5.07	6.20	8.53	6.30	5.03	4.59	7.12	5.20	2.62	2.61	3.60	4.94	6.68	3.59
Total	95.74	98.06	88.84	91.55	96.93	94.66	91.95	92.01	79.55	96.69	70.64	85.80	94.99	95.84	90.86	82.04	88.69	92.82	92.11

Sample No.	1001D	1001D	1001D	1001D	1001D	1001D	1001D	1001D	1001D	1001D	1001D	1001D	1001D	1001D	1001D	1001D	1001D	1001D
Porph. No.	5	5	5	5	5	6	6	6	6	7	7	7	7	7	8	8	8	8	8
Analysis No.	5.1	5.2	5.3	5.4	5.5	6.1	6.3	6.4	6.5	7.1	7.2	7.3	7.4	7.5	8.1	8.2	8.3	8.4	8.5
SiO_2	61.76	55.47	48.82	42.96	45.00	41.89	69.16	53.85	62.88	38.19	57.60	32.08	35.91	41.55	67.08	51.63	52.74	32.98	47.43
TiO_2	0.21	0.10	0.11	0.20	0.11	0.12	0.06	0.08	0.07	0.40	0.07	1.30	1.87	0.07	0.09	0.12	0.10	1.41	0.10
Al_2O_3	21.74	27.86	22.83	30.43	21.06	15.04	7.14	20.85	14.35	16.49	10.56	17.69	18.97	16.83	14.74	24.58	24.39	17.05	22.49
Cr_2O_3	0.02	0.01	0.01	0.00	0.03	0.00	0.02	0.01	0.00	0.00	0.00	0.09	0.16	0.00	0.00	0.01	0.03	0.06	0.00
Fe_2O_3	0.00	0.00	0.00	0.00	0.00	0.00	0.00	0.00	0.00	0.00	0.00	0.00	0.00	0.00	0.00	0.00	0.00	0.00	0.00
FeO	5.44	3.96	11.32	1.98	14.50	10.47	4.72	5.04	5.99	21.65	12.08	26.16	17.39	20.48	6.89	6.98	8.85	16.38	12.72
MnO	0.04	0.01	0.07	0.03	0.10	0.02	0.02	0.00	0.04	0.11	0.07	0.08	0.06	0.11	0.05	0.07	0.07	0.09	0.05
MgO	3.66	3.13	5.71	1.11	4.99	3.38	1.39	2.57	2.63	7.42	3.49	6.69	7.98	8.51	3.91	4.22	5.38	7.13	5.83
CaO	0.35	0.27	0.80	0.10	0.82	0.79	0.35	0.49	0.54	1.04	0.79	0.22	0.11	1.53	0.61	0.70	0.68	0.18	1.04
Na_2O	0.07	0.09	0.11	0.91	0.23	0.08	0.03	0.12	0.07	0.17	0.08	0.22	0.21	0.11	0.11	0.17	0.14	0.21	0.17
K_2O	5.79	8.24	5.04	9.18	4.63	5.71	2.52	5.97	3.85	2.85	1.84	5.84	7.91	1.39	2.63	6.19	5.72	7.83	4.13
Total	99.17	99.34	94.91	86.99	91.62	77.68	85.53	89.13	90.58	88.32	86.66	90.53	90.75	90.62	96.18	94.84	98.20	83.58	94.03

Average concentrations of selected element oxides from eight porphyroblasts from the Cordierite Zone and weighted averages

Porphyroblast No.	Avg SiO_2	1σ	Avg Al_2O_3	1σ	Avg FeO	1σ	Avg MgO	1σ
Sample 1001D								
1	52.46	5.68	23.15	4.09	7.90	3.40	3.67	1.48
2	46.08	7.60	21.52	2.70	10.17	3.74	5.31	1.31
3	54.50	19.44	18.58	5.80	5.13	4.83	2.89	0.75
4	47.07	7.99	16.84	3.79	14.33	4.52	5.49	1.54
5	50.80	7.76	24.78	4.13	7.44	5.26	3.72	1.79
6	56.94	11.84	14.35	5.62	6.55	2.66	2.49	0.82
7	41.07	9.86	16.11	3.24	19.55	5.23	6.82	1.98
8	50.37	12.22	20.65	4.49	10.36	4.11	5.29	1.30
Weighted Average	49.50	6.10 (2σ)	19.80	2.70 (2σ)	9.30	2.70 (2σ)	3.73	0.83 (2σ)

Appendix C: Zircon Geochronological Data

	COMMON LEAD		Concordance Limit		Discordance		CORRECTED RATIOS								CORRECTED AGES (Ma)							
Sample-Analysis	Correction type	Comment	% common ^{206}Pb		Central %	Min. rim %	^{207}Pb/^{206}Pb		^{207}Pb/^{235}U		^{206}Pb/^{238}U		^{208}Pb/^{232}Th		^{207}Pb/^{206}Pb		^{207}Pb/^{235}U		^{206}Pb/^{238}U		^{208}Pb/^{232}Th	
				1sd				*1sd*		*1sd*		*1sd*		*1sd*		*1sd*		*1sd*		*1sd*		*1sd*
1010B-007	None	Disc. corr: Inversely discordant	.	.	-70.8	-68.5	0.11166	0.00296	1.47130	0.03817	0.09559	0.00145	0.13143	0.00840	1827	49	919	16	589	9	2496	150
1010B-009	None	Disc. corr: Inversely discordant	.	.	-70.9	-67.2	0.09862	0.00344	1.11239	0.03758	0.08183	0.00144	0.04437	0.00351	1598	67	759	18	507	9	877	68
1010B-012	None	Concordant	.	.	-6.3	.	0.05865	0.00221	0.68015	0.02453	0.08412	0.00140	0.02638	0.00180	554	84	527	15	521	8	526	35
1010B-019A	None	Disc. corr: Inversely discordant	.	.	-47.1	-37	0.08433	0.00332	1.37513	0.05206	0.11828	0.00222	0.07343	0.00648	1300	78	878	22	721	13	1432	122
1010B-020	None	Disc. corr: Inversely discordant	.	.	-56.5	-49.3	0.07453	0.00213	0.79555	0.02188	0.07743	0.00114	0.02848	0.00170	1056	59	594	12	481	7	568	33
1010B-021	Disc	OK	4.84	0.82	-38.9	.	0.06562	0.00795	0.72517	0.08671	0.08015	0.00155	0.02450	0.00055	794	267	554	51	497	9	489	11
1010B-023	Disc	OK	43.52	1.65	>100	.	0.04605	0.01605	0.23631	0.08192	0.03722	0.00139	0.03862	0.02413		564	215	67	236	9	766	470
1010B-024	Disc	OK	2.89	0.99	-43.2	.	0.06985	0.00914	0.84288	0.10884	0.08751	0.00189	0.02656	0.00056	924	284	621	60	541	11	530	11
1010B-026	Disc	OK	75.98	5.04	>100	.	0.04605	0.15649	0.14098	0.47818	0.02221	0.00477	0.02141	0.02630		3387	134	426	142	30	428	520
1010B-027	None	Concordant	.	.	-19.3	.	0.05960	0.00197	0.63481	0.02020	0.07724	0.00121	0.02300	0.00162	589	73	499	13	480	7	460	32
1010B-028A	None	Disc. corr: Inversely discordant	.	.	-48.2	-31.5	0.07194	0.00320	0.84765	0.03579	0.08546	0.00163	0.03565	0.00353	984	93	623	20	529	10	708	69
1010B-029	None	Common Pb < det. lim.	0.72	.	-38.3	-15.9	0.06524	0.00252	0.71545	0.02629	0.07953	0.00134	0.02559	0.00221	782	83	548	16	493	8	511	44
1010B-034	Disc	OK	22.72	1.64	>100	.	0.04605	0.01426	0.69906	0.21494	0.11011	0.00416	0.04371	0.01531		499	538	128	673	24	865	297
1010B-037	Disc	OK	77.66	5.74	>100	.	0.04605	0.20605	0.16515	0.73773	0.02601	0.00679	0.00934	0.00751		3644	155	643	166	43	188	150
1010B-038	Disc	OK	36.47	2.03	-55.6	.	0.06684	0.02754	0.56464	0.23173	0.06127	0.00227	0.01869	0.00843	833	848	455	150	383	14	374	167
1010B-039	Disc	OK	29.29	3.42	-84.2	.	0.10543	0.04259	0.70232	0.28124	0.04831	0.00257	0.01403	0.00141	1722	937	540	168	304	16	282	28
1010B-045	Disc	OK	66.11	3.97	-95.2	.	0.11430	0.10133	0.25178	0.22115	0.01598	0.00193	0.00460	0.01323	1869	1811	228	179	102	12	93	266
1010B-048	None	Disc. corr: Inversely discordant	.	.	-51.3	-37.3	0.07186	0.00294	0.79400	0.03090	0.08011	0.00143	0.03975	0.00406	982	85	593	17	497	9	788	79
1010B-049	Disc	OK	65.27	5.24	>100	.	0.04605	0.12028	0.15589	0.40648	0.02455	0.00382	0.01540	0.03266		2958	147	357	156	24	309	650
1010B-050	Disc	OK	8.36	1.17	282	.	0.04859	0.01042	0.51460	0.10968	0.07680	0.00186	0.02433	0.00364	128	381	422	74	477	11	486	72
1010B-053	Disc	OK	9.43	2.45	-34.3	.	0.08739	0.02359	1.87367	0.50081	0.15550	0.00587	0.04606	0.00155	1369	591	1072	177	932	33	910	30
1010B-054	Disc	OK	37.83	2.88	>100	.	0.04605	0.03544	0.35288	0.27095	0.05558	0.00293	0.02327	0.01302		1129	307	203	349	18	465	257
1010B-055	Disc	OK	32.31	2.59	>100	.	0.04605	0.02952	0.31350	0.20049	0.04938	0.00226	0.01977	0.01201		987	277	155	311	14	396	238
1010B-057	Disc	OK	4.67	1.72	-23.9	.	0.09266	0.01636	2.51072	0.43667	0.19652	0.00601	0.05785	0.00166	1481	363	1275	126	1157	32	1137	32
1010B-059	Disc	OK	26.71	2.34	>100	.	0.04605	0.02220	0.28903	0.13881	0.04552	0.00196	0.03490	0.02666		819	258	109	287	12	693	521
1010B-061	None	Concordant	.	.	-11.2	.	0.05892	0.00181	0.65941	0.01966	0.08117	0.00122	0.03010	0.00205	564	69	514	12	503	7	599	40
1010B-062	Disc	OK	46.24	2.18	>100	.	0.04605	0.02078	0.16938	0.07599	0.02668	0.00129	0.01696	0.00677		756	159	66	170	8	340	135
1010B-067	None	Disc. corr: Inversely discordant	.	.	-56.4	-45	0.07393	0.00294	0.77732	0.02944	0.07632	0.00132	0.03333	0.00308	1040	82	584	17	474	8	663	60
1010B-070	Disc	OK	26.99	2.27	>100	.	0.04605	0.02355	0.41970	0.21399	0.06611	0.00265	0.02374	0.00672		857	356	153	413	16	474	133
1010B-072	Disc	OK	4.75	1.02	10.1	.	0.05826	0.00936	0.77176	0.12280	0.09608	0.00216	0.02977	0.00115	540	359	581	70	591	13	593	23
1010B-075	None	Disc. corr: Inversely discordant	.	.	-67.2	-63.4	0.10332	0.00343	1.39661	0.04429	0.09806	0.00160	0.06778	0.00528	1685	63	888	19	603	9	1326	100
1010B-081	Disc	OK	12.05	1.38	1.6	.	0.05776	0.01338	0.68045	0.15672	0.08545	0.00208	0.02651	0.00299	521	459	527	95	529	12	529	59
1010B-084	None	Disc. corr: Inversely discordant	.	.	-58.8	-47.9	0.07910	0.00361	0.89888	0.03916	0.08243	0.00163	0.03316	0.00321	1175	93	651	21	511	10	659	63
1010B-085	None	Disc. corr: Inversely discordant	.	.	-72.1	-68.2	0.10342	0.00403	1.18990	0.04441	0.08351	0.00151	0.05543	0.00538	1686	74	796	21	517	9	1090	103
1010B-088	None	Concordant	.	.	5.7	.	0.22604	0.00922	19.7248	0.77545	0.63404	0.01194	0.20869	0.02395	3024	67	3078	38	3166	47	3831	401
1010B-090	Disc	OK	43.37	3.36	>100	.	0.04605	0.04644	0.37236	0.37474	0.05865	0.00386	0.02064	0.00805		1227	321	277	367	23	413	159
1010B-091A	Disc	OK	4.36	1	-19.7	.	0.05915	0.00945	0.60800	0.09587	0.07455	0.00190	0.02306	0.00102	573	360	482	61	464	11	461	20
1010B-091B	None	Common Pb < det. lim.	1	.	-54.7	-35	0.07492	0.00441	0.84231	0.04686	0.08157	0.00187	0.02942	0.00430	1066	122	620	26	505	11	586	84
1010B-092	Disc	OK	86.88	3.55	-95.2	.	0.08340	0.23107	0.11994	0.33066	0.01043	0.00287	0.00310	0.01266	1279	3647	115	300	67	18	63	255
1010B-096	Disc	OK	36.59	3.47	-88.3	.	0.13383	0.05007	0.85101	0.31445	0.04612	0.00271	0.01308	0.00180	2149	861	625	172	291	17	263	36
1010B-103	Disc	OK	13.41	1.67	-59.8	.	0.07428	0.01690	0.72849	0.16458	0.07113	0.00188	0.02144	0.00071	1049	505	556	97	443	11	429	14
1010B-106	Disc	OK	22.48	1.96	-51.9	.	0.06605	0.02136	0.58498	0.18827	0.06423	0.00206	0.01962	0.00172	808	657	468	121	401	12	393	34
1010B-111	Disc	OK	3.25	0.94	-17.5	.	0.11242	0.00965	4.22423	0.34977	0.27251	0.00612	0.07863	0.00178	1839	160	1679	68	1554	31	1530	33
1010B-114A	Disc	OK	12.52	1.84	-56.9	.	0.07513	0.01853	0.80747	0.19745	0.07795	0.00248	0.02347	0.00099	1072	533	601	111	484	15	469	20
1010B-114B	Disc	OK	7.27	1.59	-61.1	.	0.08012	0.01516	0.87988	0.16453	0.07965	0.00228	0.02381	0.00064	1200	410	641	89	494	14	476	13
1010B-116	Disc	OK	1.15	0.47	-14.7	-4.9	0.14611	0.00735	7.36967	0.34550	0.36581	0.00664	0.10283	0.00206	2301	89	2157	42	2010	31	1978	38
1010B-120	None	Concordant	.	.	0.1	.	0.07667	0.00375	1.99416	0.09384	0.18890	0.00406	0.05793	0.00625	1113	100	1114	32	1115	22	1138	119
1010B-121	Disc	OK	25.21	1.67	-61.4	.	0.08207	0.02040	0.93157	0.23018	0.08233	0.00227	0.02455	0.00238	1247	550	668	121	510	14	490	47
1010B-126A	Disc	OK	55.84	4.56	-85.9	.	0.11851	0.08897	0.80488	0.59813	0.04926	0.00526	0.01414	0.00769	1934	1556	600	336	310	32	284	153
1010B-128	Disc	OK	32.88	5.49	-71.9	.	0.07517	0.06825	0.52752	0.47666	0.05090	0.00450	0.01532	0.01247	1073	1477	430	317	320	28	307	248
1010B-131	Disc	OK	2.81	1.28	-28.9	.	0.06150	0.01192	0.64643	0.12367	0.07624	0.00237	0.02348	0.00155	657	418	506	76	474	14	469	31
1010B-133A	Disc	OK	72.97	8.72	-98.4	.	0.38305	0.30628	0.70590	0.51575	0.01337	0.00434	0.00343	0.03993	3844	3052	542	307	86	28	69	804
1010B-133B	None	^{208}Pb too low for disc. corr.	.	.	-96.7	-96.5	0.72436	0.03023	3.57368	0.14367	0.03580	0.00069	0.21182	0.02334	4780	61	1544	32	227	4	3883	389

	COMMON LEAD		Concordance Limit		Discordance		CORRECTED RATIOS								CORRECTED AGES (Ma)							
Sample-Analysis	Correction type	Comment	% common ^{206}Pb		Central %	Min. rim %	$^{207}Pb/^{206}Pb$		$^{207}Pb/^{235}U$		$^{206}Pb/^{238}U$		$^{208}Pb/^{232}Th$		$^{207}Pb/^{206}Pb$		$^{207}Pb/^{235}U$		$^{206}Pb/^{238}U$		$^{208}Pb/^{232}Th$	
				1sd				*1sd*		*1sd*		*1sd*		*1sd*		*1sd*		*1sd*		*1sd*		*1sd*
1010B-136	Disc	OK	10.86	1.82	-52.3	.	0.07353	0.01823	0.83609	0.20573	0.08247	0.00254	0.02489	0.00151	1029	538	617	114	511	15	497	30
1010B-140	Disc	OK	9.46	1.06	-36.8	.	0.06388	0.01098	0.67477	0.11503	0.07662	0.00166	0.02349	0.00186	738	384	524	70	476	10	469	37
1010B-143	None	Disc. corr: Inversely discordant	.	.	-28.7	-17.3	0.08720	0.00313	2.02015	0.06990	0.16804	0.00290	0.06347	0.00560	1365	71	1122	24	1001	16	1244	106
1010B-144	Disc	OK	2.71	0.6	-5.4	.	0.07557	0.00595	1.80399	0.13847	0.17313	0.00305	0.05209	0.00099	1084	163	1047	50	1029	17	1026	19
1010B-147A	Disc	OK	50.69	3.87	-79.3	.	0.09732	0.06687	0.76717	0.52330	0.05717	0.00470	0.01674	0.00564	1573	1431	578	301	358	29	336	112
1010B-147B	Disc	OK	68.44	6.75	>100	.	0.04605	0.17456	0.34876	1.31994	0.05493	0.01196	0.02112	0.06216		3882	304	994	345	73	423	1230
1010B-152	None	Concordant	.	.	-4.5	.	0.07794	0.00337	1.99564	0.08283	0.18569	0.00357	0.07122	0.00818	1145	88	1114	28	1098	19	1391	154
1012A-003	None	Concordant	.	.	5.1	.	0.05483	0.00253	0.51553	0.02274	0.06826	0.00126	0.02315	0.00227	405	106	422	15	426	8	463	45
1012A-006A	None	Concordant	.	.	-33.6	.	0.06004	0.00300	0.54109	0.02605	0.06542	0.00140	0.02373	0.00289	605	111	439	17	409	8	474	57
1012A-006B	None	Concordant	.	.	17.9	.	0.05394	0.00204	0.51609	0.01888	0.06949	0.00120	0.02594	0.00205	369	87	423	13	433	7	518	40
1012A-013	None	Concordant	.	.	-12.2	.	0.05730	0.00216	0.56295	0.02041	0.07130	0.00118	0.02347	0.00204	503	85	453	13	444	7	469	40
1012A-014	Disc	OK	3.19	1.57	>100	.	0.04605	0.01338	0.36135	0.10451	0.05692	0.00153	0.01850	0.00175		470	313	78	357	9	370	35
1012A-021B	Disc	OK	12.59	1.19	>100	.	0.04605	0.00780	0.16687	0.02782	0.02628	0.00079	0.01648	0.00761		298	157	24	167	5	330	151
1012A-026	None	Concordant	.	.	-27.1	.	0.05895	0.00343	0.54331	0.03016	0.06700	0.00156	0.02563	0.00384	565	130	441	20	418	9	512	76
1012A-027A	None	Concordant	.	.	-15.2	.	0.07171	0.00303	1.37260	0.05580	0.13925	0.00264	0.06654	0.00754	978	88	877	24	840	15	1302	143
1012A-027B	Disc	OK	35.99	2.32	>100	.	0.04605	0.02680	0.07648	0.04439	0.01205	0.00053	0.01164	0.01346		967	75	42	77	3	234	269
1012A-028	Disc	OK	6.21	0.7	>100	.	0.04605	0.00509	0.30689	0.03318	0.04834	0.00110	0.01831	0.00402		221	272	26	304	7	367	80
1012A-030	None	Concordant	.	.	-8.6	.	0.05628	0.00217	0.52870	0.01951	0.06817	0.00113	0.02604	0.00282	463	88	431	13	425	7	520	56
1012A-032	None	Concordant	.	.	-11.3	.	0.05808	0.00258	0.61186	0.02602	0.07655	0.00147	0.02626	0.00318	533	100	485	16	475	9	524	63
1012A-039	None	Concordant	.	.	-4.2	.	0.05609	0.00199	0.54314	0.01883	0.07038	0.00117	0.02723	0.00265	456	81	440	12	438	7	543	52
1012A-042	None	Disc. corr: Inversely discordant	.	.	-32.2	-21.9	0.09084	0.00325	2.13237	0.07341	0.17031	0.00270	0.06685	0.00835	1443	70	1159	24	1014	15	1308	158
1012A-046	None	Concordant	.	.	-14.9	.	0.05704	0.00204	0.53210	0.01859	0.06775	0.00112	0.02429	0.00225	493	81	433	12	423	7	485	44
1012A-048	None	Concordant	.	.	0.4	.	0.05581	0.00163	0.55171	0.01587	0.07175	0.00107	0.02592	0.00222	445	66	446	10	447	6	517	44
1012A-053	Disc	OK	3.9	1.26	71.5	.	0.05058	0.01094	0.41862	0.08973	0.06002	0.00169	0.01892	0.00251	222	394	355	64	376	10	379	50
1012A-056	None	Common Pb < det. lim.	0.52	.	-28.3	-2.2	0.05954	0.00173	0.56102	0.01596	0.06837	0.00101	0.02262	0.00193	587	65	452	10	426	6	452	38
1012A-058	Disc	OK	1.99	0.91	22.1	.	0.05302	0.00809	0.46871	0.07061	0.06411	0.00157	0.02009	0.00186	330	328	390	49	401	9	402	37
1012A-059	None	Concordant	.	.	-2.5	.	0.05560	0.00336	0.52365	0.03059	0.06832	0.00165	0.02302	0.00412	436	138	428	20	426	10	460	81
1012A-060	None	Concordant	.	.	-18.7	.	0.05754	0.00227	0.53358	0.02049	0.06731	0.00120	0.02619	0.00298	512	89	434	14	420	7	523	59
1012A-064	Disc	OK	7.16	0.73	>100	.	0.04605	0.00539	0.28963	0.03336	0.04562	0.00094	0.01749	0.00293		232	258	26	288	6	351	58
1012A-065	None	Concordant	.	.	4.1	.	0.05504	0.00221	0.52395	0.02038	0.06906	0.00120	0.02343	0.00256	414	92	428	14	430	7	468	51
1012A-069A	None	Concordant	.	.	-22.7	.	0.05757	0.00369	0.50845	0.03130	0.06406	0.00159	0.02457	0.00327	513	145	417	21	400	10	491	65
1012A-069B	None	Concordant	.	.	-24.2	.	0.05822	0.00197	0.52974	0.01760	0.06599	0.00110	0.02445	0.00212	538	76	432	12	412	7	488	42
1012A-070	None	Disc. corr: Inversely discordant	.	.	-56.1	-46.3	0.06924	0.00219	0.63168	0.01954	0.06617	0.00107	0.02563	0.00193	906	67	497	12	413	6	512	38
1012A-071	None	Disc. corr: Inversely discordant	.	.	-28.2	-14.2	0.06203	0.00218	0.58348	0.02005	0.06822	0.00115	0.02502	0.00219	675	77	467	13	425	7	499	43
1012A-072	None	Concordant	.	.	-15.6	.	0.05773	0.00242	0.56397	0.02299	0.07085	0.00131	0.02223	0.00194	520	94	454	15	441	8	444	38
1012A-075A	Disc	OK	5.51	1	25.4	.	0.05184	0.00894	0.39577	0.06763	0.05537	0.00132	0.01740	0.00189	278	351	339	49	347	8	349	38
1012A-075B	None	Concordant	.	.	-28.6	.	0.05816	0.00489	0.49629	0.03976	0.06202	0.00192	0.02308	0.00426	536	191	409	27	388	12	461	84
1012A-083	None	Concordant	.	.	-10.5	.	0.05778	0.00193	0.60058	0.01945	0.07540	0.00119	0.02716	0.00217	521	75	478	12	441	7	542	43
1012A-090	None	Common Pb < det. lim.	2.01	.	-62.5	-51.6	0.07269	0.00307	0.63492	0.02608	0.06335	0.00121	0.02206	0.00229	1005	88	499	16	396	7	441	45
1012A-097	None	Initially inv. disc.	.	.	42	7.5	0.05265	0.00260	0.51418	0.02452	0.07082	0.00142	0.02059	0.00214	314	115	421	16	441	9	412	42
1012A-099A	None	Common Pb < det. lim.	1.34	.	-66.6	-55.1	0.07879	0.00435	0.72009	0.03839	0.06629	0.00151	0.02587	0.00336	1167	112	551	23	414	9	516	66
1012A-099B	None	Common Pb < det. lim.	-1.29	.	-51.6	-29.2	0.06529	0.00297	0.56351	0.02491	0.06260	0.00122	0.01639	0.00181	784	98	454	16	391	7	329	36
1012A-100	Disc	OK	35.09	4	-91.8	.	0.14351	0.05645	0.68344	0.26499	0.03454	0.00229	0.00973	0.00107	2270	924	529	160	219	14	196	21
1012A-104	None	Concordant	.	.	-9	.	0.05798	0.00250	0.62215	0.02569	0.07784	0.00137	0.02338	0.00182	529	97	491	16	483	8	467	36
1012A-107	None	Concordant	.	.	-22.5	.	0.05785	0.00261	0.52342	0.02263	0.06560	0.00123	0.02026	0.00174	524	101	427	15	410	7	405	34
1012A-109	None	Concordant	.	.	-22.8	.	0.05809	0.00215	0.53309	0.01913	0.06653	0.00113	0.01882	0.00136	533	83	434	13	415	7	377	27
1012A-112A	Disc	OK	17.54	1.73	-77.7	.	0.05817	0.01790	0.15495	0.04745	0.01932	0.00059	0.00599	0.00245	536	591	146	42	123	4	121	49
1012A-112B	Disc	OK	3.47	0.99	-61.2	.	0.06515	0.00924	0.44788	0.06275	0.04986	0.00109	0.01525	0.00034	779	316	376	44	314	7	306	7
1012A-115	None	Concordant	.	.	-9.3	.	0.05553	0.00218	0.48301	0.01818	0.06308	0.00106	0.02068	0.00147	434	90	400	12	394	6	414	29
1012A-131	None	Concordant	.	.	-22.2	.	0.05784	0.00190	0.52508	0.01686	0.06580	0.00105	0.02031	0.00156	524	74	429	11	411	6	406	31
1012A-133	None	Common Pb < det. lim.	1.44	.	-54.1	-41.6	0.06807	0.00241	0.62300	0.02137	0.06632	0.00111	0.02329	0.00216	871	75	492	13	414	7	465	43
1012A-137	None	Common Pb < det. lim.	0.68	.	-43.1	-12.6	0.06388	0.00303	0.60711	0.02753	0.06889	0.00138	0.02301	0.00223	738	103	482	17	429	8	460	44
1012A-140	None	Concordant	.	.	5.1	.	0.05499	0.00344	0.52579	0.03149	0.06929	0.00165	0.02077	0.00205	412	144	429	21	432	10	416	41
1012A-144	None	Concordant	.	.	-1	.	0.05547	0.00225	0.52406	0.02059	0.06850	0.00124	0.02086	0.00191	431	93	428	14	427	7	417	38
1012A-145	None	Initially inv. disc.	.	.	34.8	3	0.05247	0.00227	0.47413	0.01986	0.06550	0.00122	0.02011	0.00188	306	101	394	14	409	7	402	37

	COMMON LEAD		Concordance Limit		Discordance		CORRECTED RATIOS								CORRECTED AGES (Ma)							
Sample-Analysis	Correction type	Comment	% common ^{206}Pb		Central %	Min. rim %	$^{207}Pb/^{206}Pb$		$^{207}Pb/^{235}U$		$^{206}Pb/^{238}U$		$^{208}Pb/^{232}Th$		$^{207}Pb/^{206}Pb$		$^{207}Pb/^{235}U$		$^{206}Pb/^{238}U$		$^{208}Pb/^{232}Th$	
				1sd				*1sd*		*1sd*		*1sd*		*1sd*		*1sd*		*1sd*		*1sd*		*1sd*
1015A-003	None	Common Pb < det. lim.	-5.53	.	-79.9	-78.3	0.11477	0.00294	1.07547	0.02699	0.06798	0.00102	0.01621	0.00097	1876	47	741	13	424	6	325	19
1015A-004	None	Common Pb < det. lim.	-4.37	.	-64.4	-57.1	0.07637	0.00272	0.70011	0.02403	0.06653	0.00115	0.01535	0.00119	1105	73	539	14	415	7	308	24
1015A-007A	None	Common Pb < det. lim.	-2.47	.	-90.9	-90.3	0.20597	0.00624	1.45567	0.04322	0.05127	0.00084	0.01361	0.00105	2874	50	912	18	322	5	273	21
1015A-007B	Disc	OK	34.75	1.41	>100	.	0.04605	0.00491	0.18327	0.01865	0.02887	0.00092	0.00139	0.00027		215	171	16	183	6	28	5
1015A-008A	Disc	OK	27.24	4.57	-75.6	.	0.06450	0.05153	0.27030	0.21516	0.03039	0.00206	0.00931	0.00073	758	1246	243	172	193	13	187	15
1015A-010	None	Common Pb < det. lim.	8.77	.	-94.6	-94.3	0.26854	0.00823	1.33451	0.03995	0.03607	0.00058	0.01034	0.00081	3298	49	861	17	228	4	208	16
1015A-011A	None	Disc. corr: Inversely discordant	.	.	-87.3	-86.4	0.16300	0.00542	1.33958	0.04282	0.05960	0.00096	0.03140	0.00263	2487	57	863	19	373	6	625	52
1015A-022	None	Common Pb < det. lim.	36	.	-95.6	-95.3	0.31524	0.01113	1.40929	0.04852	0.03246	0.00057	0.00710	0.00065	3547	56	893	20	206	4	143	13
1015A-030	Disc	OK	18.96	3.08	-73.7	.	0.06123	0.03123	0.23413	0.11898	0.02773	0.00119	0.00854	0.00046	647	1017	214	98	176	7	172	9
1015A-032	Disc	OK	10.97	0.67	>100	.	0.04605	0.00402	0.39372	0.03346	0.06202	0.00123	0.02324	0.00260		190	337	24	388	7	464	51
1015A-033	Disc	OK	15.92	7.55	-93.1	.	0.13042	0.07589	0.47913	0.27519	0.02664	0.00249	0.00757	0.00045	2104	1320	397	189	170	16	153	9
1015A-036	Disc	OK	36.07	3.44	>100	.	0.04605	0.04172	0.14182	0.12822	0.02234	0.00133	0.00757	0.00101		1155	135	114	142	8	152	20
1015A-039	None	Common Pb < det. lim.	12.59	.	-90.5	-89.9	0.28626	0.00867	2.60109	0.07696	0.06601	0.00106	0.01902	0.00153	3397	48	1301	22	412	6	381	30
1015A-046	Disc	OK	33.14	1.68	>100	.	0.04605	0.01156	0.22289	0.05543	0.03511	0.00122	0.01461	0.00226		410	204	46	222	8	293	45
1015A-050	Disc	OK	24.05	0.93	>100	.	0.04605	0.00304	0.25636	0.01586	0.04038	0.00092	0.01899	0.00256		145	232	13	255	6	380	51
1015A-052	Disc	OK	18.23	4.08	-55.9	.	0.06084	0.04112	0.38212	0.25746	0.04556	0.00248	0.01405	0.00106	633	1135	329	189	287	15	282	21
1015A-059	Disc	OK	32.25	1.76	>100	.	0.04605	0.01024	0.17908	0.03930	0.02821	0.00101	0.01254	0.00215		367	167	34	179	6	252	43
1015A-060	Disc	OK	28.65	9.77	-58.4	.	0.05910	0.11374	0.31403	0.60274	0.03854	0.00540	0.01192	0.00137	571	2656	277	466	244	34	240	27
1015A-068	None	Disc. corr: Inversely discordant	.	.	-90.1	-89.4	0.23737	0.00752	2.01247	0.06106	0.06150	0.00092	0.03779	0.00337	3102	52	1120	21	385	6	750	66
1015A-070	None	Common Pb < det. lim.	-2.78	.	-64.2	-53.8	0.07479	0.00327	0.66154	0.02751	0.06422	0.00117	0.01576	0.00166	1063	90	516	17	401	7	316	33
1015A-071	Disc	OK	19.39	1.49	>100	.	0.04605	0.00446	0.25359	0.02311	0.03994	0.00131	0.02595	0.00635		203	229	19	252	8	518	125
1015A-075	Disc	OK	22.57	10.42	-86.1	.	0.08028	0.11263	0.31487	0.43964	0.02845	0.00391	0.00850	0.00080	1204	2382	278	339	181	25	171	16
1015A-077	None	Disc. corr: Inversely discordant	.	.	-91.1	-90.5	0.18019	0.00528	1.12595	0.03229	0.04533	0.00072	0.02212	0.00187	2655	50	766	15	286	4	442	37
1015A-078	Disc	OK	30.4	2.04	>100	.	0.04605	0.01780	0.14136	0.05437	0.02227	0.00086	0.00903	0.00138		632	134	48	142	5	182	28
1015A-082	None	Disc. corr: Inversely discordant	.	.	-84.2	-82.8	0.12764	0.00397	1.05338	0.03203	0.05988	0.00099	0.03003	0.00266	2066	56	731	16	375	6	598	52
1015A-083	Disc	OK	12.25	2.94	>100	.	0.04605	0.02694	0.25098	0.14649	0.03953	0.00163	0.01405	0.00175		954	227	119	250	10	282	35
1015A-088	None	Concordant	.	.	-30.8	.	0.05935	0.00253	0.53317	0.02173	0.06517	0.00119	0.02126	0.00217	580	95	434	14	407	7	425	43
1015A-089	Disc	OK	21.64	1.83	>100	.	0.04605	0.01289	0.23487	0.06520	0.03699	0.00131	0.01633	0.00268		454	214	54	234	8	327	53
1015A-094	Disc	OK	23.06	0.9	>100	.	0.04605	0.00290	0.20643	0.01215	0.03251	0.00072	0.02645	0.00342		138	191	10	206	5	528	67
1015A-096	Disc	OK	23.96	0.93	>100	.	0.04605	0.00430	0.20422	0.01851	0.03217	0.00072	0.01310	0.00144		199	189	16	204	4	263	29
1015A-099A	Disc	OK	19.32	1.09	>100	.	0.04605	0.00787	0.23423	0.03966	0.03689	0.00087	0.01402	0.00155		299	214	33	234	5	281	31
1015A-099B	Disc	OK	25.56	2.75	>100	.	0.04605	0.02885	0.16375	0.10236	0.02579	0.00111	0.00879	0.00089		996	154	89	164	7	177	18
1015A-103	Disc	OK	19.76	4.13	>100	.	0.04605	0.04203	0.24636	0.22442	0.03880	0.00221	0.01269	0.00162		1164	224	183	245	14	255	32
1015A-107	Disc	OK	38.95	11.15	-61.1	.	0.05206	0.15113	0.12761	0.36970	0.01778	0.00331	0.00558	0.00087	288	3307	122	333	114	21	113	17
1015A-110	Disc	OK	29.74	8.45	-88.9	.	0.07683	0.09973	0.22248	0.28748	0.02100	0.00260	0.00631	0.00066	1117	2049	204	239	134	16	127	13
1015A-114	Disc	OK	23.69	1.25	>100	.	0.04605	0.00764	0.21367	0.03500	0.03365	0.00089	0.01363	0.00178		291	197	29	213	6	274	36
1015A-117	Disc	OK	3.47	1.24	>100	.	0.04984	0.01063	0.41388	0.08770	0.06022	0.00146	0.01902	0.00148	188	386	352	63	377	9	381	29
1015A-120	None	Common Pb < det. lim.	13.6	.	-88.6	-87.4	0.18927	0.00931	1.57014	0.07371	0.06017	0.00124	0.01929	0.00253	2736	83	958	29	377	8	386	50
1015A-131	None	Common Pb < det. lim.	8.12	.	-83.8	-80.8	0.12382	0.00718	1.01405	0.05642	0.05943	0.00132	0.01957	0.00324	2012	106	711	28	372	8	392	64
1015A-133	Disc	OK	30.5	4.52	>100	.	0.04605	0.05053	0.20854	0.22838	0.03285	0.00234	0.01143	0.00161		1304	192	192	208	15	230	32
1019C-006A	Disc	OK	77.99	3.42	>100	.	0.04605	0.11581	0.03592	0.09015	0.00566	0.00091	0.00566	0.00615		2759	36	88	36	6	114	124
1019C-006B	Disc	OK	61.95	3.96	-81.1	.	0.06340	0.08612	0.19548	0.26471	0.02236	0.00242	0.00686	0.00921	722	1819	181	225	143	15	138	185
1019C-007A	Disc	OK	36.67	3.18	-84.3	.	0.10013	0.04422	0.62027	0.27179	0.04493	0.00248	0.01312	0.00238	1626	1010	490	170	283	15	263	48
1019C-007B	Disc	OK	27.61	1.52	>100	.	0.04605	0.01156	0.34104	0.08491	0.05372	0.00170	0.03579	0.01642		410	298	64	337	10	711	320
1019C-016	Disc	OK	73.53	5.12	-73	.	0.06866	0.16006	0.37715	0.87609	0.03984	0.00787	0.01212	0.03361	888	3350	325	646	252	49	243	671
1019C-017	Disc	OK	62.43	4.31	>100	.	0.04605	0.08896	0.25105	0.48409	0.03954	0.00474	0.01787	0.01400		1970	227	393	250	29	358	278
1019C-019A	None	Common Pb < det. lim.	0.03	.	-24.9	-19	0.18045	0.00632	9.52821	0.32197	0.38351	0.00663	0.10708	0.01107	2657	59	2390	31	2093	31	2056	202
1019C-019B	None	Concordant	.	.	-18.8	.	0.05988	0.00295	0.65318	0.03071	0.07918	0.00159	0.02736	0.00286	599	109	510	19	491	9	546	56
1019C-023B	Disc	OK	48.96	3.07	>100	.	0.04605	0.04668	0.31668	0.32034	0.04988	0.00329	0.02296	0.01848		1219	279	247	314	20	459	365
1019C-036	None	Concordant	.	.	-33.6	.	0.06376	0.00481	0.70353	0.05051	0.08004	0.00235	0.02748	0.00411	734	165	541	30	496	14	548	81
1019C-037	Disc	OK	45.99	4.44	>100	.	0.04605	0.06309	0.18877	0.25809	0.02973	0.00263	0.01213	0.00572		1455	176	220	189	16	244	114
1019C-038	Disc	OK	4.25	1.41	>100	.	0.04605	0.01194	0.86480	0.22311	0.13622	0.00347	0.04631	0.00693		422	633	121	823	20	915	134
1019C-039	Disc	OK	11.80	1.56	>100	.	0.04623	0.01441	0.57752	0.17928	0.09061	0.00252	0.02888	0.00764	10	504	463	115	559	15	576	150
1019C-040	None	Disc. corr: Inversely discordant	.	.	-45.2	-33.4	0.07118	0.00231	0.86544	0.02734	0.08819	0.00144	0.03915	0.00309	963	68	633	15	545	9	776	60
1019C-043	None	Disc. corr: Inversely discordant	.	.	-31.2	-14.6	0.08229	0.00371	1.67279	0.07199	0.14759	0.00304	0.06135	0.00510	1252	90	998	27	887	17	1203	97

	COMMON LEAD		Concordance Limit		Discordance		CORRECTED RATIOS								CORRECTED AGES (Ma)							
Sample-Analysis	Correction type	Comment	% common ^{206}Pb		Central %	Min. rim %	$^{207}Pb/^{206}Pb$		$^{207}Pb/^{235}U$		$^{206}Pb/^{238}U$		$^{208}Pb/^{232}Th$		$^{207}Pb/^{206}Pb$		$^{207}Pb/^{235}U$		$^{206}Pb/^{238}U$		$^{208}Pb/^{232}Th$	
				1sd				*1sd*		*1sd*		*1sd*		*1sd*		*1sd*		*1sd*		*1sd*		*1sd*
1019C-045	Disc	OK	22.47	0.86	>100	.	0.04605	0.00719	0.42948	0.06649	0.06765	0.00140	0.02622	0.00525		280	363	47	422	8	523	103
1019C-049	None	Common Pb < det. lim.	1.51	.	-49.4	-28.7	0.07197	0.00379	0.82969	0.04162	0.08359	0.00183	0.03030	0.00315	985	110	613	23	518	11	603	62
1019C-050B	Disc	OK	45.13	1.82	>100	.	0.04605	0.01763	0.27986	0.10649	0.04408	0.00186	0.08937	0.06335		625	251	84	278	11	1730	1175
1019C-055	Disc	OK	15.17	1.90	-17.8	.	0.06463	0.01938	0.91977	0.27431	0.10321	0.00324	0.03160	0.00564	762	604	662	145	633	19	629	111
1019C-058	Disc	OK	13.08	0.88	>100	.	0.04605	0.00747	0.20876	0.03359	0.03288	0.00068	0.01144	0.00175		286	193	28	209	4	230	35
1019C-059	Disc	OK	61.49	3.90	>100	.	0.04605	0.05949	0.30007	0.38633	0.04726	0.00510	0.13374	0.07314		1424	266	302	298	31	2537	1304
1019C-060	Disc	OK	43.24	2.70	>100	.	0.04605	0.02693	0.39071	0.22745	0.06154	0.00353	0.03804	0.01494		953	335	166	385	21	755	291
1019C-062	Disc	OK	10.82	1.84	-16.2	.	0.08972	0.01845	2.55452	0.52026	0.20650	0.00595	0.06099	0.00173	1420	438	1288	149	1210	32	1197	33
1019C-065	Disc	OK	54.72	4.72	>100	.	0.04605	0.08146	0.25975	0.45865	0.04091	0.00449	0.01610	0.00999		1810	234	370	258	28	323	199
1019C-067A	Disc	OK	33.09	2.07	>100	.	0.04605	0.02401	0.28666	0.14909	0.04515	0.00172	0.01847	0.01111		877	256	118	285	11	370	220
1019C-067B	Disc	OK	55.89	3.01	>100	.	0.04605	0.04474	0.16443	0.15930	0.02590	0.00195	0.02532	0.01831		1235	155	139	165	12	505	361
1019C-068	Disc	OK	23.28	2.89	>100	.	0.04605	0.02985	0.46613	0.30141	0.07342	0.00342	0.02437	0.00624		1000	389	209	457	21	487	123
1019C-072	Disc	OK	4.28	0.60	-2.4	.	0.05580	0.00583	0.53623	0.05517	0.06970	0.00128	0.02171	0.00058	444	238	436	36	434	8	434	11
1019C-073A	Disc	OK	61.44	2.24	>100	.	0.04605	0.01599	0.11472	0.03910	0.01807	0.00120	0.02094	0.00839		561	110	36	115	8	419	166
1019C-073B	Disc	OK	13.58	1.65	-24.5	.	0.05843	0.01608	0.53806	0.14717	0.06678	0.00197	0.02069	0.00268	546	539	437	97	417	12	414	53
1019C-078A	Disc	OK	62.89	4.01	-44.2	.	0.05320	0.08880	0.21980	0.36604	0.02996	0.00336	0.00939	0.01580	337	1938	202	305	190	21	189	316
1019C-079	Disc	OK	15.82	0.74	>100	.	0.04605	0.00621	0.41895	0.05592	0.06599	0.00125	0.02440	0.00524		250	355	40	412	8	487	103
1019C-080	Disc	OK	9.84	1.67	-58.6	-44.1	0.13638	0.01753	3.13217	0.39387	0.16657	0.00446	0.04714	0.00141	2182	235	1441	97	993	25	931	27
1019C-081A	Disc	OK	5.65	1.13	409.7	.	0.04798	0.00979	0.51842	0.10492	0.07836	0.00199	0.02486	0.00310	98	362	424	70	486	12	496	61
1019C-083	Disc	OK	37.08	1.80	>100	.	0.04605	0.01924	0.29820	0.12409	0.04697	0.00172	0.01921	0.00550		690	265	97	296	11	385	109
1019C-085	None	Concordant	.	.	-15.2	.	0.07237	0.00226	1.41393	0.04311	0.14176	0.00231	0.05114	0.00423	996	65	895	18	855	13	1008	81
1019C-087	None	Disc. corr: Inversely discordant	.	.	-63	-55.5	0.08080	0.00311	0.85551	0.03151	0.07682	0.00141	0.03755	0.00326	1217	78	628	17	477	8	745	64
1019C-088	None	Concordant	.	.	-18.4	.	0.06143	0.00416	0.73796	0.04771	0.08717	0.00234	0.02700	0.00365	654	150	561	28	539	14	538	72
1019C-090	Disc	OK	15.01	1.45	-27.3	.	0.05478	0.01428	0.35465	0.09190	0.04695	0.00129	0.01466	0.00246	403	490	308	69	296	8	294	49
1019C-091	Disc	OK	3.67	1.56	-25.6	-17.9	0.23346	0.01838	14.6429	1.08130	0.45490	0.01243	0.12228	0.00341	3076	130	2792	70	2417	55	2332	61
1019C-094	Disc	OK	26.81	2.69	>100	.	0.04605	0.02938	0.38857	0.24733	0.06120	0.00279	0.02230	0.01888		1000	333	181	383	17	446	373
1019C-095	None	Common Pb < det. lim.	1.68	.	-45.1	-30.1	0.08438	0.00438	1.42826	0.07070	0.12278	0.00281	0.04227	0.00555	1301	103	901	30	747	16	837	108
1019C-099	Disc	OK	22.13	2.67	-24.5	.	0.06031	0.02875	0.62852	0.29827	0.07558	0.00337	0.02333	0.01798	615	925	495	186	470	20	466	355
1019C-105	Disc	OK	28.91	1.70	>100	.	0.04605	0.01603	0.15482	0.05363	0.02439	0.00083	0.01793	0.01226		563	146	47	155	5	359	243
1019C-109	None	Concordant	.	.	-32.5	.	0.06439	0.00344	0.74361	0.03796	0.08377	0.00191	0.02780	0.00353	754	116	565	22	519	11	554	69
1019C-111	None	Initially inv. disc.	.	.	35.8	8	0.05523	0.00289	0.69880	0.03517	0.09181	0.00194	0.02990	0.00302	422	120	538	21	566	11	595	59
1019C-114A	Disc	OK	67.53	5.75	>100	.	0.04605	0.13175	0.15227	0.43479	0.02398	0.00439	0.06299	0.09329		3367	144	383	153	28	1235	1774
1019C-114B	Disc	OK	38.68	2.12	>100	.	0.04605	0.02345	0.36897	0.18720	0.05812	0.00251	0.04762	0.03596		852	319	139	364	15	940	694
1019C-120A	Disc	OK	16.56	1.61	-10.6	.	0.05612	0.01605	0.50853	0.14476	0.06572	0.00185	0.02046	0.00279	457	540	417	97	410	11	409	55
1019C-122	Disc	OK	14.27	2.68	2.1	.	0.05388	0.02550	0.44334	0.20893	0.05967	0.00261	0.01867	0.00405	366	881	373	147	374	16	374	80
1019C-124A	None	Concordant	.	.	1.9	.	0.05734	0.00356	0.65568	0.03907	0.08301	0.00204	0.02897	0.00391	505	141	512	24	514	12	577	77
1019C-125	Disc	OK	69.77	5.95	>100	.	0.04605	0.15527	0.14850	0.49984	0.02339	0.00472	0.02154	0.04460		3336	141	442	149	30	431	882
1019C-128	Disc	OK	9.96	1.53	-7	.	0.05302	0.01417	0.35684	0.09489	0.04881	0.00131	0.01530	0.00306	330	493	310	71	307	8	307	61
1019C-129	Disc	OK	29.19	3.53	-33.4	.	0.06465	0.04183	0.74600	0.48074	0.08369	0.00480	0.02562	0.03746	763	1155	566	280	518	29	511	738
1019C-130A	Disc	OK	14.97	2.30	-45	.	0.08378	0.02407	1.40408	0.40034	0.12155	0.00433	0.03616	0.00211	1287	622	891	169	739	25	718	41
1019C-130B	Disc	OK	33.86	3.98	-71.6	.	0.06826	0.05062	0.38977	0.28787	0.04141	0.00275	0.01260	0.02658	876	1257	334	210	262	17	253	531
1019C-133	None	Common Pb < det. lim.	1.35	.	-57.7	-50.7	0.14015	0.00815	3.37697	0.18563	0.17480	0.00419	0.05602	0.00821	2229	103	1499	43	1039	23	1102	157
1019C-141B	Disc	OK	37.49	5.99	-89.7	.	0.13604	0.08250	0.77562	0.46389	0.04135	0.00414	0.01170	0.00148	2177	1404	583	265	261	26	235	30

Appendix D: Zircon Major Element Data

Sample	1010B	1010B	1010B	1010B	1010B	1010B	1010B	1010B	1010B	1010B	1010B	1010B
Analysis	007	009	012	019A	019B	020	021	023	024	026	027	028A
SiO_2	32.50	32.97	33.03	32.90	32.45	32.48	32.87	32.59	30.35	30.48	32.79	32.59
ZrO_2	66.64	67.04	66.97	66.84	65.83	66.33	66.66	66.58	63.77	63.33	66.45	62.62
HfO_2	1.55	1.68	1.70	1.32	1.86	1.40	1.64	1.57	1.91	1.51	1.43	1.72
Y_2O_3	0.39	0.30	0.07	0.24	0.13	0.34	0.35	0.29	0.66	1.08	0.32	0.47
Total	101.09	101.98	101.77	101.30	100.27	100.55	101.52	101.03	96.70	96.40	100.99	97.40
Cations	Numbers of cations based on 4O											
Si	0.991	0.995	0.998	0.998	0.996	0.994	0.996	0.993	0.975	0.980	0.998	1.022
Zr	0.991	0.987	0.987	0.988	0.986	0.990	0.985	0.990	0.999	0.993	0.986	0.957
Hf	0.013	0.015	0.015	0.011	0.016	0.012	0.014	0.014	0.018	0.014	0.012	0.015
Y	0.006	0.005	0.001	0.004	0.002	0.006	0.006	0.005	0.011	0.019	0.005	0.008
Total	2.002	2.001	2.000	2.001	2.001	2.001	2.001	2.001	2.003	2.005	2.001	2.002
Zr+Hf+Y	1.011	1.006	1.002	1.003	1.004	1.007	1.005	1.008	1.028	1.025	1.004	0.980

Sample	1010B	1010B	1010B	1010B	1010B	1010B	1010B	1010B	1010B	1010B	1010B	1010B
Analysis	028B	029	034	037	038	039	040	045	048	049	050	053
SiO_2	29.94	32.62	32.85	30.87	32.95	32.48	28.58	27.36	32.86	31.20	32.40	32.75
ZrO_2	63.01	66.07	66.74	64.68	66.82	66.15	61.55	59.92	66.55	64.29	65.41	66.86
HfO_2	1.83	1.38	1.47	1.51	1.45	1.89	1.42	1.67	1.64	2.00	1.89	1.41
Y_2O_3	0.85	0.28	0.10	0.62	0.19	0.09	1.31	1.68	0.23	0.53	0.49	0.05
Total	95.63	100.35	101.17	97.67	101.40	100.60	92.86	90.63	101.28	98.02	100.19	101.08
Cations	Numbers of cations based on 4O											
Si	0.973	0.998	0.998	0.979	0.998	0.995	0.960	0.948	0.998	0.985	0.996	0.996
Zr	0.999	0.986	0.988	1.000	0.987	0.988	1.008	1.012	0.985	0.990	0.981	0.991
Hf	0.017	0.012	0.013	0.014	0.013	0.016	0.014	0.016	0.014	0.018	0.017	0.012
Y	0.015	0.005	0.002	0.010	0.003	0.001	0.023	0.031	0.004	0.009	0.008	0.001
Total	2.004	2.001	2.000	2.003	2.001	2.000	2.006	2.008	2.001	2.002	2.002	2.000
Zr+Hf+Y	1.030	1.003	1.003	1.024	1.003	1.006	1.045	1.060	1.003	1.017	1.006	1.004

Sample	1010B	1010B	1010B	1010B	1010B	1010B	1010B	1010B	1010B	1010B	1010B	1010B
Analysis	055	057	059	061	062	067	070	072	073	075	078	081
SiO_2	32.67	32.64	32.95	32.69	32.39	33.42	32.52	32.75	32.57	32.50	30.66	29.55
ZrO_2	65.92	66.37	66.73	66.12	66.33	66.73	66.38	65.84	65.95	66.49	64.48	62.50
HfO_2	1.74	1.27	1.33	1.61	1.55	1.43	1.34	1.57	1.75	1.39	1.34	1.55
Y_2O_3	0.24	0.20	0.36	0.34	0.12	0.11	0.34	0.21	0.12	0.15	0.55	1.47
Total	100.56	100.48	101.38	100.76	100.39	101.70	100.59	100.37	100.39	100.53	97.03	95.06
Cations	Numbers of cations based on 4O											
Si	0.999	0.998	0.998	0.998	0.993	1.006	0.994	1.002	0.998	0.994	0.978	0.968
Zr	0.983	0.989	0.986	0.984	0.992	0.980	0.990	0.982	0.985	0.992	1.003	0.998
Hf	0.015	0.011	0.012	0.014	0.014	0.012	0.012	0.014	0.015	0.012	0.012	0.014
Y	0.004	0.003	0.006	0.006	0.002	0.002	0.006	0.003	0.002	0.002	0.009	0.026
Total	2.001	2.001	2.001	2.001	2.001	2.000	2.001	2.001	2.000	2.001	2.002	2.006
Zr+Hf+Y	1.002	1.003	1.003	1.004	1.007	0.994	1.007	0.999	1.003	1.006	1.024	1.038

Sample	1010B	1010B	1010B	1010B	1010B	1010B	1010B	1010B	1010B	1010B	1010B	1010B
Analysis	082	084	085	086	088	090	091A	091B	092	096	097	098A
SiO_2	22.67	32.15	32.89	23.82	32.50	32.82	33.04	32.61	25.40	32.47	32.76	29.88
ZrO_2	53.90	65.17	66.11	52.48	66.27	66.19	66.78	65.85	56.57	65.81	65.97	61.73
HfO_2	1.49	1.61	1.61	1.42	1.54	1.58	1.23	1.36	1.55	1.39	1.98	1.58
Y_2O_3	4.16	0.32	0.24	6.35	0.05	0.21	0.09	0.23	3.78	0.32	0.33	2.07
Total	82.22	99.25	100.85	84.07	100.36	100.79	101.14	100.06	87.31	99.98	101.04	95.26
Cations	Numbers of cations based on 4O											
Si	0.888	0.997	1.001	0.910	0.996	1.000	1.001	1.000	0.925	0.998	0.998	0.976
Zr	1.030	0.985	0.982	0.978	0.990	0.984	0.987	0.985	1.004	0.986	0.980	0.983
Hf	0.017	0.014	0.014	0.016	0.014	0.014	0.011	0.012	0.016	0.012	0.017	0.015
Y	0.087	0.005	0.004	0.129	0.001	0.003	0.002	0.004	0.073	0.005	0.005	0.036
Total	2.022	2.001	2.001	2.032	2.000	2.001	2.000	2.001	2.018	2.001	2.001	2.009
Zr+Hf+Y	1.133	1.005	1.000	1.122	1.004	1.001	0.999	1.001	1.094	1.004	1.003	1.033

Sample	1010B	1010B	1010B	1010B	1010B	1010B	1010B	1010B	1010B	1010B	1010B	1010B
Analysis	103	106	111	114A	114B	116	120	121	126A	126B	128	129
SiO_2	33.35	32.50	33.01	32.93	32.83	32.50	32.80	32.56	32.48	32.41	32.73	30.49
ZrO_2	66.57	65.50	65.81	66.05	66.07	65.83	65.99	65.49	65.97	65.63	66.14	62.88
HfO_2	1.62	1.63	1.28	1.62	1.66	1.68	1.05	1.61	1.56	1.53	1.57	1.65
Y_2O_3	0.18	0.29	0.35	0.13	0.13	0.33	0.65	0.20	0.30	0.13	0.24	1.33
Total	101.72	99.92	100.44	100.73	100.68	100.34	100.49	99.86	100.30	99.71	100.69	96.36
Cations	Numbers of cations based on 4O											
Si	1.005	1.000	1.006	1.003	1.001	0.997	1.001	1.001	0.996	0.999	0.999	0.981
Zr	0.979	0.982	0.978	0.981	0.983	0.985	0.982	0.982	0.987	0.986	0.984	0.987
Hf	0.014	0.014	0.011	0.014	0.014	0.015	0.009	0.014	0.014	0.013	0.014	0.015
Y	0.003	0.005	0.006	0.002	0.002	0.005	0.011	0.003	0.005	0.002	0.004	0.023
Total	2.001	2.001	2.001	2.001	2.001	2.001	2.003	2.001	2.001	2.001	2.001	2.006
Zr+Hf+Y	0.995	1.001	0.995	0.997	0.999	1.005	1.002	1.000	1.005	1.002	1.002	1.025

Sample	1010B	1010B	1010B	1010B	1010B	1010B	1010B	1010B	1010B	1010B	1010B
Analysis	131	132A	132B	133A	133B	136	143	145	147A	147B	152
SiO_2	32.75	32.87	32.23	28.63	18.99	32.02	32.65	32.58	25.30	31.45	32.73
ZrO_2	65.94	66.36	66.04	60.63	46.99	64.97	65.68	66.02	55.56	64.41	65.80
HfO_2	1.57	1.24	1.21	1.82	1.53	1.64	1.55	1.39	1.20	1.64	1.52
Y_2O_3	0.27	0.09	0.30	1.79	5.08	0.24	0.25	0.32	4.03	0.40	0.10
Total	100.53	100.56	99.78	92.86	72.60	98.86	100.13	100.32	86.10	97.90	100.15
Cations	Numbers of cations based on 4O										
Si	1.001	1.002	0.993	0.963	0.856	0.997	1.001	0.998	0.931	0.991	1.003
Zr	0.982	0.986	0.992	0.995	1.033	0.986	0.982	0.986	0.997	0.989	0.983
Hf	0.014	0.011	0.011	0.017	0.020	0.015	0.014	0.012	0.013	0.015	0.013
Y	0.004	0.002	0.005	0.032	0.122	0.004	0.004	0.005	0.079	0.007	0.002
Total	2.001	2.000	2.001	2.008	2.030	2.001	2.001	2.001	2.020	2.002	2.000
Zr+Hf+Y	1.000	0.999	1.008	1.045	1.174	1.004	1.000	1.003	1.089	1.011	0.998

Sample	1012A	1012A	1012A	1012A	1012A	1012A	1012A	1012A	1012A	1012A	1012A	1012A
Analysis	003	006B	013	014	021A	021B	026	027A	027B	028	030	032
SiO_2	31.32	31.34	31.88	31.81	32.61	30.70	32.63	33.21	26.27	32.21	33.01	32.20
ZrO_2	68.88	68.69	69.39	68.79	67.59	61.84	66.90	67.77	53.81	66.66	67.16	65.64
HfO_2	1.69	1.48	1.32	1.29	1.41	1.66	1.62	1.46	1.32	1.47	1.42	2.03
Y_2O_3	0.09	0.14	0.05	0.18	0.22	1.42	0.26	0.31	3.09	0.20	0.20	0.51
Total	101.98	101.65	102.64	102.08	101.82	95.62	101.42	102.75	84.49	100.53	101.80	100.38
Cations	Numbers of cations based on 4O											
Si	0.957	0.960	0.964	0.967	0.987	0.992	0.992	0.994	0.971	0.988	0.997	0.991
Zr	1.027	1.026	1.024	1.020	0.998	0.974	0.991	0.989	0.970	0.997	0.989	0.985
Hf	0.015	0.013	0.011	0.011	0.012	0.015	0.014	0.012	0.014	0.013	0.012	0.018
Y	0.001	0.002	0.001	0.003	0.003	0.024	0.004	0.005	0.061	0.003	0.003	0.008
Total	2.000	2.001	2.000	2.001	2.001	2.006	2.001	2.001	2.015	2.001	2.001	2.002
Zr+Hf+Y	1.043	1.041	1.036	1.034	1.014	1.014	1.009	1.007	1.044	1.013	1.004	1.011

Sample	1012A	1012A	1012A	1012A	1012A	1012A	1012A	1012A	1012A	1012A	1012A	1012A
Analysis	039	042	046	048	053	056	058	059	060	064	065	069A
SiO_2	32.42	32.23	32.56	32.51	32.64	32.77	32.04	32.55	32.14	28.36	32.46	32.72
ZrO_2	66.89	66.71	66.85	67.26	65.98	67.25	65.50	66.70	66.33	57.32	66.67	67.36
HfO_2	1.69	1.53	1.68	1.44	1.43	1.51	1.81	1.80	1.45	1.07	1.52	1.47
Y_2O_3	0.16	0.17	0.14	0.39	0.27	0.15	0.49	0.36	0.33	2.81	0.23	0.28
Total	101.16	100.64	101.23	101.60	100.32	101.68	99.85	101.42	100.26	89.56	100.89	101.83
Cations	Numbers of cations based on 4O											
Si	0.989	0.988	0.991	0.987	0.999	0.992	0.991	0.990	0.989	0.982	0.991	0.990
Zr	0.995	0.997	0.992	0.996	0.985	0.993	0.987	0.990	0.995	0.968	0.993	0.994
Hf	0.015	0.013	0.015	0.013	0.012	0.013	0.016	0.016	0.013	0.011	0.013	0.013
Y	0.003	0.003	0.002	0.006	0.004	0.002	0.008	0.006	0.005	0.052	0.004	0.005
Total	2.001	2.001	2.001	2.002	2.001	2.001	2.002	2.001	2.001	2.013	2.001	2.001
Zr+Hf+Y	1.012	1.013	1.009	1.014	1.002	1.008	1.011	1.011	1.013	1.030	1.010	1.011

Sample	1012A	1012A	1012A	1012A	1012A	1012A	1012A	1012A	1012A	1012A	1012A	1012A
Analysis	069B	070	071	072	075B	083	090	097	099A	099B	100	104
SiO_2	32.89	32.82	32.96	32.55	32.74	32.64	32.37	32.54	32.78	32.08	32.43	29.29
ZrO_2	67.17	66.98	67.14	66.93	66.72	66.77	66.16	66.80	67.00	65.38	66.18	61.35
HfO_2	1.56	1.34	1.36	1.44	1.69	1.54	1.26	1.40	1.41	2.01	1.46	1.43
Y_2O_3	0.19	0.18	0.11	0.14	0.17	0.33	0.80	0.10	0.25	0.75	0.45	1.23
Total	101.81	101.31	101.57	101.06	101.31	101.28	100.59	100.85	101.43	100.22	100.52	93.30
Cations	Numbers of cations based on 4O											
Si	0.994	0.996	0.997	0.992	0.995	0.993	0.991	0.993	0.994	0.990	0.993	0.975
Zr	0.990	0.991	0.990	0.994	0.989	0.990	0.988	0.994	0.991	0.983	0.988	0.995
Hf	0.013	0.012	0.012	0.013	0.015	0.013	0.011	0.012	0.012	0.018	0.013	0.014
Y	0.003	0.003	0.002	0.002	0.003	0.005	0.013	0.002	0.004	0.012	0.007	0.022
Total	2.001	2.001	2.000	2.001	2.001	2.001	2.003	2.000	2.001	2.003	2.002	2.005
Zr+Hf+Y	1.007	1.005	1.004	1.009	1.006	1.009	1.012	1.008	1.007	1.013	1.008	1.031

Sample	1012A	1012A	1012A	1012A	1012A	1012A	1012A	1012A	1012A	1012A	1012A
Analysis	107	109	112A	112B	115	131	133	137	140	144	145
SiO_2	31.69	32.66	25.05	32.22	32.85	32.70	31.80	32.59	32.09	32.17	32.87
ZrO_2	64.09	66.41	52.26	65.47	66.24	66.74	66.01	66.56	66.50	66.24	66.79
HfO_2	1.43	1.49	1.24	1.60	1.65	1.52	1.44	1.40	1.48	1.55	1.39
Y_2O_3	0.54	0.33	3.30	0.75	0.62	0.14	0.17	0.30	0.40	0.27	0.22
Total	97.76	100.90	81.85	100.04	101.36	101.09	99.42	100.85	100.47	100.23	101.28
Cations	Numbers of cations based on 4O										
Si	0.997	0.996	0.960	0.993	0.998	0.995	0.987	0.994	0.986	0.990	0.997
Zr	0.983	0.987	0.976	0.984	0.981	0.990	0.999	0.990	0.996	0.994	0.988
Hf	0.013	0.013	0.014	0.014	0.014	0.013	0.013	0.012	0.013	0.014	0.012
Y	0.009	0.005	0.067	0.012	0.010	0.002	0.003	0.005	0.006	0.004	0.004
Total	2.002	2.001	2.017	2.003	2.003	2.001	2.001	2.001	2.002	2.001	2.001
Zr+Hf+Y	1.005	1.006	1.057	1.010	1.005	1.006	1.014	1.007	1.016	1.012	1.004

Sample	1015A	1015A	1015A	1015A	1015A	1015A	1015A	1015A	1015A	1015A	1015A	1015A
Analysis	003	004	007A	007B	008A	008B	010	011A	011B	022	029	030
SiO_2	30.71	30.83	23.43	26.49	24.03	27.65	23.40	23.63	24.18	24.50	18.87	22.12
ZrO_2	67.53	67.24	57.52	61.76	56.99	59.58	57.54	57.91	58.75	60.01	50.74	56.15
HfO_2	1.27	1.35	1.21	1.34	1.34	1.28	1.25	1.25	1.30	1.25	1.42	1.29
Y_2O_3	0.41	0.28	2.44	1.34	2.84	2.01	2.54	2.40	2.36	1.69	4.05	3.26
Total	99.92	99.70	84.60	90.94	85.21	90.51	84.73	85.20	86.58	87.45	75.08	82.82
Cations	Numbers of cations based on 4O											
Si	0.957	0.962	0.888	0.921	0.901	0.956	0.886	0.889	0.893	0.894	0.827	0.865
Zr	1.026	1.023	1.063	1.047	1.042	1.004	1.062	1.062	1.058	1.068	1.084	1.070
Hf	0.011	0.012	0.013	0.013	0.014	0.013	0.014	0.013	0.014	0.013	0.018	0.014
Y	0.007	0.005	0.049	0.025	0.057	0.037	0.051	0.048	0.046	0.033	0.094	0.068
Total	2.002	2.001	2.012	2.006	2.014	2.009	2.013	2.012	2.012	2.008	2.024	2.017
Zr+Hf+Y	1.045	1.039	1.125	1.085	1.113	1.054	1.127	1.123	1.118	1.114	1.196	1.152

Sample	1015A	1015A	1015A	1015A	1015A	1015A	1015A	1015A	1015A	1015A	1015A	1015A
Analysis	032	033	036	039	046	049	050	052	059	060	068	070
SiO_2	31.02	19.06	23.84	19.37	21.84	19.90	22.00	18.69	16.99	20.08	19.17	28.43
ZrO_2	67.28	51.92	59.38	53.38	49.50	45.82	57.32	50.93	47.85	53.68	54.74	63.33
HfO_2	1.52	1.20	1.32	1.26	1.45	1.27	1.23	1.16	1.22	1.30	1.45	1.39
Y_2O_3	0.46	4.60	2.28	4.29	3.34	4.20	2.31	4.49	4.40	3.97	2.11	1.35
Total	100.28	76.79	86.83	78.29	76.12	71.19	82.85	75.26	70.46	79.02	77.47	94.50
Cations	Numbers of cations based on 4O											
Si	0.963	0.819	0.882	0.816	0.915	0.899	0.859	0.819	0.801	0.833	0.814	0.944
Zr	1.018	1.087	1.071	1.097	1.011	1.009	1.091	1.088	1.100	1.086	1.133	1.025
Hf	0.013	0.015	0.014	0.015	0.017	0.016	0.014	0.014	0.016	0.015	0.018	0.013
Y	0.008	0.105	0.045	0.096	0.075	0.101	0.048	0.105	0.110	0.088	0.048	0.024
Total	2.002	2.026	2.011	2.024	2.019	2.025	2.012	2.026	2.028	2.022	2.012	2.006
Zr+Hf+Y	1.039	1.207	1.129	1.208	1.103	1.126	1.153	1.207	1.227	1.189	1.198	1.062

Sample	1015A	1015A	1015A	1015A	1015A	1015A	1015A	1015A	1015A	1015A	1015A	1015A
Analysis	071	075	077	078	082	083	088	089	094	096	099B	103
SiO_2	19.28	22.63	22.76	29.25	26.36	22.78	32.94	21.43	32.09	24.22	24.04	29.37
ZrO_2	54.76	44.50	53.45	62.62	60.10	55.73	67.25	53.59	66.29	57.25	57.02	63.01
HfO_2	1.40	1.27	1.17	1.43	1.31	1.29	1.29	1.17	1.80	1.37	1.23	1.45
Y_2O_3	3.57	3.69	4.22	1.25	1.79	3.11	0.18	3.65	0.46	2.67	3.14	1.24
Total	79.00	72.10	81.61	94.56	89.56	82.91	101.66	79.83	100.64	85.51	85.44	95.06
Cations	Numbers of cations based on 4O											
Si	0.807	0.980	0.895	0.964	0.929	0.884	0.996	0.868	0.986	0.904	0.899	0.963
Zr	1.117	0.940	1.025	1.006	1.033	1.054	0.991	1.059	0.993	1.042	1.040	1.007
Hf	0.017	0.016	0.013	0.013	0.013	0.014	0.011	0.014	0.016	0.015	0.013	0.014
Y	0.079	0.085	0.088	0.022	0.034	0.064	0.003	0.079	0.008	0.053	0.063	0.022
Total	2.020	2.021	2.022	2.005	2.008	2.016	2.001	2.020	2.002	2.013	2.016	2.005
Zr+Hf+Y	1.213	1.041	1.127	1.042	1.080	1.132	1.005	1.151	1.016	1.109	1.116	1.042

Sample	1015A	1015A	1015A	1015A	1015A	1015A	1015A		1019C	1019C	1019C	1019C
Analysis	107	110	114	117	120	131	133		006A	006B	007A	007B
SiO_2	18.41	19.43	23.36	32.40	20.80	31.18	23.67		27.37	32.81	29.73	32.66
ZrO_2	49.17	46.38	56.05	66.47	52.91	65.17	57.35		60.02	65.66	62.40	65.60
HfO_2	1.18	1.21	1.46	1.34	1.31	1.39	1.27		1.75	1.83	1.73	1.70
Y_2O_3	4.80	4.94	2.90	0.33	3.62	0.72	2.69		1.03	0.13	0.71	0.25
Total	73.56	71.96	83.77	100.54	78.63	98.46	84.97		90.17	100.42	94.57	100.20
Cations	Numbers of cations based on 4O											
Si	0.825	0.876	0.894	0.992	0.859	0.980	0.892		0.951	1.003	0.976	1.001
Zr	1.074	1.020	1.046	0.992	1.066	0.999	1.054		1.017	0.979	0.999	0.981
Hf	0.015	0.016	0.016	0.012	0.015	0.012	0.014		0.017	0.016	0.016	0.015
Y	0.114	0.118	0.059	0.005	0.079	0.012	0.054		0.019	0.002	0.012	0.004
Total	2.029	2.030	2.015	2.001	2.020	2.003	2.013		2.005	2.001	2.003	2.001
Zr+Hf+Y	1.204	1.154	1.121	1.009	1.161	1.023	1.121		1.054	0.997	1.027	1.000

Sample	1019C	1019C	1019C	1019C	1019C	1019C	1019C	1019C	1019C	1019C	1019C	1019C
Analysis	016	017	018	023A	023B	036	037	038	039	040	043	045
SiO_2	31.44	32.81	26.56	31.96	32.57	32.61	32.74	32.45	31.98	32.98	32.72	32.97
ZrO_2	64.88	65.97	59.32	64.82	65.89	65.97	64.91	65.39	65.10	66.02	65.72	65.80
HfO_2	1.85	1.44	1.55	1.71	1.79	1.58	1.45	1.77	1.12	1.68	1.12	1.53
Y_2O_3	0.28	0.34	1.71	0.45	0.14	0.10	0.53	0.31	0.65	0.17	0.58	0.08
Total	98.45	100.56	89.13	98.93	100.40	100.26	99.64	99.92	98.84	100.84	100.15	100.38
Cations	Numbers of cations based on 4O											
Si	0.987	1.002	0.938	0.995	0.998	0.999	1.007	0.999	0.995	1.004	1.002	1.006
Zr	0.993	0.982	1.022	0.984	0.985	0.986	0.974	0.982	0.987	0.980	0.981	0.979
Hf	0.017	0.013	0.016	0.015	0.016	0.014	0.013	0.016	0.010	0.015	0.010	0.013
Y	0.005	0.006	0.032	0.007	0.002	0.002	0.009	0.005	0.011	0.003	0.009	0.001
Total	2.001	2.001	2.008	2.002	2.001	2.000	2.002	2.001	2.003	2.001	2.002	2.000
Zr+Hf+Y	1.014	1.000	1.070	1.007	1.003	1.001	0.995	1.002	1.008	0.997	1.000	0.994

Sample	1019C	1019C	1019C	1019C	1019C	1019C	1019C	1019C	1019C	1019C	1019C	1019C
Analysis	049	050A	050B	055	058	059	060	062	064	065	067A	067B
SiO_2	32.98	32.47	32.40	32.89	32.51	27.11	30.46	32.81	32.08	32.98	29.02	28.27
ZrO_2	66.06	65.45	65.76	65.72	65.07	59.70	62.69	65.96	64.61	65.70	61.72	61.89
HfO_2	1.44	1.65	1.65	1.83	1.25	1.48	1.27	1.34	1.52	1.48	1.86	1.60
Y_2O_3	0.07	0.22	0.32	0.09	0.50	2.00	1.59	0.13	0.17	0.27	1.14	0.90
Total	100.55	99.79	100.13	100.54	99.34	90.28	96.01	100.24	98.39	100.43	93.74	92.66
Cations	Numbers of cations based on 4O											
Si	1.005	1.000	0.996	1.004	1.004	0.944	0.982	1.003	1.001	1.006	0.966	0.954
Zr	0.982	0.983	0.986	0.979	0.979	1.014	0.986	0.983	0.983	0.978	1.002	1.018
Hf	0.013	0.015	0.014	0.016	0.011	0.015	0.012	0.012	0.014	0.013	0.018	0.015
Y	0.001	0.004	0.005	0.002	0.008	0.037	0.027	0.002	0.003	0.004	0.020	0.016
Total	2.000	2.001	2.001	2.000	2.002	2.009	2.007	2.001	2.001	2.001	2.005	2.004
Zr+Hf+Y	0.995	1.001	1.005	0.996	0.999	1.065	1.025	0.997	1.000	0.995	1.039	1.050

Sample	1019C	1019C	1019C	1019C	1019C	1019C	1019C	1019C	1019C	1019C	1019C	1019C
Analysis	049	050A	050B	055	058	059	060	062	064	065	067A	067B
SiO_2	32.98	32.47	32.40	32.89	32.51	27.11	30.46	32.81	32.08	32.98	29.02	28.27
ZrO_2	66.06	65.45	65.76	65.72	65.07	59.70	62.69	65.96	64.61	65.70	61.72	61.89
HfO_2	1.44	1.65	1.65	1.83	1.25	1.48	1.27	1.34	1.52	1.48	1.86	1.60
Y_2O_3	0.07	0.22	0.32	0.09	0.50	2.00	1.59	0.13	0.17	0.27	1.14	0.90
Total	100.55	99.79	100.13	100.54	99.34	90.28	96.01	100.24	98.39	100.43	93.74	92.66
Cations	Numbers of cations based on 4O											
Si	1.005	1.000	0.996	1.004	1.004	0.944	0.982	1.003	1.001	1.006	0.966	0.954
Zr	0.982	0.983	0.986	0.979	0.979	1.014	0.986	0.983	0.983	0.978	1.002	1.018
Hf	0.013	0.015	0.014	0.016	0.011	0.015	0.012	0.012	0.014	0.013	0.018	0.015
Y	0.001	0.004	0.005	0.002	0.008	0.037	0.027	0.002	0.003	0.004	0.020	0.016
Total	2.000	2.001	2.001	2.000	2.002	2.009	2.007	2.001	2.001	2.001	2.005	2.004
Zr+Hf+Y	0.995	1.001	1.005	0.996	0.999	1.065	1.025	0.997	1.000	0.995	1.039	1.050

Sample	1019C	1019C	1019C	1019C	1019C	1019C	1019C	1019C	1019C	1019C	1019C	1019C
Analysis	068	071A	071B	072	073A	073B	078A	078B	079	080	081A	081B
SiO_2	32.38	26.95	26.78	32.74	32.83	33.09	26.77	27.29	29.75	32.42	32.97	30.80
ZrO_2	65.29	60.65	57.43	65.61	65.84	66.21	60.71	61.51	60.91	65.86	65.86	63.59
HfO_2	1.60	1.27	1.50	1.62	1.67	1.67	1.52	1.40	1.32	1.55	1.49	1.79
Y_2O_3	0.26	1.81	0.77	0.19	0.27	0.20	1.19	1.46	0.60	0.27	0.10	0.36
Total	99.52	90.68	86.47	100.17	100.61	101.18	90.19	91.65	92.58	100.10	100.42	96.53
Cations	Numbers of cations based on 4O											
Si	1.000	0.936	0.965	1.003	1.002	1.004	0.935	0.937	0.991	0.996	1.006	0.986
Zr	0.983	1.027	1.009	0.980	0.980	0.979	1.034	1.030	0.989	0.987	0.980	0.993
Hf	0.014	0.013	0.015	0.014	0.015	0.014	0.015	0.014	0.013	0.014	0.013	0.016
Y	0.004	0.034	0.015	0.003	0.004	0.003	0.022	0.027	0.011	0.004	0.002	0.006
Total	2.001	2.008	2.004	2.001	2.001	2.001	2.006	2.007	2.003	2.001	2.000	2.002
Zr+Hf+Y	1.001	1.073	1.039	0.998	0.999	0.997	1.071	1.070	1.012	1.005	0.994	1.015

Sample	1019C	1019C	1019C	1019C	1019C	1019C	1019C	1019C	1019C	1019C	1019C	1019C
Analysis	083	085	086	087	088	089	090	091	093	094	095	099
SiO_2	33.00	31.42	32.94	32.11	32.93	32.79	33.11	32.68	31.14	31.90	31.65	32.80
ZrO_2	65.96	64.56	65.80	65.15	65.89	65.83	66.41	65.89	63.59	64.78	64.86	65.59
HfO_2	1.38	1.61	1.28	1.32	1.14	1.62	1.36	1.12	1.06	1.72	1.26	1.08
Y_2O_3	0.29	0.63	0.38	0.38	0.42	0.19	0.12	0.59	0.57	0.41	0.33	0.51
Total	100.62	98.23	100.39	98.96	100.38	100.43	101.00	100.29	96.36	98.80	98.10	99.98
Cations	Numbers of cations based on 4O											
Si	1.005	0.988	1.005	0.997	1.005	1.002	1.005	1.000	0.994	0.995	0.993	1.005
Zr	0.980	0.990	0.979	0.986	0.980	0.981	0.982	0.983	0.989	0.985	0.992	0.980
Hf	0.012	0.014	0.011	0.012	0.010	0.014	0.012	0.010	0.010	0.015	0.011	0.009
Y	0.005	0.011	0.006	0.006	0.007	0.003	0.002	0.010	0.010	0.007	0.006	0.008
Total	2.001	2.003	2.002	2.002	2.002	2.001	2.000	2.002	2.002	2.002	2.001	2.002
Zr+Hf+Y	0.996	1.015	0.996	1.004	0.997	0.998	0.996	1.003	1.009	1.007	1.009	0.997

Sample	1019C	1019C	1019C	1019C	1019C	1019C	1019C	1019C	1019C	1019C	1019C	1019C
Analysis	083	085	086	087	088	089	090	091	093	094	095	099
SiO_2	33.00	31.42	32.94	32.11	32.93	32.79	33.11	32.68	31.14	31.90	31.65	32.80
ZrO_2	65.96	64.56	65.80	65.15	65.89	65.83	66.41	65.89	63.59	64.78	64.86	65.59
HfO_2	1.38	1.61	1.28	1.32	1.14	1.62	1.36	1.12	1.06	1.72	1.26	1.08
Y_2O_3	0.29	0.63	0.38	0.38	0.42	0.19	0.12	0.59	0.57	0.41	0.33	0.51
Total	100.62	98.23	100.39	98.96	100.38	100.43	101.00	100.29	96.36	98.80	98.10	99.98
Cations	Numbers of cations based on 4O											
Si	1.005	0.988	1.005	0.997	1.005	1.002	1.005	1.000	0.994	0.995	0.993	1.005
Zr	0.980	0.990	0.979	0.986	0.980	0.981	0.982	0.983	0.989	0.985	0.992	0.980
Hf	0.012	0.014	0.011	0.012	0.010	0.014	0.012	0.010	0.010	0.015	0.011	0.009
Y	0.005	0.011	0.006	0.006	0.007	0.003	0.002	0.010	0.010	0.007	0.006	0.008
Total	2.001	2.003	2.002	2.002	2.002	2.001	2.000	2.002	2.002	2.002	2.001	2.002
Zr+Hf+Y	0.996	1.015	0.996	1.004	0.997	0.998	0.996	1.003	1.009	1.007	1.009	0.997

Sample	1019C	1019C	1019C	1019C	1019C	1019C	1019C	1019C	1019C	1019C	1019C	1019C
Analysis	105	106	109	110A	110B	111	114A	114B	116	120A	122	124A
SiO_2	21.30	32.88	32.42	32.15	29.73	32.72	32.75	32.58	32.43	32.48	32.92	32.74
ZrO_2	53.42	65.84	65.32	64.96	62.65	65.93	65.98	65.38	65.72	65.89	66.19	65.64
HfO_2	1.95	1.34	1.33	1.63	1.70	1.32	1.43	1.97	1.19	1.42	1.42	1.67
Y_2O_3	3.54	0.17	0.16	0.31	0.77	0.22	0.15	0.11	0.39	0.13	0.16	0.19
Total	80.21	100.23	99.24	99.05	94.85	100.19	100.30	100.04	99.72	99.92	100.69	100.24
Cations	Numbers of cations based on 4O											
Si	0.864	1.005	1.002	0.998	0.974	1.002	1.002	1.001	0.998	0.998	1.003	1.003
Zr	1.056	0.981	0.984	0.983	1.000	0.984	0.984	0.980	0.986	0.988	0.983	0.980
Hf	0.023	0.012	0.012	0.014	0.016	0.012	0.012	0.017	0.010	0.012	0.012	0.015
Y	0.076	0.003	0.003	0.005	0.013	0.004	0.002	0.002	0.006	0.002	0.003	0.003
Total	2.019	2.001	2.001	2.001	2.003	2.001	2.001	2.000	2.002	2.001	2.001	2.001
Zr+Hf+Y	1.155	0.996	0.999	1.003	1.030	0.999	0.999	0.999	1.003	1.002	0.998	0.998

Sample	1019C	1019C	1019C	1019C	1019C	1019C	1019C	1019C-	1019C	1019C
Analysis	124B	125	127	128	129	130A	133	141A	141B	141C
SiO_2	32.61	27.79	31.09	30.17	33.04	32.45	31.38	32.22	24.76	32.61
ZrO_2	65.51	61.14	64.28	63.37	65.73	65.31	64.07	64.84	59.27	65.29
HfO_2	1.65	1.47	1.70	1.52	1.61	1.57	1.51	1.55	1.13	1.76
Y_2O_3	0.26	1.21	0.65	0.70	0.21	0.27	0.51	0.17	2.17	0.05
Total	100.02	91.60	97.72	95.75	100.58	99.60	97.47	98.78	87.33	99.72
Cations	Numbers of cations based on 4O									
Si	1.001	0.950	0.984	0.977	1.007	1.001	0.992	1.001	0.903	1.004
Zr	0.981	1.019	0.992	1.000	0.977	0.982	0.988	0.983	1.054	0.980
Hf	0.014	0.014	0.015	0.014	0.014	0.014	0.014	0.014	0.012	0.015
Y	0.004	0.022	0.011	0.012	0.003	0.004	0.009	0.003	0.042	0.001
Total	2.001	2.006	2.003	2.003	2.001	2.001	2.002	2.001	2.011	2.000
Zr+Hf+Y	1.000	1.056	1.019	1.026	0.994	1.000	1.010	0.999	1.108	0.996

Appendix E: Zircon Trace Element Data

Sample	1010B	1010B	1010B	1010B	1010B	1010B	1010B	1010B	1010B	1010B	1010B	1010B
Analysis	007	009	012	019A	020	021	023	024	026	027	028A	029
P	1256	695	312	1339	338	723	3666	1163	6590	345	731	331
Ti	12.2	5.6	26.6	19.5	5.5	47.6	25.4	38.3	184.1	6.2	10.9	21.9
Y	2932	2374	869	2713	1956	1617	12638	2503	20270	1311	2847	1618
Nb	1.8	4.6	2.0	1.3	3.6	4.3	7.7	3.6	16.0	5.6	2.4	1.8
La	12.36	7.91	1.01	20.09	1.67	8.20	99.15	5.43	328.08	0.48	1.52	1.12
Ce	49.4	37.0	22.4	75.8	51.5	35.4	401.9	37.2	1216.9	50.9	12.1	27.2
Pr	9.2	5.1	1.0	14.7	1.6	4.9	73.9	4.3	227.9	0.6	1.4	1.5
Nd	58.8	26.3	8.2	92.0	11.6	28.6	421.2	28.8	1306.8	4.8	14.7	13.3
Sm	42.8	19.8	8.6	56.7	12.8	16.1	275.4	22.6	622.8	7.0	18.5	15.6
Eu	10.1	3.8	1.5	15.4	4.3	4.5	81.6	7.3	225.3	1.6	2.6	1.6
Gd	101	60	29	112	49	39	468	69	1006	30	76	54
Tb	30.3	21.5	8.7	37.3	16.4	12.2	154.8	22.5	260.3	10.1	25.6	16.6
Dy	308	244	91	345	185	142	1537	239	2265	117	292	170
Ho	100	82	30	99	67	51	420	81	599	43	102	56
Er	401	339	116	368	290	237	1499	326	2046	191	418	223
Tm	86	69	24	74	62	53	295	65	377	42	85	44
Yb	862	648	235	713	596	534	2556	580	3243	413	769	393
Lu	147	103	40	124	107	98	316	101	454	73	133	65
Hf	13134	14279	14395	11206	11882	13937	13294	16184	12784	12120	14624	11687
Ta	1.19	2.26	0.99	0.75	1.25	1.86	13.20	1.47	12.47	1.98	1.05	0.84
Th	107	339	247	224	441	189	395	285	1793	451	217	371
U	673	731	429	793	489	621	2110	457	4441	489	424	454
$(Lu/La)_N$	115	126	379	60	616	115	31	179	13	1471	840	561
$(Sm/La)_N$	5.5	4.0	13.5	4.5	12.2	3.1	4.4	6.6	3.0	23.3	19.3	22.2
$(Lu/Gd)_N$	11.7	13.8	10.9	8.9	17.3	20.3	5.4	11.7	3.6	19.8	14.1	9.7
Ce/Ce*	1.09	1.37	5.23	1.03	7.42	1.31	1.10	1.81	1.04	23.13	1.92	4.97
Eu/Eu*	0.47	0.34	0.29	0.59	0.53	0.56	0.69	0.56	0.87	0.34	0.21	0.16
ΣREE	2218	1667	617	2147	1457	1264	8598	1588	14178	985	1951	1081

Sample	1010B	1010B	1010B	1010B	1010B	1010B	1010B	1010B	1010B	1010B	1010B	1010B
Analysis	034	037	038	039	045	048	049	050	053	055	057	059
P	390	6068	1033	1255	7257	568	6818	1460	446	1622	1530	295
Ti	21.8	22.6	8.3	9.6	135.8	10.4	104.2	20.7	21.3	21.8	11.1	9.2
Y	1011	26560	3368	5310	22109	1374	24894	1722	2707	4533	1567	1700
Nb	2.8	12.0	4.8	8.0	10.0	4.7	10.3	3.1	4.6	3.4	1.9	1.5
La	4.55	266.91	36.62	63.08	313.22	7.47	230.86	8.77	2.97	33.13	3.81	1.14
Ce	18.2	1007.6	117.7	220.0	1155.9	32.1	931.0	52.6	18.9	136.9	33.4	21.8
Pr	3.0	179.3	21.8	41.3	231.0	4.4	180.1	7.0	2.7	26.3	2.0	0.8
Nd	15.7	1019.0	119.9	228.8	1354.0	24.6	1062.9	38.0	21.7	157.5	13.6	7.9
Sm	8.4	612.6	74.1	115.2	750.6	14.8	652.6	21.1	21.3	103.5	11.7	10.9
Eu	2.0	236.0	19.1	38.6	311.2	4.0	231.1	3.6	4.7	40.3	4.5	2.8
Gd	28	1085	128	217	1192	33	1118	47	86	196	41	40
Tb	8.9	327.9	43.0	53.1	306.4	10.8	321.0	16.2	26.0	56.8	13.7	13.4
Dy	100	2934	433	488	2570	119	2730	168	290	515	149	156
Ho	35	768	122	159	658	43	681	54	98	148	52	57
Er	145	2567	458	646	2214	190	2198	220	389	538	223	249
Tm	29	481	96	138	413	42	386	46	76	103	51	56
Yb	276	4102	846	1350	3669	433	3078	427	673	901	490	571
Lu	47	548	118	236	498	77	420	72	109	136	84	99
Hf	12505	12790	12291	15997	14125	13944	16990	16037	11961	14755	10760	11285
Ta	0.81	5.79	3.69	2.73	8.39	3.53	15.25	2.16	1.82	1.66	0.62	0.79
Th	26	4126	238	798	577	193	970	309	118	354	117	271
U	70	2549	978	1271	3679	558	3964	675	127	941	144	284
$(Lu/La)_N$	100	20	31	36	15	100	18	79	353	40	213	836
$(Sm/La)_N$	2.9	3.6	3.2	2.9	3.8	3.1	4.5	3.8	11.4	5.0	4.9	15.2
$(Lu/Gd)_N$	13.5	4.1	7.4	8.7	3.4	18.6	3.0	12.3	10.1	5.6	16.7	20.1
Ce/Ce*	1.15	1.08	0.98	1.01	1.01	1.32	1.07	1.57	1.55	1.09	2.81	5.30
Eu/Eu*	0.39	0.88	0.60	0.75	1.01	0.56	0.83	0.35	0.34	0.87	0.62	0.41
ΣREE	722	16133	2633	3995	15636	1037	14220	1182	1821	3091	1172	1286

Sample	1010B	1010B	1010B	1010B	1010B	1010B	1010B	1010B	1010B	1010B	1010B	1010B
Analysis	061	062	067	070	072	075	081	082	084	085	088	090
P	315	5340	3334	430	700	263	431	4615	766	739	1149	744
Ti	3.3	156.3	31.6	31.8	9.2	5.2	12.9	66.2	32.4	7.6	28.7	14.7
Y	2493	11804	5856	1617	1927	837	1412	22441	1534	1594	2280	4569
Nb	28.5	5.2	7.5	2.2	4.9	1.4	6.6	13.4	2.4	3.8	5.1	4.2
La	3.17	229.12	72.79	14.17	4.28	2.62	17.69	214.00	9.87	4.96	16.06	23.10
Ce	36.4	1076.3	135.9	65.6	32.5	13.5	104.3	831.1	50.9	24.6	79.4	127.9
Pr	1.3	203.4	33.9	9.8	3.5	1.8	11.6	157.4	2.8	2.7	9.6	18.2
Nd	9.0	1205.7	170.0	56.9	23.0	10.9	65.2	920.0	16.5	18.6	55.9	120.5
Sm	9.3	505.1	92.2	34.4	15.9	7.3	40.5	573.3	12.2	12.5	34.3	83.1
Eu	9.8	283.7	18.7	11.1	4.1	1.4	14.4	204.6	3.3	3.5	9.8	35.4
Gd	47	771	239	60	47	21	68	1013	46	35	75	188
Tb	18.1	162.5	68.2	18.6	15.9	6.9	18.6	284.8	13.9	12.4	22.2	55.1
Dy	229	1237	658	172	179	77	164	2416	145	136	228	503
Ho	88	303	205	51	66	27	43	609	52	51	75	148
Er	392	958	770	198	285	121	158	2006	212	233	307	562
Tm	80	171	147	42	61	27	35	354	43	53	61	111
Yb	754	1470	1314	415	586	270	370	2995	415	533	570	1054
Lu	124	222	208	71	104	49	59	388	73	97	95	162
Hf	13618	13143	12121	11380	13287	11828	13119	12627	13644	13663	13089	13401
Ta	6.97	3.88	1.88	1.30	1.82	0.65	1.27	8.97	0.97	1.60	1.57	1.20
Th	383	2286	1088	211	171	124	516	1846	255	259	327	593
U	725	2990	867	373	331	342	1264	2905	226	700	405	599
$(Lu/La)_N$	376	9	28	48	234	181	32	17	72	189	57	67
$(Sm/La)_N$	4.7	3.5	2.0	3.9	5.9	4.4	3.6	4.3	2.0	4.0	3.4	5.7
$(Lu/Gd)_N$	21.0	2.3	7.0	9.5	17.6	18.6	7.0	3.1	12.8	22.4	10.2	6.9
Ce/Ce*	4.13	1.17	0.64	1.31	1.97	1.45	1.70	1.06	2.28	1.56	1.50	1.46
Eu/Eu*	0.55	1.39	0.39	0.75	0.46	0.35	0.84	0.82	0.43	0.52	0.59	0.87
ΣREE	1792	8798	4133	1218	1428	637	1169	12965	1096	1217	1638	3189

Sample	1010B	1010B	1010B	1010B	1010B	1010B	1010B	1010B	1010B	1010B	1010B	1010B
Analysis	091B	092	096	103	106	111	114A	114B	116	120	121	126A
P	935	7412	868	2731	2610	366	558	630	859	302	1520	1450
Ti	13.8	228.3	18.2	31.9	9.4	27.1	12.4	11.9	22.8	4.1	59.3	16.8
Y	1270	30934	3243	8002	4761	1006	1992	2387	2487	2861	7634	5922
Nb	2.8	12.3	3.8	5.7	3.5	3.2	2.3	1.9	6.5	3.8	6.2	3.2
La	4.63	385.04	45.17	92.59	27.46	3.02	3.64	2.19	17.37	0.38	51.57	67.04
Ce	20.5	1374.1	134.1	322.2	117.5	25.0	19.1	14.6	64.2	24.6	201.5	263.4
Pr	3.4	277.7	23.2	54.6	18.2	1.6	2.7	1.6	10.1	1.0	38.4	46.1
Nd	21.8	1648.9	138.2	303.0	115.8	10.2	16.3	12.4	60.5	18.4	228.3	271.2
Sm	15.2	973.3	67.5	139.1	72.7	7.2	15.7	16.8	37.0	27.5	137.1	168.1
Eu	4.2	536.4	27.2	30.1	20.3	1.6	3.1	2.1	11.0	5.6	54.4	44.2
Gd	37	1716	132	264	160	22	52	65	82	107	284	278
Tb	12.0	427.0	33.6	81.5	50.1	8.5	18.1	21.5	24.8	31.8	85.6	80.8
Dy	132	3223	302	815	505	92	202	245	256	316	743	691
Ho	43	765	92	252	159	34	69	84	85	104	202	186
Er	178	2295	351	959	648	151	284	345	355	410	725	672
Tm	37	384	67	187	136	33	59	70	81	80	140	133
Yb	353	3082	604	1640	1311	316	531	632	828	731	1311	1266
Lu	60	426	99	236	216	55	87	107	137	118	209	183
Hf	11567	13180	11768	13735	13789	10814	13732	14040	14268	8896	13681	13234
Ta	1.38	13.36	2.18	3.13	2.10	1.07	0.95	0.91	3.99	1.05	3.29	1.53
Th	212	1501	413	909	773	77	194	235	332	436	520	862
U	537	3781	761	1388	947	135	293	306	1006	299	1712	1506
$(Lu/La)_N$	126	11	21	25	76	175	230	470	76	2973	39	26
$(Sm/La)_N$	5.2	4.0	2.4	2.4	4.2	3.8	6.8	12.2	3.4	114.3	4.2	4.0
$(Lu/Gd)_N$	13.0	2.0	6.0	7.2	10.9	19.6	13.3	13.2	13.4	8.8	5.9	5.3
Ce/Ce*	1.21	0.98	0.97	1.06	1.23	2.68	1.42	1.86	1.14	9.42	1.06	1.11
Eu/Eu*	0.53	1.27	0.88	0.48	0.58	0.38	0.33	0.19	0.61	0.31	0.84	0.62
ΣREE	923	17513	2116	5376	3558	760	1362	1618	2049	1975	4412	4350

Sample	1010B	1010B	1010B	1010B	1010B	1010B	1010B	1010B	1012A	1012A	1012A
Analysis	128	131	133A	133B	136	143	147B	152	003	006A	006B
P	2558	722	6692	7370	509	1056	2293	421	216	937	612
Ti	31.4	11.2	58.1	53.0	4.9	15.7	23.1	19.5	20.9	143.6	6.6
Y	11418	2525	20758	24441	1169	3090	7495	1425	1301	7207	1735
Nb	3.8	2.7	11.8	9.8	1.4	2.3	14.6	9.1	3.2	12.5	3.3
La	184.93	6.35	315.85	452.90	3.92	2.25	114.44	2.04	40.4	218.7	3.1
Ce	528.2	28.7	1245.0	1596.3	26.8	13.2	492.7	22.0	116	1126	26
Pr	94.4	4.9	199.9	263.5	2.7	1.4	92.7	1.0	27.0	180.2	2.5
Nd	523.1	29.5	1172.1	1512.5	15.7	11.5	542.1	7.0	171	1082	17
Sm	303.2	22.0	658.1	795.5	10.0	17.4	254.0	7.1	85.4	593.3	13.6
Eu	103.2	6.3	210.6	215.9	2.5	2.2	87.7	10.3	15.8	174.2	3.1
Gd	540	68	1089	1300	30	72	398	35	141	845	39
Tb	155.7	22.7	286.3	337.4	10.2	25.5	92.9	11.9	26	164	13
Dy	1371	251	2417	2778	110	302	733	139	187	1086	154
Ho	362	87	600	714	39	111	191	52	47	250	61
Er	1237	361	2018	2341	172	480	633	221	159	812	280
Tm	231	73	367	419	37	100	115	45	31	145	60
Yb	1958	677	3112	3325	360	957	1037	421	285	1283	586
Lu	270	116	421	500	61	163	153	71	57	232	113
Hf	13304	13351	15397	12968	13891	13122	13880	12877	14359	12528	12528
Ta	2.82	1.32	106.27	66.32	1.25	0.69	7.80	1.90	1.2	4.5	1.4
Th	1303	286	1409	1673	269	176	779	135	126	691	174
U	1914	613	5353	6503	592	304	1958	247	321	1453	409
$(Lu/La)_N$	14	176	13	11	151	696	13	337	14	10.2	357
$(Sm/La)_N$	2.6	5.5	3.3	2.8	4.0	12.3	3.5	5.6	3.4	4.3	7.1
$(Lu/Gd)_N$	4.0	13.6	3.1	3.1	16.3	18.1	3.1	16.4	3.2	2.2	23.2
Ce/Ce*	0.94	1.21	1.16	1.08	1.92	1.77	1.12	3.66	0.8	1.3	2.2
Eu/Eu*	0.78	0.50	0.76	0.65	0.43	0.19	0.84	0.53	0.44	0.75	0.41
ΣREE	7861	1752	14112	16551	882	2258	4937	1036	1388	8192	1372

Sample	1012A	1012A	1012A	1012A	1012A	1012A	1012A	1012A	1012A	1012A	1012A	1012A
Analysis	013	014	021B	026	027A	027B	028	030	032	039	042	046
P	581	738	794	951	405	941	471	325	433	572	520	679
Ti	5.3	67.2	172.5	300.8	7.9	614.6	42.7	8.5	26.7	4.4	13.5	15.0
Y	1904	2139	6924	10217	2191	16440	3353	1047	2798	1821	2038	4324
Nb	4.5	3.2	16.2	20.1	9.2	27.3	5.8	2.7	4.9	4.7	3.7	3.9
La	0.3	16.7	218.1	206.6	4.9	1037.9	113.8	4.5	66.6	0.3	29.4	0.1
Ce	12	83	1156	1385	44	5975	625	24	173	11	173	19
Pr	0.1	11.8	172.9	227.0	4.5	750.4	99.3	2.7	31.9	0.3	19.5	0.3
Nd	2.2	79	1043	1400	32	4259	677	19	206	3.1	129	5.6
Sm	4.0	44.4	601.6	940.4	27.0	2318.5	317.0	10.7	93.2	4.4	70.4	13.7
Eu	0.9	9.6	197.5	216.4	3.9	509.6	88.2	3.5	46.7	0.9	17.6	4.4
Gd	30	93	865	1374	80	3011	406	26	183	27	124	87
Tb	12	24	168	303	23	528	75	8	42	11	27	32
Dy	155	235	1089	1955	234	2996	488	93	351	146	233	380
Ho	65	76	249	406	80	572	120	35	97	62	68	151
Er	308	313	775	1113	326	1416	408	167	351	305	270	678
Tm	67	62	138	176	61	210	76	37	66	69	56	144
Yb	672	584	1259	1480	574	1841	743	373	581	686	553	1404
Lu	129	111	225	252	105	297	131	74	104	133	105	272
Hf	11217	10969	12294	14179	12397	11206	12446	12021	17217	14316	12992	14225
Ta	1.7	0.7	5.4	5.6	2.3	13.3	2.6	1.3	1.4	3.2	1.8	1.3
Th	200	102	344	531	266	273	260	113	821	164	692	483
U	455	314	1988	1953	379	3096	876	313	1509	671	1157	642
$(Lu/La)_N$	3607	64	9.9	12	209	2.8	11	158	15	3933	34	42185
$(Sm/La)_N$	18.2	4.2	4.4	7.2	8.8	3.5	4.4	3.7	2.2	21.3	3.8	350.6
$(Lu/Gd)_N$	34.7	9.5	2.1	1.5	10.6	0.8	2.6	23.1	4.5	40.3	6.8	25.1
Ce/Ce*	13.7	1.4	1.4	1.5	2.2	1.6	1.4	1.6	0.9	8.2	1.7	31.3
Eu/Eu*	0.25	0.45	0.84	0.58	0.26	0.59	0.75	0.65	1.09	0.27	0.58	0.39
ΣREE	1458	1743	8158	11435	1599	25721	4367	877	2391	1458	1876	3191

Sample	1012A	1012A	1012A	1012A	1012A	1012A	1012A	1012A	1012A	1012A	1012A	1012A
Analysis	048	053	056	058	059	060	064	065	069A	069B	070	071
P	677	427	616	1468	884	626	485	614	677	483	621	558
Ti	7.6	31.2	4.2	153.0	6.4	8.3	74.1	8.6	16.7	5.8	15.6	15.7
Y	2733	2183	2768	10369	2870	2375	4032	1980	2354	2385	2662	2179
Nb	4.0	4.7	5.2	14.0	7.0	4.7	5.6	4.7	4.0	8.5	6.0	6.3
La	0.5	23.0	1.2	380.3	4.1	1.7	104.7	0.8	4.1	6.3	6.4	5.1
Ce	18	135	19	1817	32	23	462	18	34	51	52	32
Pr	0.5	18.2	1.1	297.3	2.7	1.6	81.5	0.6	3.5	5.4	6.2	3.1
Nd	5.0	120	7.6	2010	16	10.3	495	5.0	20	34	38	22
Sm	9.2	74.4	8.7	865.2	11.1	10.6	314.2	6.7	17.4	20.2	25.2	13.4
Eu	2.4	16.7	1.9	284.7	4.0	2.1	68.7	1.5	3.4	4.7	5.4	4.3
Gd	52	134	46	1285	49	46	457	33	48	56	73	46
Tb	19	30	18	226	19	17	91	13	17	19	22	16
Dy	245	253	238	1465	249	211	609	168	199	214	254	187
Ho	99	78	97	359	100	83	143	70	82	84	95	74
Er	436	320	446	1160	472	379	457	323	382	383	417	350
Tm	94	68	96	206	106	81	83	70	80	82	88	77
Yb	879	682	931	1842	1072	790	755	682	787	792	847	761
Lu	167	121	178	322	194	147	132	129	150	146	158	150
Hf	12233	12119	12843	15372	15295	12279	9084	12922	12488	13234	11345	11555
Ta	1.5	1.5	2.0	7.8	3.0	1.9	1.5	1.8	1.4	3.5	1.5	2.6
Th	342	285	311	1480	314	267	395	212	170	479	360	343
U	565	622	700	2050	921	508	699	420	347	971	588	738
$(Lu/La)_N$	3555	51	1421	8.2	457	852	12	1543	349	222	239	282
$(Sm/La)_N$	32.5	5.1	11.4	3.6	4.3	10.1	4.8	13.2	6.7	5.1	6.3	4.2
$(Lu/Gd)_N$	25.9	7.3	31.2	2.0	32.0	25.6	2.3	31.5	24.9	20.9	17.4	25.9
Ce/Ce*	8.6	1.5	3.8	1.3	2.2	3.4	1.2	5.9	2.1	2.1	1.9	1.9
Eu/Eu*	0.34	0.51	0.29	0.83	0.52	0.28	0.55	0.31	0.36	0.43	0.39	0.53
ΣREE	2026	2074	2090	12519	2331	1803	4253	1521	1828	1897	2087	1741

Sample	1012A	1012A	1012A	1012A	1012A	1012A	1012A	1012A	1012A	1012A	1012A	1012A
Analysis	072	075A	075B	083	090	097	099A	099B	100	104	107	109
P	485	790	356	552	571	785	649	1273	1103	722	763	1260
Ti	12.4	325.9	16.7	4.2	37.0	9.2	13.5	31.3	374.3	46.4	14.9	11.8
Y	2092	11920	1635	2335	5017	1946	1760	5930	9979	2598	2305	3765
Nb	3.3	16.2	2.8	6.1	6.7	2.4	1.8	13.0	19.4	6.5	4.7	5.6
La	0.1	423.2	18.5	6.7	31.1	0.7	18.6	136.9	233.8	45.1	3.3	0.0
Ce	13	2250	105	37	193	10	61	409	1637	180	33	18
Pr	0.3	327.4	15.5	3.6	30.0	0.5	10.3	67.4	284.3	28.8	2.5	0.2
Nd	3.4	2016	95	28	187	4.4	73	440	1838	175	16	3.7
Sm	7.7	1242.4	57.9	16.0	128.7	6.2	30.3	195.2	1135.4	86.7	14.0	9.0
Eu	1.7	300.2	14.9	6.4	34.1	1.7	9.6	70.1	253.3	37.9	3.4	2.0
Gd	43	1843	86	51	231	36	67	351	1538	135	47	60
Tb	15	372	21	17	57	14	17	76	280	31	18	25
Dy	193	2238	194	199	518	171	171	669	1708	278	213	322
Ho	75	444	59	81	171	69	62	210	353	90	84	133
Er	337	1157	243	373	714	314	271	856	1050	382	374	599
Tm	71	174	51	82	150	67	56	174	182	82	80	131
Yb	680	1458	494	828	1472	648	539	1629	1594	801	770	1252
Lu	125	239	91	158	271	125	105	299	272	140	145	222
Hf	12219	14297	14297	13039	10713	11886	11926	17057	12400	12096	12160	12626
Ta	1.2	2.1	1.4	2.8	1.7	0.9	0.9	5.4	4.4	2.3	1.6	1.6
Th	232	1161	193	272	1164	158	123	810	683	219	205	310
U	348	1485	401	655	1226	293	277	1585	1220	691	454	565
$(Lu/La)_N$	9447	5.4	47	228	84	1830	54	21	11	30	424	86957
$(Sm/La)_N$	95.2	4.7	5.0	3.8	6.6	15.0	2.6	2.3	7.7	3.1	6.7	582.8
$(Lu/Gd)_N$	23.2	1.0	8.5	24.9	9.4	27.6	12.5	6.8	1.4	8.3	24.7	29.8
Ce/Ce*	17.4	1.4	1.4	1.8	1.5	4.3	1.0	1.0	1.5	1.2	2.7	66.2
Eu/Eu*	0.29	0.61	0.64	0.68	0.60	0.35	0.65	0.82	0.59	1.07	0.40	0.26
ΣREE	1567	14484	1545	1885	4186	1467	1491	5584	12359	2493	1803	2777

Sample	1012A	1012A	1012A	1012A	1012A	1012A	1012A	1012A	1012A	1015A	1015A
Analysis	112A	112B	115	131	133	137	140	144	145	003	004
P	1403	1261	498	965	1028	790	398	750	456	1136	1068
Ti	637.7	208.5	13.3	5.1	24.9	15.8	15.6	8.0	5.5	45	16
Y	13633	9067	1858	2770	3869	2592	1309	2192	1366	2996	2830
Nb	29.7	18.2	2.8	3.9	11.7	3.9	1.8	4.8	1.7	235	78
La	430.7	247.4	9.7	4.0	90.8	19.9	0.1	0.0	0.3	19	12
Ce	2292	1350	44	35	309	87	11	12	9	315	120
Pr	392.5	225.6	5.9	2.8	46.0	14.6	0.1	0.1	0.3	33	11
Nd	2424	1425	36	22	269	85	2.1	1.5	2.6	234	65
Sm	1639.5	868.7	23.5	17.9	121.6	42.8	5.0	4.8	5.7	174	48
Eu	367.9	230.5	4.5	3.3	32.2	15.4	1.4	1.1	1.4	7.7	2.9
Gd	2275	1239	56	62	212	88	26	32	27	260	103
Tb	419	219	16	21	50	24	9	14	10	58	30
Dy	2507	1391	171	248	452	251	117	184	125	452	306
Ho	492	321	62	94	141	91	45	76	49	115	103
Er	1321	999	282	436	570	406	205	354	214	426	442
Tm	223	177	63	97	114	84	46	80	49	89	94
Yb	2023	1589	644	1006	1072	831	451	796	472	890	915
Lu	317	268	126	184	185	152	85	143	84	149	155
Hf	10477	13577	14015	12852	12242	11861	12585	13145	11813	10799	11417
Ta	5.7	6.6	1.1	2.0	4.8	1.4	0.8	1.8	0.8	16.3	4.2
Th	426	1070	222	487	1025	268	109	181	105	1890	1124
U	2399	1954	383	1002	1644	468	169	424	220	948	860
$(Lu/La)_N$	7.1	10	125	441	20	74	14945	48200	2611	77	124
$(Sm/La)_N$	6.0	5.6	3.8	7.1	2.1	3.4	143.7	264.6	29.5	14.9	6.4
$(Lu/Gd)_N$	1.1	1.7	18.0	23.9	7.0	13.9	26.5	35.9	24.9	4.6	12.1
Ce/Ce*	1.3	1.3	1.3	2.5	1.1	1.2	35.1	63.1	7.2	3.0	2.4
Eu/Eu*	0.58	0.68	0.38	0.31	0.61	0.77	0.37	0.27	0.35	0.11	0.12
ΣREE	17125	10551	1544	2232	3663	2192	1004	1700	1047	3221	2407

Sample	1015A	1015A	1015A	1015A	1015A	1015A	1015A	1015A	1015A	1015A	1015A	1015A
Analysis	007A	007B	008A	010	011A	022	029	030	032	033	036	039
P	6058	5981	7663	10506	5519	11056	8624	11381	2391	12331	13455	8284
Ti	334	431	399	455	262	587	450	377	131	452	566	365
Y	16385	18594	22211	24590	15917	26230	27171	25985	8220	24607	35166	24079
Nb	1799	2596	3083	2922	1685	3517	3403	2832	423	2903	4444	3061
La	81	347	148	196	78	270	214	108	28	130	306	227
Ce	1332	5963	2083	2814	997	2674	3332	1911	314	1533	3206	3074
Pr	182	456	290	306	160	373	493	281	50	225	441	427
Nd	1375	2957	2180	2204	1132	2652	3922	2361	357	1687	2987	3349
Sm	1150	1646	1647	1710	994	1873	2630	1927	347	1548	2259	2294
Eu	62	77	87	92	51	108	116	91	19	102	135	95
Gd	1707	2239	2617	2719	1662	2842	3303	2662	666	2573	4049	2827
Tb	411	511	580	652	436	632	632	562	166	631	1005	546
Dy	2971	3681	3958	4618	3231	4417	4183	4009	1303	4539	7019	3635
Ho	692	828	893	1033	753	1026	972	962	341	1037	1518	861
Er	2245	2589	2706	3218	2417	3174	2998	3073	1216	3244	4582	2732
Tm	418	455	471	577	447	576	545	571	243	593	800	512
Yb	3596	3774	3857	4824	3888	4868	4579	4952	2229	5078	6498	4522
Lu	499	528	543	664	527	678	674	705	333	680	858	660
Hf	10279	11384	11355	10623	10573	10611	12032	10926	12908	10204	11194	10643
Ta	76.2	215.7	75.4	104.3	68.5	69.5	67.0	40.3	12.6	62.5	118.3	50.2
Th	11420	40676	11418	19376	5664	23270	21719	11832	2017	13911	18636	15029
U	2627	2369	3410	4014	2883	3910	2732	3969	1846	3981	6101	2637
$(Lu/La)_N$	60	15	35	33	65	24	30	63	116	50	27	28
$(Sm/La)_N$	22.6	7.5	17.7	13.9	20.3	11.0	19.6	28.2	20.0	18.9	11.7	16.0
$(Lu/Gd)_N$	2.3	1.9	1.7	2.0	2.5	1.9	1.6	2.1	4.0	2.1	1.7	1.9
Ce/Ce*	2.6	3.5	2.4	2.7	2.1	2.0	2.4	2.6	2.0	2.1	2.0	2.3
Eu/Eu*	0.14	0.12	0.13	0.13	0.12	0.14	0.12	0.12	0.12	0.16	0.14	0.11
ΣREE	16720	26052	22061	25629	16771	26163	28593	24176	7612	23599	35662	25761

Sample	1015A	1015A	1015A	1015A	1015A	1015A	1015A	1015A	1015A	1015A	1015A	1015A
Analysis	046	049	050	052	059	060	068	070	071	075	077	078
P	9331	17284	6449	11026	10155	9578	8055	965	8952	10096	6645	15583
Ti	447	439	355	380	402	564	371	14	448	536	187	459
Y	24468	40633	16111	25974	24857	25754	14798	2766	24775	24976	18562	35590
Nb	4168	4190	3002	2746	3543	4055	3528	86	3126	3124	1435	3804
La	253	278	221	127	180	121	133	5	168	171	47	184
Ce	2830	3177	2160	1686	2595	2350	1488	118	2243	2146	638	2338
Pr	497	358	314	200	313	300	264	9	381	303	78	250
Nd	3644	2518	2169	1432	2225	2361	1656	61	3083	2206	572	1741
Sm	2003	2172	1230	1471	1715	1869	744	37	2165	1895	829	2052
Eu	75	133	51	83	87	92	32	2.7	98	116	46	116
Gd	2669	4178	1673	2837	2889	2879	1149	92	2778	2918	1838	4005
Tb	519	1056	318	770	709	642	231	27	546	679	583	1151
Dy	3621	7606	2259	5524	5006	4489	1808	291	3841	4738	4559	8507
Ho	887	1672	568	1186	1090	1024	518	100	919	1056	1009	1777
Er	2874	5053	1934	3603	3344	3123	1910	426	2954	3279	3194	5496
Tm	545	881	358	637	609	578	377	92	546	586	583	1009
Yb	4882	7023	3182	5300	5109	4870	3475	905	4827	4887	4910	8177
Lu	705	917	486	692	674	674	532	151	675	656	605	1044
Hf	12268	10803	10397	9817	10324	11003	12298	11745	11891	10796	9943	12158
Ta	91.7	121.8	41.0	53.5	126.4	120.0	51.1	5.0	50.7	75.3	45.9	176.9
Th	12963	28487	6411	11938	11904	17343	9704	863	9006	19708	6350	20063
U	4103	4635	3558	4352	3941	3809	3837	764	3527	3558	2621	5401
$(Lu/La)_N$	27	32	21	52	36	54	39	269	39	37	125	55
$(Sm/La)_N$	12.6	12.4	8.8	18.4	15.2	24.5	8.9	10.9	20.4	17.6	28.3	17.7
$(Lu/Gd)_N$	2.1	1.8	2.3	2.0	1.9	1.9	3.7	13.2	2.0	1.8	2.6	2.1
Ce/Ce*	1.9	2.4	1.9	2.5	2.6	2.9	1.9	4.0	2.1	2.2	2.5	2.6
Eu/Eu*	0.10	0.13	0.11	0.12	0.12	0.12	0.11	0.14	0.12	0.15	0.11	0.12
ΣREE	26006	37025	16922	25549	26545	25374	14318	2318	25227	25636	19491	37847

Sample	1015A	1015A	1015A	1015A	1015A	1015A	1015A	1015A	1015A	1015A	1015A	1015A
Analysis	082	083	088	094	096	099B	103	107	110	114	117	120
P	7921	7522	564	9412	12071	5604	4693	13991	11862	10836	720	8664
Ti	321	390	9	339	589	231	227	404	467	504	16	455
Y	18160	21929	3877	25695	29019	15053	12098	29138	25005	24415	2653	20801
Nb	2054	2400	27	2848	3432	1518	1416	3391	2855	2919	77	2797
La	81	38	5	208	131	93	68	313	230	139	7	97
Ce	1329	930	54	3163	2205	1393	903	4932	2152	1902	87	1491
Pr	250	214	4	383	329	161	128	490	290	304	9	204
Nd	2090	1950	24	2699	2550	1105	922	3297	2029	2149	66	1521
Sm	1598	1794	29	1739	1976	950	808	2104	1551	1584	50	1216
Eu	76	84	3.8	68	114	47	48	99	83	84	2.8	67
Gd	1946	2344	106	2568	2956	1533	1325	3187	2405	2515	98	2001
Tb	381	487	35	554	674	385	331	739	571	576	28	456
Dy	2647	3461	396	4055	4873	2874	2416	5179	4244	4185	281	3319
Ho	646	812	137	977	1126	650	535	1149	983	959	96	791
Er	2178	2680	581	3204	3527	2060	1672	3583	3074	3062	408	2595
Tm	411	492	124	594	645	372	303	642	574	550	88	482
Yb	3722	4344	1180	5173	5487	3223	2618	5263	4899	4669	861	4227
Lu	542	619	197	755	773	443	358	745	674	658	146	604
Hf	11091	10921	10942	15273	11577	10472	12257	10015	10263	12372	11335	11095
Ta	30.5	37.3	2.6	45.7	70.9	49.4	69.1	136.1	47.7	47.0	5.4	50.7
Th	5945	9986	691	8971	17984	8542	6324	25460	17890	13686	723	15801
U	3202	3161	868	5364	4171	2929	2339	4169	4077	4417	920	3331
$(Lu/La)_N$	65	159	419	35	57	46	51	23	28	46	189	60
$(Sm/La)_N$	31.4	75.8	10.2	13.3	24.0	16.2	18.9	10.7	10.7	18.1	10.6	19.8
$(Lu/Gd)_N$	2.2	2.1	15.0	2.4	2.1	2.3	2.2	1.9	2.2	2.1	12.0	2.4
Ce/Ce*	2.2	2.4	3.1	2.6	2.5	2.7	2.3	2.9	1.9	2.2	2.5	2.5
Eu/Eu*	0.13	0.13	0.21	0.10	0.14	0.12	0.14	0.12	0.13	0.13	0.12	0.13
ΣREE	17896	20250	2875	26139	27366	15289	12434	31723	23760	23336	2227	19070

Sample	1015A	1019C	1019C	1019C	1019C	1019C	1019C	1019C	1019C	1019C	1019C
Analysis	133	006A	006B	007A	007B	016	017	023B	036	037	038
P	9131	15843	10507	3065	4833	5181	2045	1958	321	5704	1701
Ti	395	267.3	181.6	87.8	19.0	87.0	44.5	49.2	16.7	51.4	23.9
Y	22760	16642	8725	5909	2245	4901	4428	3125	1739	13574	4993
Nb	2778	18.9	17.4	8.1	8.1	5.2	4.8	5.1	1.3	4.3	2.5
La	203	558.1	195.3	116.6	33.1	63.9	34.1	34.6	0.11	147.6	5.7
Ce	3069	2022	875	374	110	272	164	141	24	596	41
Pr	384	418.8	206.0	74.3	18.8	60.0	31.4	29.2	0.2	123.5	6.7
Nd	2755	2893	1579	509	111	400	228	199	4.41	823	49
Sm	1719	1218	675	202	47	180	144	108	9.25	445	43
Eu	72	473.2	327.6	138.8	23.3	209.1	102.6	95.7	2.6	310.9	11.0
Gd	2352	1630	845	321	88	286	246	178	46	772	130
Tb	511	281	136	66	22	65	60	38	14	176	43
Dy	3620	1972	984	609	221	553	517	337	162	1464	478
Ho	842	511	270	199	75	158	141	104	61	428	173
Er	2719	1741	984	767	321	581	507	392	256	1611	729
Tm	497	338	200	157	68	121	98	83	54	338	153
Yb	4258	3079	1919	1457	639	1176	896	806	523	3271	1392
Lu	605	489	287	228	106	189	144	123	87	536	227
Hf	10735	14821	15476	14673	14404	15708	12206	15198	13401	12305	15007
Ta	43.0	21.1	17.2	5.3	4.2	4.2	2.2	3.1	0.8	2.2	1.2
Th	14473	4208	1471	997	519	1020	813	508	242	2660	535
U	3949	10653	3497	2272	1184	2432	1099	1311	242	2467	710
$(Lu/La)_N$	29	8.4	14	19	31	28	41	34	7794	35	381
$(Sm/La)_N$	13.4	3.5	5.5	2.8	2.2	4.5	6.7	4.9	137.1	4.8	11.9
$(Lu/Gd)_N$	2.1	2.4	2.7	5.7	9.7	5.3	4.7	5.5	15.1	5.6	14.0
Ce/Ce*	2.6	0.98	1.02	0.94	1.03	1.03	1.17	1.04	37	1.03	1.54
Eu/Eu*	0.11	1.03	1.32	1.67	1.11	2.82	1.67	2.11	0.38	1.62	0.45
ΣREE	23607	17625	9483	5218	1882	4312	3314	2668	1243	11042	3481

Sample	1019C	1019C	1019C	1019C	1019C	1019C	1019C	1019C	1019C	1019C	1019C	1019C
Analysis	039	040	043	045	049	050B	055	058	059	060	062	065
P	940	409	284	1083	154	2253	852	4513	2860	4620	521	3441
Ti	16.6	42.9	14.1	11.0	7.8	83.9	26.6	42.9	145.3	61.7	10.4	82.1
Y	2285	1820	929	1236	439	4777	1661	7866	7612	12865	1635	6475
Nb	0.85	6.2	3.6	2.0	1.05	4.2	4.0	4.6	6.7	3.9	3.2	7.9
La	4.2	0.41	0.17	12.7	0.13	22.0	8.9	52.4	33.6	17.2	9.9	59.6
Ce	26	9	10	72	12	153	56	271	249	140	64	348
Pr	5.6	0.3	0.2	9.2	0.1	33.8	9.7	56.8	55.1	24.7	6.6	64.9
Nd	44	1.99	1.75	55	1.86	265	63	422	424	189	44	487
Sm	35	3.55	4.09	25	2.04	153	39	303	295	146	25	243
Eu	11.7	0.6	0.7	27.7	1.2	159.6	18.4	186.8	369.5	129.3	11.3	215.8
Gd	91	28	17	45	8.50	246	74	538	457	413	63	391
Tb	27	12	6.67	12	2.95	58	20	133	110	128	16	83
Dy	261	154	84	113	33	517	187	1031	885	1375	165	692
Ho	81	62	31	38	14	147	59	265	228	453	57	204
Er	312	286	145	166	65	533	246	918	780	1784	232	792
Tm	63	63	32	39	17	107	55	175	154	370	48	162
Yb	576	600	328	416	179	980	589	1519	1388	3385	456	1556
Lu	92	108	61	83	38	151	104	238	210	509	79	259
Hf	9531	14250	9504	13005	12212	14006	15519	10580	12520	10802	11361	12570
Ta	0.7	2.9	1.1	1.4	0.5	2.4	2.8	3.2	5.9	1.8	1.2	3.6
Th	297	337	68	615	126	147	308	852	669	1406	264	1621
U	705	866	89	1108	236	1371	826	1869	1900	1303	498	1690
(Lu/La)N	210	2524	3431	63	2812	66	113	44	60	285	77	42
(Sm/La)N	13.3	13.7	37.6	3.1	25.0	11.0	6.9	9.2	13.9	13.4	4.0	6.5
(Lu/Gd)N	8.1	31.0	29.3	14.7	35.6	5.0	11.4	3.6	3.7	9.9	10.2	5.3
Ce/Ce*	1.28	5.81	13.20	1.55	21	1.32	1.40	1.16	1.35	1.59	1.84	1.31
Eu/Eu*	0.63	0.19	0.26	2.51	0.90	2.52	1.05	1.41	3.07	1.61	0.87	2.14
ΣREE	1631	1328	721	1114	374	3526	1528	6107	5639	9065	1276	5556

Sample	1019C	1019C	1019C	1019C	1019C	1019C	1019C	1019C	1019C	1019C	1019C	1019C
Analysis	067A	067B	068	072	073A	073B	078A	079	080	081A	083	085
P	3414	5674	750	862	6591	681	3970	1133	2000	297	11797	673
Ti	111.8	181.5	25.4	14.4	235.3	13.7	116.1	16.3	60.3	41.0	27.8	15.6
Y	6573	10084	1707	2406	8671	1208	7037	1975	3483	565	2532	3431
Nb	5.8	8.1	5.5	2.6	6.3	2.6	7.7	3.8	6.2	1.9	2.8	10.4
La	60.2	121.9	3.2	4.7	161.5	7.4	79.0	13.2	28.9	1.36	66.4	2.2
Ce	297	576	58	36	583	53	373	56	161	18	196	38
Pr	67.8	129.9	3.4	8.2	106.0	6.7	86.9	11.3	32.2	0.9	28.9	3.0
Nd	539	992	22	69	709	47	714	75	231	6.78	177	24
Sm	351	604	21	47	341	24	422	43	150	6.58	92	23
Eu	237.5	416.1	22.1	26.1	310.3	24.0	293.6	21.8	101.1	3.0	40.0	5.5
Gd	512	885	54	92	513	47	609	81	241	17	158	78
Tb	100	171	16	25	101	11	112	22	56	5.13	39	27
Dy	753	1224	172	247	811	111	794	215	439	54	324	315
Ho	201	308	59	81	232	36	201	70	113	18	87	118
Er	724	1031	244	326	855	157	679	282	390	74	313	519
Tm	146	193	51	67	167	36	127	58	79	17	61	110
Yb	1400	1762	500	631	1591	381	1154	556	787	154	574	1058
Lu	214	263	86	102	270	69	173	89	122	28	89	173
Hf	15744	13552	13538	13722	14175	14188	12882	11227	13103	12623	11661	13669
Ta	3.8	6.3	2.2	2.2	4.7	1.8	5.6	2.5	2.8	1.1	1.8	3.5
Th	517	1069	425	191	2497	361	907	275	866	203	474	457
U	1800	2898	457	658	2993	687	2496	701	1638	370	538	1239
(Lu/La)N	34	21	260	211	16	90	21	65	41	199	13	749
(Sm/La)N	9.3	7.9	10.4	16.1	3.4	5.2	8.5	5.2	8.2	7.7	2.2	16.6
(Lu/Gd)N	3.3	2.4	12.9	8.9	4.2	11.7	2.3	8.8	4.1	13.3	4.5	17.7
Ce/Ce*	1.09	1.07	4.1	1.37	1.04	1.77	1.05	1.07	1.24	3.8	1.05	3.4
Eu/Eu*	1.71	1.74	2.02	1.20	2.27	2.15	1.77	1.12	1.63	0.88	1.01	0.39
ΣREE	5603	8674	1311	1763	6751	1014	5817	1594	2931	404	2243	2493

Sample	1019C	1019C	1019C	1019C	1019C	1019C	1019C	1019C	1019C	1019C	1019C	1019C
Analysis	087	088	090	091	094	095	099	105	109	111	114A	114B
P	583	320	1219	239	891	350	497	5286	832	404	2746	2261
Ti	18.0	10.4	47.0	8.1	27.2	7.8	13.6	104.7	135.9	9.4	76.6	48.7
Y	1686	1721	1671	1496	2183	1009	1546	10887	2243	1174	4950	3370
Nb	3.8	2.3	4.1	2.2	3.4	2.7	2.2	6.8	4.3	3.0	6.0	5.7
La	3.0	0.3	16.6	0.8	11.2	4.3	4.0	113.7	1.2	0.5	34.2	22.3
Ce	20	5.21	70	24	63	28	22	516	56	9.42	232	149
Pr	3.7	0.5	14.8	1.2	13.7	2.8	4.5	117.3	1.6	0.7	49.9	27.3
Nd	27	7.85	101	11	103	17	36	833	15	6.09	361	194
Sm	21	13	75	13	68	12	22	513	23	6.07	205	118
Eu	12.6	2.2	42.8	5.0	55.3	5.3	18.2	257.0	6.8	3.3	246.9	129.6
Gd	50	54	106	48	112	27	50	768	101	25	312	194
Tb	14	17	24	14	28	8.20	15	167	34	8.91	71	48
Dy	156	187	190	152	242	89	159	1325	415	106	574	399
Ho	56	62	53	53	68	33	52	341	148	41	153	113
Er	244	256	199	215	254	151	220	1187	625	180	554	434
Tm	54	50	44	46	52	36	48	244	132	40	118	93
Yb	539	473	456	438	479	374	505	2371	1273	391	1168	945
Lu	94	78	76	75	78	68	83	347	204	67	190	158
Hf	11159	9688	11515	9527	14562	10672	9165	16503	11304	11176	12095	16708
Ta	1.7	1.1	10.5	0.7	1.4	1.2	1.5	6.1	1.4	1.4	4.4	5.1
Th	157	129	211	119	225	273	83	564	1096	205	208	307
U	427	257	544	221	901	393	453	3453	845	402	1568	1506
(Lu/La)N	298	2358	44	885	67	154	199	29	1688	1256	54	68
(Sm/La)N	11.1	62.6	7.2	26.4	9.7	4.3	8.8	7.2	31.7	18.8	9.5	8.4
(Lu/Gd)N	15.2	11.6	5.8	12.6	5.7	20.3	13.3	3.6	16.2	21.7	4.9	6.5
Ce/Ce*	1.40	2.92	1.04	5.8	1.19	1.89	1.21	1.05	9.6	3.73	1.31	1.41
Eu/Eu*	1.18	0.26	1.47	0.60	1.94	0.92	1.65	1.25	0.43	0.8	2.98	2.61
ΣREE	1294	1205	1467	1097	1627	855	1238	9100	3037	885	4269	3024

Sample	1019C	1019C	1019C	1019C	1019C	1019C	1019C	1019C	1019C	1019C
Analysis	120A	122	124A	125	127	128	129	130A	133	141B
P	1021	1065	3961	4282	7302	2283	2298	970	1195	2840
Ti	18.3	30.2	33.2	137.0	176.6	35.6	58.1	112.8	58.7	68.2
Y	2139	2731	9155	8779	14065	3166	4451	2225	1806	4976
Nb	3.3	2.7	6.8	9.3	11.7	2.9	2.6	4.6	1.9	5.6
La	11.3	12.3	76.5	55.9	76.6	27.6	13.0	19.9	17.6	74.9
Ce	57	69	345	462	598	153	100	93	94	283
Pr	10.3	13.6	72.7	112.2	149.1	35.5	23.6	8.6	15.6	44.7
Nd	78	100	481	838	1182	278	174	56	108	305
Sm	47	66	278	462	719	152	115	35	61	181
Eu	43.1	39.3	168.2	478.2	599.4	83.5	135.5	15.8	58.2	144.8
Gd	88	128	488	647	1039	225	199	74	109	318
Tb	22	33	116	134	213	48	52	22	25	71
Dy	212	301	1006	1002	1591	371	478	223	199	569
Ho	68	91	294	253	423	104	139	75	55	149
Er	285	351	1131	832	1498	392	542	323	209	513
Tm	62	73	232	155	307	82	115	71	44	98
Yb	617	695	2292	1407	2935	823	1131	730	438	894
Lu	100	116	358	208	442	139	175	126	73	132
Hf	12015	12051	14171	12468	14450	12852	13625	13326	12822	9560
Ta	2.1	1.0	3.1	6.7	10.4	2.6	1.4	1.5	0.9	1.4
Th	327	380	2009	733	774	593	217	212	556	1668
U	613	670	1867	2940	5198	1564	1404	406	810	1164
(Lu/La)N	85	90	45	36	56	48	130	61	40	17
(Sm/La)N	6.7	8.5	5.8	13.1	14.9	8.8	14.1	2.8	5.5	3.8
(Lu/Gd)N	9.1	7.3	5.9	2.6	3.4	4.9	7.0	13.7	5.4	3.3
Ce/Ce*	1.24	1.26	1.08	1.37	1.31	1.15	1.34	1.66	1.33	1.15
Eu/Eu*	2.04	1.31	1.40	2.67	2.12	1.38	2.74	0.95	2.18	1.84
ΣREE	1700	2088	7337	7045	11773	2914	3393	1871	1506	3777